AFRL-AFOSR-VA-TR-2023-0351

Boundary Layer Transition (BOLT) Post-Flight Research and BOLT II Flight Test Support

Wheaton, Bradley
JOHNS HOPKINS UNIV BALTIMORE MD
3400 NORTH CHARLES STREET
BALTIMORE, MD,
US

04/27/2023
Final Technical Report

Air Force Research Laboratory
Air Force Office of Scientific Research
Arlington, Virginia 22203
Air Force Materiel Command

REPORT DOCUMENTATION PAGE

PLEASE DO NOT RETURN YOUR FORM TO THE ABOVE ORGANIZATION.

1. REPORT DATE
20230427

2. REPORT TYPE
Final

3. DATES COVERED

START DATE 20200311	**END DATE** 20230310

4. TITLE AND SUBTITLE
Boundary Layer Transition (BOLT) Post-Flight Research and BOLT II Flight Test Support

5a. CONTRACT NUMBER	**5b. GRANT NUMBER** FA9550-20-1-0043	**5c. PROGRAM ELEMENT NUMBER** 61102F
5d. PROJECT NUMBER	**5e. TASK NUMBER**	**5f. WORK UNIT NUMBER**

6. AUTHOR(S)
Bradley Wheaton

7. PERFORMING ORGANIZATION NAME(S) AND ADDRESS(ES)
JOHNS HOPKINS UNIV BALTIMORE MD
3400 NORTH CHARLES STREET
BALTIMORE, MD
US

8. PERFORMING ORGANIZATION REPORT NUMBER

9. SPONSORING/MONITORING AGENCY NAME(S) AND ADDRESS(ES)
Air Force Office of Scientific Research
875 N. Randolph St. Room 3112
Arlington, VA 22203

10. SPONSOR/MONITOR'S ACRONYM(S)
AFRL/AFOSR RTA1

11. SPONSOR/MONITOR'S REPORT NUMBER(S)
AFRL-AFOSR-VA-TR-2023-0351

12. DISTRIBUTION/AVAILABILITY STATEMENT
A Distribution Unlimited: PB Public Release

13. SUPPLEMENTARY NOTES

14. ABSTRACT
This report summarizes the three-year research effort by the Johns Hopkins University Applied Physics Laboratory (APL) under grant number FA9550-20-1-0043 from the Air Force Office of Scientific Research (AFOSR) to conduct postflight analysis of the BOLT flight experiment and to support the development, execution, and analysis of data from BOLT-2: The Holden Mission. Key accomplishments from this research included characterization of supersonic transition flight data received from the BOLT experiment, investigation and identification of the probably cause of unexpected flight behavior that occurred in the BOLT flight, significant independent analysis of the BOLT-2 flight during the pre- and postflight research phases, and new Spatial BiGlobal stability calculations of the BOLT geometry in support of the BOLT-2 flight analysis and a NATO STO-AVT-346 working group activities. The research resulted in seven conference papers with an eighth paper planned. The research led to advances in understanding of supersonic transition, flight dynamics, aeroelastic effects on aerodynamics, thermal analysis methodology for low-cost sounding rocket experiments, and advancements in the use of Spatial BiGlobal stability on the BOLT geometry. APL plans to continue research on many of these topics in a new grant from AFOSR, FA9550-22-1-0357, that will also support a re-flight attempt of the BOLT experiment called BOLT-1B.

15. SUBJECT TERMS

16. SECURITY CLASSIFICATION OF:

a. REPORT	**b. ABSTRACT**	**c. THIS PAGE**
U	U	U

17. LIMITATION OF ABSTRACT
UU

18. NUMBER OF PAGES
25

19a. NAME OF RESPONSIBLE PERSON
DOUGLAS SMITH

19b. PHONE NUMBER *(Include area code)*
314 235 6013

Standard Form 298 (Rev.5/2020)
Prescribed by ANSI Std. Z39.18

JOHNS HOPKINS
APPLIED PHYSICS LABORATORY

FA9550-20-1-0043 Final Report
10 March 2023
APL Project FGX75

To: Dr. Doug Smith
Acting Program Officer - High Speed Aerodynamics
AFOSR/RTA
875 N. Randolph St., Suite 325, Room 3112
Arlington, VA 22203-1768

From: Dr. Bradley M. Wheaton (Principal Investigator)
Dr. Daniel B. Araya (Co-Investigator)
Dr. Dennis C. Berridge (Co-Investigator)
Dr. Cameron S. Butler
Dr. Gregory R. McKiernan
Mr. Prasad M. Kutty
Mr. Jim B. Fortier
Dr. John T. Melcher
Mr. Eliott J. Radcliffe
Mr. David M. Gers
Mr. Ryan L. Eby
Mr. Thomas D. Wolf
Ms. Deana M. Prosniewski (Financial Manager)
Mr. Rubbel Kumar (Program Manager)

Subject: Final Performance Report for Boundary Layer Transition (BOLT) Post-Flight Research and BOLT II Flight Test Support (Grant FA9550-20-1-0043, period 11 March 2020 through 10 March 2023)

Distribution Statement A: Approved for Public Release; Distribution Unlimited.

Cover Page Data

- **Federal Agency and Organization Element to Which the Report is Submitted:**
  Air Force Research Laboratory Air Force Office of Scientific Research (AFRL/AFOSR)
- **Federal Grant or Other Identifying Number Assigned by Agency:**
  FA9550-20-1-0043
- **Project Title:**
  Boundary Layer Transition (BOLT) Post-Flight Research and BOLT II Flight Test Support
- **Project Director/Principal Investigator (PD/PI):**
  Dr. Bradley M. Wheaton
  Senior Professional Staff
  Bradley.Wheaton@jhuapl.edu
  +1 240-228-6470
- **Co-Investigator:**
  Dr. Daniel B. Araya
  Senior Professional Staff
  Daniel.Araya@jhuapl.edu
  +1 240-592-2302
- **Co-Investigator:**
  Dr. Dennis C. Berridge
  Senior Professional Staff
  Dennis.Berridge@jhuapl.edu
  +1 240-228-4399
- **Submission Date:**
  10 March 2023
- **Recipient Organization (Name and Address):**
  Johns Hopkins Applied Physics Laboratory
  11100 Johns Hopkins Rd., Laurel, MD 20723
- **Project/Grant Period (Start Date, End Date):**
  11 March 2020 to 10 March 2023
- **Total Funding:**
  $825,000
- **Reporting Period End Date:**
  10 March 2023
- **Report Term or Frequency (annual, semi-annual, quarterly, other)**
  Annual
- **Final Report?**
  Yes

Abstract

This report summarizes the three-year research effort by the Johns Hopkins University Applied Physics Laboratory (APL) under grant number FA9550-20-1-0043 from the Air Force Office of Scientific Research (AFOSR) to conduct postflight analysis of the BOLT flight experiment and to support the development, execution, and analysis of data from BOLT-2: The Holden Mission. Key accomplishments from this research included characterization of supersonic transition flight data received from the BOLT experiment, investigation and identification of the probable cause of unexpected flight behavior that occurred in the BOLT flight, significant independent analysis of the BOLT-2 flight during the pre- and postflight research phases, and new Spatial BiGlobal stability calculations of the BOLT geometry in support of the BOLT-2 flight analysis and a NATO STO-AVT-346 working group activities. The research resulted in seven conference papers with an eighth paper planned. The research led to advances in understanding of supersonic transition, flight dynamics, aeroelastic effects on aerodynamics, thermal analysis methodology for low-cost sounding rocket experiments, and advancements in the use of Spatial BiGlobal stability on the BOLT geometry. APL plans to continue research on many of these topics in a new grant from AFOSR, FA9550-22-1-0357, that will also support a re-flight attempt of the BOLT experiment called BOLT-1B.

Contents

1 Introduction and Research Objectives 5
2 Accomplishments 7
2.1 BOLT Postflight Analysis of Experiment Conditions and Supersonic Transition Data 7
2.2 BOLT Postflight Analysis of Flight Dynamics 8
2.3 BOLT-2 Knowledge Transfer and Advisory Activities 10
2.4 BOLT-2 Independent Analysis 11
2.4.1 Preflight Aerodynamics Analysis 12
2.4.2 Preflight Thermal/Structural Analysis 13
2.4.3 Preflight Trajectory Analysis and Application of BOLT-1 Lessons Learned 15
2.4.4 BOLT-2 Postflight Data Analysis 17
2.5 BiGlobal Stability Analysis of BOLT and BOLT-2 19
2.6 NATO AVT-346 Working Group Support 20
2.7 Conference Papers and Publications 21
3 Impacts 21
4 Changes/Problems 23
A Year 1 Interim Report (Archived Copy) 26
B Year 2 Interim Report (Archived Copy) 137

1. Introduction and Research Objectives

Prediction of hypersonic boundary-layer physics is critical to optimize the design of hypersonic vehicles for maximum range, thermal survivability, and controllability. Physics-based prediction methods are under development that have the potential to improve the ability of hypersonic vehicle designers to estimate transition and turbulent flow effects. These methods require extensive validation with ground and flight test data that is often not available for the geometry of interest. To date, much of the available validation data are on simple conical geometries.

The Johns Hopkins University Applied Physics Laboratory (APL) proposed this Boundary Layer Transition (BOLT) Post-Flight Research and BOLT-2 Flight Test Support to assist the Air Force Office of Scientific Research (AFOSR) and university researchers in obtaining and analyzing critical hypersonic boundary layer physics validation data in the flight environment. The research was conducted within a three-year project period with a total funding of $825K ($275K/year). Previous technical contributions have been summarized in detail in the grant annual performance reports from Years 1 and 2 [1, 2]. Archived copies of the previously-submitted Year 1 and 2 interim reports are included for the record as Appendix A and Appendix B, respectively.

The primary objective of this research was to continue to utilize the BOLT (also called BOLT-1 in this report) boundary-layer transition flight test data that was to be obtained in a previous grant (AFOSR Award Number FA9550-17-2-0001) to discover and document the salient physics of the laminar-to-turbulent transition process observed during the flight experiment, as well as to disseminate the findings and test data at the direction of the AFOSR to other investigators within the AFOSR portfolio. Although the BOLT experiment, which was conducted in 2021, did not achieve its intended hypersonic conditions, the current grant supported a detailed analysis of supersonic transition data achieved during the flight [3, 4]. In addition the grant supported research into the flight dynamics that led to the unexpected behavior of the BOLT experiment [5, 6].

The secondary objective of this project was to strengthen the development of the Texas A&M and CUBRC BOLT-2: The Holden Mission flight test to study turbulent flow phenomena by leveraging the expertise and significant experience of the APL team who led the BOLT flight experiment. APL performed independent aerodynamic and thermal analyses to ensure the BOLT-2 flight experiment would be delivered at the desired experimental conditions and that the experiment hardware would survive through the flight environment. The success of the BOLT-2 flight offered new validation data for APL spatial BiGlobal and planar-marching Parabolized Stability Equations (PSE) calculations at hypersonic flight conditions [7]. APL assisted the BOLT-2 team in post-processing the flight data and co-authored several papers with members of the BOLT-2 team including CUBRC, NASA Langley, and Texas A&M [8–10].

The research objectives and related activities as originally proposed are shown in Figure 1. The final grant spending versus the original (linear) planned spending profile are shown in Figure 2. Specific accomplishments and impacts from these research activities will be described in this report.

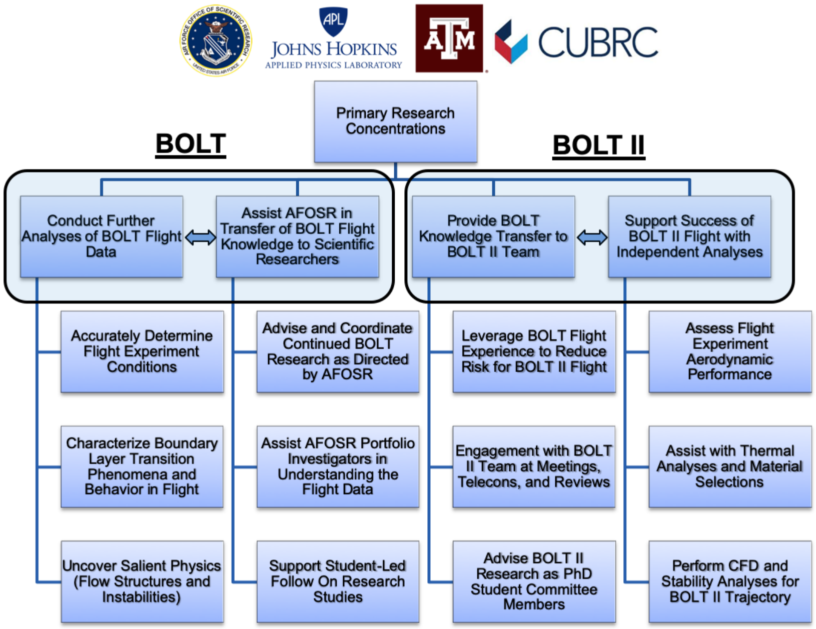

Figure 1. Research objectives and related activities as originally proposed by APL.

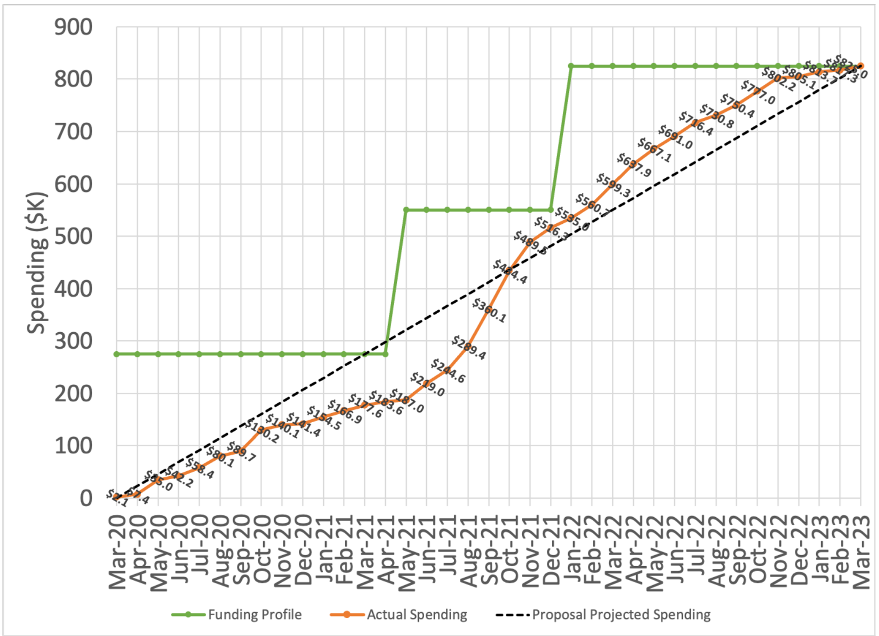

Figure 2. Grant actual spending versus proposed

2. Accomplishments

2.1. BOLT Postflight Analysis of Experiment Conditions and Supersonic Transition Data

Postflight analysis of the BOLT experiment was to be the major focus of the present grant. When this grant was originally awarded in 2020, the BOLT flight had not yet occurred due to delays incurred from the COVID-19 global pandemic. The flight experiment did not occur until Year 2 of this grant in June 2021. Due to unexpected behavior of the flight vehicle carrying the BOLT experiment, the experiment did not reach its intended Mach 5–7 conditions in flight. The vehicle entered a coning motion and achieved large angles of attack during the ascent phase which complicated the analysis of the experimental data that was ultimately obtained at supersonic conditions (Mach ≈ 3) during the descent phase of flight. Unfortunately, reentry to the atmosphere occurred several minutes sooner than anticipated due to the much lower apogee, resulting in only one of the three scientific data telemetry streams being active during the descent phase. Thus, a limited number of instrument data on the order of 90 channels were received during the BOLT descent. APL analyzed the available data to obtain a summary of the boundary-layer transition events which may be inferred at various points during the supersonic descent. This analysis was coupled with a computational investigation performed for the flight conditions, allowing for direct comparisons of surface heat flux. These computations were also leveraged to conduct preliminary stability analyses meant to identify potential transition mechanisms encountered in flight. Initial results from the flight experiment were published in Wheaton et al. [3] while the final analysis of the supersonic data obtained during descent were published in Butler et al. [4]. Full details are described in the Year 2 annual report [2] which is also included in the present document as Appendix B.

The first major task of the BOLT postflight research was to determine the experiment conditions from the flight. APL worked with the Air Force Research Laboratory Aerospace Systems Directorate (AFRL/RQ) as well as the Air Force Weather Agency to obtain a reconstructed estimated atmosphere from the June 2021 flight experiment. The reconstruction of the atmospheric conditions was aided significantly by the AFOSR MURI balloon team that supported the BOLT flight campaign with detailed pressure, temperature, and dew point measurements of the atmosphere. A second major effort included reconstructing the vehicle attitude during the BOLT flight. APL generated a database of inviscid computational fluid dynamics (CFD) solutions that was used along with measured surface pressure sensors on the BOLT forebody to reconstruct an estimated vehicle attitude. The predictions of angle of attack and sideslip angle were then compared against reconstructions of the attitude from the vehicle IMU provided by AFRL/RQ. There were two IMU's on board, however due to the wild trajectory of the vehicle, the DLR DMARS IMU was saturated and not useful during most of the flight. Together, all data sources were compared and used to produce the Best Estimated Trajectory (BET) for the BOLT flight. The BET was version controlled and is stored along with the scientific data for future use by researchers wishing to analyze the BOLT data.

APL developed scripts and processing methods to reduce the measured BOLT surface sensor data to pressure fluctuation magnitude and heat transfer rates for potential identification and characterization of supersonic boundary-layer transition during the flight. It was decided that due to the large angles of attack achieved on the ascent phase, that APL would concentrate analysis of boundary-layer transition to the supersonic descent phase of the experiment. APL also performed new postflight CFD and boundary-layer stability analysis using the NASA LASTRAC code for portions of the descent phase of flight in order to compare against the experimental measurements. Because the BOLT vehicle did not perform a re-pointing maneuver as originally planned, the reentry phase of flight had an erratic attitude. APL worked carefully to compare the vehicle attitude solution to measurements of pressure and transition to make sure that vehicle motion was properly understood. Discrete times were selected for analysis where the vehicle briefly achieved relatively low angle of attack, and these conditions were analyzed with CFD and published in a conference paper [4]. The same paper published the conclusion of transition behavior inferred from the flight measurements during descent. Highlights of the analysis are shown in Figure 3.

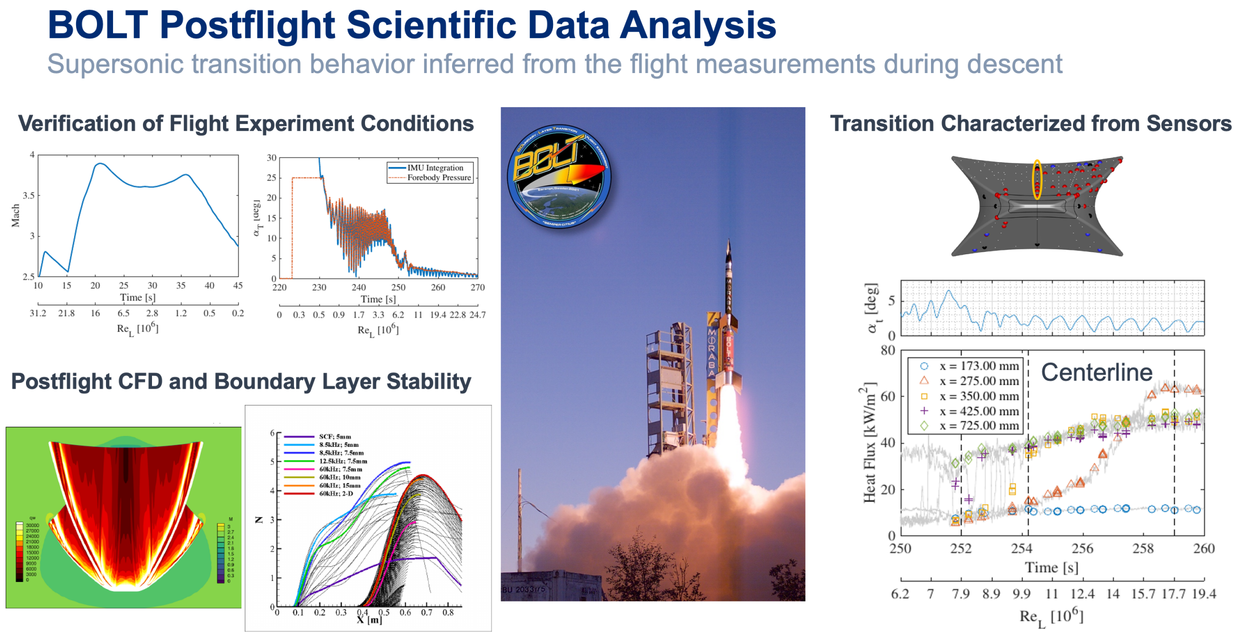

Figure 3. Highlights of postflight supersonic transition analysis of the BOLT flight descent phase.

The postflight scientific data analysis effort was not as extensive as originally proposed, due to the lack of achieving the desired flight experiment conditions and also the limited amount of flight instrument data actually received from the flight (due to a pre-planned telemetry stream shutoff at the actual reentry times). After discussion with the Program Officer, and since both activities were within the scope of the proposed research, it was decided to prioritize assistance in analysis of the BOLT-2 flight data rather than continue further analysis of the BOLT supersonic transition data.

2.2. BOLT Postflight Analysis of Flight Dynamics

Supported by funding from this grant, APL lead a post flight analysis of the BOLT flight unexpected behavior from the June 2021 flight event. The investigation was a collaborative effort with flight partners AFRL/RQ and DLR and was conducted with full participation of the AFOSR Program Officer Dr. Popkin. A small advisory committee was formed to investigate the flight behavior.

The committee consisted of members of the BOLT team from AFRL, DLR, and APL. In addition, a small number of additional staff from APL and Sandia National Laboratory were brought in as Subject Matter Experts to assist with particular aspects of the investigation. The investigation initiated in August 2021, and results were briefed to AFOSR at two reviews: (1) an interim investigation review on 20 September 2021 as well as (2) a final review on 19 November 2021. APL published four AIAA papers documenting the post flight research phase as seen in Wheaton et al. [3] from SciTech 2022, as well as three papers for AVIATION 2022 (Butler et al. [4], Kutty et al. [5], and Melcher et al. [6]). The advisory committee developed a fault tree to guide the investigation efforts.

APL was able to leverage its organizational expertise to simulate flight vehicle trajectories to explore the dynamics of the instability that occurred during the BOLT flight. This included developing a model for the BOLT second stage in the Sandia Trajectory Analysis and Optimization Software (TAOS). Unlike preflight modeling, the new APL model represented the vehicle aerodynamics in an asymmetric manner which was key to uncovering unstable flight behavior. APL led a literature search and found old papers from the 1970's that described the impacts of asymmetric spinning vehicle dynamics on the susceptibility of a vehicle to enter pitch-roll resonance [11, 12]. APL also leveraged subject matter expertise in aeroelastic effects to model the coupled impact of the bending modes of the vehicle with the aerodynamics and flight dynamics. This was the first time at APL that these effects had been combined into a complete vehicle model. Although the aeroelastic effects were simulated for linearized aerodynamic loading valid only at small angles of attack, the aeroelastic model was suitable to recreate the behavior observed in flight. Figure 4 shows the APL postflight 6-DOF modeling (in yellow) against the flight data (in black). The orange and blue lines show the impact of flexible body aerodynamics on the critical pitch and yaw frequencies, which is not typically modeled in standard preflight planning.

It was found that the preliminary cause of the observed flight deviation was a significant reduction in the second stage aerodynamic static stability relative to preflight predictions. As a result of reduced stability, the critical pitch frequency was in close proximity to the roll rate during the initial portion of the coast phase following separation of the first stage ($t > 11$ s) enabling roll resonance "lock-in" (roll rate locks-into the critical pitch frequency). Roll resonance "lock-in" caused exponential growth in the vehicle angle of attack. The primary contributor was aeroelastic flexure of the 2nd stage during the coast phase exacerbated by high dynamic pressure and the significant lift produced by the forebody in the pitch plane. Aeroelastic flexure was also expected to create a large divergence of the pitch plane and yaw plane critical frequencies, caused by the asymmetric shape of the vehicle outer mold line, and exacerbated by a loss of static margin due to significant aeroelastic effects. The divergence of the pitch plane and yaw plane critical frequencies also expanded the region in which the vehicle was susceptible to entering roll-pitch coupling.

The BOLT investigation and resulting lessons learned provided new knowledge and modeling capabilities for determining flight dynamic stability of asymmetric sounding rockets. Full details are described in the Year 2 annual report [2] also included in Appendix B. The APL team remained in communication with the BOLT-2: The Holden Mission team to ensure that the lessons learned from the BOLT flight were applied ahead of the flight experiment of BOLT-2. The new knowledge is currently being applied by APL in the development of the BOLT-1B experiment that will attempt to re-fly the original BOLT-1 experiment on a new rocket.

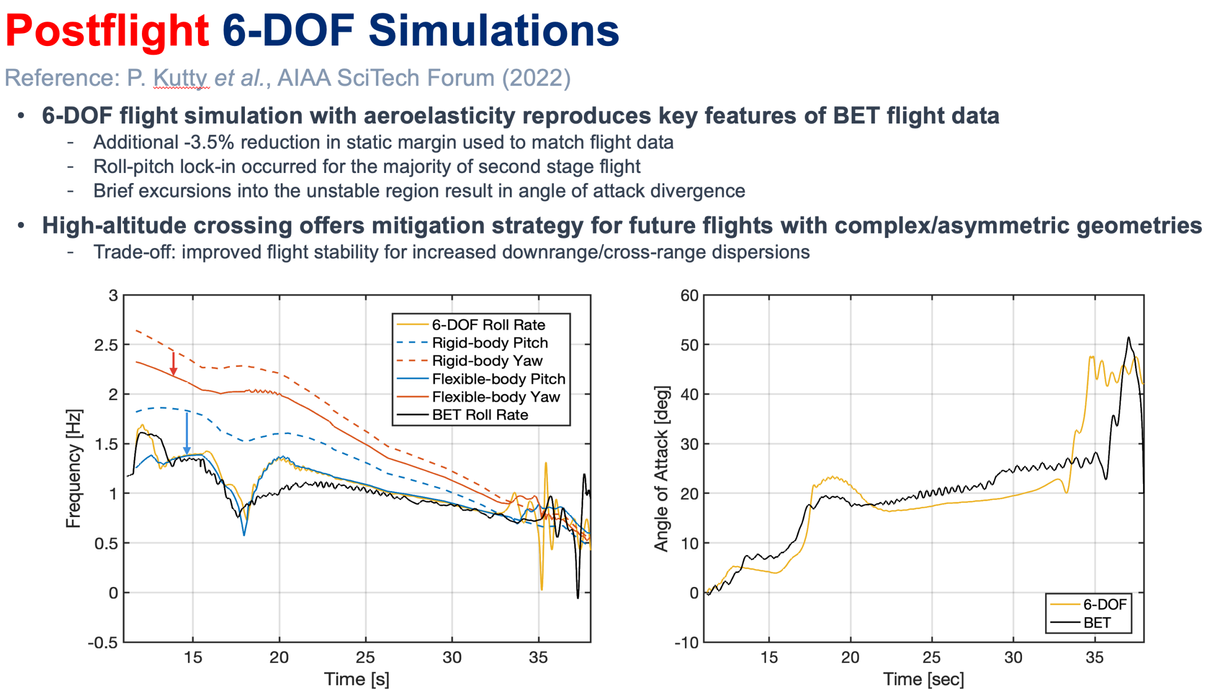

Postflight 6-DOF Simulations

Reference: P. Kutty *et al.*, AIAA SciTech Forum (2022)

- **6-DOF flight simulation with aeroelasticity reproduces key features of BET flight data**
  - Additional -3.5% reduction in static margin used to match flight data
  - Roll-pitch lock-in occurred for the majority of second stage flight
  - Brief excursions into the unstable region result in angle of attack divergence
- **High-altitude crossing offers mitigation strategy for future flights with complex/asymmetric geometries**
  - Trade-off: improved flight stability for increased downrange/cross-range dispersions

Figure 4. APL's final 6-DOF recreation of the BOLT flight behavior (yellow) compared against the flight data (black).

2.3. BOLT-2 Knowledge Transfer and Advisory Activities

A major research focus of this grant, as proposed, was to make available the APL staff members who led the development of the original BOLT flight experiment for transferring experience and knowledge to the follow-on BOLT-2: The Holden Mission team (led by Texas A&M University and CUBRC).

While leading the development of BOLT, APL gained valuable knowledge specific to hypersonic flow over a low-curvature, concave surface with swept leading-edges. Sharing this knowledge and experience helped serve to reduce risk in the design of the BOLT-2 flight experiment. As such, a key component of the activities supported in this grant was for APL to engage in knowledge transfer and advisory activities with the BOLT-2 team. Here "knowledge transfer" is sharing of BOLT design experience and data, while "advisory activities" include all other collaboration with the BOLT-2 team outside of the technical work for independent analysis that will be described later. While this portion of the research did not always produce defined products, the support of the APL BOLT team to engage with the larger BOLT-2 team was integral to developing the follow on flight.

Some of the knowledge transfer and advisory activities to the BOLT-2 team are summarized briefly here. Since March 2020, APL staff supported regular bi-weekly technical discussion phone calls with the BOLT-2 team to observe the current status of experiment design work and related issues.

APL has in most cases conducted follow up communications via e-mail and/or telecons to support the BOLT-2 team researchers and students in various aspects of their research to design their flight experiment. APL provided CAD and other design materials from BOLT-1 directly to the BOLT-2 team and hosted meetings at APL with CUBRC designers and instrumentation specialists to review potential areas for improvement in the design of BOLT-2. Advice and documentation from APL's BOLT experience has been communicated in aspects such as material selection, thermal modeling techniques, detailed mechanical design questions, aerodynamic considerations, experience with designing an aerodynamic fairing, wind-tunnel testing, wind-tunnel results, computational fluid dynamics, instrumentation selection, instrumentation layout considerations, data sampling considerations, version control, flow phenomena, and flight range operations.

APL staff members also supported the BOLT-2 Preliminary Design Review (PDR) and Critical Design Review (CDR) in Year 1 of this research grant, and provided feedback via Requests for Actions (RFA's) in both reviews. APL staff then assisted the BOLT-2 team in responding to the RFA's.

In many instances, APL was encouraged to interact directly with student researchers who were leading aspects of the development of BOLT-2. This allowed the students an outside subject matter expert perspective on their work. Early in the project, APL aerodynamics subject matter experts helped review and assist in the development of the BOLT-2 aerodynamic database that was led by students from Texas A&M. Later in the project, the lessons learned from the design of the BOLT-1 instrumentation layout were communicated to students who were leading the selection of BOLT-2 instrumentation locations. Following the flight experiment, APL staff assisted students analyzing the flight data by suggesting potential analyses and reviewing interim research findings prior to publication.

Throughout the project, APL interacted increasingly with NASA Wallops as details of the BOLT postflight investigation became apparent. APL interacted with NASA Wallops including reviewing latest flight trajectory Monte Carlo studies leading up to the BOLT-2 Mission Readiness Review (MRR) that occurred in the weeks prior to the flight. APL's contributions were highlighted by NASA Wallops / NASA Sounding Rocket Operations Contractor (NSROC) in their official postflight self-assessment from the Technical Mission Closeout Report (TCMR):

> *The NSROC self-assessment of the 46.027 Holden mission performance is "Excellent". NSROC used recently added TAOS to analyze the non-axisymmetric BOLT 2 payload, working with the SRPO Chief Engineer for TAOS questions, TAMU students running CFD, and APL for an independent review. In addition, NSROC worked with the Exp team to reconfigure an unstable payload to allow the mission to proceed, designed through the pandemic shutdown, and maintained consistency in the team through work being stopped because funding. The results were the first successful sounding rocket flight of a payload with a non-axisymmetric front end.*

2.4. BOLT-2 Independent Analysis

A major set of research activities conducted under this grant included a variety of independent analyses conducted by APL to support the preflight planning and postflight data analysis of BOLT-

2: The Holden Mission. As a University Affiliated Research Center (UARC), APL brings expertise and analysis capabilities not typically found in academia in areas critical to the planning and execution of flight experiments. For the BOLT-2 flight, APL employed these capabilities to assess the vehicle aerodynamics, thermal environment, and structural response of the experiment to the planned flight environment. The analysis was in many cases a “second set of eyes” to check results generated by other members of the BOLT-2 team including students. Contributions of independent analysis to the preflight planning and postflight data analysis will be summarized here. Highlights of some of the APL contributions are shown in Figure 5.

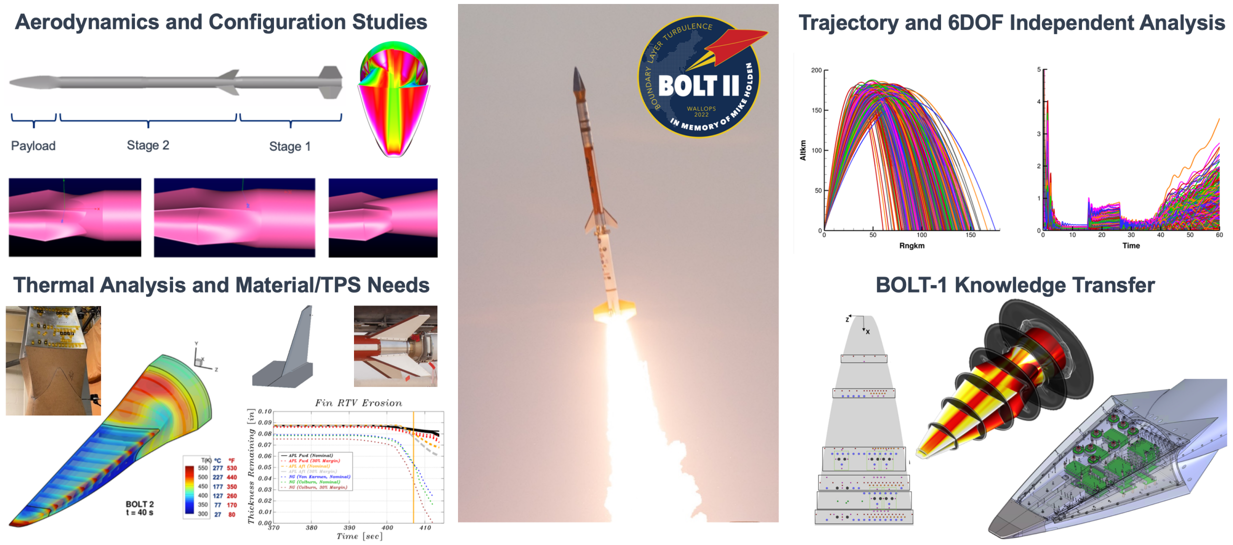

Figure 5. Highlights of APL contributions to BOLT-2: The Holden Mission enabled by this research grant.

2.4.1. Preflight Aerodynamics Analysis

Most of the early independent analysis by APL in this grant was to perform an assessment of the aerodynamic force and moment databases being generated by Texas A&M. APL has significant subject matter expertise in this area and typically supports major hypersonics programs in the generation and validation of aerodynamic databases. As BOLT-2 was the first flight at NASA Wallops of a vehicle with a nonaxisymmetric forebody, NASA required the BOLT-2 team to provide the aerodynamic database as they did not have their own Computational Fluid Dynamics (CFD) capabilities. The primary lead for generation of the BOLT-2 area database was Texas A&M University, and the main data was being generated by graduate students. Because aerodynamic data generated by students would be used directly in preflight predictions by NASA Wallops including vehicle dynamics and range safety, APL’s role under this grant was to support the students and perform verification of the aerodynamic data being generated.

In preparation for the BOLT-2 PDR (held on June 19, 2020), APL conducted a limited set of inviscid and viscous CFD simulations of the BOLT-2 second stage configuration (Payload + Stage 2 rocket motor). This was done to assess the accuracy of the aerodynamic database utilized in the trajectory analysis and to provide feedback for potential improvements to the aerodynamics modeling for future design iterations. Predictions of center of pressure location, X_{cp}, as well as inviscid drag and total drag for total angle of attack = 0° ($CA_{inviscid}$ and CA_0, respectively) were the focus of the assessment. Full details are described in the Year 1 annual report [1] (also included in its entirety in Appendix A). Generally, good agreement was found between the new APL results and the Texas A&M aerodynamic database for the vehicle center of pressure, a key term in the calculation of static margin to meet the flight requirements. Some small discrepancies in drag terms were noted that prompted further discussions with NASA Wallops about the buildup of drag for their flight modeling.

Following PDR, APL conducted a trade study to examine the stability impacts of three different fairing concepts under consideration by the BOLT-2 team leading up to CDR (held on October 28, 2020). The major conclusions from this analysis were to show that the "short" fairing increased stability and drag, while the "long" fairing decreased both stability and drag relative to the "PDR" fairing design. However, the short fairing was found to have higher local heating. Thus the analysis drove the BOLT-2 team to maintain the fairing outer mold line from PDR for the final flight.

2.4.2. Preflight Thermal/Structural Analysis

Another major accomplishment in this grant was the work by APL to perform preflight thermal analysis that directly supported key design decisions for materials by the BOLT-2 team. The majority of this research was performed in a short time period ahead of the BOLT-2 PDR in 2020. The rapid turnaround of a complete preflight transient thermal analysis to support the PDR was enabled by previous BOLT-1 models and experience developed by APL. Many of the grids, tools, and thermal models were developed under the original BOLT-1 project and available for immediate application to support BOLT-2, with limited modifications//updates to the models required.

The initial support by APL to the BOLT-2 team in the area of thermal modeling utilized correlation-based heating predictions and an existing BOLT-1 model developed previously in the MSLRAD–ATLAS (Missile Radiance/Aerothermal Loads And Stresses) thermal solver developed by APL. MSLRAD–ATLAS is an in-house suite of aerothermal prediction tools developed over many years by APL. It has the powerful capability of rapidly generating correlation-based heating inputs on complex geometries for a given trajectory. APL was provided with a preflight design trajectory generated by NASA Wallops and asked by CUBRC to begin running trade studies of potential materials that were under consideration for the BOLT-2 forebody design. The new BOLT-2 trajectory was less thermally stressing that the original BOLT-1 design trajectory due to an expected lower flight Mach number. APL generated correlation-based heating predictions as well as temperature predictions for the BOLT-2 trajectory using the original material set from BOLT-1 as well as additional materials for BOLT-2. In this early phase of design, the APL results along with close collaboration with CUBRC were critical to identifying and selecting the Nickel 201 nosetip for BOLT-2 along with the 410 stainless steel frustum.

Once the candidate materials had been identified, APL conducted a higher fidelity transient thermal analysis using heating derived from viscous CFD solutions, rather than from empirical correlations. Full details of this analysis are summarized in an AIAA paper that was presented after the flight [8]. Once again, this effort was conducted prior to PDR on a tight schedule and heavily leveraged CFD grids and methods developed under BOLT-1. Because of the longer length of the BOLT-2 forebody, the CFD grids were modified to include the additional length of the BOLT-2 forebody as well as the geometry of the transition module section of the payload. The fluid grid utilized a quarter geometry as the assumption of zero angle of attack was made, and the grid was comprised of 28.5M hexagonal cells (fully structured). Three variations of the grid utilizing the same topology and cell count were generated for different portions of the trajectory. A standard grid was utilized for most of the ascent and descent experiment portions as the outer boundaries were sufficient to capture the outer shock, and the wall spacing remained favorable for the desired $y^+ < 0.5$ condition sought for accurate heat flux. A grid with expanded outer boundaries was utilized early during the supersonic portions of the ascent phase in order to capture the outer shock. Late in the descent phase, a third grid was utilized with a smaller wall spacing to maintain the $y^+ < 0.5$ at higher Reynolds numbers. The transient thermal analysis was completed with a finite volume formulation of the transient heat equation developed within the CFD++ "solids only mode" analysis feature developed by Metacomp. This section describes the use of this capability in CFD++ such that the CFD solutions and resulting thermal response for a simple, short-duration ballistic trajectory such as BOLT-2 can be computed within the same solver. All preflight thermal modeling was completed using the assumption of fully turbulent heating throughout the entire trajectory. In addition, a $C = 1.2$ safety factory was applied to the thermal boundary condition profiles on top of the turbulent heating.

Temperature statistics from each material component were calculated from the transient thermal simulation including the maximum and volume-averaged (bulk) temperatures of each simulated component (nose, frustum, internal bulkhead at the base of the BOLT-2 forebody, the transition section, and the cylindrical booster section). With conservative assumptions, the preflight analysis predicted that the Nickel 201 nose maximum temperature was near 850 K (1070 °F) during ascent and reached a peak value of 980 K (1300 °F) at end of flight. These temperatures were provided to CUBRC for a detailed structural analysis, allowing the final design of the BOLT-2 forebody and transition section to be completed. One other impact of the APL analysis is that relatively high temperatures in the aluminum transition section were noted when a cork thermal protection layer was not modeled. Ultimately, cork was applied on the payload in this region as a result of the APL thermal modeling.

Following PDR, APL also supported several other thermal modeling studies again with the APL MSLRAD–ATLAS code. The MSLRAD–ATLAS code includes the ability to model gas/surface interaction problems such as ablation. APL was asked to perform a trade study to select the thermal protection methods on the BOLT-2 transition section and performed analysis of RTV and cork at various thicknesses in this region. The analysis identified the final thickness of cork that was applied to the TSM. In addition, APL was asked to perform an independent analysis of the RTV thermal protection layer on the second stage Improved Malemute fins. There was concern that the RTV would ablate and expose the fins to high temperatures during the end of flight descent leg, which could have led to fin failure before the end of the BOLT-2 descent phase science experiment window. A primary analysis was being performed by Northrop Grumman in support of NASA Wallops, but APL also performed a MSLRAD/ATLAS analysis showing that the recession of RTV was likely sufficient until the end of flight. APL also performed viscous CFD of the fin geometry at various flight conditions to ensure that the correlation-based heating predictions being used to analyze the fin RTV recession were within expected ranges.

APL supported CUBRC in understanding previously completed structural analysis of the BOLT flight experiment, such that a similar analysis could be completed by CUBRC for the BOLT-2 design. Although BOLT-2 featured different materials than BOLT, the overall design of the interface joints remains common between the two missions. BOLT-2 featured a single joint at the location of the BOLT "downstream isolator/frustum" joint. A potential issue was raised regarding how to model the interaction between differential thermal expansion, pre-flight bolt torque values, and related uncertainties in the initial/pre-flight torque of bolts connecting the parts. APL revisited the BOLT structural analysis with a new ABAQUS structural model that included new details of the bolts within the joints. The new analysis determined that the bolt loads are unlikely to cause failure in flight for the BOLT mission, and remained within acceptable limit loads. The results were shared with the BOLT-2 team and in particular to support the CUBRC structural analysis. It was determined that due to the materials used in BOLT-2, the load environment on the bolts was not of concern and a similar analysis did not need to be completed for BOLT-2. The new analysis helped to verify acceptable levels of risk for the BOLT flight and also allowed both the BOLT and BOLT-2 teams to gain new understanding of the behavior of the joint bolt structural loads through the stressing hypersonic flight environment.

2.4.3. Preflight Trajectory Analysis and Application of BOLT-1 Lessons Learned

APL conducted several preflight reviews of modeling the BOLT-2 trajectory utilizing the Trajectory Analysis and Optimization Software (TAOS) trajectory code and inputs provided by the NASA Wallops team. The first initial review came before the BOLT-2 PDR, very early in the NASA Wallops trajectory modeling process. NASA shared early TAOS modeling directly with APL for an independent review. Along with a general examination of the TAOS input files, four separate cases were considered for analysis: (1) a single nominal trajectory, (2) a single trajectory with reduced stage 2 total drag, (3) a set of 50 Monte Carlo simulations with given dispersions, and (4) a set of 50 Monte Carlo simulations with modified dispersions. The first goal of the trajectory studies was to quantify the potential impact on a reduction in second stage drag, as the initial APL aerodynamic database review noted a potential overprediction of drag by the BOLT-2 team for the second stage. The second goal of the trajectory studies was to explore the flight dynamics associated with NASA's initial scheme for fin cants of the first and second stage, and their corresponding roll rates.

Both the nominal trajectory simulation and simulation with reduced stage 2 total drag remained statically stable (static margin $>$ 2 calibers) for the majority of the flight; only a slight decrease below 2 calibers was noted in the first 30 seconds of flight. It was noted in APL's Year 1 report [1] that the main impact of reduced stage 2 total drag would be a $\sim 10\%$ increase in Mach number on reentry, which could slightly increase heating. It should be noted that in the actual flight the Mach number was higher than anticipated, although it is unclear whether this increase can be attributed entirely to a potential error in calculating the preflight expected drag. Preliminary conversations between APL and NASA Wallops have indicated that there might be other factors associated with the increased Mach number in the actual flight.

The initial APL trajectory modeling highlighted the potential for pitch-roll coupling in the BOLT-2 flight due to the roll rate early in the Stage 2 burn aligning with the expected natural pitch frequency. Without corrections, the first set of Monte Carlo simulations showed a potential for dynamic instability during coast after Stage 1 separation (1 in 50 simulations failed). APL then performed additional Monte Carlo sets with a proposed correction to the fin cant of the second stage that demonstrated improved performance (0 of 50 simulations failed). These results were shared with NASA Wallops. Ultimately, NASA Wallops would go on to devise an even better fin cant and roll rate scheme for BOLT-2 that targeted a CONOPS for extremely low (near zero) roll rate of the second stage to remain below the critical pitch and yaw frequencies.

In retrospect, the susceptibility of the BOLT-2 vehicle to enter pitch-roll coupling for certain roll rate schemes should have highlighted the need to revisit the BOLT-1 mission CONOPS. For BOLT-1, detailed six degree of freedom (6-DOF) Monte Carlo modeling such as employed by APL in this grant and also by NASA Wallops had not been performed before the flight. Instead, other tools had been employed for BOLT-1 that assumed rotationally-symmetric aerodynamics (later found to be insufficient to model the pitch-roll coupling susceptibility of asymmetric spinning vehicles [5, 6]). A detailed 6-DOF Monte Carlo analysis of BOLT-1, which was a completely different vehicle configuration from BOLT-2, was not considered before the flight. The BOLT-1 flight, as mentioned previously, would go on to experience pitch-roll coupling. A major lesson learned from the current grant (from both the BOLT-2 preflight modeling and BOLT-1 postflight investigation modeling) was that a nonaxisymmetric spinning vehicle is inherently susceptible to pitch-roll coupling and must be analyzed with 6-DOF Monte Carlo modeling that considers the asymmetry of the aerodynamics as well as terms that are important to contributing to nonzero trim angle of attack. While this lesson was learned too late to impact the BOLT-1 flight in June 2021, APL was able to complete the BOLT-1 investigation in time to assess the risk of the same issue occurring in the BOLT-2 flight in March 2022.

In the several months before the BOLT-2 flight, APL completed additional trajectory modeling with 6-DOF Monte Carlo methods of the final BOLT-2 flight configuration to determine the risk of pitch-roll coupling occurring in the BOLT-2 flight. The BOLT investigation concluded in November 2021, leaving only four months between the conclusion of the investigation and the expected launch of the BOLT-2 experiment. Following the BOLT investigation, APL worked with NASA Wallops to evaluate the Wallops TAOS trajectory modeling for BOLT-2 and provide an independent analysis of the 6DOF modeling to ensure that terms found to be important to the BOLT pitch roll coupling behavior were incorporated adequately into the BOLT-2 modeling.

APL obtained the BOLT-2 TAOS model from NASA Wallops in late January 2022 as well as a description of the modeled Monte Carlo parameters in the simulation. Due to the unknown sensitivity of the models, results are not plotted here but were provided separately to NASA and AFOSR. On initial receipt of the TAOS model, APL noted that the Wallops modeling did not include a blanket uncertainty on center of pressure. APL typically recommends a 5% body length uncertainty on center of pressure. APL performed independent simulations of the BOLT-2 trajectory with Monte Carlo parameters that included a 5% and 10% (unrealistic but stressing) body length center of pressure uncertainty. In addition, knowing from the BOLT investigation that the moment bias terms provide the initial seeding for angle of attack amplification, APL performed additional simulations with a 3X multiplier on the Wallops tailcan misalignment term (the term responsible for providing these moment biases).

The results showed that the BOLT-2 vehicle was much more robust to these terms due to the selection of a low roll rate that avoided pitch-roll crossings at high dynamic pressures. APL presented the results to Wallops in January 2022. The analysis was deemed a complete check of the phenomena from the BOLT investigation and satisfied the Wallops team that the preflight analysis did not miss any unexpected behavior. BOLT-2 had a successful launch in late March 2022.

2.4.4. BOLT-2 Postflight Data Analysis

Under support from this grant, APL assisted the BOLT-2 team in receiving, post-processing, and understanding portions of the flight data received from the successful experiment. Primary postflight analysis of the BOLT-2 data was led by Texas A&M and CUBRC, but APL contributed to an analysis of a subset of the flight data (from the functioning Medtherm coaxial thermocouples) and also provided a complete set of laminar and turbulent Reynolds Averaged Navier Stokes (RANS) CFD data computed from the as-flown BOLT-2 trajectory. APL coordinated directly with Texas A&M regarding the postflight analysis and also worked directly with one of the Texas A&M students who was leading the postflight analysis. APL discovered that the simple Cook-Felderman [13] analytical solution was likely sufficient to convert the Medtherm temperature data to estimated heat flux in most regions of the BOLT-2 forebody where spanwise conduction effects were low. APL also contributed an initial BiGlobal stability analysis at BOLT-2 flight conditions, described further in the next section. Figure 6 summarizes research highlights from this project that contributed to initial understanding of the BOLT-2 postflight data.

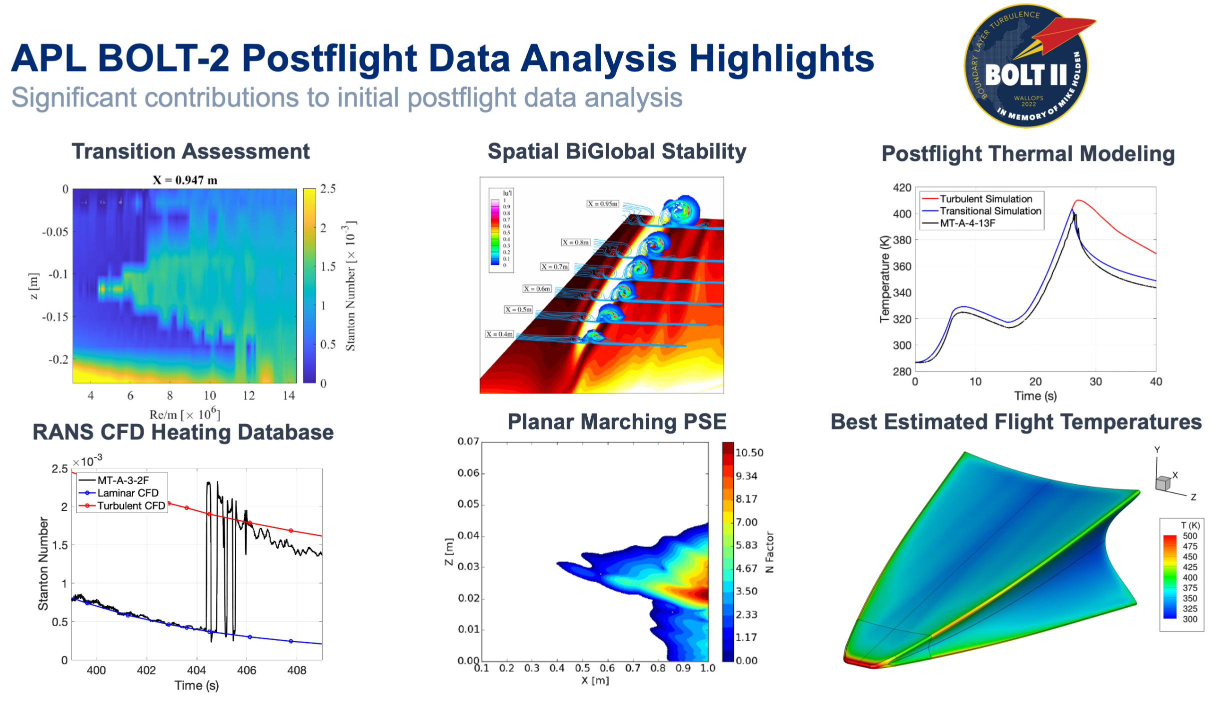
APL BOLT-2 Postflight Data Analysis Highlights

Significant contributions to initial postflight data analysis

Transition Assessment

Spatial BiGlobal Stability

Postflight Thermal Modeling

RANS CFD Heating Database

Planar Marching PSE

Best Estimated Flight Temperatures

Figure 6. Highlights from APL's contributions to the initial BOLT-2 postflight data analysis.

As mentioned, APL focused BOLT-2 experimental data analysis efforts under this grant on analysis of the Medtherm coaxial thermocouples from the flight. The purpose of the APL analysis was to identify suitable transition onset conditions from the BOLT-2 flight for planned postflight

CFD and BiGlobal/Planar Marching PSE stability analysis. In addition, the temperature data from the surface Medtherms represented the final validation of all the APL BOLT-1 and BOLT-2 preflight thermal modeling, and the temperatures were used to compare against a new postflight thermal analysis of the BOLT-2 experiment performed by APL and presented at AIAA SciTech 2023 (Wheaton and Dufrene [8]).

First, a new database of RANS CFD was generated with both laminar and turbulent heating using the same CFD grids and methods from the APL preflight analysis. CFD predictions of laminar and turbulent heat flux, as well as shear stress, were extracted at the BOLT-2 flight sensor coordinates and provided as a database to Texas A&M for further comparison against their postprocessed experimental data. These comparisons will be shown in an upcoming joint AIAA paper at AVIATION 2023 written by Texas A&M and APL [10]. Data were also provided to NASA Langley for the purpose of understanding the Side B experiment of the BOLT-2 flight and resulted in a joint paper led by NASA and contributed to by APL [9]. The APL heating inputs generated by the postflight RANS CFD were critical to understanding the initial boundary layer transition and turbulent flow data on the BOLT-2 flight.

The RANS CFD inputs were then used by APL for a complete postflight thermal analysis using the same methods described earlier for the preflight analysis. The thermal modeling methodology was validated against the flight-measured surface temperatures. The flight data provided the opportunity to assess conservatism in the preflight analysis and to determine best practices for future transient thermal analyses. The temperatures realized in the actual flight were lower than in the preflight analysis, due to conservative assumptions used in the preflight modeling (fully turbulent heating plus a 1.2 safety factor on heat transfer coefficient). It was found that modeling of transitional heating during ascent was crucial to matching the measured ascent surface temperatures. The CFD heating was compared to estimated heat transfer rates from the flight and showed good agreement.

A set of estimated three-dimensional surface temperature distributions were also a product of the postflight thermal modeling, and were found to be a good match to the available flight data. These surface temperature distributions were anchored using measured frustum surface temperatures. APL has made these estimated surface temperature distributions from the BOLT-2 flight available to other researchers who wish to use them as boundary conditions in new simulations, as they offer more accurate temperatures than the assumed constant-temperature isothermal wall condition typically used in CFD analysis.

The postflight best estimated temperature distributions within the nosetip were given to CUBRC and used to estimate the differential thermal expansion at the nosetip/frustum joint interface at the end of flight. Due to the conservatism in the preflight analysis, the differential thermal expansion at the nosetip joint is expected to be smaller than indicated in the preflight analysis.

Overall, the postflight APL thermal analysis and associated CFD database was incredibly impactful to early scientific analysis of the BOLT-2 flight data. Data were generated and shared with relevant BOLT-2 team partners for assistance in understanding the flight data. The postflight thermal modeling will also have a direct impact on the future APL-led BOLT-1B flight experiment as the same methods (now flight validated) can be applied to this future experiment.

2.5. BiGlobal Stability Analysis of BOLT and BOLT-2

The recent success of the BOLT-2 flight experiment has yielded a wealth of hypersonic flight data to compare against computational tools. After discussions with the BOLT-2 team and the AFOSR Program Officer Dr. Sarah Popkin, it was decided that APL should focus some of the final portions of the present grant on detailed boundary-layer stability studies of the BOLT-2 flight conditions using BiGlobal stability analysis. The studies included a computational assessment of boundary-layer instabilities at a single condition in the as-flown trajectory, including comparisons to the flight data. The chosen condition occurs at a Mach number of 6.2 and freestream Reynolds number of $8 \times 10^6/m$, at which point boundary-layer transition is observed in both the near-centerline and outboard regions of the vehicle acreage. The heat flux data collected in flight reveals a transition pattern dominated by two independent fronts in the near-centerline and midspan of the vehicle acreage. The stability analyses conducted for this study focused separately on these two regions.

A limited effort was made to ascertain the degree of grid dependence displayed by the flow topology and resulting stability analysis, though grid convergence is likely not attained in this study. The laminar heating predicted by both grids demonstrated satisfactory agreement with the flight measurements. It also appears that the near-centerline thermocouples capture the motion of heating streaks caused by small variations in vehicle attitude. For both grids employed, the near-centerline region is dominated by the roll-up of two large vortex structures, with increased grid resolution enhancing the degree of roll-up displayed by the outer vortex. Greater grid dependence of the flow resolution was observed in the outboard region where vortex structures are seen developing within the higher-resolution baseflow. It is believed that further increasing the spanwise grid resolution in this region would yield more mature vortex structures.

BiGlobal stability analysis showed the near-centerline region to be dominated by shear instabilities housed within the two vortex structures. Planar-PSE computations show the most-amplified vortex instabilities to initiate within the inner vortex and reach N factors of approximately 16 by the end of the vehicle, regardless of which grid resolution is considered. Although this instability remains confined to the inner vortex with the coarse baseflow, it was shown to spread substantially to the outer vortex for the more highly-resolved baseflow. This instability is believed to precipitate the near-centerline transition observed in flight. Furthermore, it was shown that the enhanced vortex roll-up which accompanies greater resolution of the laminar mean flow produces a new, strongly-amplified instability family within the stem of the outer vortex. This instability was shown to reach N factors in excess of 15, nearly as high as the dominant inner-vortex instability. Significant spatial overlap of the various vortex instabilities is noted as it demonstrates the potential for nonlinear modal interactions, which are outside the scope of this study.

The stability analysis within the outboard region was found to be more susceptible to issues with resolution of the laminar baseflow. Upstream of any significant roll-up, BiGlobal analysis predicts this region to house various families of second-mode instabilities. Planar-PSE marches show these second-mode disturbances amplify substantially downstream as they are modulated by the roll-up predicted by the laminar computations and disturbance energy enters the vortex shear layer. However, the greatest N factors predicted by the Planar-PSE analysis with the highest-resolution grid are approximately 11.5, likely insufficient to cause the transition observed in flight, and occur inboard of the observed transition front.

It is noted that the N factor predictions within this study are meant merely as lower bounds to the actual disturbance amplification, as only a limited number of initial marching locations were surveyed and the neutral points of the various instabilities have yet to be established. Future work in an upcoming grant from AFOSR will seek to remedy this shortcoming in order to yield true maximum N factors. Furthermore, additional effort will be put in to attaining satisfactory grid-convergence of the laminar basic state.

That said, this work provided some quantitative measure of the sensitivity of the BiGlobal/Planar Parabolzed Stability Equations (PPSE) analysis methodology to the resolution of the laminar basic state. Conclusions regarding transition of the near-centerline vortex structure would be largely unimpacted by the choice of grid in this study, and these conclusions are apparently corroborated by the flight data. The same cannot be said for the outboard region, where the in-flight transition behavior was not predicted on either grid, but increased grid resolution produces a significant increase in disturbance amplification. All together, this highlights the need for development of best-practices in grid design and BiGlobal/PPSE stability analysis to avoid incorrect conclusions in studies where experimental data is not available. This work is meant to be a step towards defining these best-practices for the study of complex hypersonic configurations. The results as of the end of this grant were summarized in Butler et al. [7].

2.6. NATO AVT-346 Working Group Support

This grant supported Dr. Bradley Wheaton and Dr. Cameron Butler as members of the North Atlantic Treaty Organization (NATO) Science and Technology Organization (STO) Air Vehicles Technology (AVT-346) working group “Predicting Hypersonic Boundary-Layer Transition on Complex Geometries.” The AVT-346 working group consists of boundary-layer transition subject matter exports from across NATO ally nations to“facilitate an international collaboration of leading experimentalists and numerical simulation experts towards improved hypersonic prediction capabilities.” The simulation approaches will be mechanism-based and the team will use new opportunities for validation in ground facilities.

APL’s involvement in the AVT-346 working group was brought on by the selection of BOLT as a focus geometry for the working group subtask “transition due to the interaction of multiple instability modes.” The BOLT geometry was identified as producing concurrent instability modes (second mode and crossflow) within the same regions of the geometry. APL’s leadership of BOLT and knowledge of available ground test validation data as well as the state of CFD and boundary layer stability surrounding the geometry are extremely beneficial to the working group. Under the working group, new wind tunnel testing of the BOLT geometry are being conducted by the German Aerospace Center (DLR) and the French Aerospace Lab (ONERA) in their wind tunnels. APL is contributing new CFD and BiGlobal analysis of the wind-tunnel cases to the working group. APL, NASA, DLR, and ONERA are working on a chapter together for the AVT-346 final report expected in 2024. The APL support of the AVT-346 working group will continue under a new grant from AFOSR following the conclusion of the present research grant.

2.7. Conference Papers and Publications

This grant supported APL contributions to many AIAA conference papers, reporting research findings from the BOLT-1 postflight analysis as well as describing pre- and postflight analysis of BOLT-2: The Holden Mission. The papers are summarized below:

- [3] Wheaton, B. M., Butler, C. S., McKiernan, G. R., & Berridge, D. C. (2022). Initial Results from the BOLT Flight Experiment. AIAA Paper 2022-0345. `https://doi.org/10.2514/6.2022-0345`
- [4] Butler, C. S., Araya, D. B., McKiernan, G. R., & Wheaton, B. M. (2022). Supersonic Transition Measurements During the BOLT Flight Experiment Descent Phase. AIAA Paper 2022-4099. `https://doi.org/10.2514/6.2022-4099`
- [5] Kutty, P. M., Butler, C. S., Wheaton, B. M., & Fortier, J. B. (2022). 6DOF Simulation Analysis for the Post-Flight Investigation of the Boundary Layer Transition (BOLT) Experiment. AIAA Paper 2022-3884. `https://doi.org/10.2514/6.2022-3884`
- [6] Melcher, J. T., Radcliffe, E. J., Butler, C. S., & Wheaton, B. M. (2022). Effects of Aeroelasticity on Flight Stability of the Boundary Layer Transition (BOLT) Experiment. AIAA Paper 2022-3748. `https://doi.org/10.2514/6.2022-3748`
- [7] Butler, C. S., McKiernan, G. R., & Wheaton, B. M. (2023). Initial BiGlobal Stability Analysis of the BOLT II Flight Experiment. AIAA Paper 2023-0291. `https://doi.org/10.2514/6.2023-0291`
- [8] Wheaton, B. M., & Dufrene, A. T. (2023). Thermal and Structural Analysis of BOLT-2: The Holden Mission. AIAA Paper 2023-0685. `https://doi.org/10.2514/6.2023-0685`
- [9] Berry, S. A., & Wheaton, B. M. (2023). BOLT II Roughness-Side Flight Results. AIAA Paper 2023-0684. `https://doi.org/10.2514/6.2023-0684`
- [10] Wirth, J., Morreale, B., Bowersox, R. D., & Wheaton, B. M. (2023). Boundary Layer Turbulence Flight Experiment in Memory of Mike Holden: Side A Flight Data 2. Abstract Submitted to AIAA AVIATION 2023.

3. Impacts

This section documents the distinctive contributions, major accomplishments, innovations, successes, or any change in practice or behavior that has come about as a result of this project:

- Although the BOLT flight did not reach its intended hypersonic experiment conditions, the postflight scientific analysis of the supersonic descent phase of the flight supported by this grant resulted in a new flight validation dataset for supersonic transition that complements previous datasets (such as HIFiRE-5A [14]);
- This project supported APL and its partners to identify the cause of the BOLT unexpected flight behavior, and to reconstruct the flight behavior in a postflight simulation;

- The BOLT postflight investigation efforts resulted in new knowledge of sounding rocket flight dynamics that will influence the practices of planning for new low-cost flight experiments with complex asymmetric forebodies;
- This research project supported the first ever implementation of aeroelastic effects into 6-DOF modeling at APL, whereby the aerodynamic force and moment coefficients were a function of dynamic pressure in addition to typical parameters (Mach number and angle of attack). This implementation of aeroelastic effects not typically modeled in sounding rocket flight planning was documented and available for future flight experiment plans;
- The lessons learned from the BOLT flight investigation were directly applied by APL in assessing the risk of similar flight behavior in the successful BOLT-2 flight that would follow;
- This project supported the original BOLT-1 team as team members of BOLT-2: The Holden Mission to assist with knowledge transfer and advisory activities. The involvement of APL in this manner significantly reduced the development cost, timeline, and risks for the BOLT-2 flight;
- APL subject matter experts in aerodynamics, flight dynamics, thermal analysis, and structural analysis were able to mentor the BOLT-2 team including graduate students in their own analysis for planning the BOLT-2 experiment. This mentorship helped improve the resulting BOLT-2 planning and also helped foster improved workforce development for the students;
- APL's independent aerodynamic analysis for the BOLT-2 flight provided a much needed independent check on the results being generated by graduate students for the flight. The independent analysis by APL was cited by NASA Wallops as critical to reducing risk of the first flight at Wallops with user-supplied aerodynamic databases;
- APL performed independent trajectory modeling that influenced the roll-rate scheme employed for the BOLT-2 flight to mitigate unwanted pitch/roll resonance instabilities;
- Trade studies performed by APL with transient thermal modeling and correlation-based heating were instrumental in helping the BOLT-2 team select suitable materials for the design of the flight experiment;
- APL conducted the primary thermal analysis from a database of viscous CFD simulations for the BOLT-2 flight ahead of the program PDR;
- APL assisted in independent thermal analysis of the BOLT-2 transition module and second stage fin thermal protection systems ahead of the program CDR;
- APL assisted the BOLT-2 team in receiving, post-processing, and understanding portions of the flight data;
- APL conducted an independent post-processing analysis of the BOLT-2 Medtherm coaxial thermocouples and identified a reduced-form of reduction of the measured temperatures to heat flux via the Cook-Felderman analytical solution. This method only requires a surface measurement rather than a surface and inner measurement;

- A complete postflight RANS database of laminar and turbulent CFD solutions of the BOLT-2 as-flown flight trajectory were generated by APL, providing computational heat transfer rates and shear stress predictions that assisted the BOLT-2 team in understanding the experimentally-measured flight data;
- A postflight thermal analysis performed by APL of the BOLT-2 flight provided best estimated temperature distributions suitable for use as boundary conditions to future computations performed by others seeking to understand the impacts of temperature distribution on transition and turbulence;
- The postflight BOLT-2 thermal analysis provided validation of the preflight process used to predict temperatures for the flight, and documented the conservatism inherent to preflight assumptions of turbulent heating throughout the flight;
- The postflight thermal analysis of BOLT-2 allowed CUBRC to estimate the expected differential thermal expansion at the nosetip joint in the actual flight;
- This grant supported new CFD and Spatial BiGlobal stability analysis of the BOLT-2 flight experiment at the flown conditions;
- This grant supported APL to participate in the NATO AVT-346 working group, which seeks to understand the behavior of transition in the presence of multiple mechanisms using the BOLT geometry. APL provided new analysis of wind tunnel data on the BOLT geometry gathered by NATO partners.
- APL subject matter experts were able to directly mentor graduate students working on the BOLT-2 flight, providing unique perspective and workforce development.

4. Changes/Problems

In coordination with the AFOSR PO, Dr. Sarah Popkin, the APL team successfully navigated several challenges encountered during this research project:

- The availability of the BOLT flight data was critical to many of the planned research efforts related to postflight analysis of this data in the present project. Due to the COVID-19 global pandemic, the BOLT flight experiment was delayed from May 2020 to June 2021. This meant that the BOLT flight did not occur until approximately mid-way through the 3-year research effort, rather than at the beginning of the project as planned originally. The APL team was able to redirect early project effort to support of the BOLT-2 preflight planning instead. To mitigate the delay in obtaining the BOLT flight data, the spending on the grant in Year 1 was lower than planned and was followed by higher than planned spending in Years 2 and 3 of the grant when the BOLT data was available (see Figure 2).
- The project objectives were to analyze hypersonic flight experiment data from the BOLT flight, however the flight did not achieve this conditions. Instead, a smaller research effort centered on analyzing that data that was received from the flight at supersonic conditions, which still provides value to the field;

- Following the BOLT flight unexpected behavior, research effort was re-prioritized within the scope of the grant to support a postflight investigation of the flight dynamics. This investigation meant a greater emphasis on aerodynamics and flight dynamics research compared to the proportion originally planned in the proposal;
- Since the original proposal, APL developed new capabilities to perform higher-fidelity BiGlobal stability analysis along with planar marching PSE by using the Sandia LSTPACK code. These new capabilities required additional computing resources that were not anticipated in the original project proposal, and were not generally available within APL's existing internal computational resources. APL was able to apply for and be granted a supplemental allocation of computing hours from the Department of Defense (DoD) High Performance Computing Modernization Program (subproject AFOSR49332933). This allocation of resources greatly enhanced the ability of the APL team to meet the research objectives of this project.

Acknowledgments

This work was supported by the Air Force Office of Scientific Research under award number FA9550-20-1-0043 (PO: Dr. Sarah Popkin). Any opinions, finding, and conclusions or recommendations expressed in this material are those of the author(s) and do not necessarily reflect the views of the United States Air Force. This work was supported in part by high-performance computer time and resources from the Department of Defense (DoD) High Performance Computing Modernization Program.

References

[1] Wheaton, B. M., "FA9550-20-1-0043 Year 1 Annual Report," *Grant deliverable to the Air Force Office of Scientific Research*, 2021.

[2] Wheaton, B. M., "FA9550-20-1-0043 Year 2 Annual Report," *Grant deliverable to the Air Force Office of Scientific Research*, 2022.

[3] Wheaton, B. M., Butler, C. S., McKiernan, G. R., and Berridge, D. C., "Initial Results from the BOLT Flight Experiment," *AIAA Paper 2022-0345*, 2022. doi:10.2514/6.2022-0345, URL `https://arc.aiaa.org/doi/10.2514/6.2022-0345`.

[4] Butler, C. S., Araya, D. B., McKiernan, G. R., and Wheaton, B. M., "Supersonic Transition Measurements During the BOLT Flight Experiment Descent Phase," *AIAA Paper 2022-4099*, 2022. doi:10.2514/6.2022-4099, URL `https://arc.aiaa.org/doi/10.2514/6.2022-4099`.

[5] Kutty, P. M., Butler, C. S., Wheaton, B. M., and Fortier, J. B., "6DOF Simulation Analysis for the Post-Flight Investigation of the Boundary Layer Transition (BOLT) Experiment," *AIAA Paper 2022-3884*, 2022. doi:10.2514/6.2022-3884, URL `https://arc.aiaa.org/doi/abs/10.2514/6.2022-3884`.

[6] Melcher, J. T., Radcliffe, E. J., Butler, C. S., and Wheaton, B. M., "Effects of Aeroelasticity on Flight Stability of the Boundary Layer Transition (BOLT) Experiment," *AIAA*

Paper 2022-3748, 2022. doi:10.2514/6.2022-3748, URL `https://arc.aiaa.org/doi/10.2514/6.2022-3748`.

[7] Butler, C. S., McKiernan, G. R., and Wheaton, B. M., "Initial BiGlobal Stability Analysis of the BOLT II Flight Experiment," *AIAA Paper 2023-0291*, 2023. doi:10.2514/6.2023-0291, URL `https://arc.aiaa.org/doi/10.2514/6.2023-0291`.

[8] Wheaton, B. M., and Dufrene, A. T., "Thermal and Structural Analysis of BOLT-2: The Holden Mission," *AIAA Paper 2023-0685*, 2023. doi:10.2514/6.2023-0685, URL `https://arc.aiaa.org/doi/10.2514/6.2023-0685`.

[9] Berry, S. A., and Wheaton, B. M., "BOLT II Roughness-Side Flight Results," *AIAA Paper 2023-0684*, 2023. doi:10.2514/6.2023-0684, URL `https://arc.aiaa.org/doi/10.2514/6.2023-0684`.

[10] Wirth, J., Morreale, B., Bowersox, R. D., and Wheaton, B. M., "Boundary Layer Turbulence Flight Experiment in Memory of Mike Holden: Side A Flight Data 2," *Abstract submitted to AIAA AVIATION 2023*, 2023.

[11] Hodapp, A. E., "Effects of Unsymmetrical Stability Derivative Characteristics on Re-Entry Vehicle Trim Angle Behavior," *Journal of Spacecraft and Rockets*, Vol. 11, No. 5, 1974, pp. 300–307. doi:10.2514/3.62067, URL `https://arc.aiaa.org/doi/10.2514/3.62067`.

[12] Hodapp, A. E., "Effects of unsymmetrical stability derivative characteristics on re-entry vehicle transient angular motion," *Journal of Spacecraft and Rockets*, Vol. 13, No. 2, 1976, pp. 82–90. doi:10.2514/3.27887, URL `https://arc.aiaa.org/doi/10.2514/3.27887`.

[13] Cook, W. J., and Felderman, E. J., "Reduction of Data from Thin-Film Heat-Transfer Gages: A Concise Numerical Technique," *AIAA Journal*, Vol. 4, No. 3, 1966, pp. 561–562. doi:10.2514/3.3486.

[14] Kimmel, R. L., Adamczak, D. W., Borg, M. P., Jewell, J. S., Juliano, T. J., Stanfield, S. A., and Berger, K. T., "First and fifth hypersonic international flight research experimentation's flight and ground tests," *Journal of Spacecraft and Rockets*, Vol. 56, No. 2, 2019, pp. 421–431. doi:10.2514/1.A34287.

A. Year 1 Interim Report (Archived Copy)

The following pages of this appendix section contain an archived copy of the previously-submitted interim/annual report for the first year of this grant. Inclusion of this report supplements the final performance report with a copy of any previously-referenced analysis.

JOHNS HOPKINS
APPLIED PHYSICS LABORATORY

FA9550-20-1-0043 Year 1 Annual Report
10 March 2021
JHU/APL Project Number FGX75

To: Dr. Sarah Popkin
Program Officer - High Speed Aerodynamics
AFOSR/RTA
875 N. Randolph St., Suite 325, Room 3112
Arlington, VA 22203-1768

From: Dr. Bradley M. Wheaton (Principal Investigator)
Dr. Daniel B. Araya (Co-Investigator)
Dr. Dennis C. Berridge (Co-Investigator)
Dr. Kerri B. Phillips (Program Manager)

Subject: Boundary Layer Transition (BOLT) Post-Flight Research and BOLT II Flight Test Support (Grant FA9550-20-1-0043 Year 1 Annual Report, period 11 March 2020 through 10 March 2021)

This report summarizes the first year of research efforts by the Johns Hopkins University Applied Physics Laboratory (JHU/APL) under grant number FA9550-20-1-004 from the Air Force Office of Scientific Research (AFOSR), consisting of research to analyze the flight data from the Boundary Layer Transition (BOLT) flight experiment as well as to support the execution of BOLT II: The Holden Mission.

Contents

1 Introduction **3**
1.1 Description of Research . . . 3
1.2 Year 1 Major Activities . . . 4
1.3 COVID-19 Impacts . . . 4
1.4 Financial Status . . . 4

2 BOLT II Support **5**
2.1 Overview of Year 1 Activities . . . 5
2.2 Independent Analysis . . . 5
2.2.1 Aerodynamics Analysis . . . 5
2.2.2 Trajectory Analysis . . . 7
2.2.3 Thermal Analysis . . . 12
2.2.4 Structural Analysis of Fasteners . . . 17
2.3 Knowledge Transfer and Advisory . . . 18

3 Anticipated Year 2 Activities **19**

4 BOLT Post-Flight Research **20**
4.1 Post Flight Analysis Scripts . . . 21
4.2 CART3D Database for Attitude Determination . . . 23
4.3 Instrumentation Coordinates . . . 23
4.4 Inverse Heat Transfer Analysis . . . 23
4.5 Anticipated Year 2 Activities . . . 26

A Appendices **29**
A.1 BOLT II PDR Aerodynamics and Trajectory Analysis . . . 30
A.2 BOLT II PDR Thermal Analysis . . . 62
A.3 BOLT II Independent Fin Heating CFD Analysis . . . 105

1. Introduction

1.1. Description of Research

Prediction of hypersonic boundary-layer physics is critical to optimize the design of hypersonic vehicles for maximum range, thermal survivability, and controllability. Physics-based prediction methods are under development that have the potential to improve the ability of hypersonic vehicle designers to estimate transition and turbulent flow effects. These methods require extensive validation with ground and flight test data that is often not available for the geometry of interest. To date, much of the available validation data are on simple conical geometries. The Johns Hopkins University Applied Physics Laboratory (JHU/APL) proposes this Boundary Layer Transition (BOLT) Post-Flight Research and BOLT II Flight Test Support to assist the Air Force Office of Scientific Research (AFOSR) and university researchers in obtaining and analyzing critical hypersonic boundary layer physics validation data in the flight environment. The proposed research will be conducted within a three-year project period with a requested total funding of $825K ($275K/year).

The primary objective of this research is to continue to utilize the BOLT boundary-layer transition flight test data to be obtained in a previous grant (AFOSR Award Number FA9550-17-2-0001) to discover and document the salient physics of the laminar-to-turbulent transition process observed during the flight test, as well as to disseminate the findings and test data at the direction of the AFOSR to other investigators within the AFOSR portfolio. JHU/APL will complete a thorough core analysis of the BOLT flight experiment data that will result in a final postprocessed dataset along with characterization of the observed transition front behavior and physics from the flight data. JHU/APL will then transition into a role supporting long-term data analysis of the BOLT flight data at the behest of AFOSR, whereby JHU/APL will assist AFOSR in the dissemination of the flight data to the larger portfolio of researchers and will assist AFOSR in coordinating and supporting those analyses by other researchers.

The secondary objective of this proposal is to strengthen the development of the planned Texas A&M and CUBRC BOLT II: The Holden Mission flight test to study turbulent flow phenomena by leveraging the expertise and significant experience of the JHU/APL team who led the BOLT flight experiment. JHU/APL will perform independent aerodynamic and thermal analyses to ensure the BOLT II flight experiment will be delivered at the desired experimental conditions and that the experiment hardware will survive through the flight environment. JHU/APL will also assist the BOLT II team in post-processing the flight data.

The availability of the BOLT and BOLT II data will permit designers to compare these results to their respective program-specific test data and improve their modeling tools, ultimately resulting in a higher-performing weapon system platform for the DoD. Better understanding of boundary-layer transition and turbulent flow effects is of critical importance to achieving the ambitious performance goals for production hypersonic weapons, while concurrently minimizing the complexity and risk of the design, thereby reducing system costs.

1.2. Year 1 Major Activities

The majority of the Year 1 activities on this grant were focused on support of the BOLT II flight experiment via independent analysis in the aerodynamics and thermal analysis areas. Additional support has been given in the knowledge transfer and advisory of BOLT information to the BOLT II team. The BOLT II activities in Year 1 are summarized in Section 2. While the BOLT flight data is not yet available to commence the initially planned post-flight research activities, initial effort in Year 1 of the grant was spent to develop some post-flight tools as well as to complete some preliminary analysis needed for the post-flight data research. The BOLT research conducted in Year 1 is summarized in Section 4.

1.3. COVID-19 Impacts

This grant began in March 2020 during the initial phases of the COVID-19 global pandemic, and has experienced some impacts on the proposed work due to the pandemic.

Some activities related to planned travel in support of the BOLT II research have been postponed indefinitely until travel restrictions and social distancing measures can be relaxed. Approximately $7K in travel costs had been anticipated in Year 1 of this project to support meetings at Texas A&M and CUBRC. These trips have not happened, and most of these interactions have occurred virtually (via ZoomGov or Microsoft Teams). Additional labor hours had been planned to host the BOLT II team at JHU/APL for several in-person meetings. The associated labor costs for these trips have also been reduced, resulting in a general underspending in the BOLT II support activities for Year 1 in the “Knowledge Transfer and Advisory” category.

In addition, the BOLT flight campaign was postponed from its originally planned May 2020 date and is now anticipated to occur in June 2021. Some initial post-flight data analysis activities had been planned for Year 1 of the grant. However, with the flight delay these activities are postponed into the second year of this grant.

1.4. Financial Status

As a result of underspending in the BOLT II knowledge transfer and advisory activities due to travel restrictions, the grant balance at the end of Year 1 is higher than anticipated. It is anticipated that JHU/APL will carry over approximately $100K of Year 1 funds into Year 2 of the grant. These funds will be used to conduct the previously planned meetings in support of BOLT II once the COVID-19 pandemic has ended, or they can be used for additional BOLT post-flight research work. JHU/APL has communicated to the AFOSR PO the anticipated underspending in Year 1 and will work with Dr. Popkin to agree upon a new spending plan for the carryover funds.

2. BOLT II Support

2.1. Overview of Year 1 Activities

In support of both the Preliminary Design Review (PDR) and Critical Design Review (CDR) for the BOLT II Holden Mission, APL performed independent assessments of aerodynamics, trajectory, and thermal response to compliment work by the Texas A&M University, NASA Wallops, and CUBRC teams. The scope of the APL work was intentionally limited to minimize duplicating efforts while providing sufficient crosschecks for building confidence in both the PDR and CDR designs. A summary of the work completed by APL and major takeaways from the independent analyses are included in this section. The source material can be found in APL presentation slides delivered to the BOLT II team and included in their entirety in the Appendix.

2.2. Independent Analysis

The following subsections detail various independent analyses conducted by JHU/APL in support of designing the BOLT II flight experiment. These analyses were conducted for assessing aerodynamics, trajectory performance, stability, and experimental conditions, as well as thermal and structural analysis. This section will provide a high level summary of the analyses and additional details are presented in the appendices.

2.2.1. Aerodynamics Analysis

In preparation for the BOLT II PDR (held on June 19, 2020), APL conducted a limited set of inviscid and viscous CFD simulations of the BOLT II Stage 2 configuration (Payload + Stage 2 rocket motor). This was done to assess the accuracy of the aerodynamic database utilized in the trajectory analysis and to provide feedback for potential improvements to the aerodynamics modeling for future design iterations. Predictions of center of pressure location, X_{cp}, as well as inviscid drag and total drag for total angle of attack = 0° ($CA_{inviscid}$ and CA_0, respectively) were the focus of the assessment. Full details are shown in Appendix A.1. Major takeaways from the pre-PDR analysis were the following:

(1) Good agreement found between APL and TAMU predictions of X_{cp}, as shown in Figure 1. APL results predicted slightly increased stability (larger X_{cp}) but all values are within approximately 0.3 calibers across the Mach regime.

(2) APL results showed reasonable agreement with TAMU predictions of $CA_{inviscid}$, with APL predicting slightly decreased drag in the low to mid-supersonic regime (Mach < 4), as shown in Figure 2. Note that this figure is a corrected version of what was originally presented to the BOLT II team before PDR and included in the appendix. The difference is accounted by the reference area, S_{ref}, that was used. Originally the plot of $CA_{inviscid}$ vs. Mach used $S_{ref} = 201 in^2$ for the TAMU data (same as the APL data). The corrected figure (c.f. Figure 2) uses $S_{ref} = 234 in^2$ for the TAMU data and was presented to the BOLT II team after PDR.

(3) APL total drag predictions at sea-level show significantly lower values ($\sim 40\%$ less) across

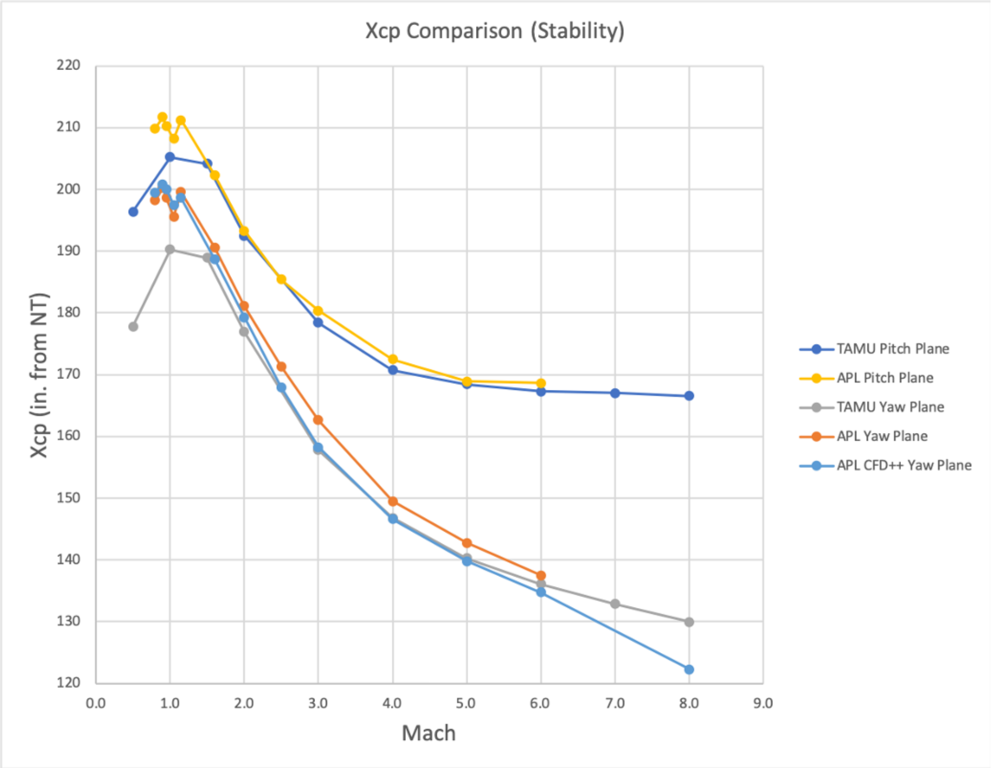

Figure 1. BOLT II Stage 2 X_{cp} comparison

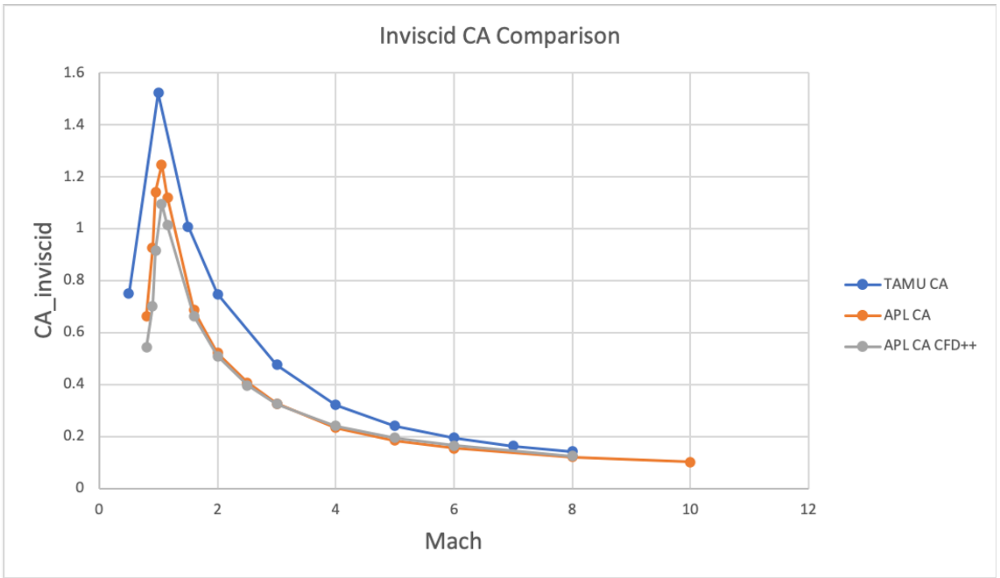

Figure 2. BOLT II Stage 2 $CA_{inviscid}$ comparison

the Mach regime when compared to the trajectory inputs for Stage 2 coast drag. This total drag comparison is shown in Figure 3. Understanding this discrepancy prompted further inquiry into how base/viscous drag contributions are implemented into the trajectory code used by the NASA Wallops team.

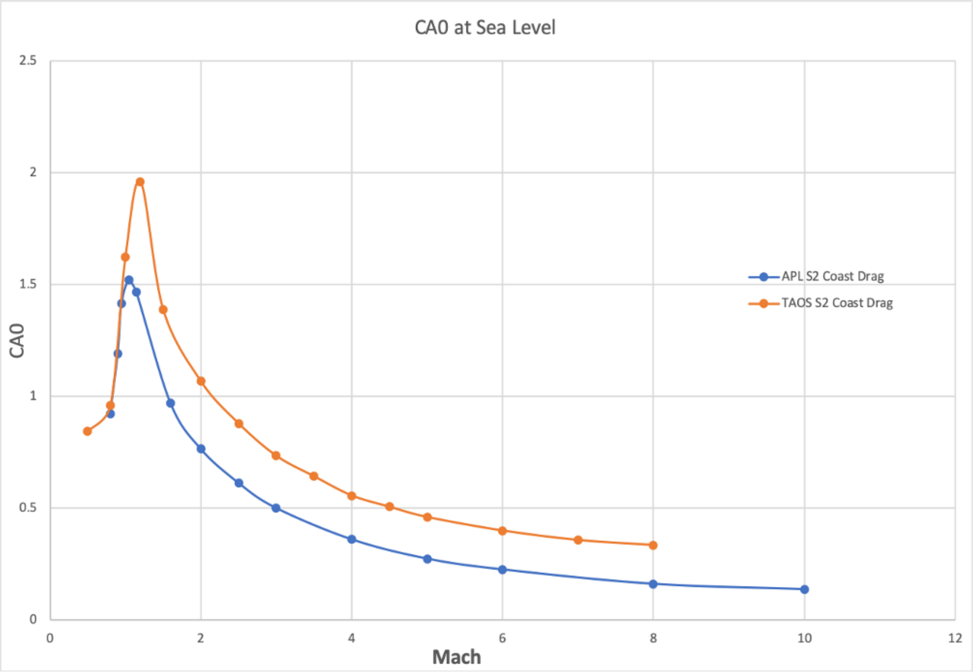

Figure 3. BOLT II Stage 2 $CA_{inviscid}$ comparison

Following PDR, APL conducted a limited trade study to examine the stability impacts of three different fairing concepts under consideration by the BOLT II team leading up to CDR (held on October 28, 2020). These three fairing concepts are shown in Figure 4. RANS CFD simulations were conducted with Metacomp CFD++ software using the SA turbulence model and assuming sea level conditions. Reference values for the drag calculation included a reference length of L_{ref}=16in (1 caliber = 16in) and an a reference area of $S_{ref} = 201.05$in^2. The major conclusions from this analysis were to show that the "short" fairing increased stability and drag, while the "long" fairing decreased both stability and drag relative to the "PDR" fairing design. The stability comparison among the three fairing concepts is shown in Figure 5 and the inviscid drag comparison is shown in Figure 6.

2.2.2. Trajectory Analysis

APL conducted a review of modeling the BOLT II trajectory utilizing the Trajectory Analysis and Optimization Software (TAOS) trajectory code and inputs provided by the NASA Wallops team. Along with a general examination of the TAOS input files, four separate cases were considered for analysis: (1) a single nominal trajectory, (2) a single trajectory with reduced stage 2 total

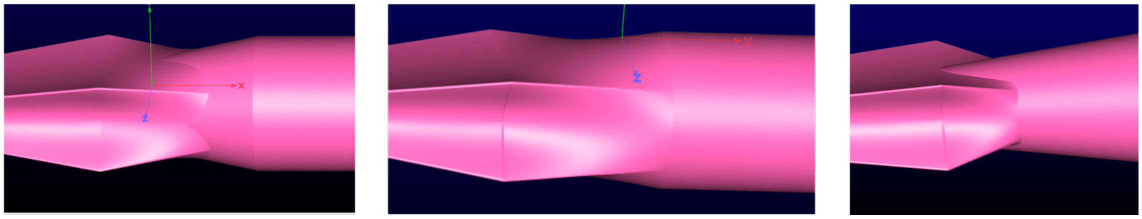

(a) "PDR" Fairing Design. (b) "Long" Fairing Design. (c) "Short" Fairing Design.

Figure 4. BOLT II Pre-CDR Fairing Design concepts.

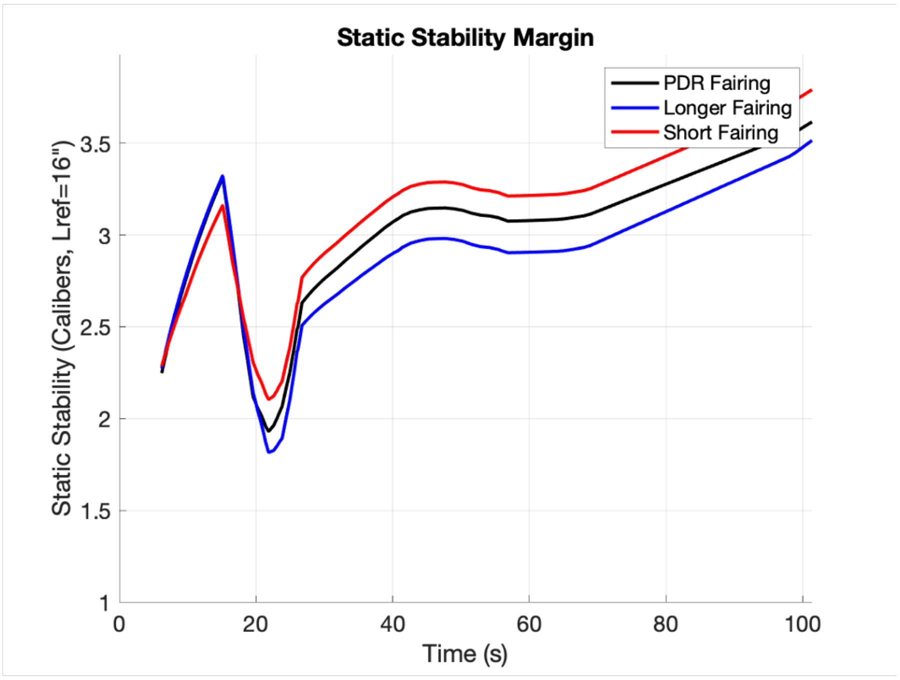

Figure 5. BOLT II fairing design aerodynamic stability comparison

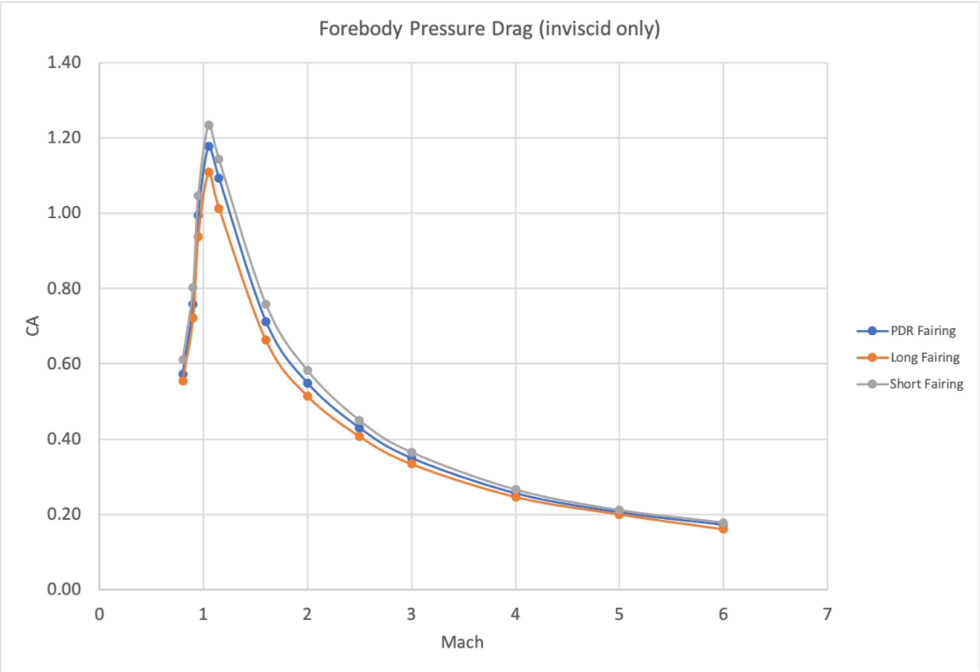

Figure 6. BOLT II fairing design inviscid drag comparison. Drag comparison does not include viscous effects, base drag, or protuberance increments.

drag, (3) a set of 50 Monte Carlo simulations with given dispersions, and (4) a set of 50 Monte Carlo simulations with modified dispersions. Full details are shown in Appendix A.1. The major takeaways from this analysis were the following:

(1) Both the nominal trajectory simulation and simulation with reduced stage 2 total drag remained statically stable (static margin $>$ 2 calibers) for the majority of the flight; only a slight decrease below 2 calibers was noted in the first 30 seconds of flight. This is shown in Figure 7.

(2) The main impact of reduced stage 2 total drag is $\sim$ 10% increase in Mach number on reentry, shown in Figure 8, which could slightly increase heating.

(3) Without corrections, the first set of Monte Carlo simulations showed a potential for dynamic instability during coast after stage1 separation; 1 in 50 simulations failed shown in Figure 9.

(4) With adjustments to the stage 1 fin cant angle and expanded aerodynamics uncertainty bounds, a second set of Monte Carlo simulations showed the feasibility of mitigating the dynamic instability; 0 of 50 simulations failed shown in Figure 10.

(5) APL recommended to the BOLT II team to include aerodynamic uncertainties in future Monte Carlo simulations, particularly to drag, rolling moment and roll damping coefficients.

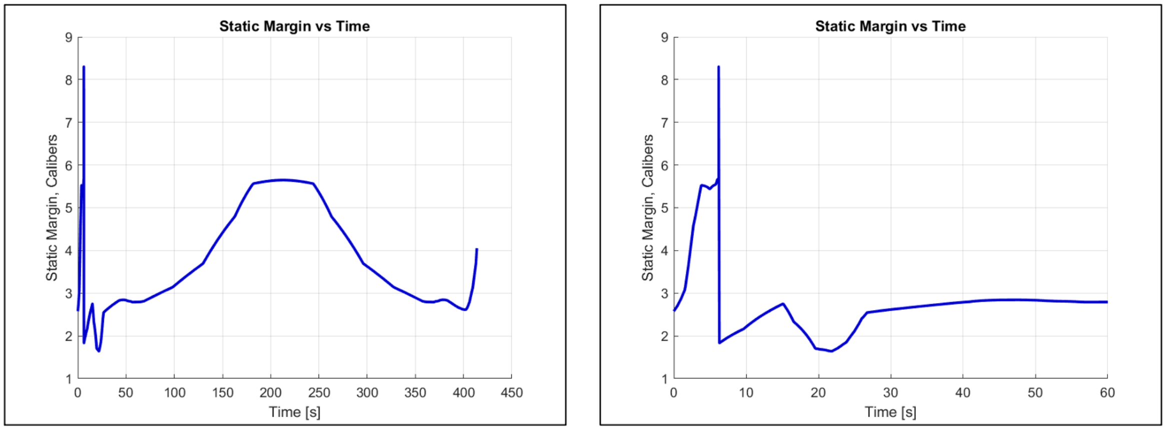

(a) (b)

Figure 7. BOLT II TAOS prediction of static margin for nominal simulation (a) of entire trajectory (b) of first 60 seconds during trajectory.

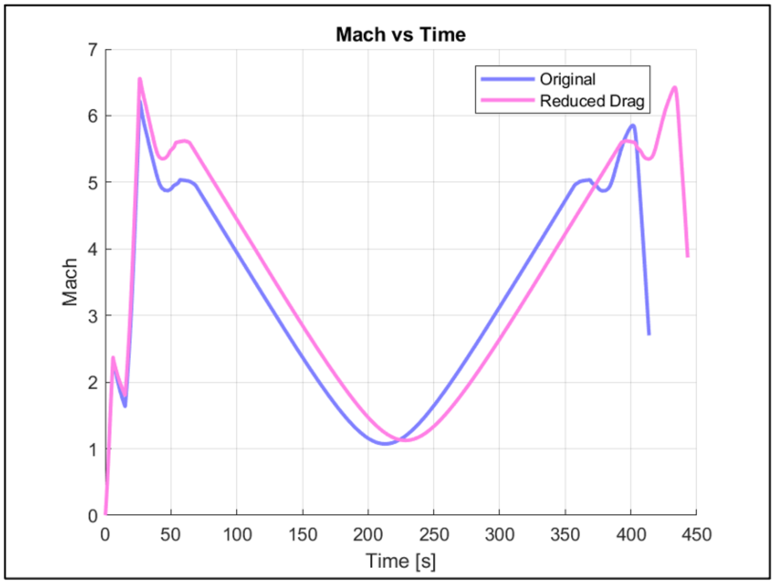

Figure 8. BOLT II TAOS prediction of Mach number for nominal trajectory and reduced stage 2 drag simulations.

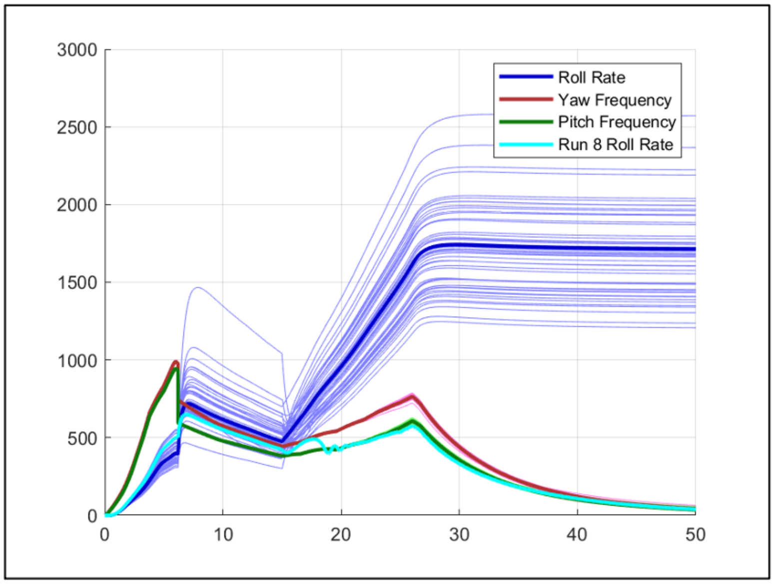

Figure 9. BOLT II TAOS Monte Carlo demonstrating Roll-Pitch coupling resulting in failure of 1 (Run 8) out of 50 trajectory simulations. Horizontal axis is trajectory time (s) and vertical axis is rate (rad/s).

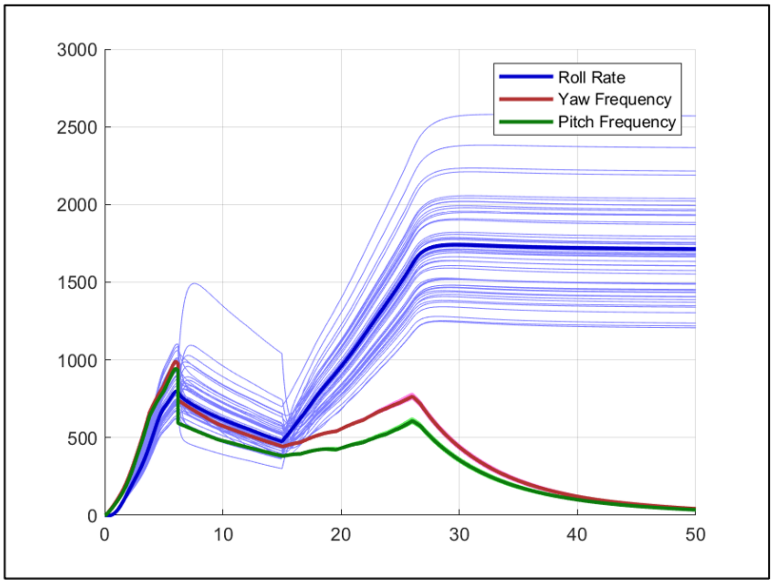

Figure 10. BOLT II TAOS Monte Carlo with no failures in 50 trajectory simulations after adjustments made to stage 1 fin cant angle. Horizontal axis is trajectory time (s) and vertical axis is rate (rad/s).

2.2.3. Thermal Analysis

One of the primary areas of research that JHU/APL has conducted within the first year of this grant has been to support the BOLT II team with independent thermal analysis. JHU/APL was approached by Texas A&M and CUBRC in April 2020 regarding an urgent need for analysis to assist in the selection of materials of the BOLT II flight vehicle. Utilizing existing BOLT thermal analysis models, in-house modeling and simulation techniques, and subject matter expertise, JHU/APL was able to provide analysis at various levels of fidelity. The analysis first consisted of lower-fidelity correlation-based heating analysis to examine a variety of candidate materials. Once the materials of interest were selected, a higher-fidelity CFD-based thermal analysis was conducted ahead of the BOLT II program PDR in June 2020. The PDR thermal analysis was subsequently used for a variety of purposes by JHU/APL and the BOLT II team, including structural analysis at CUBRC as well as instrumentation suite design and assessment of measurement uncertainties in the flight experiment by Texas A&M.

Initial correlation-based heating thermal analysis resulted were generated with JHU/APL's in-house MSLRAD/ATLAS thermal solver. This code was used previously by JHU/APL to predict temperatures for the BOLT flight [1]. Due to similarities in the geometry and design between BOLT and BOLT II, the previously existing model from MSLRAD/ATLAS could be leveraged to quickly run new trajectories and generate results. Texas A&M and CUBRC provided JHU/APL with the desired materials properties and trajectory to analyze, and initial temperature results were generated by JHU/APL within two weeks using correlation-based fully turbulent heating. Some of these initial results are shown in Figure 11 for the BOLT II ascent and descent phases of flights. The figure shows mean (volume-averaged) as well as maximum (surface) temperatures during flight for two candidate frustum materials: aluminum 6061 and 410 stainless steel. The end of the flight experiment is denoted as a vertical yellow line. The results showed that for BOLT II's comparatively less thermally stressing trajectory (compared to BOLT), a steel material did not produce concerning temperatures. The use of steel would also add weight into the BOLT II payload itself via the high density of the material, which would alleviate the need for extra ballast to maintain aerodynamic stability. In addition to plots, JHU/APL also generated full data files of payload temperatures for all components for CUBRC to use to assess the materials selection decision.

After it became apparent that a stainless steel frustum (specifically, 410 stainless) was feasible, JHU/APL supported the BOLT II team with additional trade studies of candidate materials for the nosetip. With a less thermally stressing trajectory than BOLT, it was thus possible to avoid the application of expensive Iridium coating on the nosetip, provided that a suitable oxidation-resistant material could be found. In addition, high conductivity is desired in the nosetip to avoid issues due to thermal shock during flight. CUBRC suggested interest in a Nickel alloy nosetip and asked if JHU/APL could perform some trade studies to assess the likely temperatures that would be experienced with that material. A follow-on round of correlation-based heating analysis was conducted on a Nickel alloy nosetip with a 410 stainless frustum, and results were generated and compared to temperatures on the original BOLT analysis (Figure 12). The results showed that a Nickel alloy nosetip resulted in comparable temperatures near the stagnation point to those expected in the BOLT flight (with its TZM nosetip). The analysis provided preliminary data showing that Nickel 201 appeared feasible for use in the nosetip of BOLT II. The use of Nickel 201 for this flight avoided the need for an oxidation-resistant coating of a material such as Iridium, saving

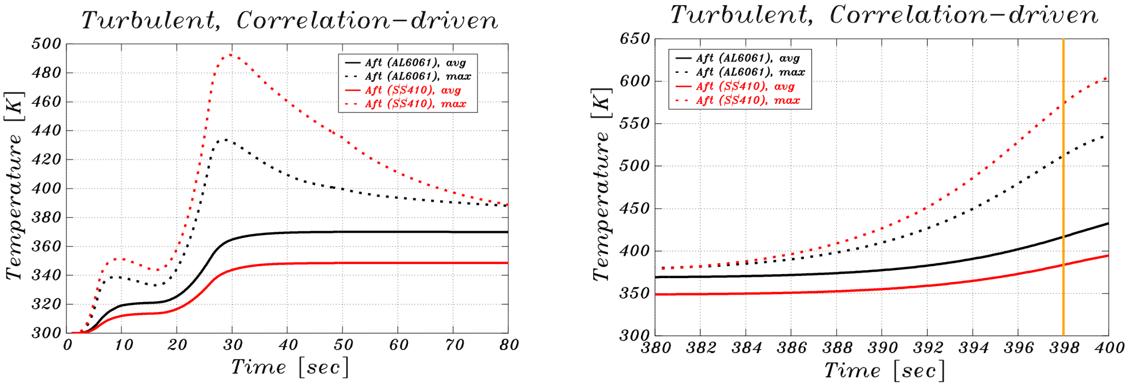

(a) Ascent

(b) Descent

Figure 11. Correlation-based heating analysis showing the effect of material (Aluminum 6061 vs. 410 Stainless Steel) on predicted BOLT II temperatures.

significant expense (the BOLT Iridium coating cost approximately $60K). Nickel 201 also had a higher coefficient of thermal expansion compared to the aft 410 stainless material, and thus the parts could be machined flush and any differential expansion would create a backwards facing step. Thus, the challenge of designing and manufacturing cold-wall steps into the material joints could be avoided for BOLT II. JHU/APL also performed trade studies on the effect of assumed material emmisivity on the results, since there was a lack of data for these materials, and showed that the effect was negligible.

The correlation-based heating analyses were highly impactful and came at a critical time in the BOLT II program (ahead of the PDR). The availability of data to conduct these material trades allowed a downselection to the Nickel 201/410-stainless configuration ahead of PDR. Once the candidate materials had been identified, JHU/APL conducted a higher fidelity transient thermal analysis using heating derived from viscous CFD solutions, rather than from empirical correlations.

The CFD-based thermal analysis was completed in May 2020, approximately three weeks prior to the BOLT II PDR. Details of the analysis are provided as PowerPoint slides in Appendix A.2. The analysis involved generating new CFD grid suitable for accurate heat transfer rates, and the new grid leveraged previous BOLT work and topologies. The grid was created in LINK3D and also included the extended BOLT II experiment geometry as well as the transition section and a portion of the second stage booster. CFD solutions were generated at various times across the trajectory. Figure 13 shows an example of one of these mean flows.

Heating results were then collected and applied to a thermal solution. A detailed grid of the BOLT II components was created and the heat transfer coefficient and recovery temperature distributions from CFD solutions were applied throughout the trajectory. The thermal response was then simulated across the entire trajectory. Figure 14 shows the thermal response of the BOLT II payload configuration at $t = 40$ s, following the ascent phase. Transparent surfaces are used to

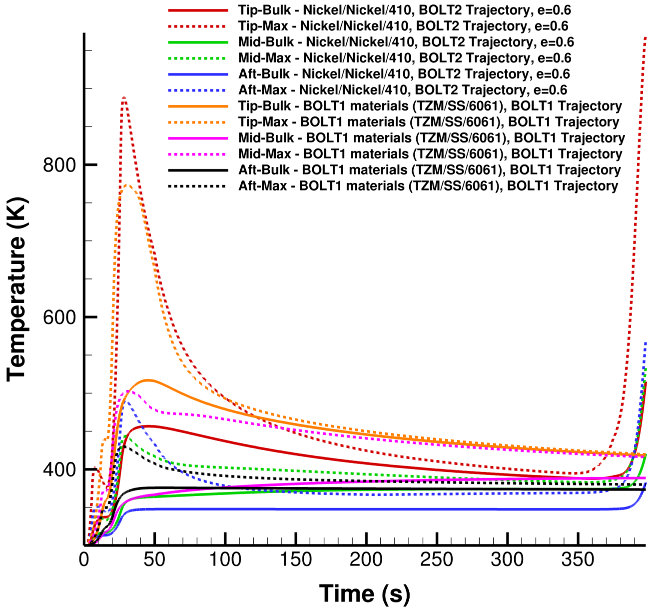

Figure 12. Additional correlation-based heating results comparing a Nickel/410 stainless BOLT II configuration to the original BOLT trajectory results.

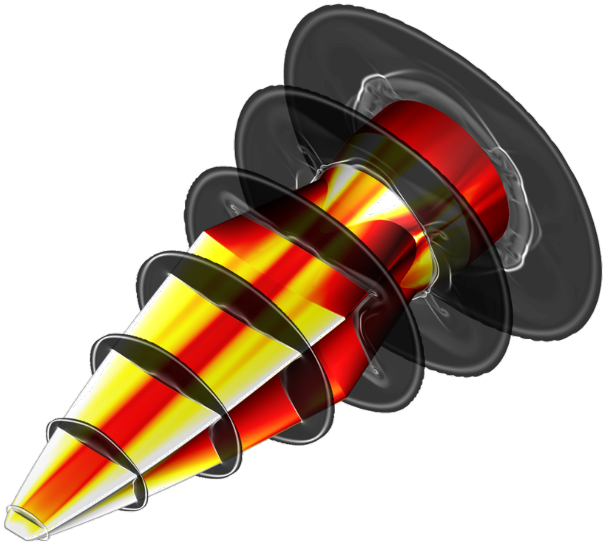

Figure 13. Example JHU/APL BOLT II mean flow results, showing surface heating in orange, and numerical schlieren in grayscale.

visualize the in-depth temperature distributions throughout the material. A full three-dimensional temperature datasets were generated every 200 ms during the ascent and descent phases. The exoatmospheric portion of flight was simulated using adiabatic boundary conditions, neglecting radiation heat transfer, to model the degree of equilibrium obtained via long-term conduction during that phase of flight. Additional data statistics were captured in other files, such as the minimum, maximum, and average temperatures in each component.

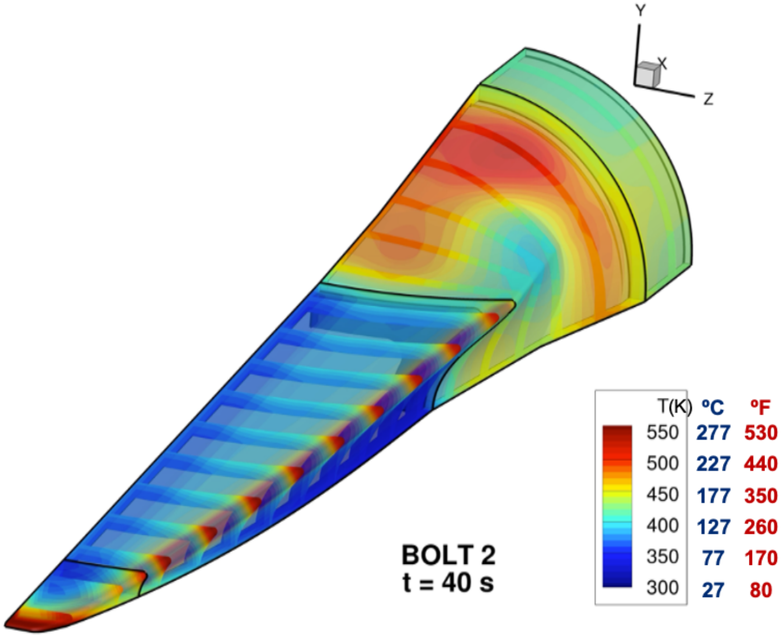

Figure 14. Temperature response at $t = 40$ s from the JHU/APL thermal analysis.

The complete transient thermal simulations by JHU/APL were used for several follow-on studies by the BOLT II team. Results and data files were provided by JHU/APL on request to support activities including instrumentation layout design by Texas A&M as well as structural analyses by CUBRC. For the former, Tecplot solution files of transient temperature distributions were used by Texas A&M to assess the ability of the instrumentation suite to account for spanwise temperature gradients. For the latter, temperature distribution point clouds were provided by JHU/APL to CUBRC so that structural analyses of the design for the BOLT II flight vehicle would include temperature-dependent properties and stresses from nonuniform temperature gradients and thermal expansion.

JHU/APL also supported the BOLT II team including NASA Wallops with thermal analyses to assess the need for thermal protection additions to portions of the BOLT II payload, including the transition section as well as portions of the second stage attitude control module. These assessments included trade studies on the effect of candidate thermal protection techniques (cork, RTV) on structural temperatures, as well as trade studies assessing the effect of TPS thickness on temperatures of the structure. These studies were performed with the APL MSLRAD/ATLAS code and were provided to the BOLT II team for use in making decisions on TPS techniques. For later analyses by CUBRC, JHU/APL provided heat transfer coefficient and recovery temperatures at various points of interest from the transient thermal solutions.

JHU/APL also performed a quick CFD study to examine the heating differences between a baseline and an alternate transition section design (Figure 15). The results showed that fairing length changes the shock/boundary-layer interaction regions on the transition section and thus the location of peak heating.

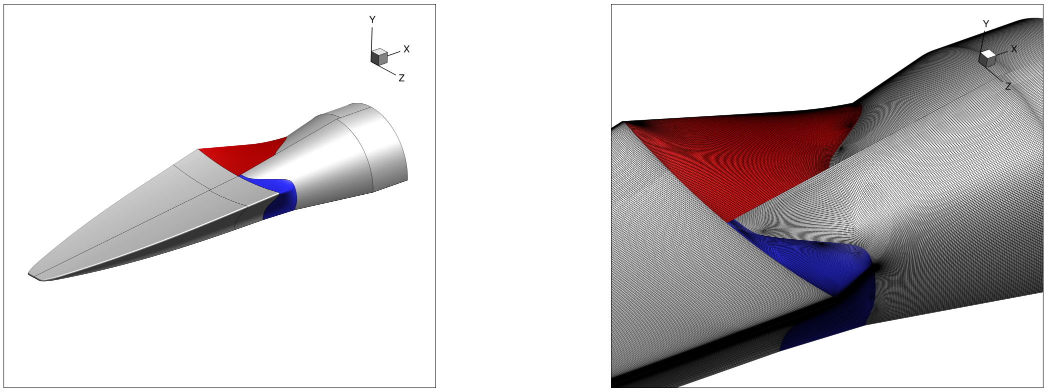

(a) Transition section alternates

(b) Transition section grids

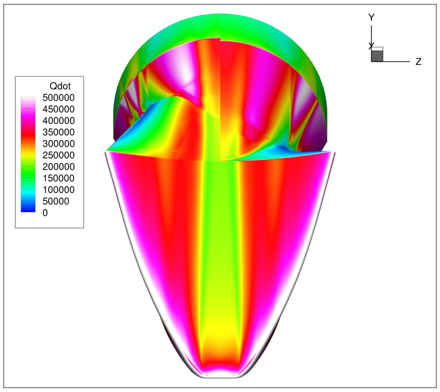

(c) Heat flux comparison

Figure 15. CFD prediction of heating on candidate alternate transition section designs

Finally, JHU/APL performed independent analysis on heating and expected temperatures for the second stage fin in collaboration with NASA Wallops. The heating on the second stage fin was an area of concern for BOLT II ahead of the program CDR. While NASA Wallops/Northrop Grumman performed analysis of the expected heating, and independent analysis was also desired. Predicted erosion of the fin RTV TPS was compared to the NASA Wallops/Northrop Grumman baseline and it was found that the fin RTV layer recession predicted by JHU/APL did not exceed that of the primary predictions (Figure 16). To spot check the correlation-based heating results from the Northrop Grumman analysis, JHU/APL conducted independent CFD simulations of the second stage fin and found good agreements with the correlation-based heating rates. Details of the CFD heating comparisons are shown in Appendix A.3.

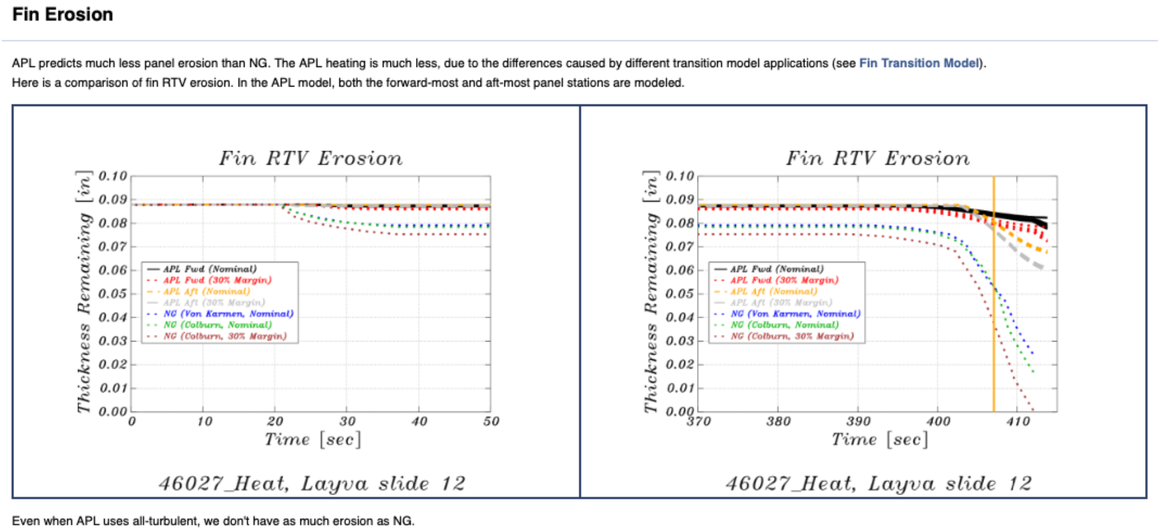

Fin Erosion

APL predicts much less panel erosion than NG. The APL heating is much less, due to the differences caused by different transition model applications (see Fin Transition Model).
Here is a comparison of fin RTV erosion. In the APL model, both the forward-most and aft-most panel stations are modeled.

Even when APL uses all-turbulent, we don't have as much erosion as NG.

Figure 16. Fin RTV erosion rates predicted by JHU/APL compared to Northrop Grumman results.

2.2.4. Structural Analysis of Fasteners

JHU/APL supported CUBRC in understanding previously completed structural analysis of the BOLT flight experiment, such that a similar analysis could be completed by CUBRC for the BOLT II design. Although BOLT II features different materials than BOLT, the overall design of the interface joints remains common between the two missions. BOLT II features a single joint at the location of the BOLT "downstream isolator/frustum" joint. A potential issue was raised regarding how to model the interaction between differential thermal expansion, pre-flight bolt torque values, and related uncertainties in the initial/pre-flight torque of bolts connecting the parts.

With permission of the AFOSR program officer, Dr. Popkin, JHU/APL revisited the BOLT structural analysis with a new ABAQUS structural model that included new details of the bolts within the joints. Figure 17b shows a new ABAQUS finite element grid of the nosetip, isolator, frustum, and interface joint features (bolts and gaps) for the BOLT flight experiment. Using existing thermal models, a temperature distribution from the BOLT flight was superimposed on the structural model and the temperature-dependent properties of the materials were simulated to determine the combined loads felt by the bolts. Figure 17b shows equivalent plastic strain within the bolts and joint interfaces expected for various times in flight during the BOLT mission. The new analysis determined that the bolt loads are unlikely to cause failure in flight for the BOLT mission, and remain within acceptable limit loads. The results were shared with the BOLT II team and in particular to support the CUBRC structural analysis. It was determined that due to the materials used in BOLT II, the load environment on the bolts was not of concern and a similar analysis did not need to be completed for BOLT II. The new analysis helped to verify acceptable levels of risk for the BOLT flight and also allowed both the BOLT and BOLT II teams to gain new understanding of the behavior of the BOLT structural loads through the stressing hypersonic flight environment.

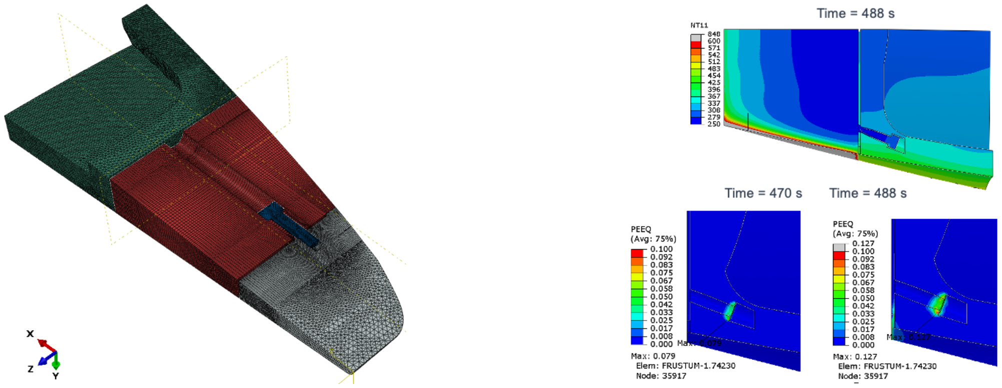

(a) ABAQUS Grid

(b) Plastic Strain

Figure 17. Exploratory finite element simulations of expected bolt structural loads for the BOLT mission, completed to understand modeling of similar phenomena for BOLT II.

2.3. Knowledge Transfer and Advisory

While leading the development of BOLT, JHU/APL gained valuable knowledge specific to hypersonic flow over a low-curvature, concave surface with swept leading-edges. Sharing this knowledge and experience would serve to reduce risk in the design of the BOLT II flight experiment. As such, a key component of the present activities are for JHU/APL to engage in knowledge transfer and advisory activities with the BOLT II team. Here “knowledge transfer” is intended to specify sharing of BOLT design experience and data, while “advisory activities” include all other collaboration with the BOLT II team outside of the technical work described earlier in Section 2.2. While this portion of the research does not necessarily produce defined products or research findings, the support of the JHU/APL BOLT team to engage with the larger BOLT II team has been integral to developing a follow on flight.

Some of the initial activities in Year 1 to support of knowledge transfer and advisory activities to the BOLT II team are summarized briefly here. Since March 2020, JHU/APL staff have supported regular bi-weekly technical discussion phone calls with the BOLT II team to observe present design work and related issues. JHU/APL has in most cases conducted follow up communications via e-mail and/or telecons to support the BOLT II team researchers and students in various aspects of their research to design their flight experiment. Advice and documentation from JHU/APL’s BOLT experience has been communicated in aspects such as material selection, thermal modeling techniques, detailed mechanical design questions, aerodynamic considerations, experience with designing an aerodynamic fairing, wind-tunnel testing, wind-tunnel results, computational fluid dynamics, instrumentation selection, instrumentation layout considerations, data sampling considerations, version control, flow phenomena, and flight range operations.

JHU/APL staff members also supported the BOLT II Preliminary Design Review (PDR) and Critical Design Review (CDR) in Year 1 of this research grant, and provided feedback via Requests for Actions (RFA's) in both reviews. JHU/APL staff then assisted the BOLT II team in responding to the RFA's.

3. Anticipated Year 2 Activities

JHU/APL anticipates its support of BOLT II to continue in Year 2 of the grant in the form of any needed independent analysis activities and via continued knowledge transfer and advisory activities. The BOLT II mission will be scheduled for a flight experiment in September 2021 during the second year of this grant. JHU/APL staff are prepared to support Texas A&M and CUBRC in the expected fabrication, instrumentation, and pre-flight activities as well as at the flight campaign at NASA Wallops.

4. BOLT Post-Flight Research

A major focus of this research grant is to continue to utilize the Boundary Layer Transition (BOLT) flight test data to discover and document the salient physics of the laminar-to-turbulent transition process observed during the flight test, as well as to disseminate the findings and test data at the direction of the AFOSR to other investigators within the AFOSR portfolio.

A previous AFOSR grant awarded to JHU/APL (FA9550-17-2-0001 with PI's Drs. Wheaton and Berridge) was used to gain fundamental understanding of boundary layer transition flow phenomena surrounding the BOLT geometry consisting of a low-curvature concave surface with highly swept leading edges [1–9]. For that grant, JHU/APL coordinated and executed a rapid-paced effort to design a set flight experiment hardware ("Flight Geometry") to obtain in-flight measurements of temperature, pressure, and heat flux during the planned flight campaign. The flight data had been expected to be obtained near the conclusion of the first grant, however it was delayed due to COVID-19. There are two planned research thrusts within this present research grant as follow-on activities for the BOLT flight data here:

(1) Complete a thorough core data analysis of the BOLT flight experiment data that will result in a final postprocessed dataset along with characterization of the observed transition front behavior and physics from the flight data

(2) Transition JHU/APL into a role supporting long-term data analysis of the BOLT flight data, whereby JHU/APL will assist AFOSR in the dissemination of the flight data to the larger portfolio of researchers and will assist AFOSR in coordinating and supporting those analyses by other researchers

The phased approach of these research thrusts will first ensure that a complete and thorough vetting and understanding of the BOLT flight test data is obtained by the JHU/APL team. Following the core analysis phase, the second phase will ensure that JHU/APL will be able to support the transition of this flight data to the extended AFOSR portfolio of researchers who will use it for advances in the fundamental understanding of boundary-layer transition and for improvement in tools and methods for prediction of transition on future complex geometries.

Due to the delay of the BOLT flight campaign from its originally scheduled May 2020 date, to a later date now anticipated in June 2021, there is not currently and flight test results to use for either thrust (1) and (2) above. As such, work on BOLT post-flight research has largely been postponed. A limited amount of initial work began in Year 1 of the present grant on activities that do not require the availability of BOLT flight data. These activities included:

(1) Initial development of a software repository and initial post-flight analysis script development utilizing sample telemetry data,

(2) Development of a database of expected surface pressure sensors from CART3D simulations to be used for future vehicle attitude determination,

(3) Extraction of new instrumentation coordinates based on the final dimensions of the fabricated flight hardware, and

(4) Initial development of required grids and computational methods that will enable inverse heat transfer calculations based on measured surface temperatures

The progress on these initial activities in Year 1 related to BOLT post-flight research will be briefly summarized here.

4.1. Post Flight Analysis Scripts

JHU/APL has begun the process of developing scripts and tools for the future analysis of the BOLT flight experiment data. Using sample telemetry data provided by the Air Force Research Laboratory Aerospace Systems Directorate (AFRL/RQ), initial scripts have been developed to read in the data files for all instrumentation and to make the data ready for future manipulation and processing.

The investigators of this grant first determined a common set of philosophies for an approach to developing the post-flight tools:

(1) To use MATLAB for majority of analysis, with some Tecplot outputs for plotting (both tools being common use software among researchers)

(2) Source and version control of all data and tools

(3) Traceability from the telemetry data input to all processed outputs

(4) Common/agreed-upon coordinate system

(5) Extensive documentation for future distribution of the tools to other researchers

Based on the above philosophies, it was decided that the BOLT post-flight data analysis tools will be securely hosted on JHU/APL's internal network via an enterprise implementation of Gitlab. Gitlab is software to securely manage Git repositories for code development and version control. It allows the simultaneous development of post-flight data analysis tools from multiple users while maintaining agreed upon master versions of the codes. All versions are backed up and available in case of problems introduced via changes to the tools.

Figure 18 shows some of the initial development of the post-flight tools in Gitlab accomplished in Year 1 of this grant. Figure 18a shows the initial script for reading in the BOLT telemetry data and the image shows two versions of the script in Gitlab, highlighting changes to various lines of the script. Figure 18b shows a sample entry into the Gitlab's wiki, which is being used by JHU/APL to document every step of development of the data analysis tools. The wiki will be able to be exported and converted into documentation that will assist future AFOSR researchers utilizing the BOLT data.

At the conclusion of Year 1 of the grant, the BOLT post-flight tool development process has been established and an initial set of scripts has been developed to convert the telemetry data into usable format.

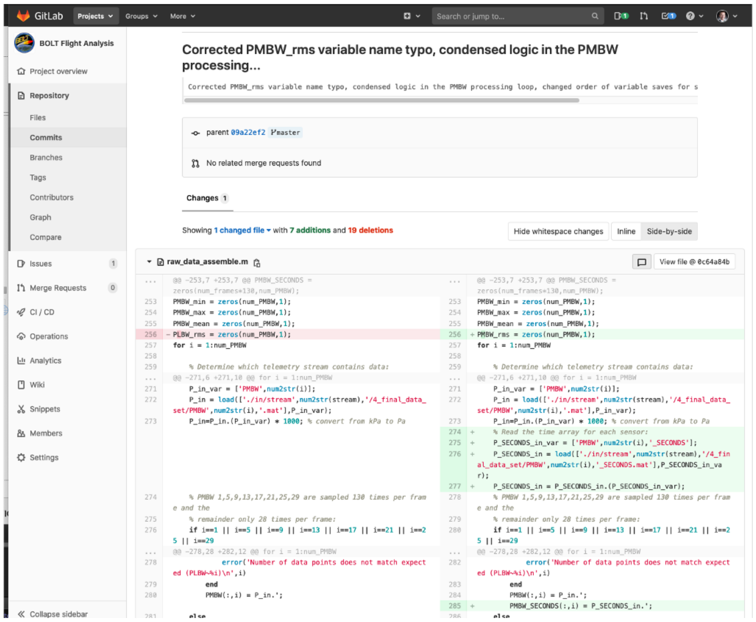

Corrected PMBW_rms variable name typo, condensed logic in the PMBW processing...

```
Corrected PMBW_rms variable name typo, condensed logic in the PMBW processing loop, changed order of variable saves for s
```

parent 09a22ef2 master

No related merge requests found

Showing 1 changed file with 7 additions and 19 deletions

raw_data_assemble.m

```
@@ -253,7 +253,7 @@ PMBW_SECONDS =
zeros(num_frames*130,num_PMBW);
PMBW_min = zeros(num_PMBW,1);
PMBW_max = zeros(num_PMBW,1);
PMBW_mean = zeros(num_PMBW,1);
- PLBW_rms = zeros(num_PMBW,1);
for i = 1:num_PMBW

    % Determine which telemetry stream contains data:
@@ -271,6 +271,10 @@ for i = 1:num_PMBW
    P_in_var = ['PMBW',num2str(i)];
    P_in = load(['./in/stream',num2str(stream),'/4_final_data_set/PMBW',num2str(i),'.mat'],P_in_var);
    P_in=P_in.(P_in_var) * 1000; % convert from kPa to Pa
    % PMBW 1,5,9,13,17,21,25,29 are sampled 130 times per frame and the
    % remainder only 28 times per frame:
    if i==1 || i==5 || i==9 || i==13 || i==17 || i==21 || i==25 || i==29
@@ -278,28 +282,12 @@ for i = 1:num_PMBW
            error('Number of data points does not match expected (PLBW~%i)\n',i)
        end
        PMBW(:,i) = P_in.';

    else
```

```
@@ -253,7 +253,7 @@ PMBW_SECONDS =
zeros(num_frames*130,num_PMBW);
PMBW_min = zeros(num_PMBW,1);
PMBW_max = zeros(num_PMBW,1);
PMBW_mean = zeros(num_PMBW,1);
+ PMBW_rms = zeros(num_PMBW,1);
for i = 1:num_PMBW

    % Determine which telemetry stream contains data:
@@ -271,6 +271,10 @@ for i = 1:num_PMBW
    P_in_var = ['PMBW',num2str(i)];
    P_in = load(['./in/stream',num2str(stream),'/4_final_data_set/PMBW',num2str(i),'.mat'],P_in_var);
    P_in=P_in.(P_in_var) * 1000; % convert from kPa to Pa
+    % Read the time array for each sensor:
+    P_SECONDS_in_var = ['PMBW',num2str(i),'_SECONDS'];
+    P_SECONDS_in = load(['./in/stream',num2str(stream),'/4_final_data_set/PMBW',num2str(i),'_SECONDS.mat'],P_SECONDS_in_var);
+    P_SECONDS_in = P_SECONDS_in.(P_SECONDS_in_var);
    % PMBW 1,5,9,13,17,21,25,29 are sampled 130 times per frame and the
    % remainder only 28 times per frame:
    if i==1 || i==5 || i==9 || i==13 || i==17 || i==21 || i==25 || i==29
@@ -278,28 +282,12 @@ for i = 1:num_PMBW
            error('Number of data points does not match expected (PLBW~%i)\n',i)
        end
        PMBW(:,i) = P_in.';
+        PMBW_SECONDS(:,i) = P_SECONDS_in.';
    else
```

(a) Code version control

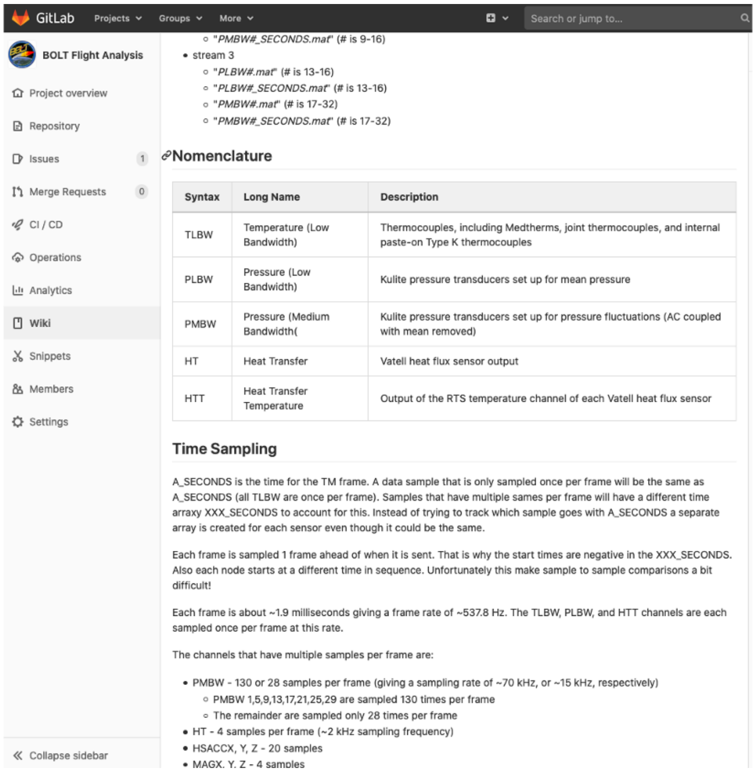

  - "*PMBW#_SECONDS.mat*" (# is 9-16)
- stream 3
  - "*PLBW#.mat*" (# is 13-16)
  - "*PLBW#_SECONDS.mat*" (# is 13-16)
  - "*PMBW#.mat*" (# is 17-32)
  - "*PMBW#_SECONDS.mat*" (# is 17-32)

Nomenclature

Syntax	Long Name	Description
TLBW	Temperature (Low Bandwidth)	Thermocouples, including Medtherms, joint thermocouples, and internal paste-on Type K thermocouples
PLBW	Pressure (Low Bandwidth)	Kulite pressure transducers set up for mean pressure
PMBW	Pressure (Medium Bandwidth(	Kulite pressure transducers set up for pressure fluctuations (AC coupled with mean removed)
HT	Heat Transfer	Vatell heat flux sensor output
HTT	Heat Transfer Temperature	Output of the RTS temperature channel of each Vatell heat flux sensor

Time Sampling

A_SECONDS is the time for the TM frame. A data sample that is only sampled once per frame will be the same as A_SECONDS (all TLBW are once per frame). Samples that have multiple sames per frame will have a different time arraxy XXX_SECONDS to account for this. Instead of trying to track which sample goes with A_SECONDS a separate array is created for each sensor even though it could be the same.

Each frame is sampled 1 frame ahead of when it is sent. That is why the start times are negative in the XXX_SECONDS. Also each node starts at a different time in sequence. Unfortunately this make sample to sample comparisons a bit difficult!

Each frame is about ~1.9 milliseconds giving a frame rate of ~537.8 Hz. The TLBW, PLBW, and HTT channels are each sampled once per frame at this rate.

The channels that have multiple samples per frame are:

- PMBW - 130 or 28 samples per frame (giving a sampling rate of ~70 kHz, or ~15 kHz, respectively)
  - PMBW 1,5,9,13,17,21,25,29 are sampled 130 times per frame
  - The remainder are sampled only 28 times per frame
- HT - 4 samples per frame (~2 kHz sampling frequency)
- HSACCX, Y, Z - 20 samples
- MAGX, Y, Z - 4 samples

(b) Wiki for documentation

Figure 18. JHU/APL internally hosted Gitlab repository for BOLT post-flight analysis tool development and version control.

4.2. CART3D Database for Attitude Determination

Due to the design of the BOLT flight test, the vehicle will be constantly changing angle of attack and roll throughout the experimental window. This behavior will induce a constant oscillatory behavior in the recorded surface measurements. In order to accurately characterize the behavior of boundary-layer transition with respect to vehicle attitude in the post-flight data, a prediction of the real-time angle of attack and roll is necessary. Therefore, a database of CFD solutions spanning the predicted Mach numbers, angles of attack, and roll angles has been calculated in preparation for determination of vehicle attitude. These simulations were performed with the NASA CART3D code and the surface pressure distributions will be extracted for comparison to measured surface pressures in flight. Table 1 shows the range and step increment of each variable utilized for the database. Work is ongoing to post-process these solutions into a database that can be used to interpolate a least-squares fit of the measured flight surface pressure to accurately determine the AoA and roll at all times. This was based on work completed by Jewell et al. [10] on the HiFIRE-5b flight test, where the same procedure was successfully used.

Table 1. CART3D database parameters for BOLT attitude determination

	Mach Number	Total AoA	Roll Angle
Range	1–9	0–6°	0–180°
Resolution	0.5	0.5°	10°

4.3. Instrumentation Coordinates

The final machined BOLT flight geometry features some small changes with respect to the baseline shape used for pre-flight analyses. The isolator component was lengthened by approximately 1 mm (0.040 in.) to create two rear-facing steps at the material interface joints. As a result of this change, some of the sensor hole coordinates needed to be updated by the JHU/APL team prior to beginning analysis on the flight data. The coordinate updates are small, representing nominally a 0.3 mm shift in location relative to the physical nosetip. In addition, the coordinates are now referenced to a new origin at the physical nosetip of the manufactured parts. Coordinates are being updated in a master CAD assembly in Solidworks and exported to a spreadsheet for tracking the new locations. While updating the coordinates in Solidworks, labels are being added to the sensor locations within the CAD assembly to enhance understanding by all researchers on the exact locations of each sensor. Figure 19 shows some of the initial updated sensor labels completed in Year 1 of the grant. The remainder of the locations will be updated within Year 2 of the grant, as initially only the locations needed for a subset of the thermocouple analysis were completed.

4.4. Inverse Heat Transfer Analysis

Because of the highly complex shape of the BOLT Flight Geometry, a significantly higher amount of spanwise conduction of heating is expected within the flight experiment compared to previous HIFiRE flight experiments with conical bodies. As a result, a semi-one-dimensional approximation

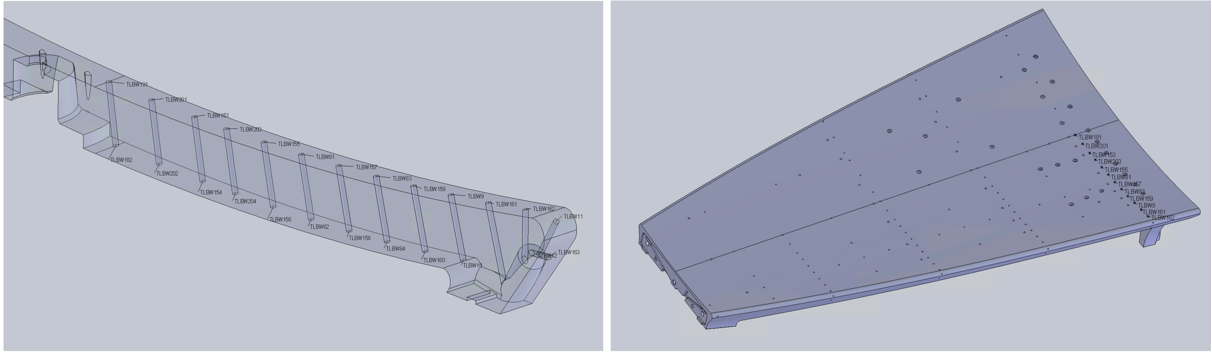

(a) 800 mm Station

(b) Primary frustum component

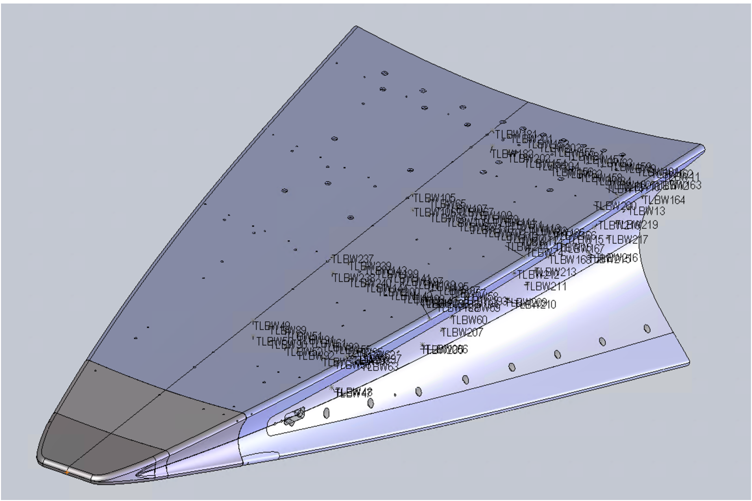

(c) Labeled sensor locations

Figure 19. Instrumentation coordinate updates and labeling in Solidworks CAD assembly.

to the coaxial thermocouples cannot be used to convert measured temperatures in flight to heat transfer. JHU/APL devised a methodology for reducing temperatures to heat transfer for highly-instrumented spanwise arrays of sensors placed at four axial stations (350 mm, 500 mm, 650 mm, and 800 mm). A conceptual study conducted within the original BOLT grant proved that a two-dimensional inverse heat transfer calculation at these axial stations seemed feasible for use in the BOLT post-flight analysis.

Initial work in Year 1 of this grant has been spent to begin to generate computational grids for these highly instrumented spanwise slices. In Year 2, scripts will be written to generate a time-dependent external and internal boundary condition based on measured temperatures with interpolation schemes between sensor locations. It is expected within Year 3 that the methodology to perform inverse heat transfer calculations will be completed and tested on the anticipated flight data.

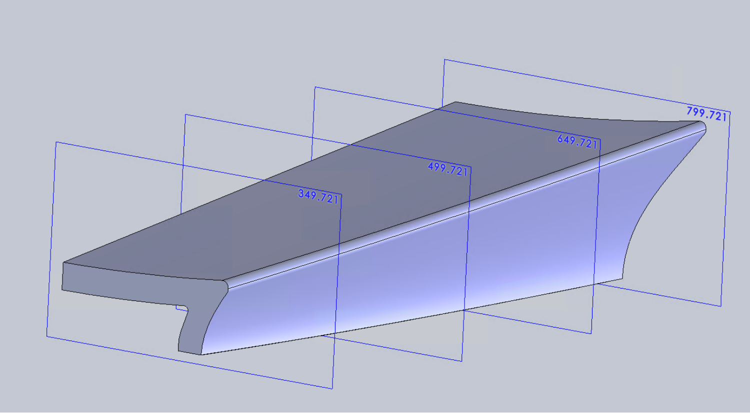

(a) CAD representing axial stations

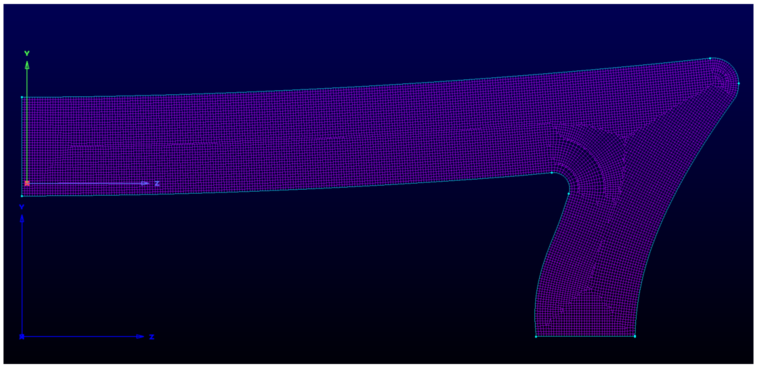

(b) Initial thermal grid

Figure 20. Year 1 progress on implementing inverse 2D calculations of heat transfer based on highly-instrumented axial stations.

4.5. Anticipated Year 2 Activities

It is anticipated that BOLT flight data will be available within the weeks following the June 2021 scheduled flight campaign, in the absence of any further delays due to COVID-19. This schedule would mean that flight data could be available with approximately 21 months remaining in the 36-month grant period of performance. It would make sense within Year 2 for JHU/APL to attempt to make nearly complete progress on the proposed "Core Data Analysis" activity, including:

(1) analyses to ensure that the BOLT scientific measurement raw data are selected from the best combination of telemetry stream and receiving station data,

(2) gather and analyze weather balloon data from the flight in order to develop a best estimated atmospheric profile for the as-flown trajectory,

(3) develop a best estimated Flight Geometry orientation,

(4) develop a best estimated surface wall temperature distribution to provide to researchers who wish to study the impact of surface temperature on the boundary layer physics,

(5) complete new computational analyses at the final flight conditions to assist in understanding the flight data,

(6) implement two-dimensional inverse heat transfer solver methodology that can be used to extract heat transfer rates from the spanwise arrays of Medtherm coaxial thermocouples,

(7) characterize amplitudes of narrowband and broadband pressure fluctuations within the laminar, transitional, and turbulent boundary layer states for instability and transition assessment,

(8) assess the spatial characteristics of streamwise laminar and transitional heating streak structures in flight, and

(9) conduct an analysis of the PCB132B pressure sensors to identify potential instability modes.

While it is not likely that all of the above activities will be completed in Year 2 of this grant, JHU/APL will strive to make extensive progress on as many as feasible to accelerate the timeline for full core analysis of the BOLT flight data.

Acknowledgments

This work was supported by the Air Force Office of Scientific Research under award number FA9550-20-1-0043 (PO: Dr. Sarah Popkin). Any opinions, finding, and conclusions or recommendations expressed in this material are those of the author(s) and do not necessarily reflect the views of the United States Air Force.

References

[1] Wheaton, B. M., Berridge, D. C., Wolf, T. D., Araya, D. B., Stevens, R. T., McGrath, B. E., Kemp, B. L., and Adamczak, D. W., "Final Design of the Boundary Layer Transition (BOLT) Flight Experiment," *Journal of Spacecraft and Rockets*, Vol. 58, No. 1, 2021, pp. 6–17. doi:10.2514/1.A34809, URL `https://doi.org/10.2514/1.A34809`.

[2] Leyva, I. A., and Cummings, R. M., "Introduction to the Special Section on the Boundary Layer Transition (BOLT) Flight Experiment," *Journal of Spacecraft and Rockets*, Vol. 58, No. 1, 2021, pp. 4–5. doi:10.2514/1.A34872, URL `https://arc.aiaa.org/doi/10.2514/1.A34872`.

[3] Hörschgen-Eggers, M., Kirchhartz, R. M., Jung, W., Schoppmann, K., Ettl, J., and Wittkamp, M., "Boundary Layer Transit Flight Experiment: Mission Overview, Launch Vehicle and Payload Subsystems," *Journal of Spacecraft and Rockets*, Vol. 58, No. 1, 2021, pp. 26–37. doi:10.2514/1.A34877, URL `https://arc.aiaa.org/doi/10.2514/1.A34877`.

[4] McKiernan, G. R., Chynoweth, B. C., Schneider, S. P., Berridge, D. C., and Wheaton, B. M., "Boundary Layer Transition Preflight Experiments in a Mach-6 Quiet Tunnel," *Journal of Spacecraft and Rockets*, Vol. 58, No. 1, 2021, pp. 54–66. doi:10.2514/1.A34772, URL `https://doi.org/10.2514/1.A34772`.

[5] Moyes, A. J., and Reed, H. L., "Preflight Boundary-Layer Stability Analysis of BOLT Geometry," *Journal of Spacecraft and Rockets*, Vol. 58, No. 1, 2021, pp. 78–89. doi:10.2514/1.A34792, URL `https://doi.org/10.2514/1.A34792`.

[6] Rieken, E. F., Berry, S. A., Mason, M. L., and Greene, F. A., "Aerothermodynamic Ground Tests in Support of the Boundary Layer Transition Flight Experiment," *Journal of Spacecraft and Rockets*, Vol. 58, No. 1, 2021, pp. 38–53. doi:10.2514/1.A34803, URL `https://doi.org/10.2514/1.A34803`.

[7] Knutson, A. L., Thome, J. S., and Candler, G. V., "Numerical Simulation of Instabilities in the Boundary-Layer Transition Experiment Flowfield," *Journal of Spacecraft and Rockets*, Vol. 58, No. 1, 2021, pp. 90–99. doi:10.2514/1.A34599, URL `https://doi.org/10.2514/1.A34599`.

[8] Kostak, H. E., and Bowersox, R. D. W., "Preflight Ground Test Analyses of the Boundary Layer Transition (BOLT) Flight Geometry," *Journal of Spacecraft and Rockets*, Vol. 58, No. 1, 2021, pp. 67–77. doi:10.2514/1.A34858, URL `https://doi.org/10.2514/1.A34858`.

[9] Berry, S. A., Wheaton, B. M., and Chynoweth, B. C., "Secondary Side Considerations for Boundary Layer Transition Flight Experiment," *Journal of Spacecraft and Rockets*, Vol. 58, No. 1, 2021, pp. 18–25. doi:10.2514/1.A34778, URL `https://doi.org/10.2514/1.A34778`.

[10] Jewell, J. S., Kimmel, R. L., Adamczak, D. W., Poggie, J., Porter, K. M., and Juliano, T. J., "HIFiRE-5b Flow Computations and Attitude Determination via Comparison with Flight Data," *Journal of Spacecraft and Rockets*, Vol. 55, No. 6, 2018, pp. 1356–1368. doi:10.2514/1.A34162, URL `https://arc.aiaa.org/doi/10.2514/1.A34162`.

A. Appendices

The appendices of this annual report contains selected results from work in Year 1 of the research. Appendix A.1 shows the trajectory analysis of the BOLT II mission. Appendix A.2 shows the thermal analysis of BOLT II completed for the BOLT II Preliminary Design Review (PDR). Appendix A.3 shows the independent heating analysis of the BOLT II second stage fin completed using CFD.

A.1. BOLT II PDR Aerodynamics and Trajectory Analysis

The following appendix contains details of the aerodynamics and trajectory analysis JHU/APL conducted for the BOLT II Preliminary Design Review (PDR).

APL BOLTII Aerodynamics and Trajectory assessment for PDR geometry

09 June 2020

David Gers – APL Aerodynamics SME
Hailey Palensky – APL Trajectory SME
Prasad Kutty – APL Trajectory SME

Brad Wheaton – APL BOLT II Support PI
Daniel Araya – APL BOLT II Support Co-PI

This material is based upon work supported by the Air Force Office of Scientific Research under award number FA9550-20-1-0043.

Summary

Aerodynamics Analysis

- APL completed CFD analysis of both Xcp and CA_0 for the Stage 2 configuration.
  - Analysis tools include:
    - Inviscid Cart3D forebody results
    - SkinFriq -- APL skin friction correlation tool using Cart3D results
    - APL Base Drag correlation tool -- Moore and Honeywell correlations
    - Viscous CFD++ spot checks.
  - Xcp comparisons with current aero model in TAOS looked good (**slide 5**).
  - Total drag coefficient left questions that need feedback from NASA Wallops (**slide 7**).
    - We observe significantly lower total drag (inviscid + viscous + base) and thus ~10% higher Mach on reentry.

TAOS trajectory analysis

- APL Trajectory team has reviewed NASA Wallops TAOS simulation
  - Completed nominal trajectory run and run with reduced stage 2 total drag to reflect aero findings – both remain statically stable (static margin > 2 majority of flight; **slides 18 & 29**)
  - Limited set of MC runs showed potential for dynamic instability during coast after stage1 separation that is a concern (**slide 46**).
  - Second set of limited MC runs with adjustments to fin cant on stage 1 and aerodynamic uncertainties showed feasibility of mitigating dynamic instability (**slide 61**).
  - Additional feedback was compiled from reviewing the input files (listed on **slides 10 & 11**)
  - APL recommends including aerodynamic uncertainties in future Monte Carlo simulations, particularly to drag, rolling moment and roll damping coefficients.

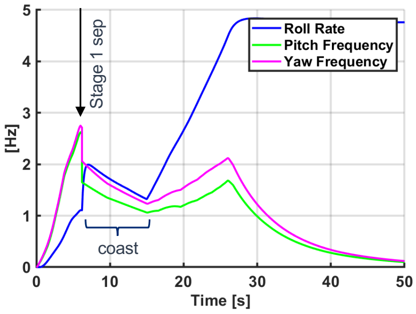

JOHNS HOPKINS
APPLIED PHYSICS LABORATORY

BOLT II Independent Aero Analysis

David Gers

BOLTII Independent Aero Quick-Look

- APL performed a quick-look independent assessment of the BOLTII aero stability and drag
  - Initial QL performed using Cart3D
  - CFD++ spot-check runs also completed using updated fin leading edges
- Cart3D comparison showed good agreement with TAMU stability predictions
  - APL shows slightly increased stability, but Xcp predictions within .3 calibers of each other across the Mach regime
- APL QL inviscid drag prediction shows reasonable agreement with TAMU inviscid predictions
  - APL shows decreased drag in the mid-supersonic regime, but within reasonable uncertainty margin for Cart3D
- APL total drag predictions at sea-level show significant discrepancy with values in TAOS input deck for Stage 2 coast drag
  - Unclear how base/viscous drag is being combined and implemented to get values in the TAOS input deck
  - TAOS is using 16” Lref, TAMU aero data was calculated at 17.25” Lref - if data was not converted, may result in part (but not all) of the discrepancy.

Stability Comparison

- Plot shows Xcp comparison as measured from the physical nosetip. All curves except “APL CFD++ Yaw Plane” correspond to Cart3D predictions
- APL Xcp values calculated at Total Angle of Attack=2°
- Xcp values within 0.3 calibers of each other across the Mach number regime for a given plane.
- Viscous CFD spot-checks (CFD++) show excellent agreement with inviscid (Cart3D) Xcp predictions.

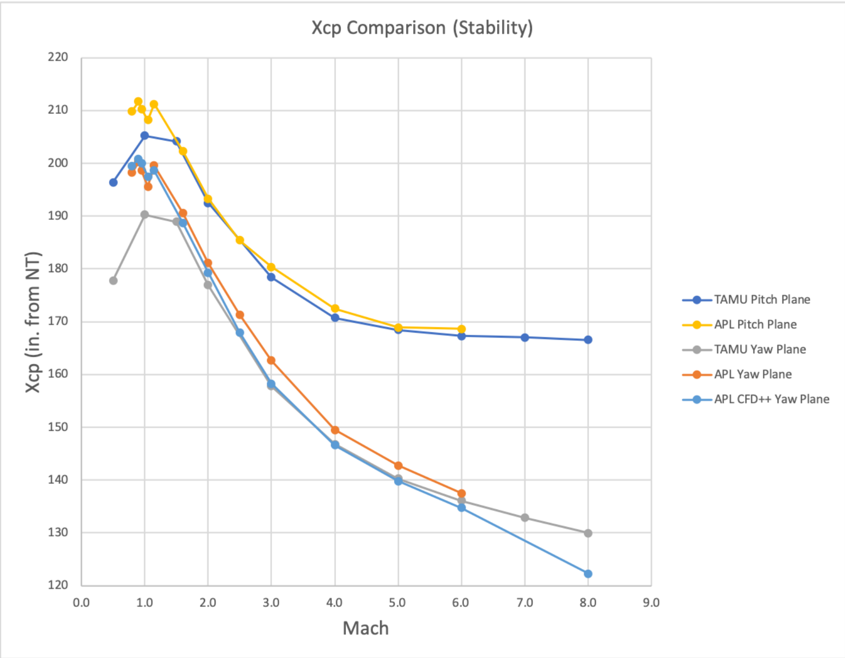

Inviscid Drag Comparison

- Plot shows inviscid axial force component (CA_inviscid) at total angle of attack=0° for coasting Stage 2 configuration.
- APL shows decreased drag relative to TAMU data in the mid-supersonic regime, but within reasonable uncertainty margin for Cart3D results.
- APL comparison between Cart3D predictions and inviscid component of viscous CFD spot-checks (“APL CA CFD++”) is very good.
- Data shown is using Sref=201.06 in^2 (16” Lref)
  - TAMU data converted to this Sref
- APL data is forebody only (no base contribution)

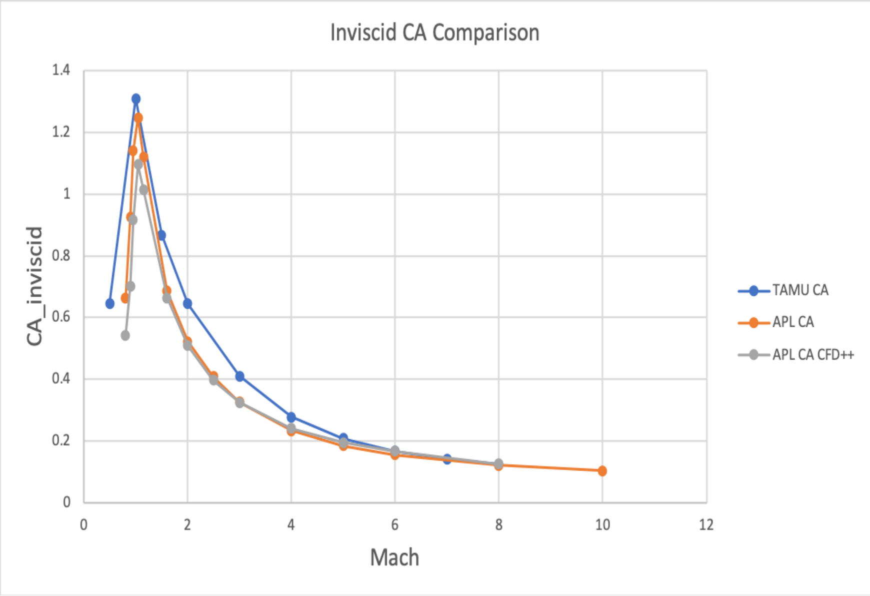

Total Drag Comparison at Sea-Level

- Plot shows total axial force at total angle of attack=0° for coasting Stage 2 configuration.
- Data shown is using Sref=201.06 in^2 (16” Lref)
  - Both APL and TAOS data use this Sref
- APL data includes:
  - Inviscid Cart3D forebody results
  - SkinFriq (APL skin friction correlation tool using Cart3D results)
  - APL Base Drag correlation tool (Moore and Honeywell correlations)
- Open Questions:
  - What is being used for base drag in TAOS buildup?
  - What other geometry feature drag estimates are included in the TAOS drag model that weren’t in the CAD? (i.e., launch lugs, protuberances, raceways, etc?)
  - Difference in Sref from TAMU data to TAOS data – was it accounted for?

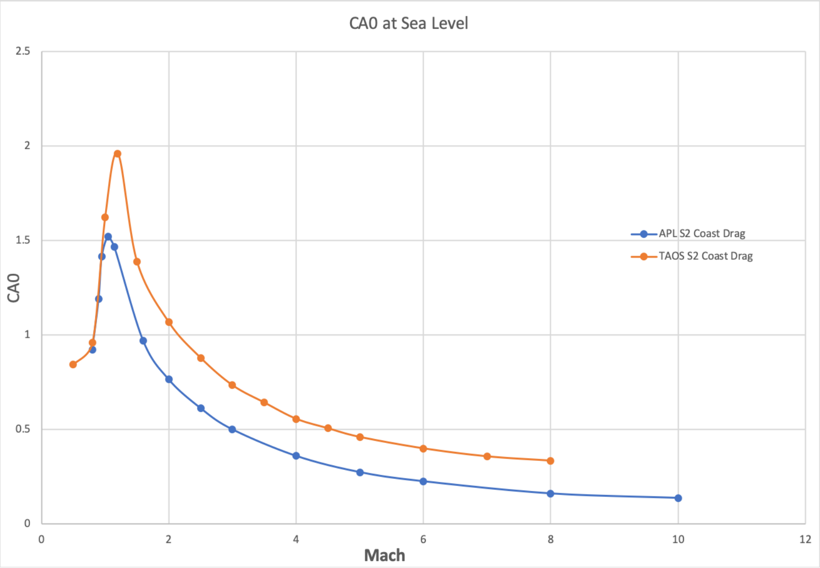

JOHNS HOPKINS
APPLIED PHYSICS LABORATORY

BOLTII Nominal Trajectory Overview

Hailey Palensky
Prasad Kutty

BOLTII Vehicle Overview

Description

Target Vehicle:
- Two Stage
  - Terrier MK-70
  - Improved Malemute
- Payload does not separate from Malemute

Nominal Launch Settings*:
Azimuth = 105.0°
Elevation = 83.0°
Latitude = 37.838°N
Longitude = 75.484°W

Nominal Performance:
Range = 117.88 km
Apogee = 182.00 km

Guidance:
- Unguided
- ACS utilized to trim vehicle for re-entry

BOLT II Full Vehicle Stack

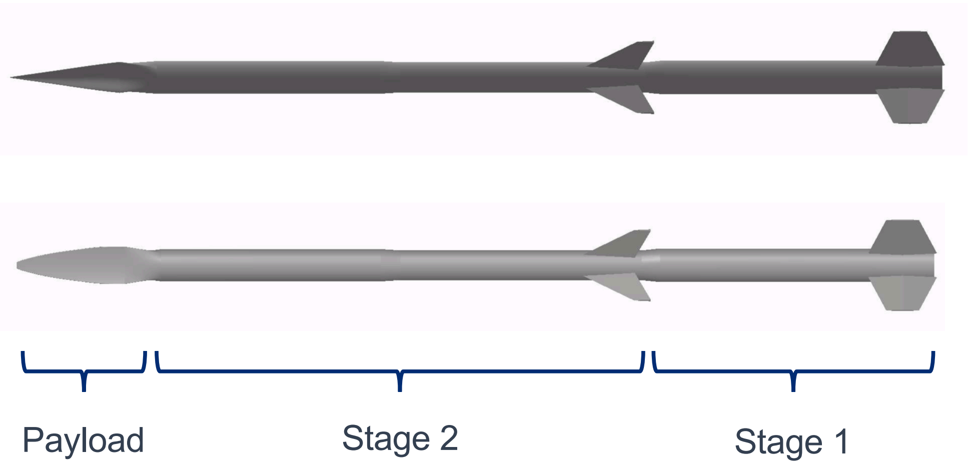

BOLTII TAOS File Notes

- BOLTII Weight:
  - 2019-07-16-BOLT2-TC presentation
    - Total launch without payload reported by BOLT II team but not published here
    - Payload Launch Config = 915.76 lb
  - TAOS File
    - Total launch weight without payload in model but not published here
    - Payload = 890.1 lb

- Atmosphere
  - RCC Wallops July atmospheric model used
    - RCC Wallops atmosphere in TAOS defined up to altitude of 70 km. From 70 km – 150 km, RCC Wallops atmosphere is merged with 1976 U.S. standard atmosphere. Above 150 km, only 1976 U.S. standard atmosphere is used.
  - MC dispersions used for uncompensated winds, with no winds nominally
    - Mean monthly/annual wind profile is not implemented

BOLTII TAOS File Notes (contd.)

- Incomplete uncertainty model for C_Y, C_Z, C_m, C_n
  - Fin misalignments are dispersed but additional uncertainty on component terms needed
  - No dispersion on C_{mq}/C_{nr}
  - No dispersion on tail X_{cp}
- Incomplete uncertainty model for C_l
  - Stage 1: No dispersion on Fin Cant
  - Stage 1: C_{lp} not being multiplied by Fin Cant (non-issue if fin cant is 1 and not dispersed)
  - Both stages: No dispersions on component terms ($C_{l,alpha}$, $C_{l,beta}$, C_{lp}) or total C_l
- No uncertainties applied to X-CG (uncertainties are applied to Y/Z-CG)
- Comment in TAOS problem file regarding Stage 1 Fin Cant value is unclear on what correct value should be

---

BOLTII Timeline

	Nominal Time (s)	Nominal Alt (km)
Target Launch	0.0	0.0
Stage 1 Burnout	6.00	2.31
Stage 1 Separation	6.20	2.47
Stage 2 Ignition	15.00	8.02
Stage 2 Burnout	26.73	20.01
Yoyo Despin	60.0	73.70
Apogee	212.89	182.00
100 km Descent (ACS Initiation)	346.01	100.0
Impact	413.76	0.0

CONOPS

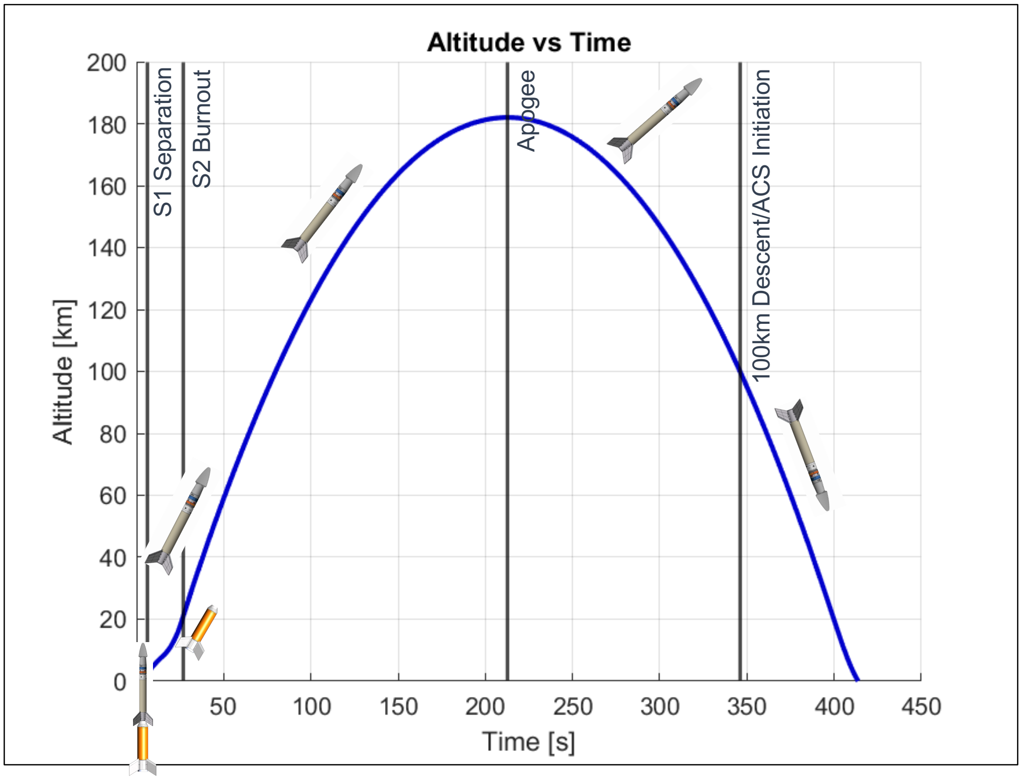

Trajectory Shape

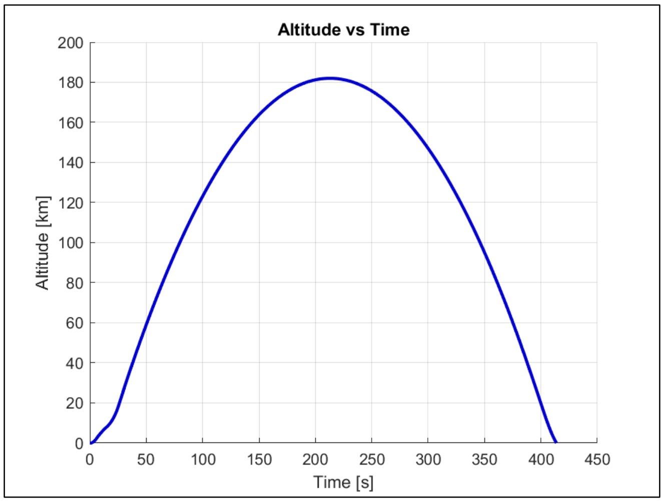

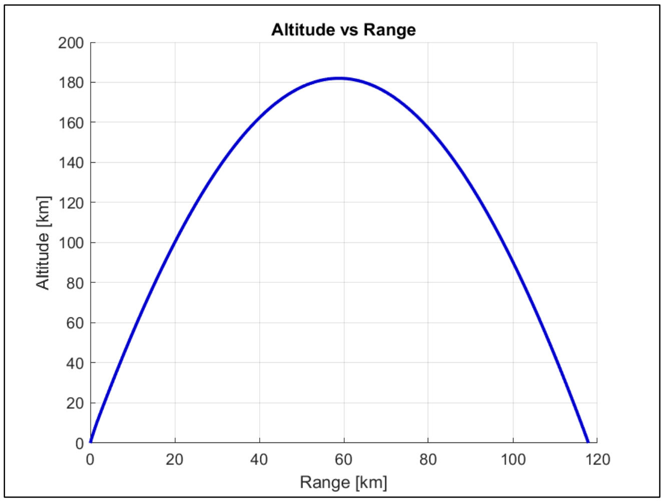

Velocity and Mach

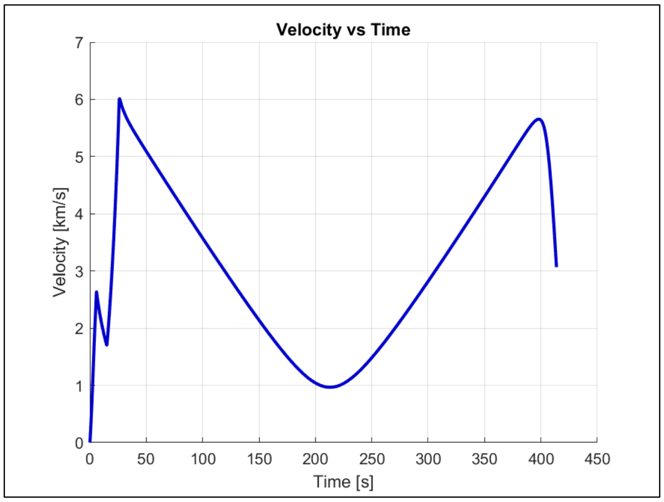

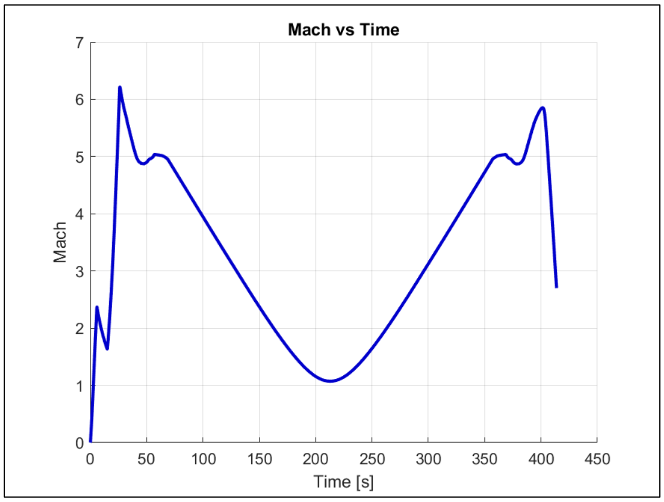

Attitude

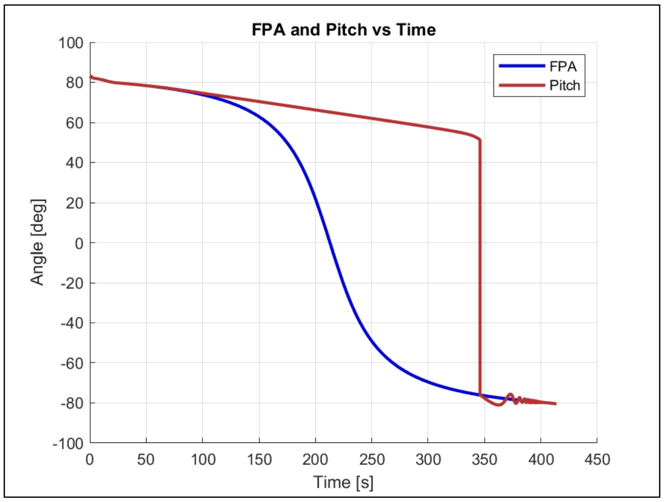

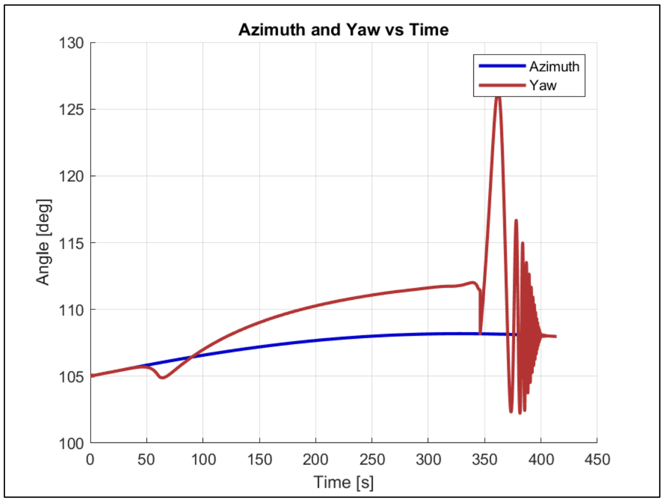

Angle of Attack

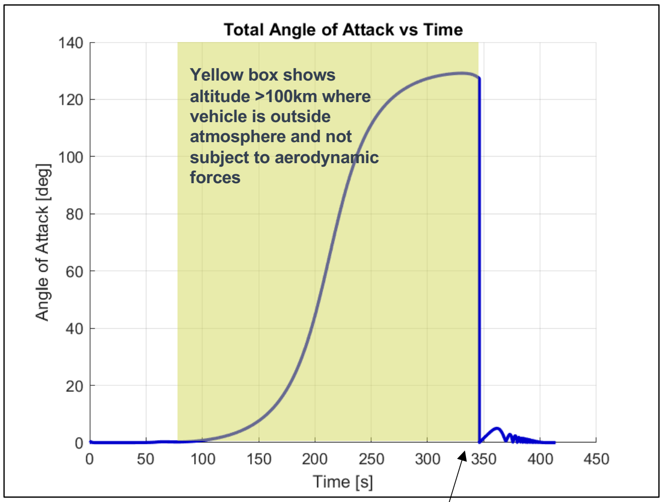

Yellow box shows altitude >100km where vehicle is outside atmosphere and not subject to aerodynamic forces

Total angle of attack was reset to 0 in TAOS problem file at 100 km descent altitude to represent Attitude Control

---

Static Margin

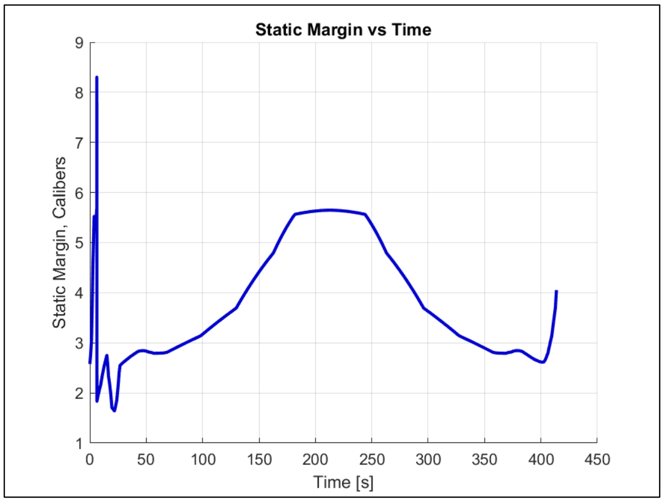

Boost

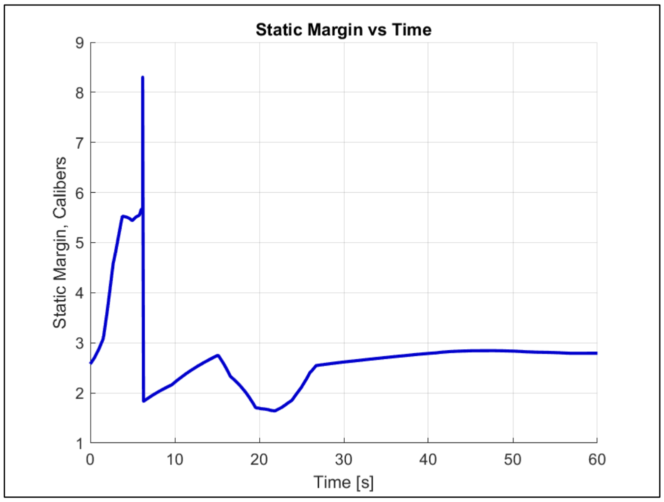

$$\text{Static Margin, Calibers} = \frac{X_{cg} - X_{cp}}{17.25''}$$

Body Rates

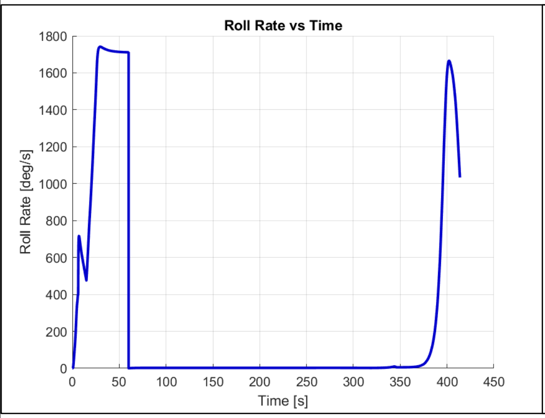
Roll Rate vs Time

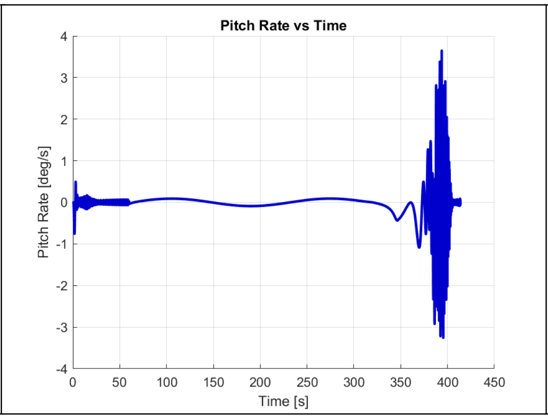
Pitch Rate vs Time

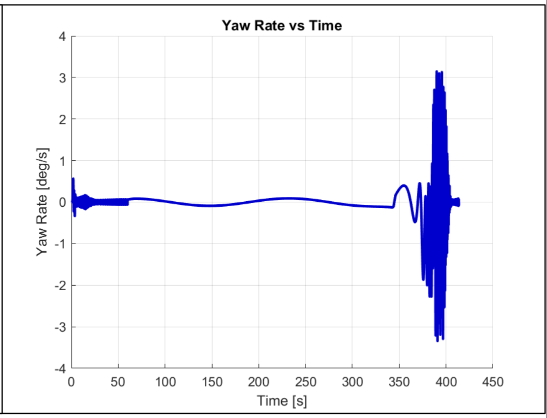
Yaw Rate vs Time

MC Parameters

MC Parameter	Units	Mean	1-sigma
Wind Vel	fps	0.0	2.50
Wind Direction	deg	90.0	90.0
Launch QE	deg	83.0	0.1667
Launch Azimuth	deg	105.0	0.6067
Struct Weight Delta	lb	0.0	10.0
Sustainer Ignition	sec	15.0	0.0333
Booster Impulse	%	1.0	0.01
Sustainer Impulse	%	1.0	0.0133
Booster Drag	%	-1.0	0.0333
Sustainer Drag	%	-1.0	0.0333
IM Fin Cant	min	25.0	0.333
T70 CG Offset – Y	ft	0.0	0.0064
T70 CG Offset – Z	ft	0.0	0.0064
Thrust Misalignment – Epsilon	deg	0.0	0.0667
Thrust Misalignment – Phi	deg	90.0	90.0

MC Parameters

MC Parameter	Units	Mean	1-sigma
T70 Thrust Offset – Y	ft	0.0	0.0064
T70 Thrust Offset - Z	ft	0.0	0.0064
T70 Fin Misalignment – Pitch	deg	0.0	0.06667
T70 Fin Misalignment – Yaw	deg	0.0	0.06667
IM CG Offset – Y	ft	0.0	0.0064
IM CG Offset – Z	ft	0.0	0.0064
IM Thrust Misalignment – Epsilon	ft	0.0	0.1
IM Thrust Misalignment – Phi	ft	90.0	90.0
IM Thrust Offset – Y	ft	0.0	0.0064
IM Thrust Offset – Z	ft	0.0	0.0064
IM Fin Misalignment – Pitch	deg	0.0	0.06667
IM Fin Misalignment – Yaw	deg	0.0	0.06667
Rail Exit Pitch Rate	dps	0.0	0.3333
Rail Exit Yaw Rate	dps	0.0	0.3333

JOHNS HOPKINS
APPLIED PHYSICS LABORATORY

BOLTII Reduced Drag Comparison

Hailey Palensky
Prasad Kutty

Reduced Drag

- Reduced second stage drag by 30%
  - Changed Sustainer Drag MC parameter from a mean of -1.0 to -0.7

BOLTII Timeline

	Original Nominal Time (s)	Original Nominal Alt (km)	Reduced Drag Nominal Time (s)	Reduced Drag Nominal Alt (km)
Target Launch	0.0	0.0	0.0	0.0
Stage 1 Burnout	6.00	2.31	6.00	2.31
Stage 1 Separation	6.20	2.47	6.20	2.47
Stage 2 Ignition	15.00	8.02	15.00	8.02
Stage 2 Burnout	26.73	20.01	26.73	20.01
Yoyo Despin	60.00	73.70	60.00	79.25
Apogee	212.89	182.00	228.39	209.61
100 km Descent (ACS Initiation)	346.01	100.0	382.87	100.0
Impact	413.76	0.0	443.13	0.0

Trajectory Shape

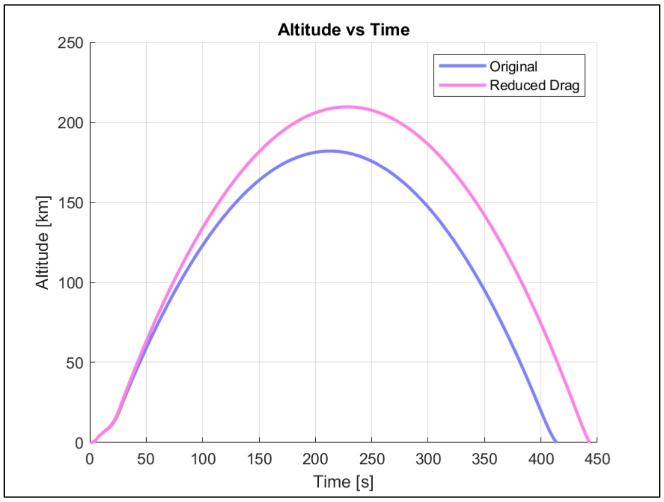
Altitude vs Time

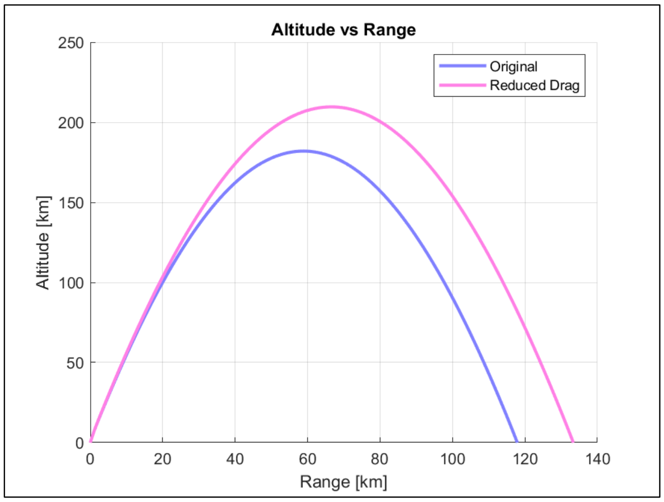
Altitude vs Range

	Original	Reduced Drag
Apogee	182.00 km	209.61 km

	Original	Reduced Drag
Range	117.88 km	133.35 km

Velocity and Mach

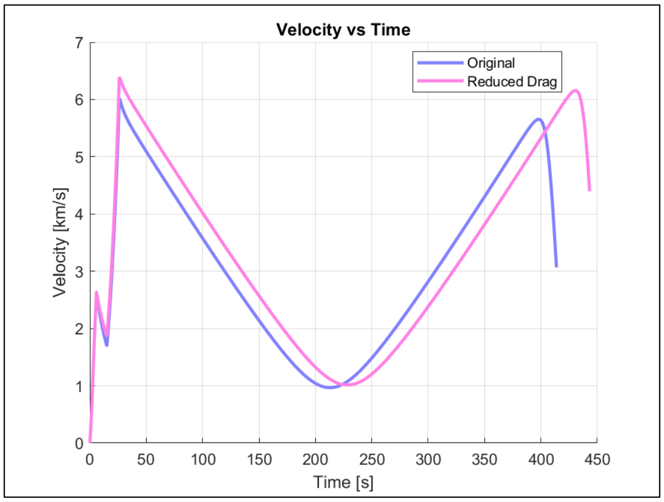
Velocity vs Time

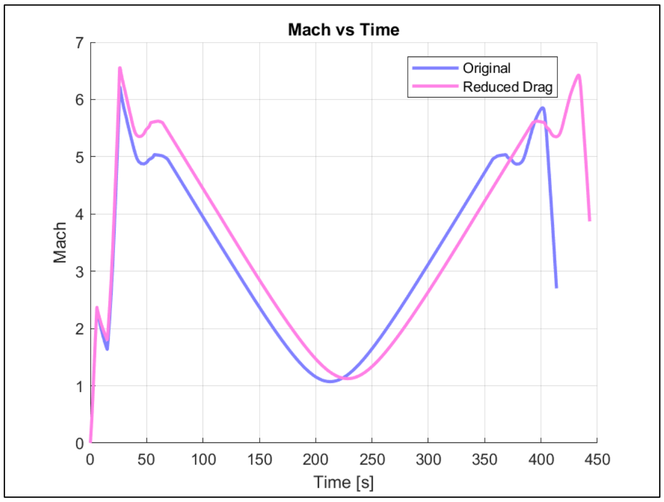
Mach vs Time

Attitude

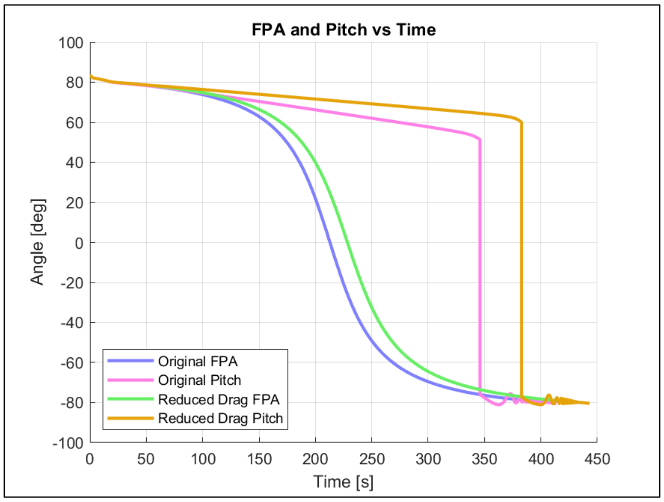

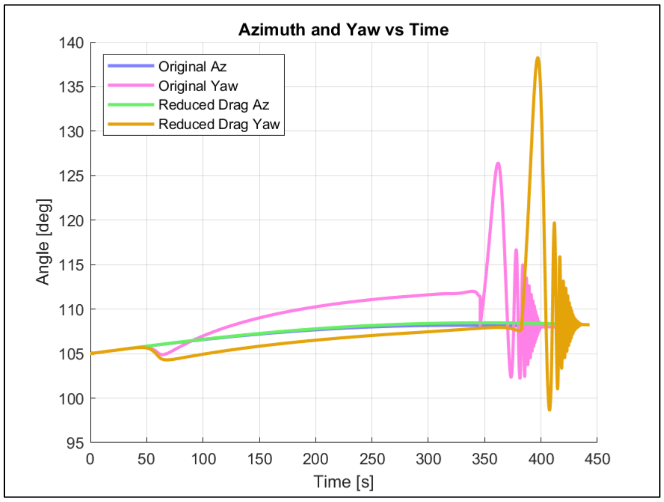

Angle of Attack

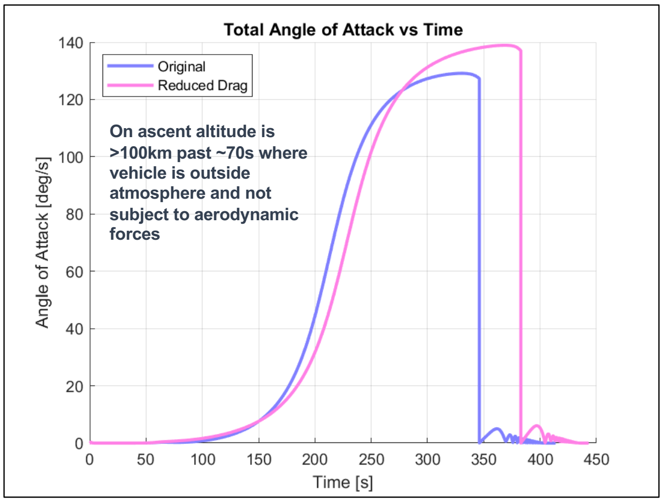

On ascent altitude is >100km past ~70s where vehicle is outside atmosphere and not subject to aerodynamic forces

Static Margin

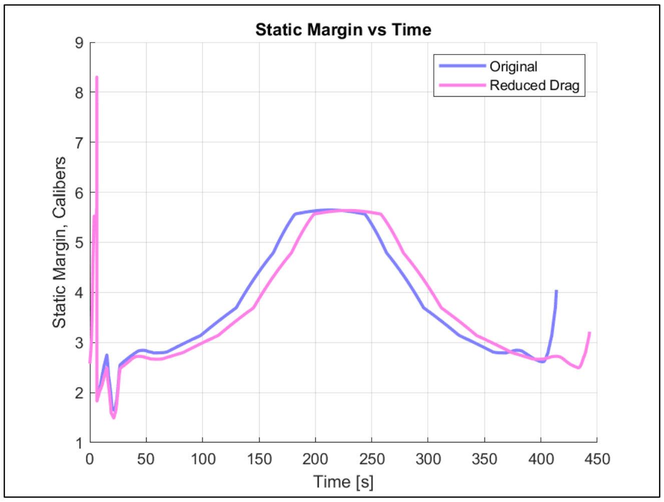

Boost

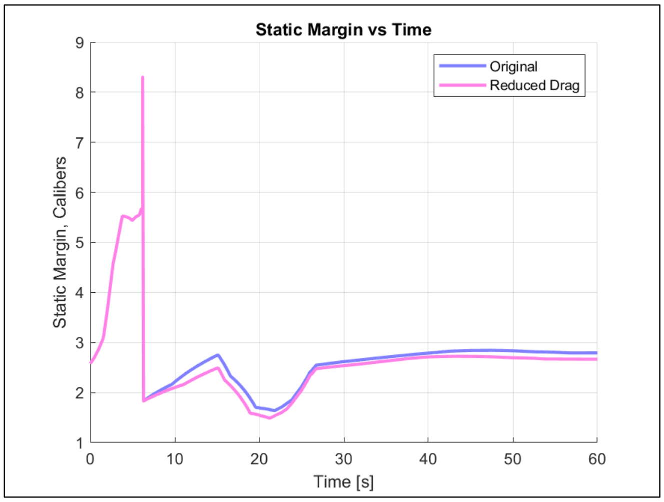

$$\text{Static Margin, Calibers} = \frac{\text{Xcg – Xcp}}{17.25''}$$

Body Rates

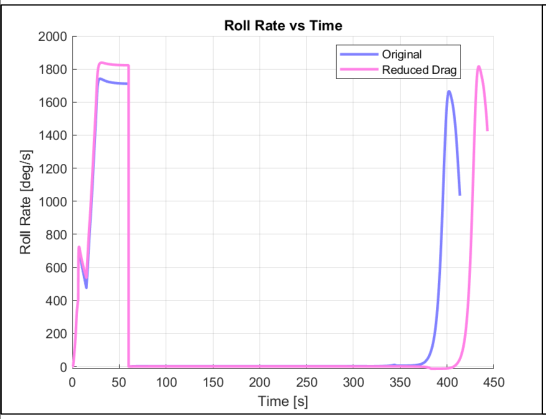

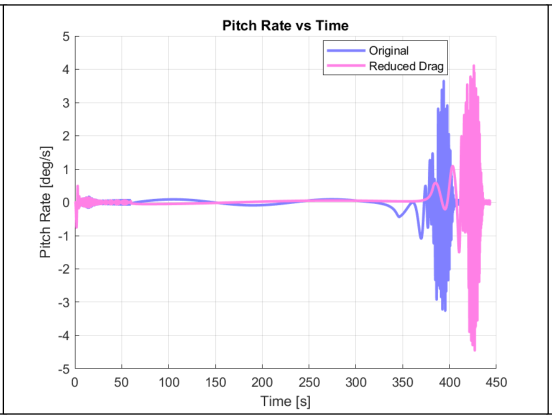

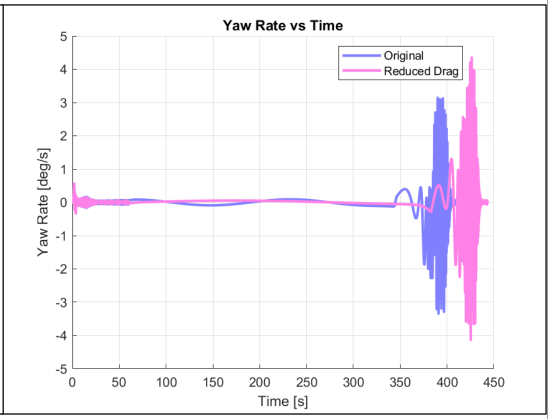

JOHNS HOPKINS
APPLIED PHYSICS LABORATORY

BOLTII TAOS 50 Run MC Trajectory Overview

Hailey Palensky
Prasad Kutty

MC Parameters

- Trajectory set includes 49 monte carlo runs and 1 nominal (50 total runs)

MC Parameter	Units	Mean	1-sigma
Wind Vel	fps	0.0	2.50σ
Wind Direction	deg	90.0	90.0σ
Launch QE	deg	83.0	0.1667σ
Launch Azimuth	deg	105.0	0.6067σ
Struct Weight Delta	lb	0.0	10.0σ
Sustainer Ignition	sec	15.0	0.0333σ
Booster Impulse	-	1.0	0.01σ
Sustainer Impulse	-	1.0	0.0133σ
Booster Drag	-	-1.0	0.0333σ
Sustainer Drag	-	-1.0	0.0333σ
IM Fin Cant	min	25.0	0.6667σ*
T70 CG Offset – Y	ft	0.0	0.0064σ
T70 CG Offset – Z	ft	0.0	0.0064σ
Thrust Misalignment – Epsilon	deg	0.0	0.0667σ
Thrust Misalignment – Phi	deg	90.0	90.0σ
T70 Thrust Offset – Y	ft	0.0	0.0064σ
T70 Thrust Offset - Z	ft	0.0	0.0064σ

* - Additional/Modified Aero Uncertainties

MC Parameters

MC Parameter	Units	Mean	1-sigma
T70 Fin Misalignment – Pitch	deg	0.0	0.06667σ
T70 Fin Misalignment – Yaw	deg	0.0	0.06667σ
IM CG Offset – Y	ft	0.0	0.0064σ
IM CG Offset – Z	ft	0.0	0.0064σ
IM Thrust Misalignment – Epsilon	deg	0.0	0.1σ
IM Thrust Misalignment – Phi	deg	90.0	90.0σ
IM Thrust Offset – Y	ft	0.0	0.0064σ
IM Thrust Offset – Z	ft	0.0	0.0064σ
IM Fin Misalignment – Pitch	deg	0.0	0.06667σ
IM Fin Misalignment – Yaw	deg	0.0	0.06667σ
Rail Exit Pitch Rate	dps	0.0	0.3333σ
Rail Exit Yaw Rate	dps	0.0	0.3333σ
T70 Fin Cant*	min	60.0	0.6667σ*
S1 Roll Damping*	-	1.0	0.1667σ*
S2 Roll Damping (First Coast)*	-	1.0	0.1667σ*
S2 Roll Damping (Remainder of Traj)*	-	0.8583	0.1667σ*

* - Additional/Modified Aero Uncertainties

Updated Aero Uncertainties

MC Parameter	Units	Mean	Original 1-sigma	New 1-sigma
IM Fin Cant	min	25.0	0.3333σ	0.6667σ
T70 Fin Cant	min	60.0	0.0σ	0.6667σ
S1 Roll Damping	-	1.0	0.0σ	0.1667σ
S2 Roll Damping (First Coast)	-	1.0	0.0σ	0.1667σ
S2 Roll Damping (Remainder of Traj)	-	0.8583	0.0σ	0.1667σ

Note: The stage 2 roll damping multiplier changed in the TAOS files through the phase of flight. The first coast period after separation used a multiplier of 1.0 and the remainder of the trajectory used a multiplier of 0.8583.

AUR/Stage 1 Aerodynamic Coefficient Buildups

- $C_X = C_{X0}(alt, Mach) * \sigma_{C_{D1}} + C_{X\alpha}(Mach) + C_{X\beta}(Mach)$
  - $\sigma_{C_{D1}}$ = Stage 1 Drag Uncertainty
- $C_Y = C_{Y0} + C_{Y\beta}(Mach)$
  - C_{Y0} = $-C_{N,Tail1}(Mach) * \xi_{Stage1} - C_{N,Tail2}(Mach) * \xi_{Stage2}$
  - ξ = Yaw Fin Misalignment
- $C_Z = C_{Z0} + C_{Z\alpha}(Mach)$
  - C_{Z0} = $-C_{N,Tail1}(Mach) * \zeta_{Stage1} - C_{N,Tail2}(Mach) * \zeta_{Stage2}$
  - ζ = Pitch Fin Misalignment
- $C_l = C_{l0}(Mach) * \theta_{Stage1} + C_{l,apha}(Mach) + C_{l,beta}(Mach) + C_{lp}(Mach)$
  - θ_{Stage1} = Stage 1 Fin Cant (constant value)
- $C_m = C_{m0} + C_{m,alpha}(Mach) + C_{mq}$
  - C_{m0} = $-C_{N,Tail1}(Mach) * \zeta_{Stage1} * (x_{cg} - x_{CP,Tail1}(Mach)) / l_{refx}$ + $-C_{N,Tail2}(Mach) * \zeta_{Stage2} * (x_{cg} - x_{CP,Tail2}(Mach)) / l_{refx}$
  - C_{mq} = $-2 * [C_{N,Tail1}(Mach) * (x_{cg} - x_{CP,Tail1}(Mach))^2] / l_{refx}^2$ + $-2 * [C_{N,Tail2}(Mach) * (x_{cg} - x_{CP,Tail2}(Mach))^2] / l_{refx}^2$
- $C_n = C_{n0} + C_{n,beta}(Mach) + C_{nr}$
  - C_{n0} = $C_{N,Tail2}(Mach) * \xi_{Stage2} * (x_{cg} - x_{CP,Tail2}(Mach)) / l_{refx}$
  - $C_{nr} = C_{mq}$

- **Denote MC parameters:**
  - $\sigma_{C_{D1}}$ = Stage 1 Drag Uncertainty
  - ξ = Yaw Fin Misalignment (Stage 1 and 2)
  - ζ = Pitch Fin Misalignment (Stage 1 and 2)
  - θ_{Stage1} = NOT DISPERSED for Stage 1

Denote look-up tables in TAOS

Stage 2 Aerodynamic Coefficient Buildups

- $C_X = C_{X0}(alt, Mach) * \sigma_{C_{D2}} + C_{X\alpha}(Mach) + C_{X\beta}(Mach)$
  - CX0(alt, Mach) exist for both coasting and thrusting
  - $\sigma_{C_{D2}}$ = Stage 2 Drag Uncertainty
- $C_Y = C_{Y0} + C_{Y\beta}(Mach)$
  - C_{Y0} = $- C_{N,Tail2}(Mach) * \xi_{Stage2}$
  - ξ = Yaw Fin Misalignment
- $C_Z = C_{Z0} + C_{Z\alpha}(Mach)$
  - C_{Z0} =$- C_{N,Tail2}(Mach) * \zeta_{Stage2}$
  - ζ = Pitch Fin Misalignment
- $C_l = C_{l0}(Mach) * \theta_{Stage2} + C_{l,apha}(Mach) + C_{l,beta}(Mach) + C_{lp}(Mach) * \theta_{Stage2}$
  - θ_{Stage2} = Stage 2 Fin Cant
- $C_m = C_{m0} + C_{m,alpha}(Mach) + C_{mq}$
  - C_{m0} = $-C_{N,Tail2}(Mach) * \zeta_{Stage2} * (x_{cg} - x_{CP,Tail2}(Mach)) / l_{refx}$
  - C_{mq} = $-2* [C_{N,Tail2}(Mach) * (x_{cg} - x_{CP,Tail2}(Mach))^2] / l_{refx}^2$
- $C_n = C_{n0} + C_{n,beta}(Mach) + C_{nr}$
  - C_{n0} = $C_{N,Tail2}(Mach) * \xi_{Stage2} * (x_{cg} - x_{CP,Tail2}(Mach)) / l_{refx}$
  - $C_{nr} = C_{mq}$

- **Denote MC parameters:**
  - $\sigma_{C_{D2}}$ = Stage 2 Drag Uncertainty
  - ξ = Yaw Fin Misalignment
  - ζ = Pitch Fin Misalignment
  - θ_{Stage2} = Fin Cant

Denote look-up tables in TAOS

Run #8

- Run #8 showed outlier behavior and became unstable in flight

MC Parameter	Units	Mean	1-sigma	Run #8 value	Run #8 sigma
IM Fin Cant	min	25.0	0.6667σ	24.379	0.9312σ
T70 Fin Cant	min	60.0	0.6667σ	60.112	0.1694σ
S1 Roll Damping	-	1.0	0.1667σ	0.7927	1.2439σ
S2 Roll Damping (First Coast)	-	1.0	0.1667σ	1.0870	0.5218σ
S2 Roll Damping (Remainder of Traj)	-	0.8583	0.1667σ	1.1864	1.968σ

- Run 8 additional aero MC parameters are well within 3-sigma

---

BOLTII Timeline

	Early (s)	Nominal Time (s)	Nominal Alt (km)	Late (s)	Run #8 Time (s)
Target Launch	0.0	0.0	0.0	0.0	0.0
Stage 1 Burnout	6.00	6.00	2.31	6.00	6.00
Stage 1 Separation	6.20	6.20	2.47	6.20	6.20
Stage 2 Ignition	14.93	15.00	8.02	15.09	14.98
Stage 2 Burnout	26.66	26.73	20.01	26.82	26.71
Yoyo Despin	60.00	60.00	73.70	60.00	60.00
Apogee	204.00	213.00	182.00	223.17	145.80
100 km Descent (ACS Initiation)	323.85	346.01	100.0	370.60	N/A
Impact	396.67	413.76	0.0	433.59	296.74

Note: Early and Late start times do not include Run #8

CONOPS

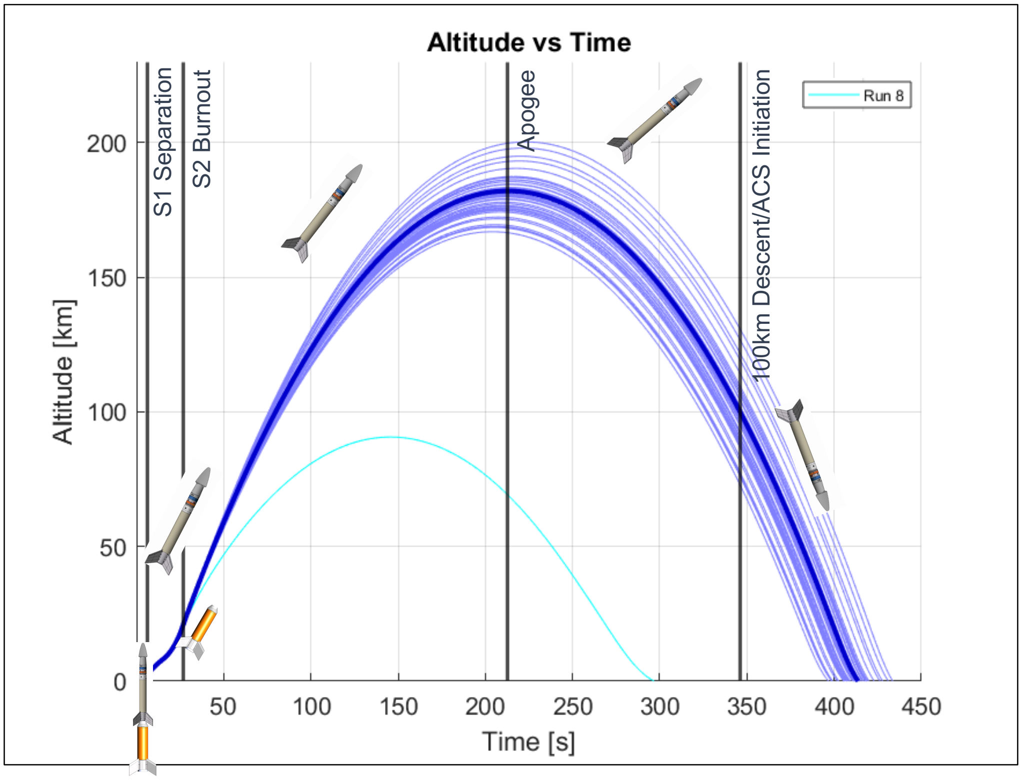

Trajectory Shape

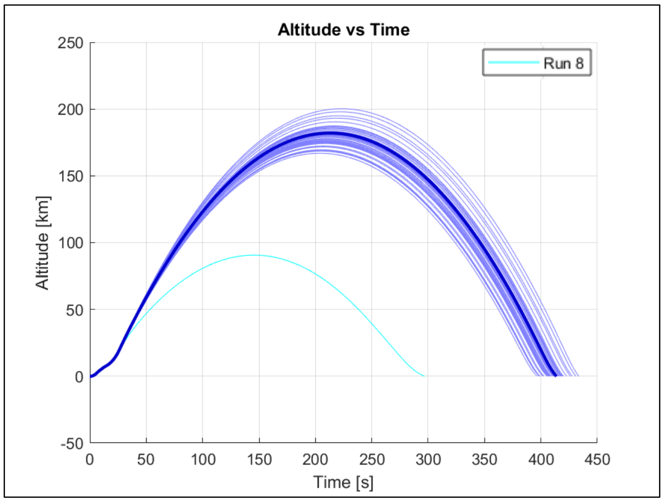

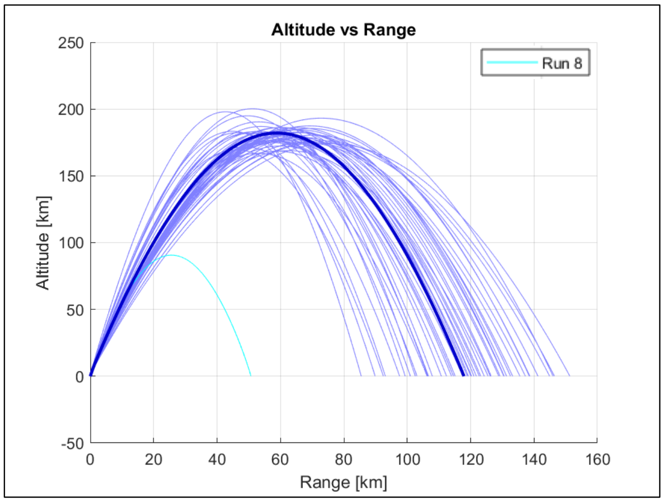

Velocity and Mach

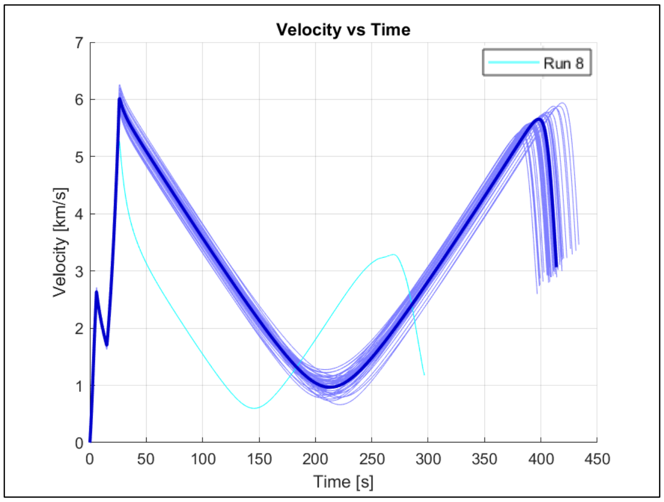

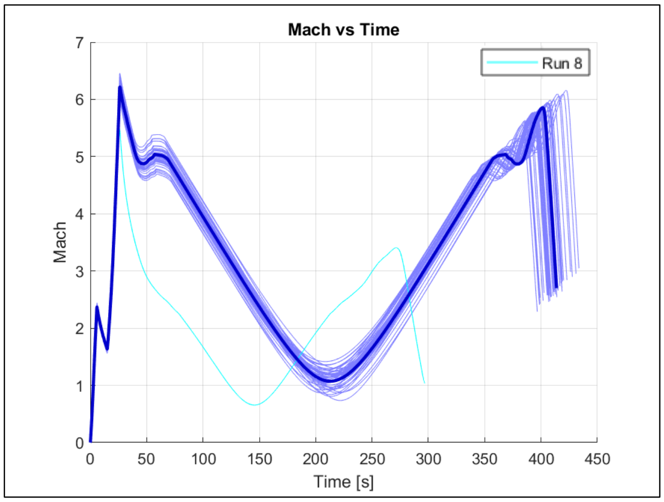

Attitude

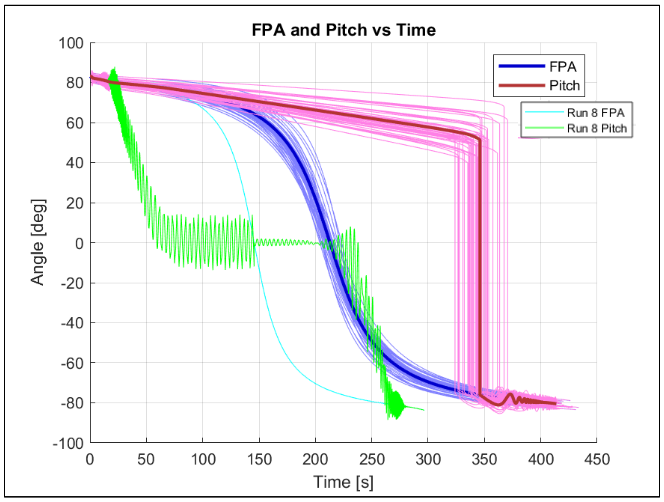

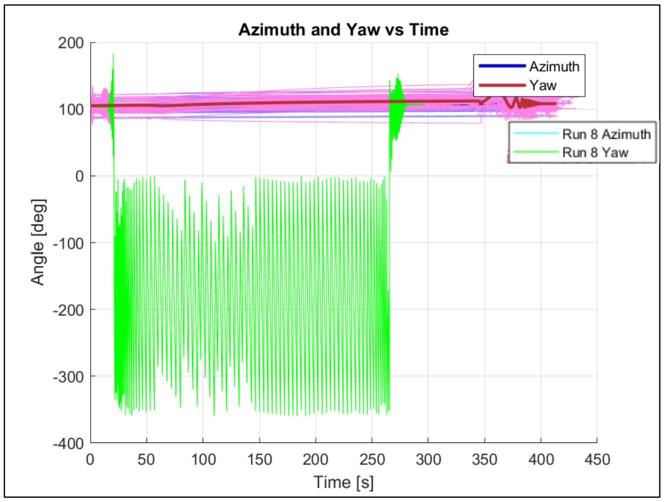

Angle of Attack

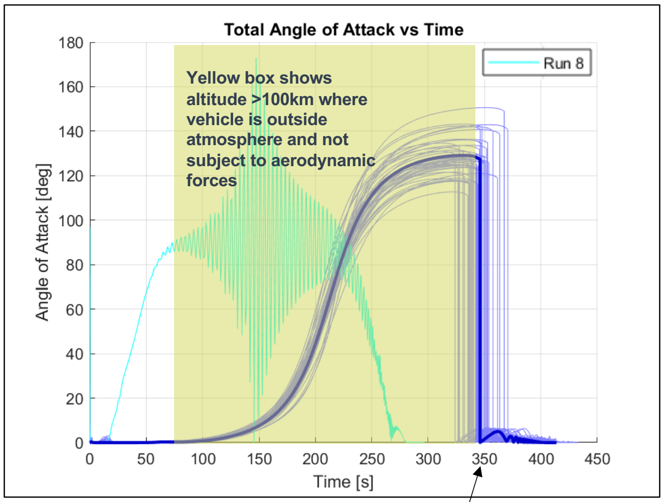

Yellow box shows altitude >100km where vehicle is outside atmosphere and not subject to aerodynamic forces

Boost

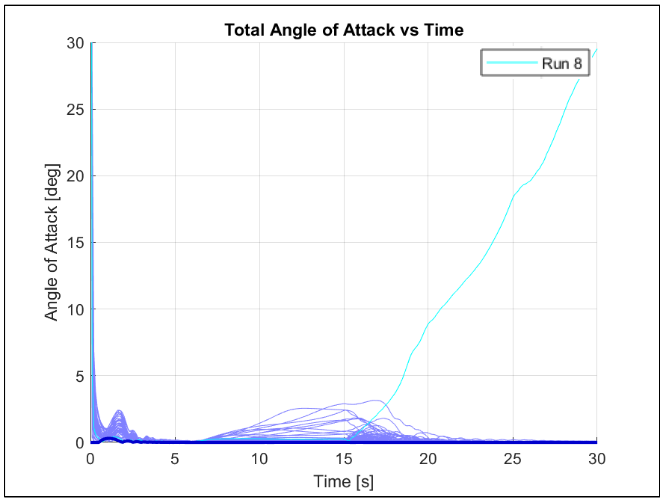

Total angle of attack was reset to 0 in TAOS problem file at 100 km descent altitude to represent Attitude Control

---

Static Margin

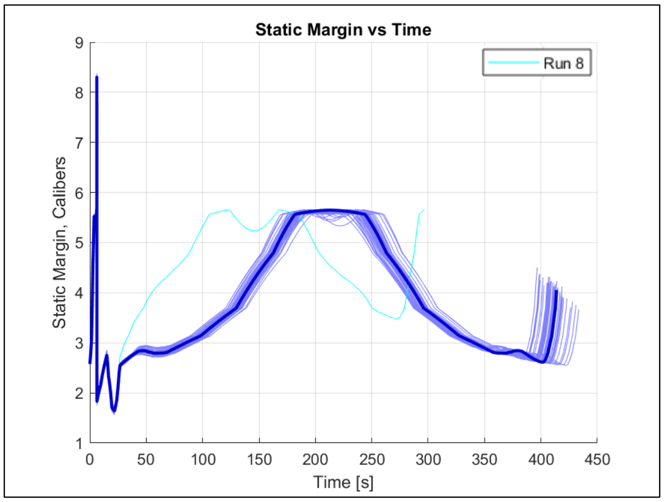

Boost

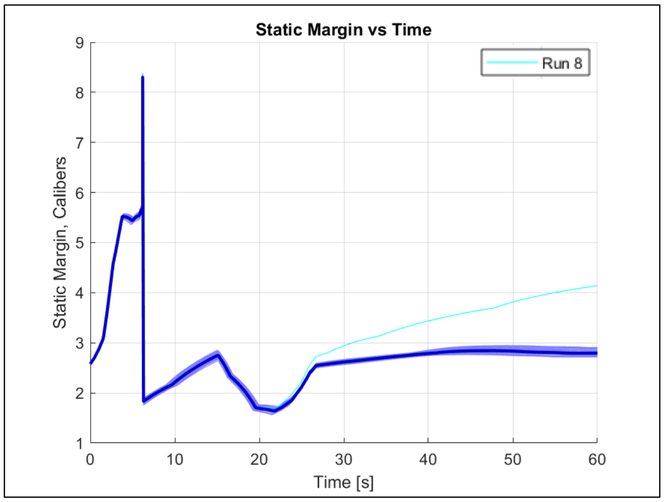

$$\text{Static Margin, Calibers} = \frac{X_{cg} - X_{cp}}{17.25''}$$

Body Rates

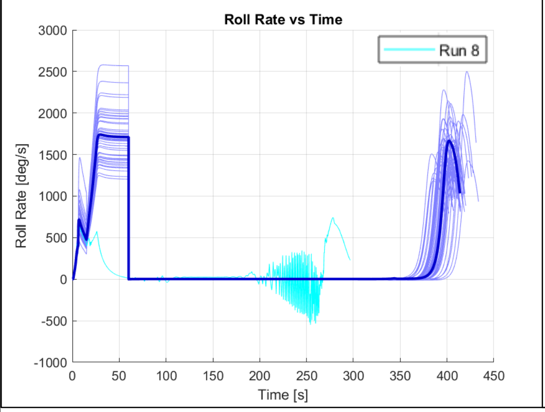

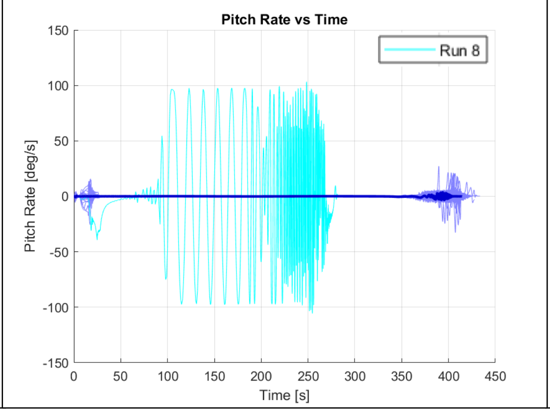

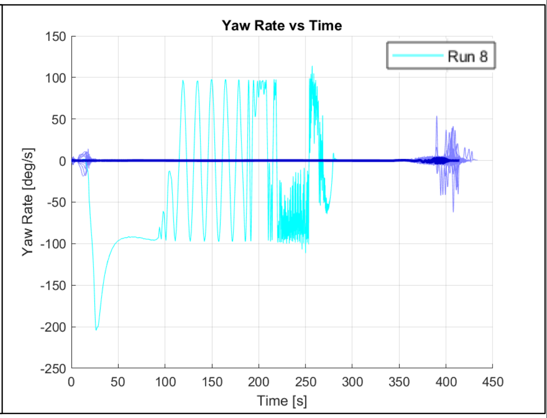

Roll-Pitch Coupling

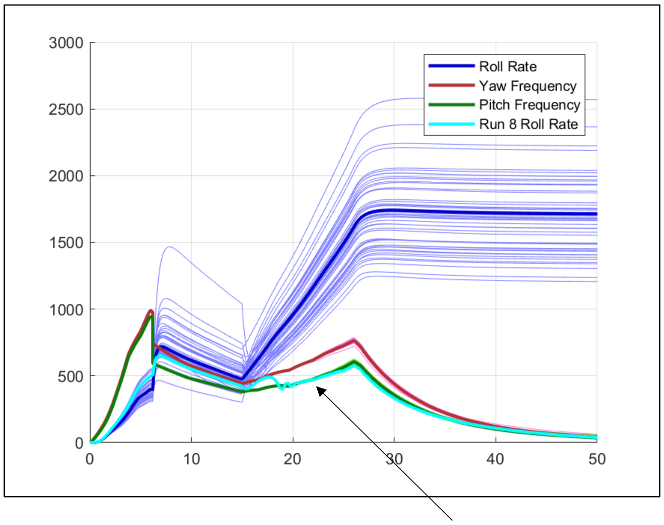

Run 8

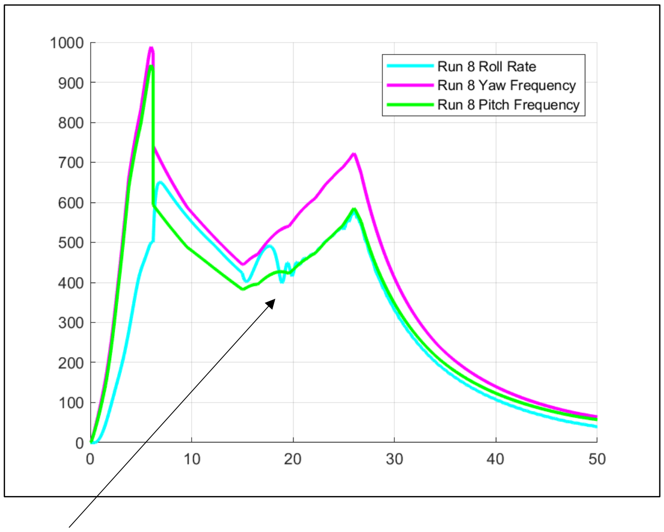

Run 8 roll rate aligns with its pitch frequency for the remainder of the trajectory and becomes unstable

JOHNS HOPKINS
APPLIED PHYSICS LABORATORY

BOLTII TAOS 50 Run MC Trajectory Overview with Increased S1 Fin Cant

Hailey Palensky
Prasad Kutty

MC Parameters

- Trajectory set includes 49 monte carlo runs and 1 nominal (50 total runs)

MC Parameter	Units	Mean	1-sigma
Wind Vel	fps	0.0	2.50σ
Wind Direction	deg	90.0	90.0σ
Launch QE	deg	83.0	0.1667σ
Launch Azimuth	deg	105.0	0.6067σ
Struct Weight Delta	lb	0.0	10.0σ
Sustainer Ignition	sec	15.0	0.0333σ
Booster Impulse	-	1.0	0.01σ
Sustainer Impulse	-	1.0	0.0133σ
Booster Drag	-	-1.0	0.0333σ
Sustainer Drag	-	-1.0	0.0333σ
IM Fin Cant	min	25.0	0.6667σ*
T70 CG Offset – Y	ft	0.0	0.0064σ
T70 CG Offset – Z	ft	0.0	0.0064σ
Thrust Misalignment – Epsilon	deg	0.0	0.0667σ
Thrust Misalignment – Phi	deg	90.0	90.0σ
T70 Thrust Offset – Y	ft	0.0	0.0064σ
T70 Thrust Offset - Z	ft	0.0	0.0064σ

* - Additional/Modified Aero Uncertainties

MC Parameters

MC Parameter	Units	Mean	1-sigma
T70 Fin Misalignment – Pitch	deg	0.0	0.06667σ
T70 Fin Misalignment – Yaw	deg	0.0	0.06667σ
IM CG Offset – Y	ft	0.0	0.0064σ
IM CG Offset – Z	ft	0.0	0.0064σ
IM Thrust Misalignment – Epsilon	deg	0.0	0.1σ
IM Thrust Misalignment – Phi	deg	90.0	90.0σ
IM Thrust Offset – Y	ft	0.0	0.0064σ
IM Thrust Offset – Z	ft	0.0	0.0064σ
IM Fin Misalignment – Pitch	deg	0.0	0.06667σ
IM Fin Misalignment – Yaw	deg	0.0	0.06667σ
Rail Exit Pitch Rate	dps	0.0	0.3333σ
Rail Exit Yaw Rate	dps	0.0	0.3333σ
T70 Fin Cant*	min	120.0	0.6667σ*
S1 Roll Damping*	-	1.0	0.1667σ*
S2 Roll Damping (First Coast)*	-	1.0	0.1667σ*
S2 Roll Damping (Remainder of Traj)*	-	0.8583	0.1667σ*

* - Additional/Modified Aero Uncertainties

Updated Aero Uncertainties

MC Parameter	Units	Mean	Original 1-sigma	New 1-sigma
IM Fin Cant	min	25.0	0.3333σ	0.6667σ
T70 Fin Cant	min	120.0*	0.0σ	0.6667σ
S1 Roll Damping	-	1.0	0.0σ	0.1667σ
S2 Roll Damping (First Coast)	-	1.0	0.0σ	0.1667σ
S2 Roll Damping (Remainder of Traj)	-	0.8583	0.0σ	0.1667σ

Note: The stage 2 roll damping multiplier changed in the TAOS files through the phase of flight. The first coast period after separation used a multiplier of 1.0 and the remainder of the trajectory used a multiplier of 0.8583.

*Based on parametric study about unstable run (Run #8) in previous MC trajectory set

AUR/Stage 1 Aerodynamic Coefficient Buildups

- $C_X = C_{X0}(\text{alt, Mach}) * \sigma_{C_{D1}} + C_{X\alpha}(\text{Mach}) + C_{X\beta}(\text{Mach})$
  - $\sigma_{C_{D1}}$ = Stage 1 Drag Uncertainty
- $C_Y = C_{Y0} + C_{Y\beta}(\text{Mach})$
  - $C_{Y0} = -C_{N,Tail1}(\text{Mach}) * \xi_{Stage1} - C_{N,Tail2}(\text{Mach}) * \xi_{Stage2}$
  - ξ = Yaw Fin Misalignment
- $C_Z = C_{Z0} + C_{Z\alpha}(\text{Mach})$
  - $C_{Z0} = -C_{N,Tail1}(\text{Mach}) * \zeta_{Stage1} - C_{N,Tail2}(\text{Mach}) * \zeta_{Stage2}$
  - ζ = Pitch Fin Misalignment
- **Denote MC parameters:**
  - $\sigma_{C_{D1}}$ = Stage 1 Drag Uncertainty
  - ξ = Yaw Fin Misalignment (Stage 1 and 2)
  - ζ = Pitch Fin Misalignment (Stage 1 and 2)
  - θ_{Stage1} = NOT DISPERSED for Stage 1
- $C_l = C_{l0}(\text{Mach}) * \theta_{Stage1} + C_{l,apha}(\text{Mach}) + C_{l,beta}(\text{Mach}) + C_{lp}(\text{Mach})$
  - θ_{Stage1} = Stage 1 Fin Cant (constant value)
- $C_m = C_{m0} + C_{m,alpha}(\text{Mach}) + C_{mq}$
  - $C_{m0} = -C_{N,Tail1}(\text{Mach}) * \zeta_{Stage1} * (x_{cg} - x_{CP,Tail1}(\text{Mach})) / l_{refx} + -C_{N,Tail2}(\text{Mach}) * \zeta_{Stage2} * (x_{cg} - x_{CP,Tail2}(\text{Mach})) / l_{refx}$
  - $C_{mq} = -2 * [C_{N,Tail1}(\text{Mach}) * (x_{cg} - x_{CP,Tail1}(\text{Mach}))^2] / l_{refx}^2 + -2 * [C_{N,Tail2}(\text{Mach}) * (x_{cg} - x_{CP,Tail2}(\text{Mach}))^2] / l_{refx}^2$
- $C_n = C_{n0} + C_{n,beta}(\text{Mach}) + C_{nr}$
  - $C_{n0} = C_{N,Tail2}(\text{Mach}) * \xi_{Stage2} * (x_{cg} - x_{CP,Tail2}(\text{Mach})) / l_{refx}$
  - $C_{nr} = C_{mq}$

Denote look-up tables in TAOS

Stage 2 Aerodynamic Coefficient Buildups

- $C_X = C_{X0}(\text{alt, Mach}) * \sigma_{C_{D2}} + C_{X\alpha}(\text{Mach}) + C_{X\beta}(\text{Mach})$
  - CX0(alt, Mach) exist for both coasting and thrusting
  - $\sigma_{C_{D2}}$ = Stage 2 Drag Uncertainty
- $C_Y = C_{Y0} + C_{Y\beta}(\text{Mach})$
  - $C_{Y0} = - C_{N,Tail2}(\text{Mach}) * \xi_{Stage2}$
  - ξ = Yaw Fin Misalignment
- $C_Z = C_{Z0} + C_{Z\alpha}(\text{Mach})$
  - $C_{Z0} = - C_{N,Tail2}(\text{Mach}) * \zeta_{Stage2}$
  - ζ = Pitch Fin Misalignment
- **Denote MC parameters:**
  - $\sigma_{C_{D2}}$ = Stage 2 Drag Uncertainty
  - ξ = Yaw Fin Misalignment
  - ζ = Pitch Fin Misalignment
  - θ_{Stage2} = Fin Cant
- $C_l = C_{l0}(\text{Mach}) * \theta_{Stage2} + C_{l,apha}(\text{Mach}) + C_{l,beta}(\text{Mach}) + C_{lp}(\text{Mach}) * \theta_{Stage2}$
  - θ_{Stage2} = Stage 2 Fin Cant
- $C_m = C_{m0} + C_{m,alpha}(\text{Mach}) + C_{mq}$
  - $C_{m0} = -C_{N,Tail2}(\text{Mach}) * \zeta_{Stage2} * (x_{cg} - x_{CP,Tail2}(\text{Mach})) / l_{refx}$
  - $C_{mq} = -2 * [C_{N,Tail2}(\text{Mach}) * (x_{cg} - x_{CP,Tail2}(\text{Mach}))^2] / l_{refx}^2$
- $C_n = C_{n0} + C_{n,beta}(\text{Mach}) + C_{nr}$
  - $C_{n0} = C_{N,Tail2}(\text{Mach}) * \xi_{Stage2} * (x_{cg} - x_{CP,Tail2}(\text{Mach})) / l_{refx}$
  - $C_{nr} = C_{mq}$

Denote look-up tables in TAOS

BOLTII Timeline

	Early (s)	Nominal Time (s)	Nominal Alt (km)	Late (s)
Target Launch	0.0	0.0	0.0	0.0
Stage 1 Burnout	6.00	6.00	2.31	6.00
Stage 1 Separation	6.20	6.20	2.47	6.20
Stage 2 Ignition	14.93	15.00	8.02	15.09
Stage 2 Burnout	26.66	26.73	20.01	26.82
Yoyo Despin	60.00	60.00	73.70	60.00
Apogee	204.00	213.00	182.00	223.17
100 km Descent (ACS Initiation)	323.85	346.01	100.0	370.60
Impact	396.67	413.76	0.0	433.59

- The timeline did not change between the two MC sets
- Total range value increased slightly from 117.88 km to 117.92 km

---

CONOPS

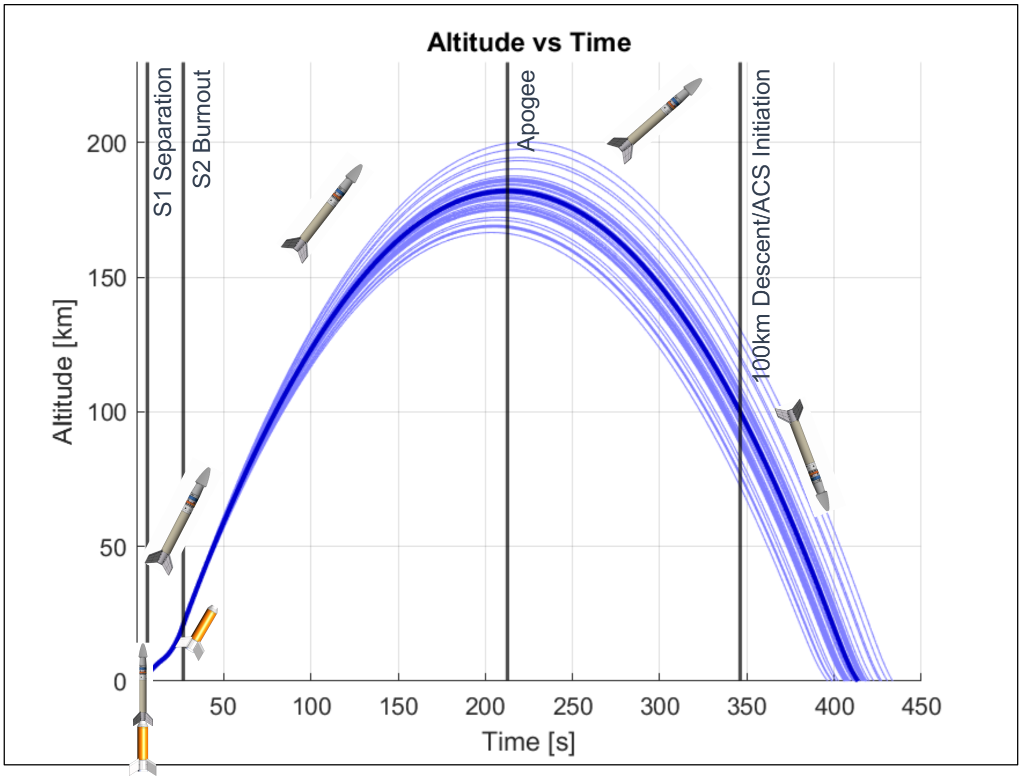

Trajectory Shape

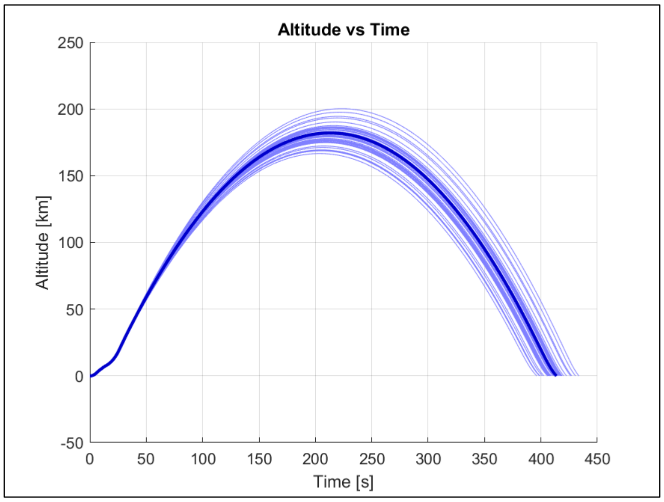

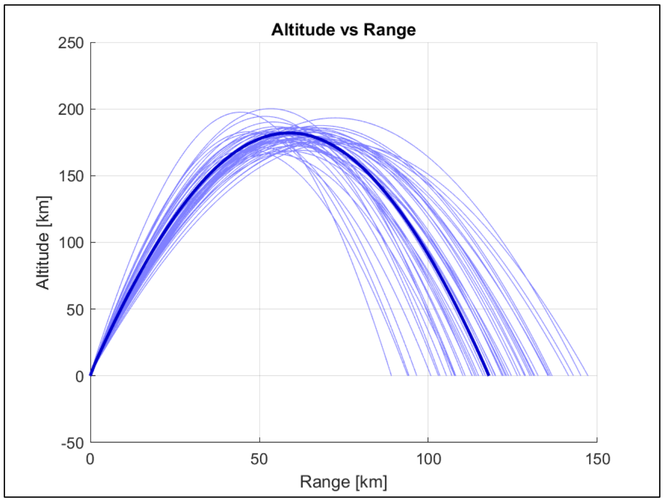

Velocity and Mach

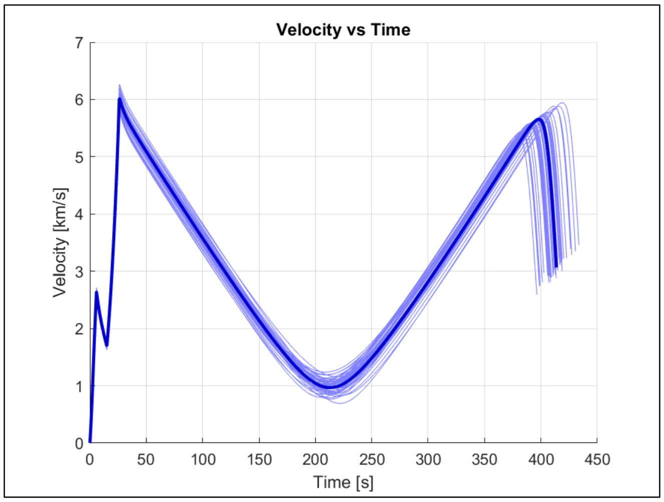

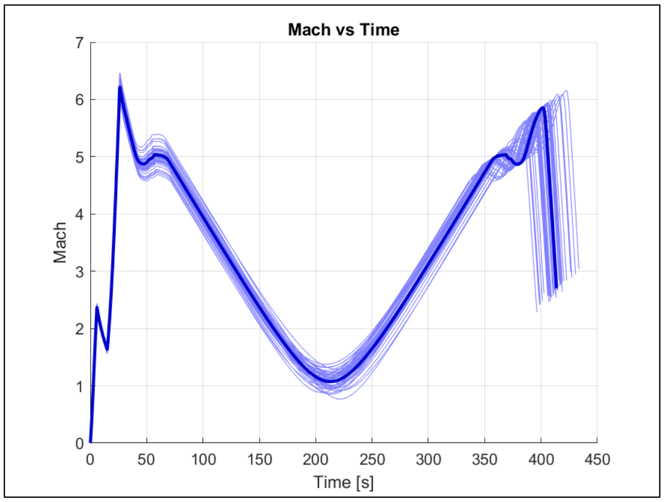

Attitude

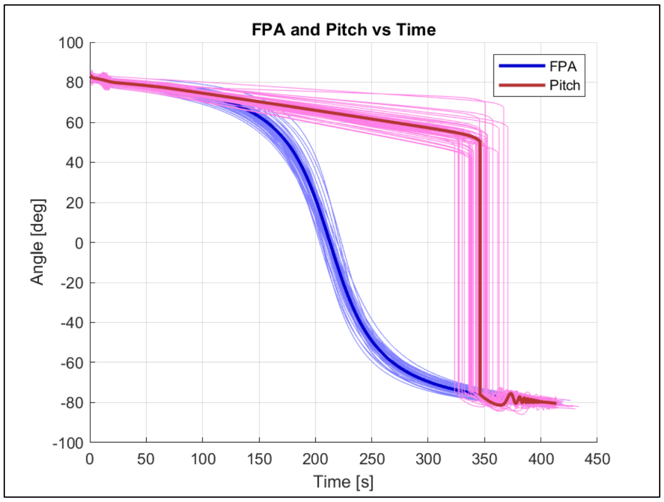

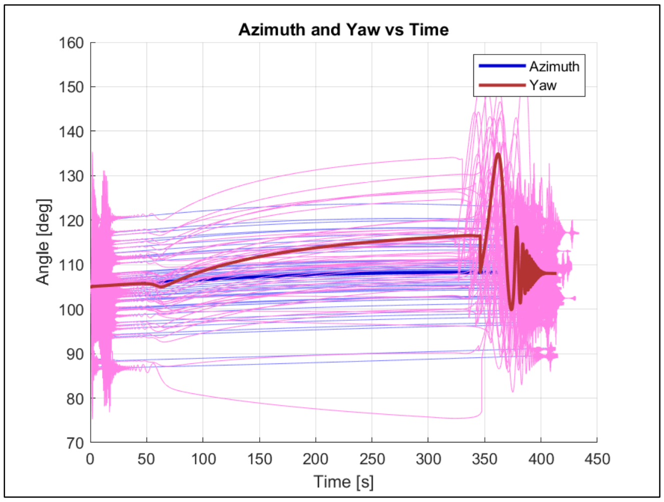

Angle of Attack

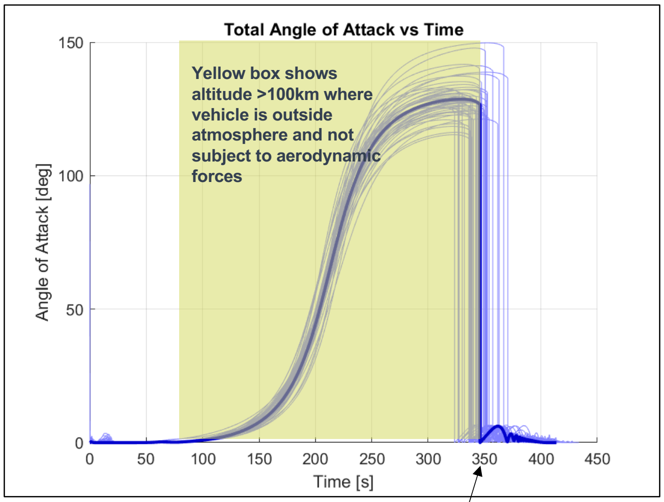

Yellow box shows altitude >100km where vehicle is outside atmosphere and not subject to aerodynamic forces

Total angle of attack was reset to 0 in TAOS problem file at 100 km descent altitude to represent Attitude Control

Boost

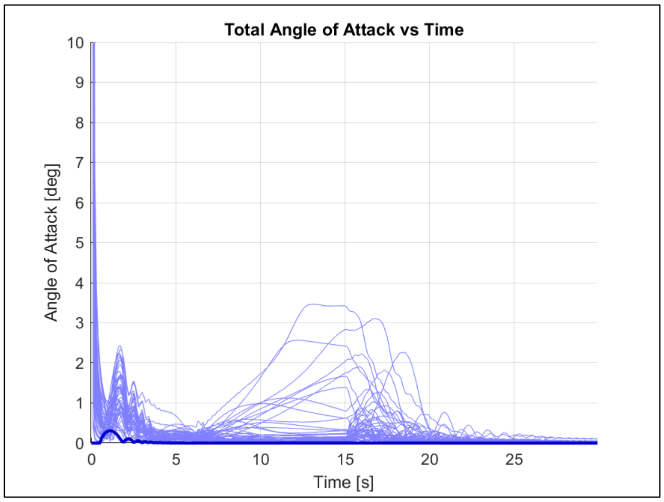

Static Margin

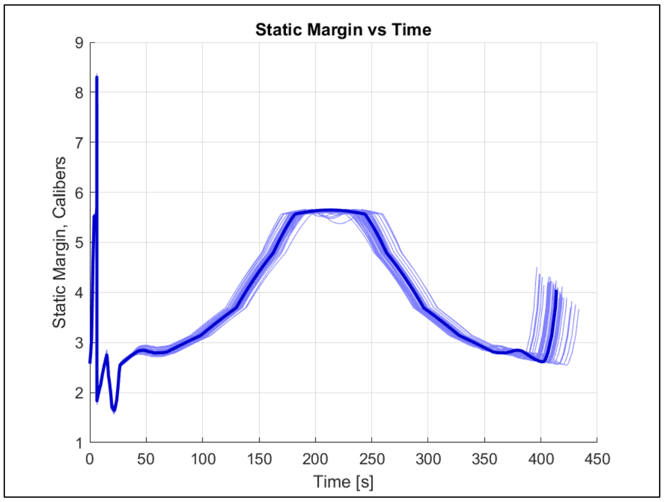

Boost

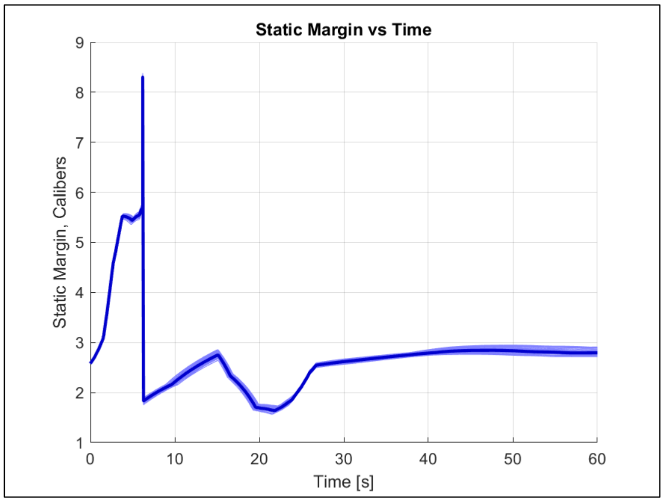

$$\text{Static Margin, Calibers} = \frac{\text{Xcg – Xcp}}{\text{17.25”}}$$

Body Rates

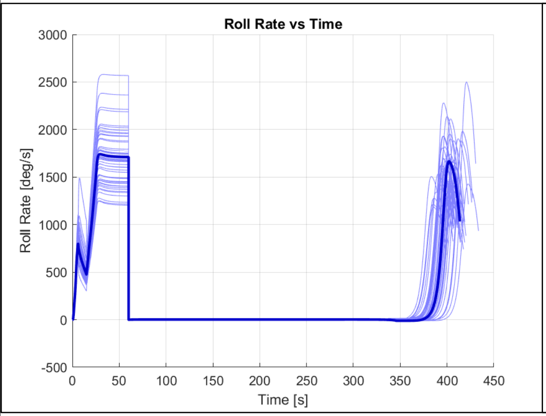

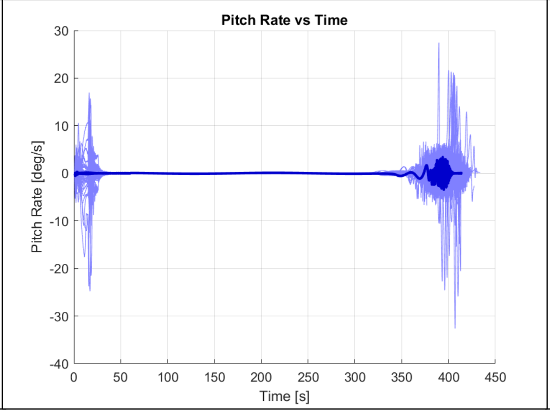

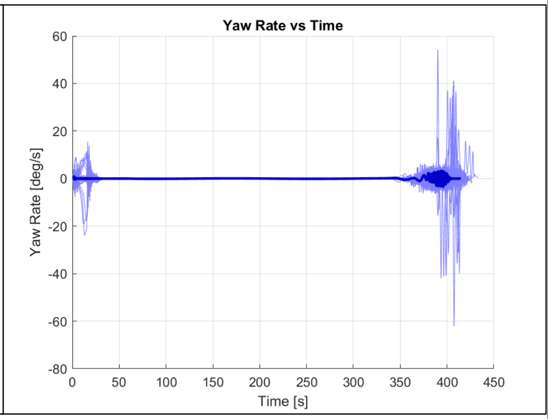

Roll-Pitch Coupling

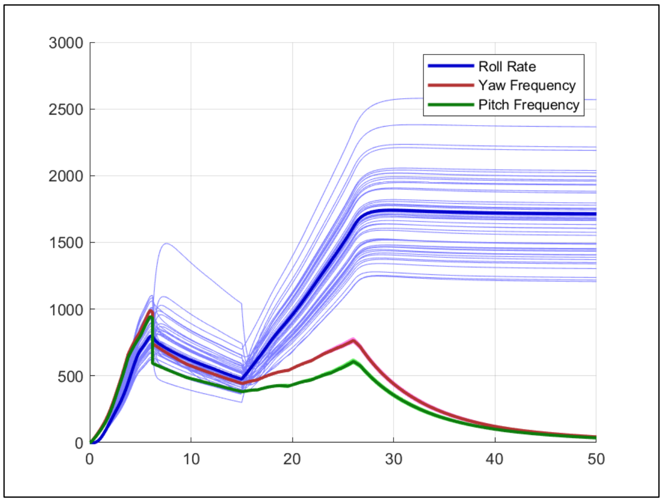

No runs exhibit unstable behavior with increased Stage 1 Fin Cant

A.2. BOLT II PDR Thermal Analysis

The following appendix contains details of the thermal analysis JHU/APL conducted for the BOLT II Preliminary Design Review (PDR).

JOHNS HOPKINS
APPLIED PHYSICS LABORATORY

This work was supported by the Air Force Office of Scientific Research under award number FA9550-20-1-0043 (PO: Dr. Sarah Popkin). Any opinions, finding, and conclusions or recommendations expressed in this material are those of the author(s) and do not necessarily reflect the views of the United States Air Force.

BOLT2 Holden Mission: CFD-Based Thermal Analysis for PDR

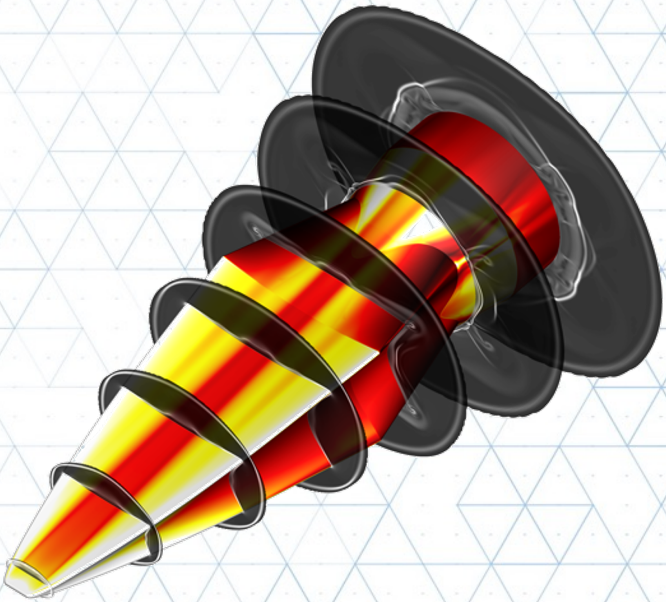

Brad Wheaton (JHU/APL)
Aaron Dufrene (CUBRC)
Daniel Mullen (Texas A&M)

BOLT2 Preliminary Design Review (PDR) Thermal Analysis

- Objective: Provide an initial transient thermal analysis using viscous CFD based heating to guide materials selection for BOLT2 Holden Mission
- Intention is that further thermal analysis will be performed ahead of CDR for any significant changes in trajectory and vehicle outer mold line (OML)
- Significant assumptions and details are provided in these slides, and the results should be verified prior to finalizing design

Background: BOLT Thermal Work

Background: BOLT Thermal Work

- JHU/APL performed several rounds of thermal analysis for the BOLT flight supporting design work for CoDR, PDR, and eventually CDR
- Initial results from correlation-based models performed for CoDR
- Viscous-based CFD with full transitional flow modeling used for refined thermal model at PDR to close material choices
    - Anchored with CUBRC wind tunnel data
    - Various additional quality checks performed on the CFD-based heating rates (i.e. comparison to independent calculations)
- Also developed multiple thermal modeling processes using different codes for the transient analysis (MSLRAD/ATLAS, CFD++)
- Able to leverage existing grids, tools, knowledge base from BOLT to apply to quick-turnaround BOLT2 analyses!

BOLT CFD Methods

- Developed full structured hexahedral cell grid for BOLT
- 17M cells for ¼ geometry
- Fine wall spacing determined for BOLT trajectory (0.7 microns, 3e-5 in.) enables y+ < 0.5 over most flow conditions for BOLT
- Metacomp CFD++ finite volume flow solver used for all CFD solutions:
  - Second order spatial discretization
  - Laminar, tripped, and fully turbulent cases all were run
  - 1-equation Spalart-Allmaras turbulence model chosen for all turbulent heating rates (due to efficiency and compatibility with tripping locations)

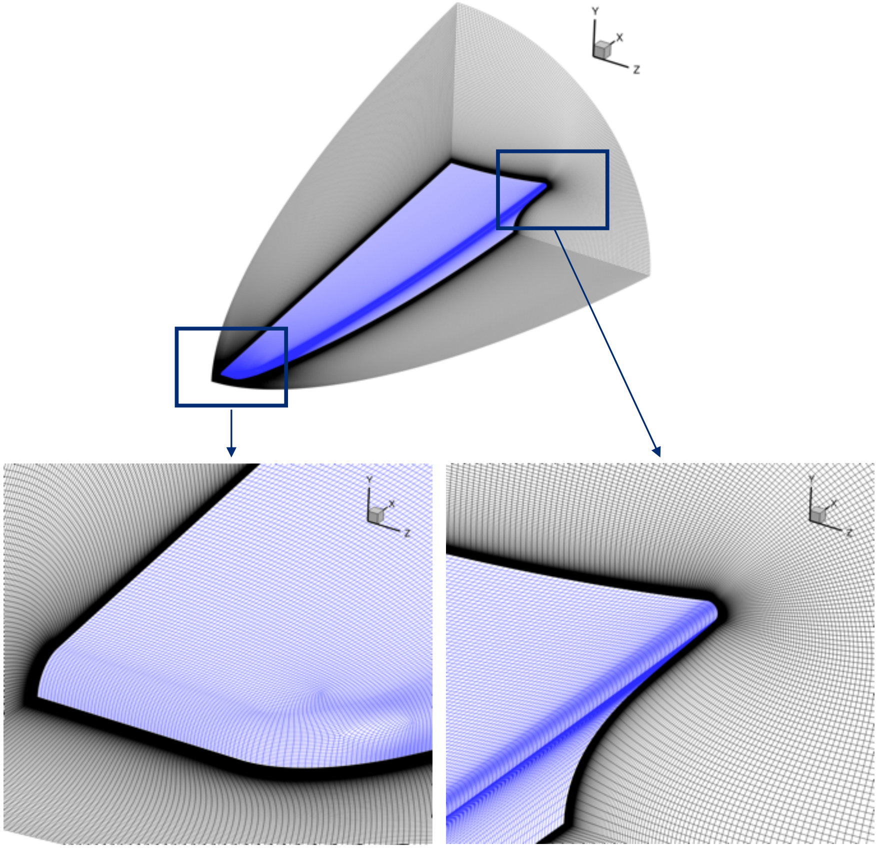

BOLT CUBRC Results Used to Validate CFD Heating Predictions

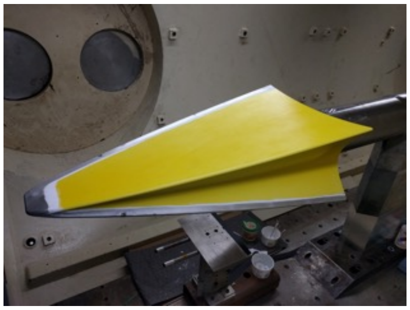

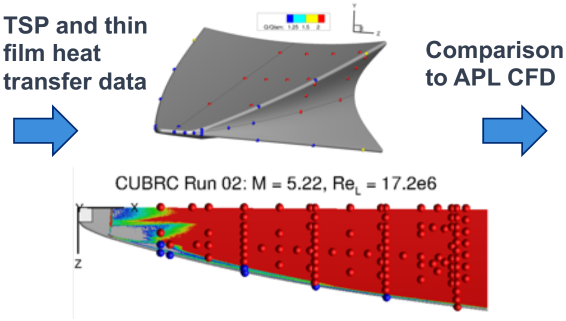

TSP and thin film heat transfer data

Comparison to APL CFD

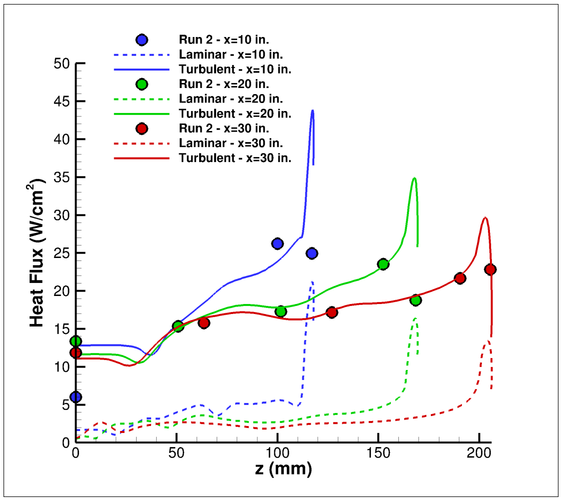

Thin film heat transfer data from Run 02 at three axial stations (x = 10, 20, and 30 in.) compared to laminar (dashed lines) and turbulent (solid lines) CFD from JHU/APL grid. Predicted turbulent heat transfer from CFD showed excellent agreement to turbulent regions of the model.

- Eight runs completed at CUBRC with temperature-sensitive paint and thin-film heat flux sensors
- CFD calculations using same grid and code (CFD++) performed at CUBRC conditions, showing great agreement to test data
- Confidence in CFD-based heating and observed transition behavior allowed thermal analysis to be completed and a final structural analysis to be performed at CDR
- Sample results shown here for Run 2 (Mach 5.22, Re=20e6/m), most turbulent case and relevant to BOLT2 trajectory

Comparison of CFD++ Heat Flux to CUBRC Data

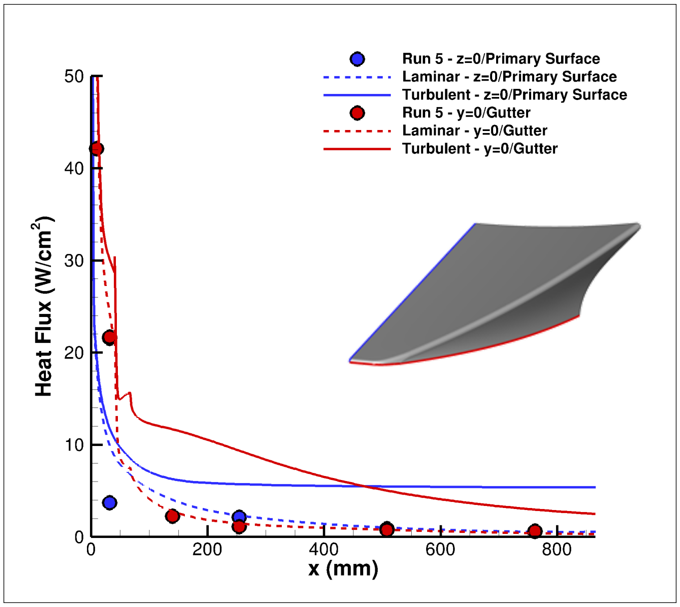

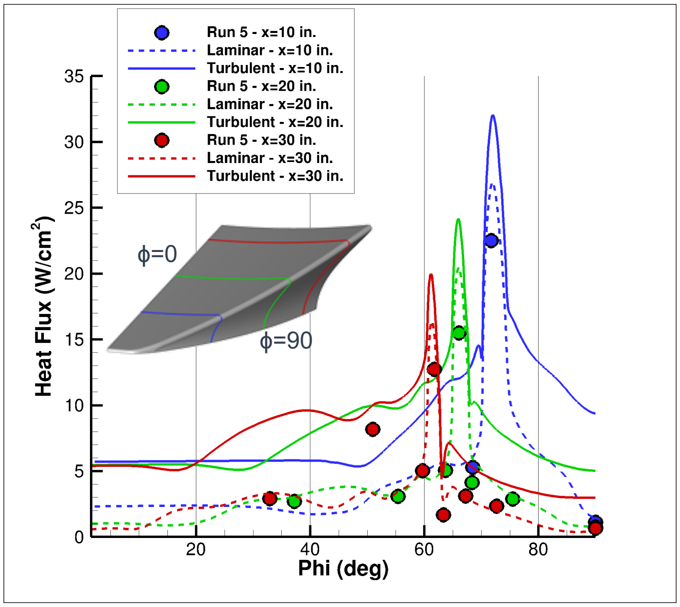

- Laminar heat flux with CFD++ agrees well with CUBRC thin-film data
- Run 5 – Mach 7, Re_L=2.7e6 (mainly laminar)

Comparison of CFD++ Heat Flux to CUBRC Data

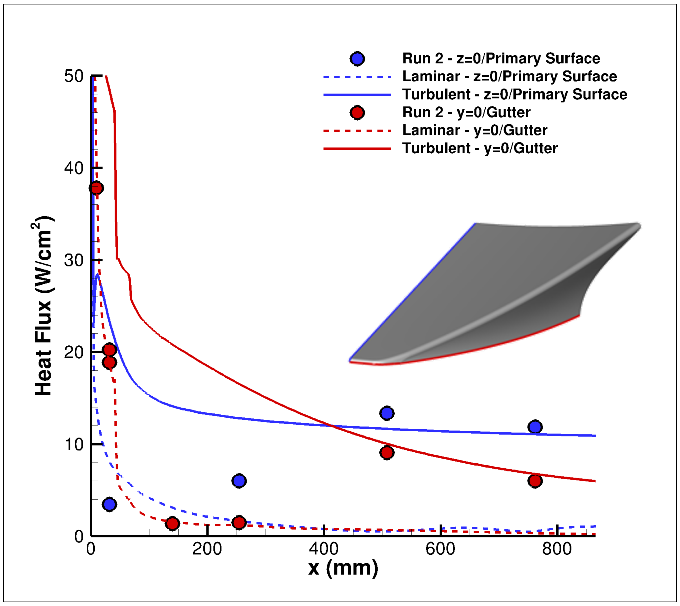

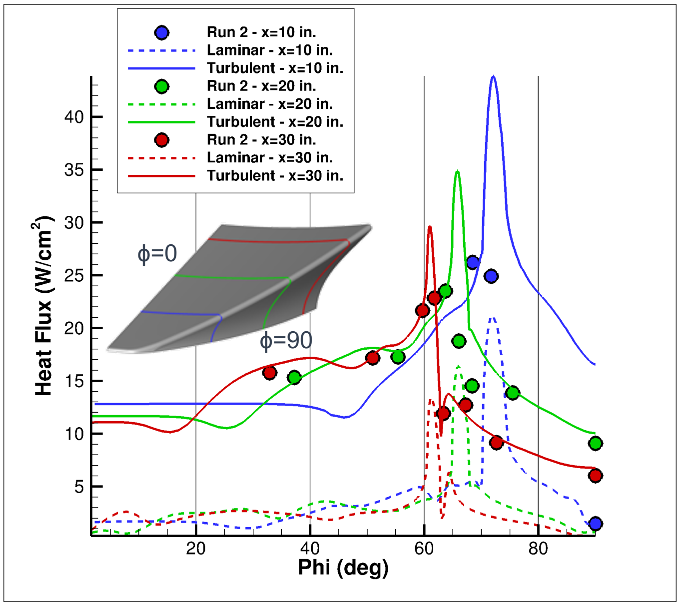

- Turbulent heat flux with CFD++ SA model agrees well with CUBRC thin-film data
- Run 2 – Mach 5.22, Re_L=17.2e6 (mainly turbulent)

Independent US3D Calculations Used as Quality Check

- APL turbulent heat transfer rates compared against independent results in US3D performed by John Thome at University of Minnesota
- Source: “2018-03-05-APL-vs-UMN-Turbulent-Heating.pptx”
- Plot shows turbulent heating comparisons between CFD++ and US3D
  - Solid lines = CFD++
  - Dashed lines = US3D
  - Colors = axial station (x, where x=0 is nosetip)
- Overall agreement is very good considering:
  - Different grids
  - Different flow solvers
  - Different turbulence model implementations (both are Spalart-Allmaras models)
- CFD++ heat fluxes are slightly higher, by a few percent

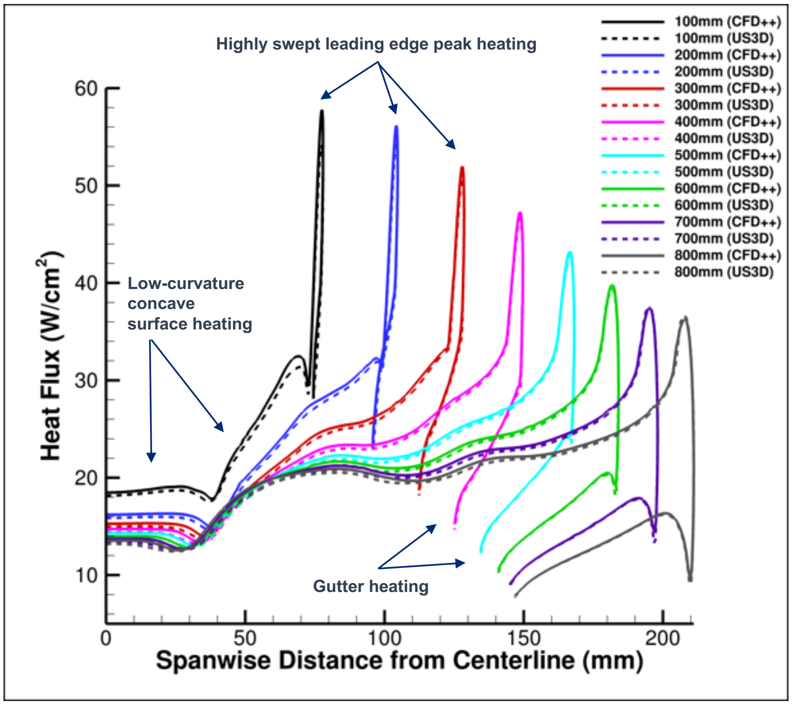

BOLT CFD Points Calculated Across Nominal Trajectory

JHU/APL made complete database of CFD solutions for the payload forebody (“Flight Geometry”), eventually switching to a full viscous-CFD based heating database for final analyses at PDR and CDR

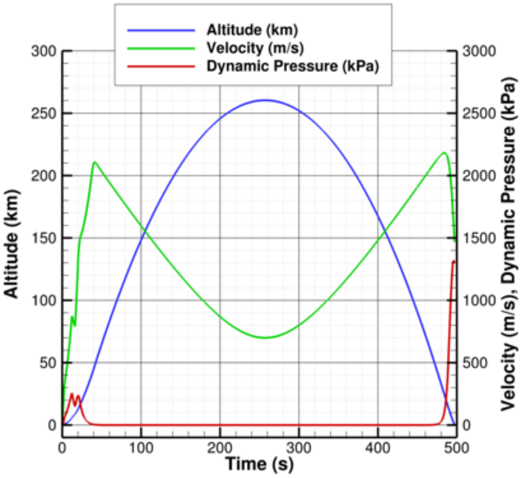

Notional Trajectory for Thermal Analyses

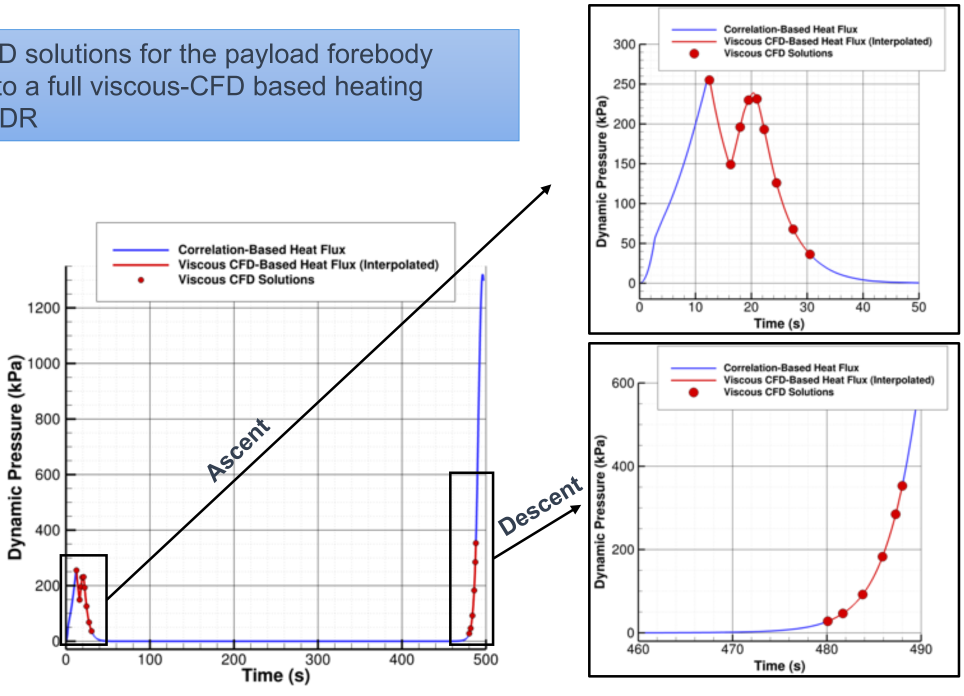

Dynamic Pressure w/ Viscous CFD Points Shown

Thermal Analyses of BOLT – from APL MSLRAD code

- Maximum nosetip Iridium-Coated TZM temperature remains below 1100 K
- Maximum stainless-steel mid-section temperature remains below 750K
- Primary focus is maximum temperature of aft aluminum component at <u>end of experiment</u>
  - Occurs at swept leading edge
  - 550-600 K range comparable to peak aluminum temperatures on HIFiRE-5B (Juliano et al. AIAA 2017-3134)
  - Bulk temperature largely below 500 K

Ascent Temperatures (Tripped Case)

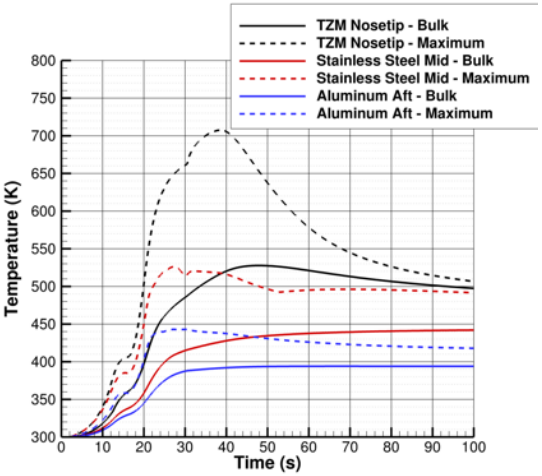

Descent Temperatures (Tripped Case)

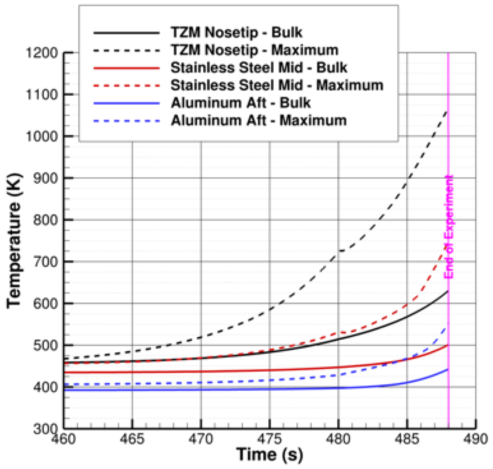

Effect of Transition Assumption on Maximum Temperatures (K) at End of Flight (t = 488.0 s)

Section	Fully Laminar	Tripped at $Re_\theta/M_e = 150$	Fully Turbulent
TZM Nosetip	1028	1068	1113
Stainless Steel Mid	624	748	802
Aluminum Aft	442	554	616

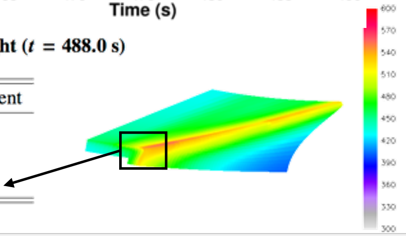

CFD++ Thermal Solver

- During BOLT, APL worked with Metacomp to facilitate implementation of new boundary conditions into CFD++'s existing conjugate heat transfer solver
- Goal → complementary but slightly more limited transient thermal solver to MSLRAD, useful for spot checking MSLRAD results, able to be run easily by CFD++ users
- Initial comparisons were made to full BOLT geometry to gain confidence in CFD++ solver
- CFD++ solver eventually used for BOLT fairing analysis performed post-CDR

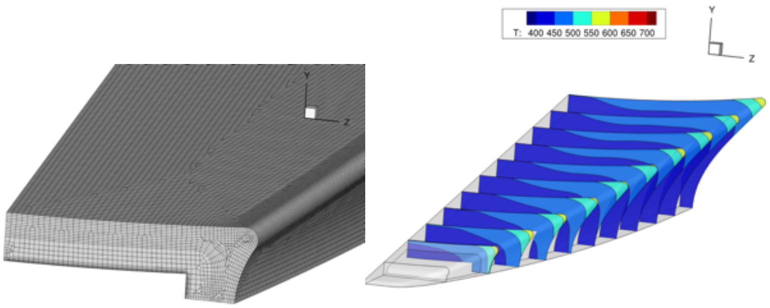

Pre-PDR CFD++ thermal model development. Comparisons to MSLRAD performed internally.

t = 488.0s (end of descent)

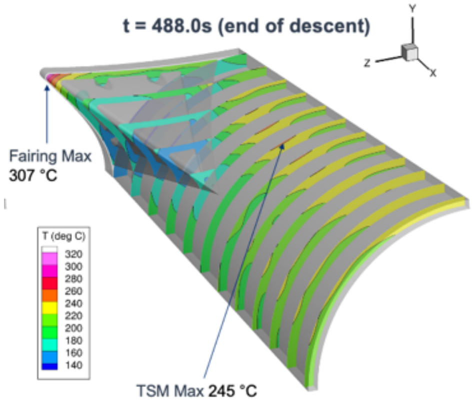

Development matured such that CFD++ was used for post-CDR aerodynamic fairing thermal analysis

BOLT Thermal Summary

- BOLT2 able to leverage significant development work for quick-turnaround thermal analysis ahead of PDR
- Existing grid topologies, flow solutions, and wall spacing and clustering parameters directly applied to create new BOLT2 CFD solutions

---

BOLT2 CAD and CFD Grid

BOLT2 CAD Used for CFD Solutions

- “20200308_BOLT2_Meter_Full_Stack_Minimum_Transition9_Quarter.IGS” provided by Bryan Morreale and Eric Swinny at TAMU, as this geometry version was previously certified by Wallops as meeting aerodynamic stability standards

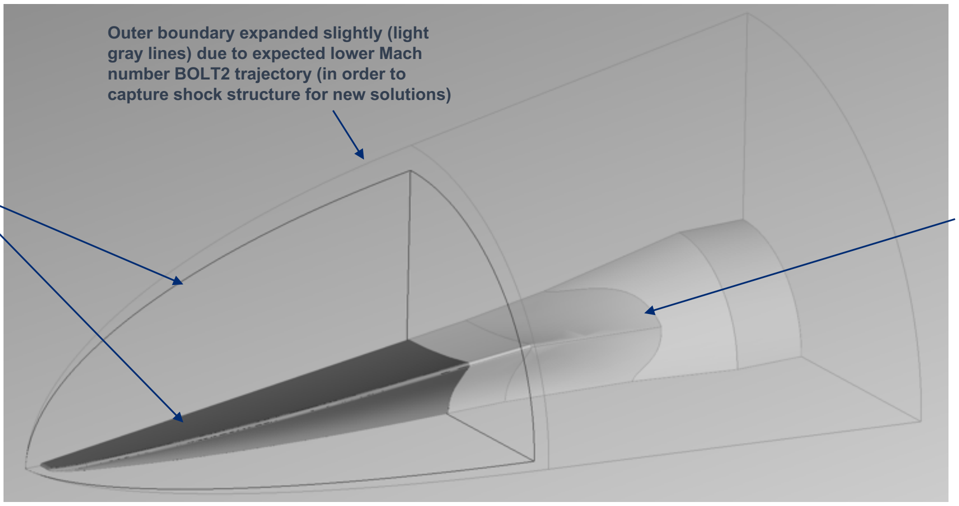

Outer boundary expanded slightly (light gray lines) due to expected lower Mach number BOLT2 trajectory (in order to capture shock structure for new solutions)

Dark gray is existing BOLT1 geometry, black lines are previous BOLT1 outer shock boundary

BOLT2 extension, fairing, conical transition section, and initial portion of service modules included in PDR CFD solutions

CAD w/ Baseline Outer Boundary Imported to LINK3D for Grid Generation

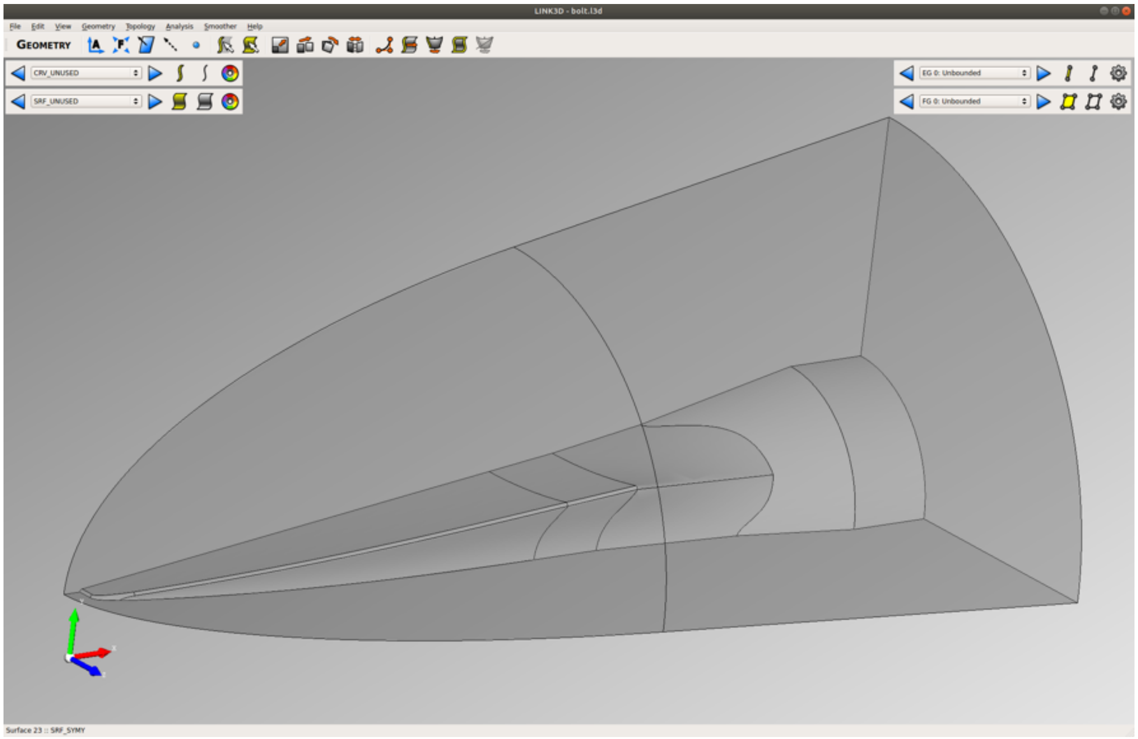

BOLT1 Grid Topology Imported

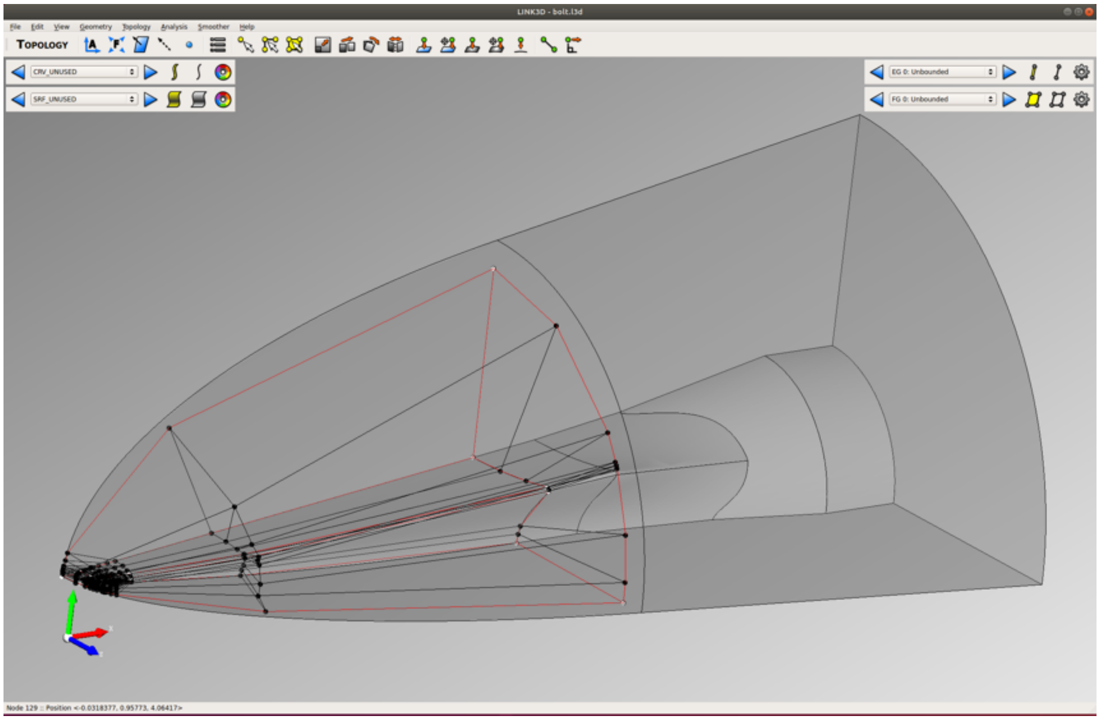

Node 129 :: Position <-0.0318377, 0.95773, 4.06417>

Grid Topology Expanded to Entire BOLT2 Geometry

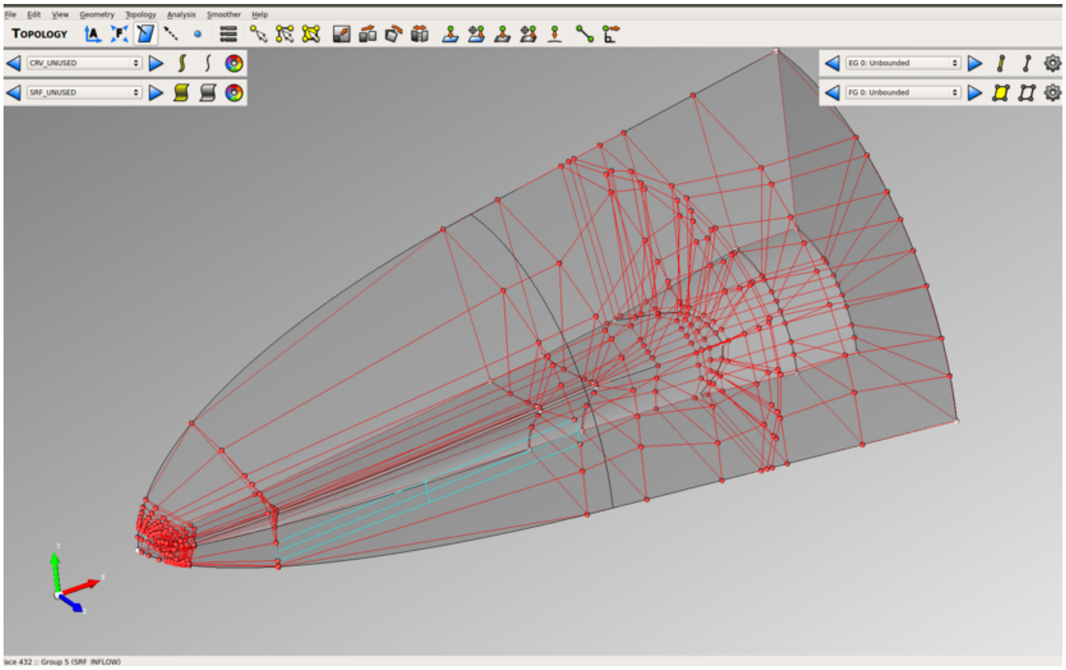

ace 432 :: Group 5 (SRF INFLOW)

New Grid Solved in LINK3D w/ Same BOLT1 Parameters

Grid Size 29M Cells

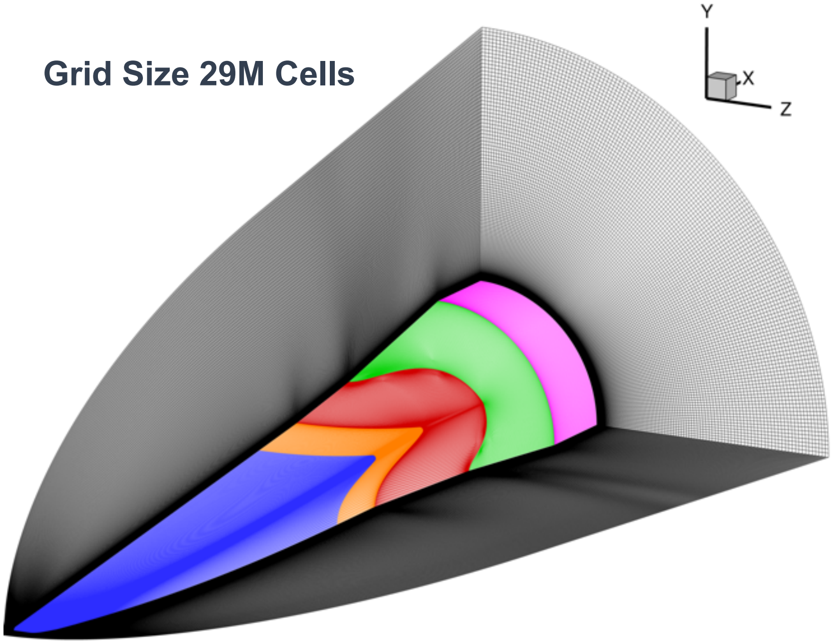

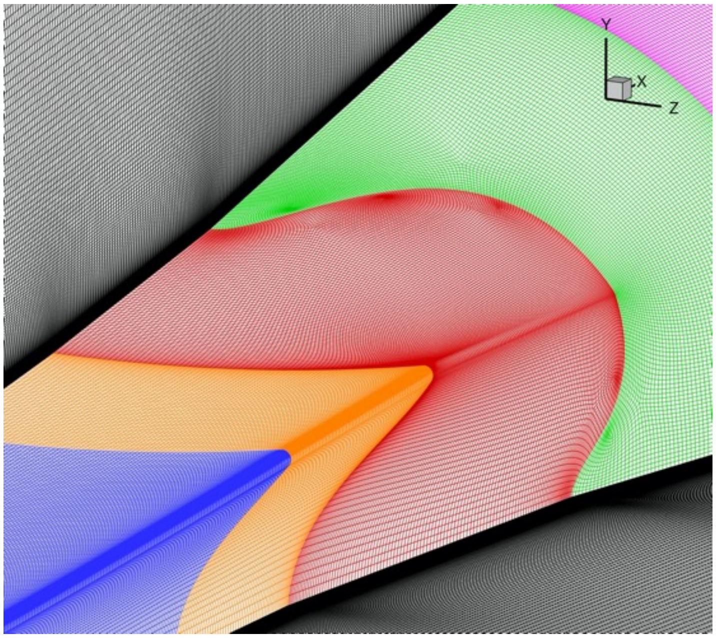

New Grid Solved in LINK3D w/ Same BOLT1 Parameters

Grid Size 29M Cells

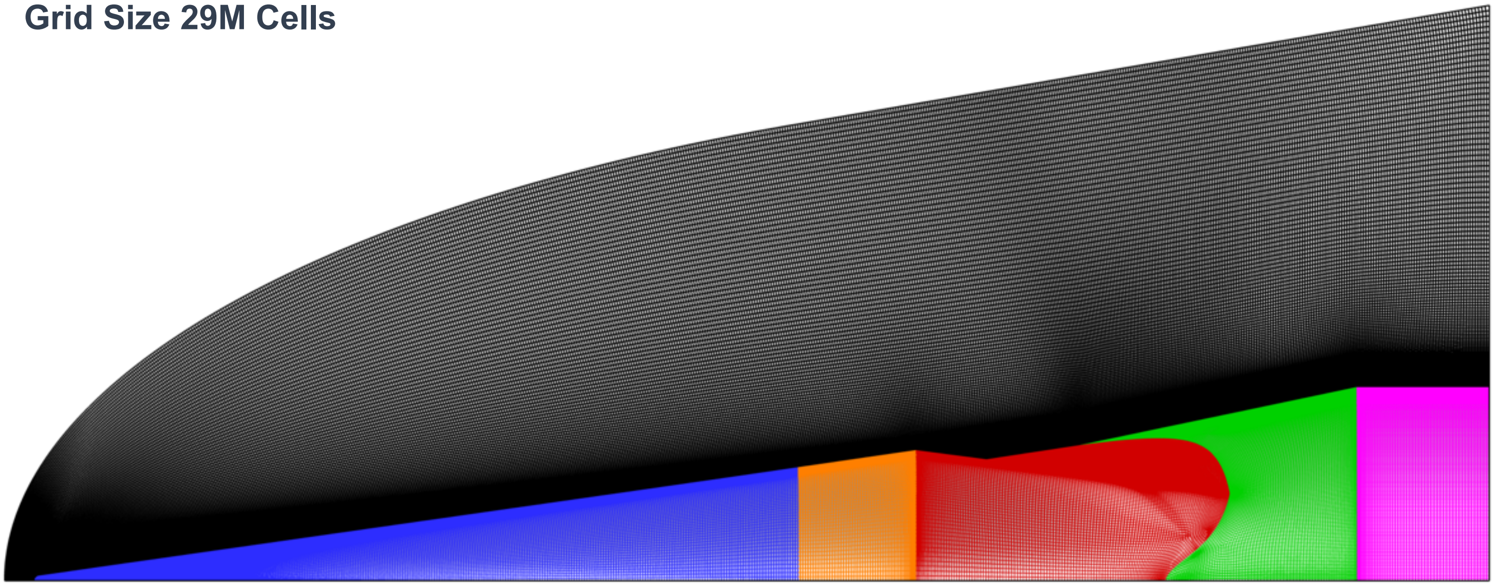

Multiple Grid Versions Needed

- Baseline grid shown previously used for majority of flow simulations. Two alternate grids were also created:
  - 1. “Low Mach”, expanded outer boundary to ensure capture of shock at low Mach numbers after launch
  - 2. “End of Descent”, same outer boundary as baseline grid, but wall spacing reduced from 0.76 microns to 0.253 microns (33%) to maintain low y+ values at extreme high Reynolds numbers at end of flight

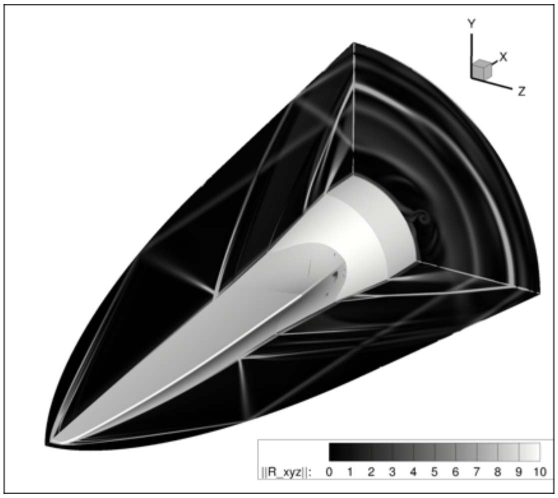

Flow solutions both at BOLT2 t=12.0s, 6.2 km altitude, Mach 1.8. Density gradient magnitude is shown.

At Mach numbers below ~3, the baseline grid outer boundary (LEFT) did not capture the shock and unwanted reflections were created.

The “Low Mach” grid with expanded outer boundary (RIGHT) was used for these cases.

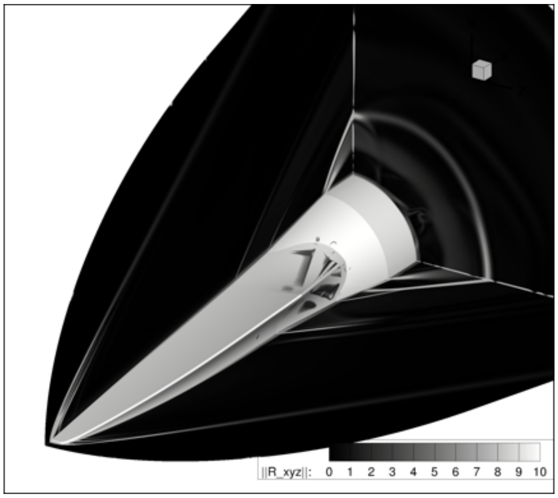

BOLT2 Trajectory and Selection of CFD Solution Points

Thermal Analysis Nominal Trajectory

- “BOLTII Trajectory 1m - Version 1.xlsx” provided to APL via Heather Kostak
- Assumed to be nominal trajectory, but verified against 5/5/2020 BOLT2 telecon plots of Monte Carlo spreads (magenta dashed lines)
- Trajectory falls within Monte Carlo spread and appears nominal.
- Nominal trajectory to be used w/ excursions accounted for by adding a safety factor on CFD-based heating.

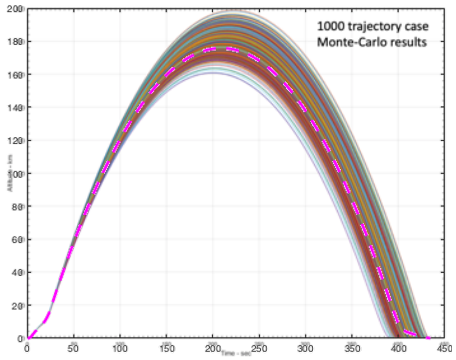

Altitude vs. Time

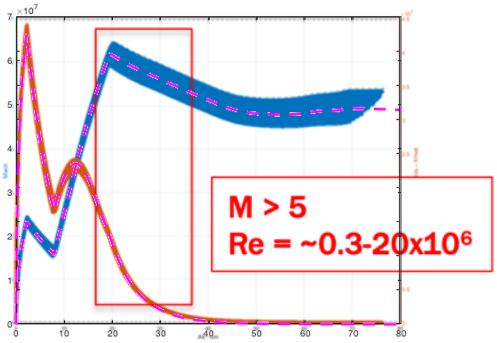

M > 5
Re = ~0.3-20x10⁶

Mach and Unit Reynolds Number vs. Altitude (ascent)

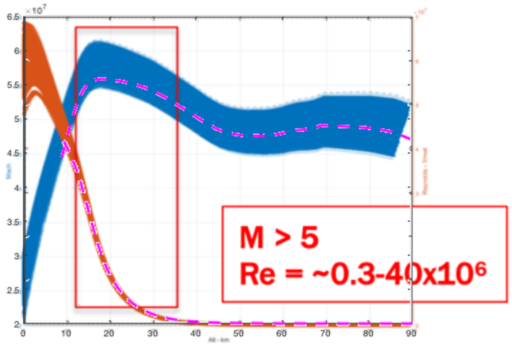

M > 5
Re = ~0.3-40x10⁶

Mach and Unit Reynolds Number vs. Altitude (descent)

Atmosphere Model

- Per Dave Kilcoyne e-mail, Wallops TAOS simulation run with “Range Commander’s Council (RCC) NASA Wallops Island, VA atmospheric model for July. Some may know this but the TAOS trajectory simulation includes an option to use the 1976 standard atmosphere and/or atmosphere models developed by the RCC that are based on measurements of the atmosphere at specific sites. I believe the RCC atmosphere tables are defined up to 70 km and then the 1976 U.S. standard atmosphere is applied in TAOS above that.”
- To maintain consistency, CFD freestream conditions extracted from the Wallops trajectory results rather than 1976 Standard Atmosphere.
  - The different atmospheric temperature profile is shown to the right between the two models.
  - Temperature extracted from provided “Mach” and “Velocity”
  - Density extracted from provided “Dynamic Pressure” and “Velocity”

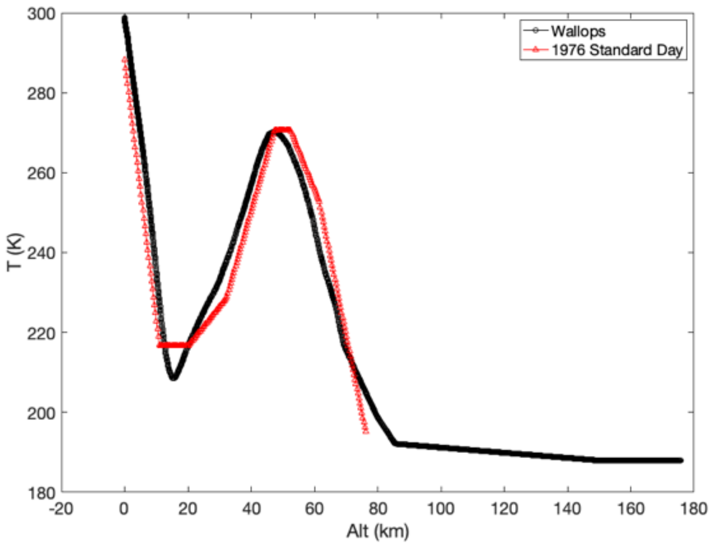

Selection of CFD Solution Points

- Trajectory examined and 23 solution points were identified for the CFD heating solutions (red circles)
- All solutions below ~33km altitude to avoid rarefied flow regimes and capture peak heating portions
- Rho*u^3 (energy flux) examined to capture peaks and expected heating variations
- Mach number examined to ensure continuity in adiabatic recovery temperature
- Two CFD solutions completed at each time (46 total cases):
  - 1. “Cold wall” solution with 300K isothermal wall boundary condition (used for cold-wall heat flux)
  - 2. “Adiabatic” solution with adiabatic wall boundary condition (used for recovery temperature)

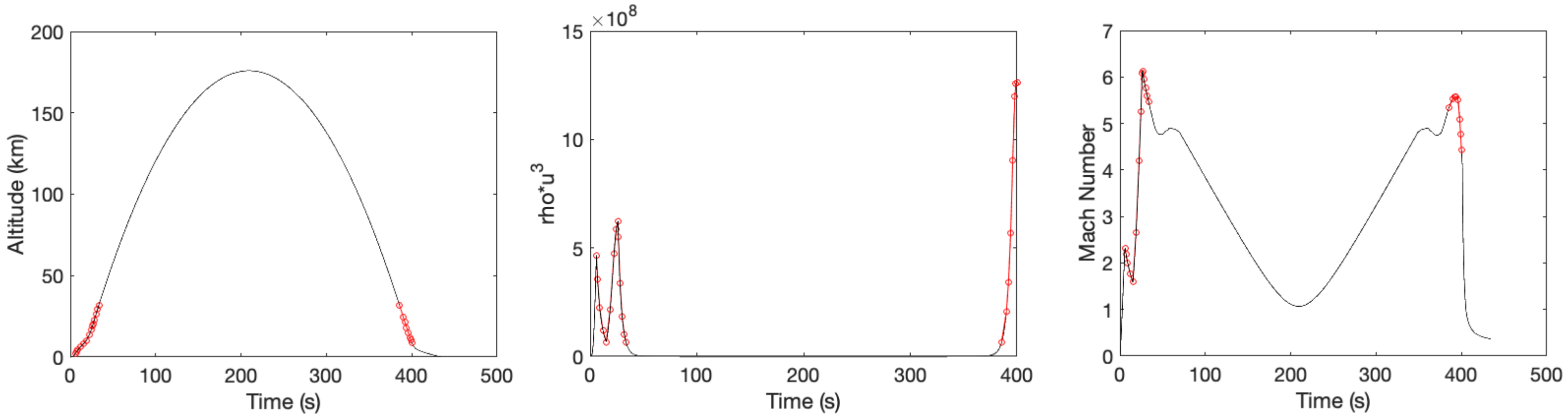

Freestream Conditions / Grid Used

Time (s)	Alt (km)	Mach #	p (Pa)	T (K)	u (m/s)	Grid
5.9	2.2	2.3	78707.08	286.04	785.12	"Low Mach"
7.0	3	2.2	71225.07	281.32	738.37	"Low Mach"
9.0	4.4	2.0	60038.06	273.5	664.39	"Low Mach"
12.0	6.2	1.8	47530.49	262.58	575.5	"Low Mach"
15.1	7.9	1.6	38199.7	251.41	504.17	"Low Mach"
18.8	10.2	2.6	27376.52	233.63	810.66	"Low Mach"
22.4	13.8	4.2	15780.21	211.48	1221.95	Baseline
24.5	16.6	5.3	9949.5	209.74	1524.56	Baseline
26.0	19.1	6.1	6715.33	214.61	1788.42	Baseline
26.5	20	6.1	5834.27	216.42	1803.89	Baseline
28.0	22.6	5.9	3866	221.2	1771.87	Baseline
30.0	26	5.8	2285.4	226.87	1736.79	Baseline
32.0	29.4	5.6	1380.35	232.04	1708.16	Baseline
33.5	31.9	5.5	955.82	237.38	1689.26	Baseline
385.5	31.8	5.3	972.52	237.12	1651.22	Baseline
390.0	24.5	5.5	2895.67	224.39	1658.64	Baseline
392.0	21.2	5.6	4783.02	218.84	1649.92	Baseline
394.0	18	5.6	7974.77	212.27	1629.67	Baseline
396.0	14.8	5.5	13378.28	208.91	1594.34	"End of Descent" (Baseline w/ smaller wall spacing)
398.0	11.8	5.1	21845.79	222.33	1518.54	"End of Descent" (Baseline w/ smaller wall spacing)
399.0	10.3	4.8	27214.17	233.32	1457.27	"End of Descent" (Baseline w/ smaller wall spacing)
400.0	8.9	4.4	33267.19	244.05	1385.69	"End of Descent" (Baseline w/ smaller wall spacing)

All solutions run at 0º angle of attack with quarter symmetry grid

CFD Solution Convergence, Quality Checks, and Flow Features

Solution Convergence

- Most solutions ran for 10,000 iterations
- Each solution checked for convergence after completion monitoring:
  - Global RHS residuals
  - Asymptotic trend for viscous (skin friction) drag component on entire body

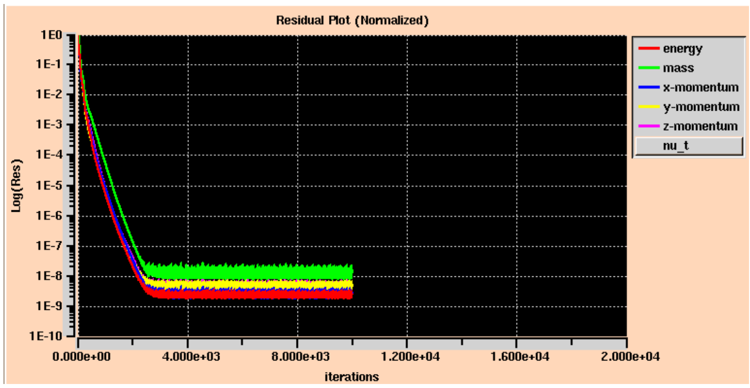

Residuals

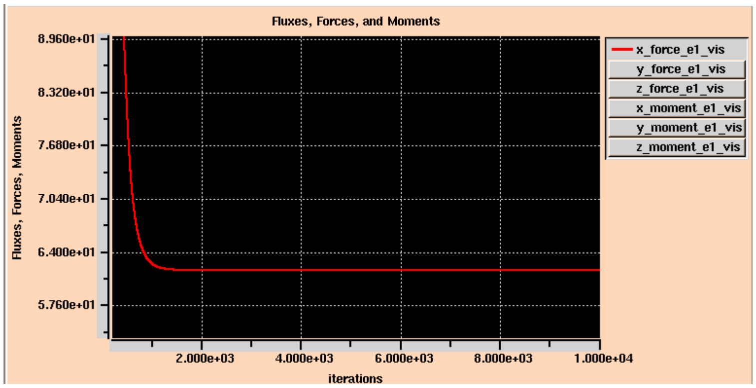

Viscous Drag Force

Ensuring Capture of Heat Transfer Rates

- All solutions checked to ensure y+ < 1.0 over the majority of the body (threshold) with y+ < 0.5 desired
- Plot shows line cuts from all cold-wall solutions using the appropriately selected grids:
  - Colors:
    - Blue = early ascent “Low Mach” grid
    - Green = mid ascent
    - Black = late ascent
    - Orange = early descent
    - Red = late descent “End of Descent” grid
  - Cuts:
    - z = 0 mm (centerline, to show nose y+)
    - z = 75 mm (off centerline, to show swept leading edge, BOLT2 acreage, fairing, and conical transition section)
- Some solutions exceeded y+ >1 only in small regions on the shoulder of the nosetip

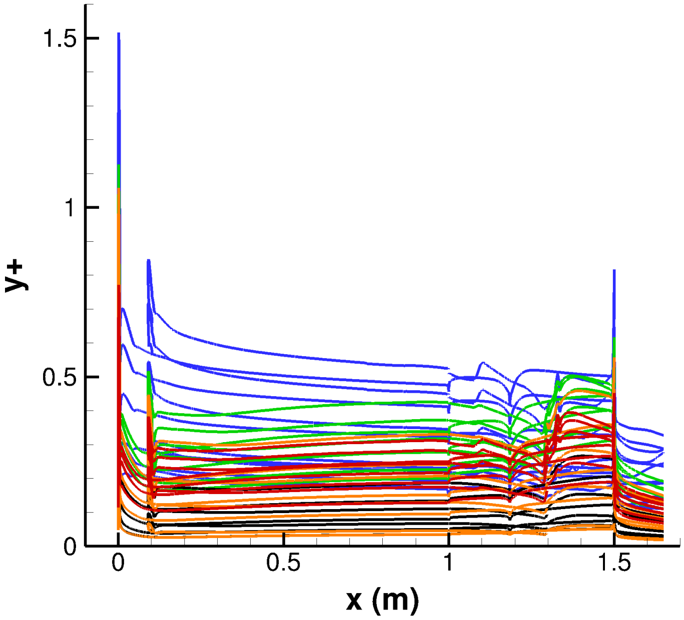

Spot Check Against BOLT1 Heating

- One extra case was run at a BOLT trajectory point to compare against the previous grid and solutions used in the first flight (t = 24.5s, Mach 5.2, Re = 11.5M/m)
- Heating showed excellent agreement on the matching portion of the geometry (forebody)
- Local heating rates are higher, respectively, on the BOLT2 conical section which is not shielded by the forebody as in BOLT

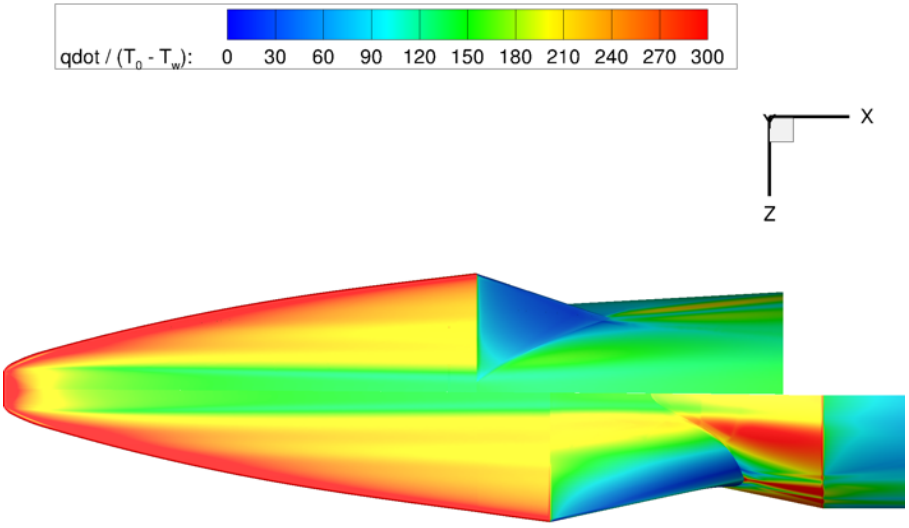

BOLT2 Flow Field

- Surface contours of heat flux shown
- Density gradient magnitude plotted to visualize boundary layer and shocks
- BOLT2 creates a complex flow field
- Fairings and conical transition section, like on BOLT, experience expansion and recompression along with shock/BL interactions

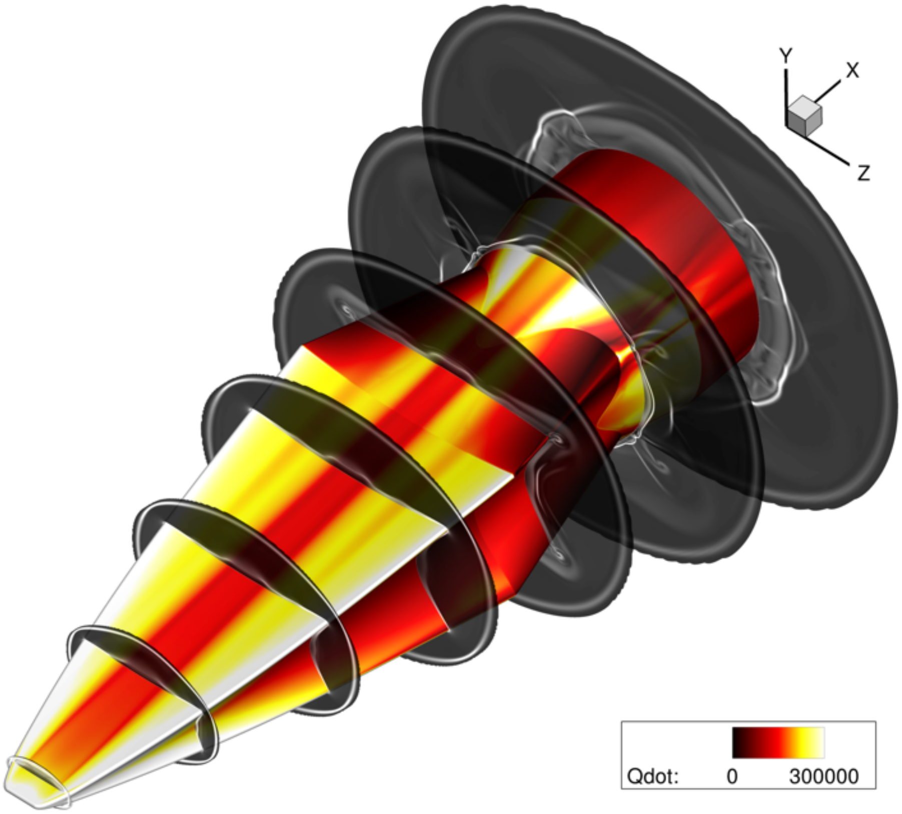

Thermal Grid

Internal Geometry CAD

- Simplified internals CAD file provided by Aaron Dufreneat CUBRC: “BOLT_CDR_Full_Stack_Transition9_STEP_0507-11_2020.stp”
- Similar forebody to BOLT1 except:
  - BOLT1 nose and isolator combined into one solid part
  - Aft bulkhead is a separate part
- CAD aeroshell thickness designed to match mass properties from PDR converged aerodynamic stability analysis
  - 0.35” thickness shell used in transition section and initial portion of booster modules
- Tungsten ballast mass ignored in current analysis, assumed to be in poor thermal contact with the inner mold line

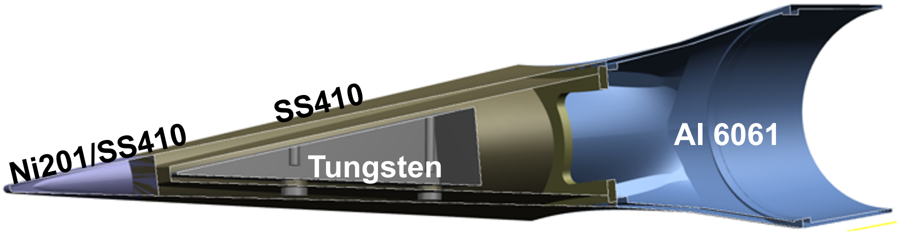

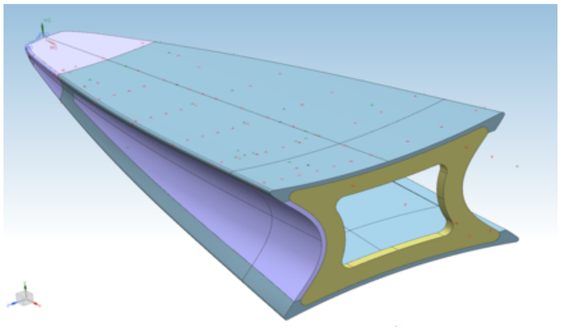

Thermal Grid Generation

- Thermal grid created in Pointwise using the T-Rex unstructured meshing algorithms
  - Allows creation of predominantly hex elements
  - Grids can be generated very quickly
  - This thermal grid created in under 8 hours
- Grid contains five separate parts, all are point matched at interfaces to avoid flux-stitching in the conduction across parts:
  - Nosetip (Nickel 201 or 410 Stainless Steel)
  - Frustum (410 SS)
  - Bulkhead (410 SS)
  - Transition Section = Fairing plus conical (6061 Aluminum)
  - Booster Module (6061 Aluminum

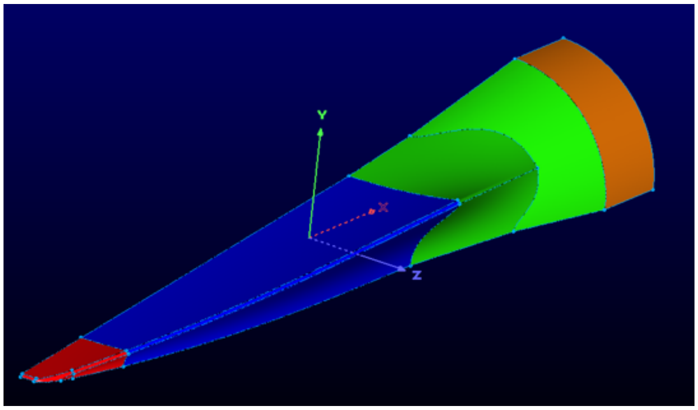

Thermal Grid Images

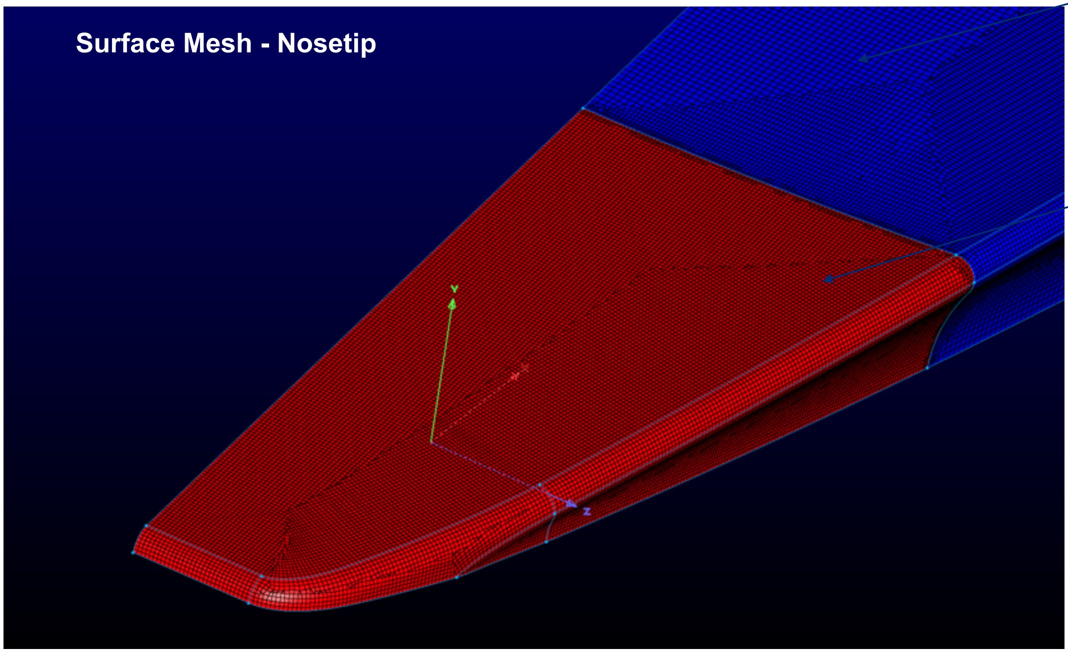

To reduce mesh size, larger elements were used near centerline of BOLT2 frustum where large spanwise gradients are not expected

Advancing front ortho surface domains used to create mesh dominated by isotropic quads on the surface

Thermal Grid Images

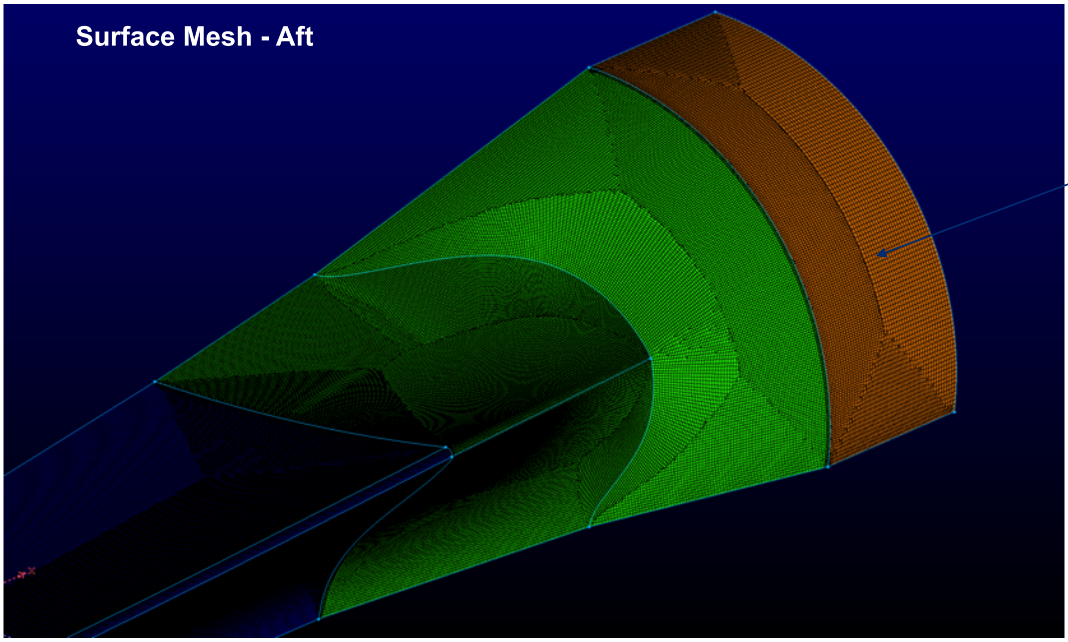

Grid de-refined near end of geometry

Thermal Grid Images

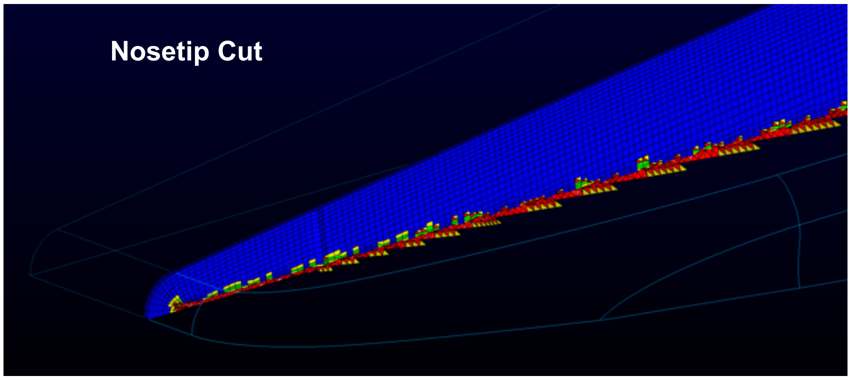
Nosetip Cut

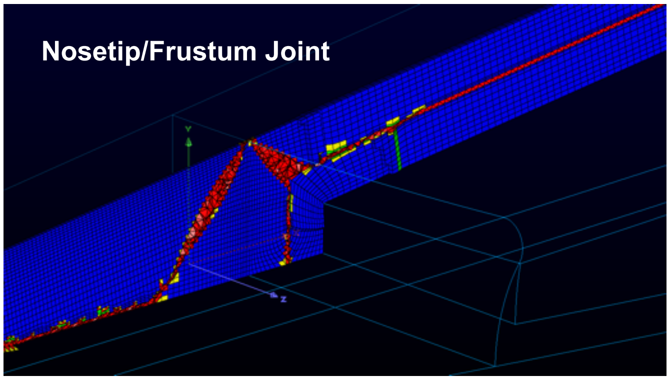
Nosetip/Frustum Joint

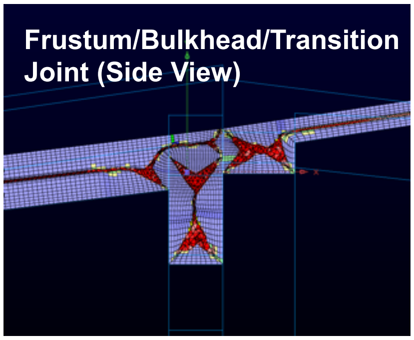
Frustum/Bulkhead/Transition Joint (Side View)

Spanwise cut of volume shows automatically generated hex elements perpendicular to surfaces where conduction gradients are important (outer surfaces and abutting solid parts)

Red cells are filled in triangle elements mostly limited to inner portions of the parts

---

Thermal Grid Images

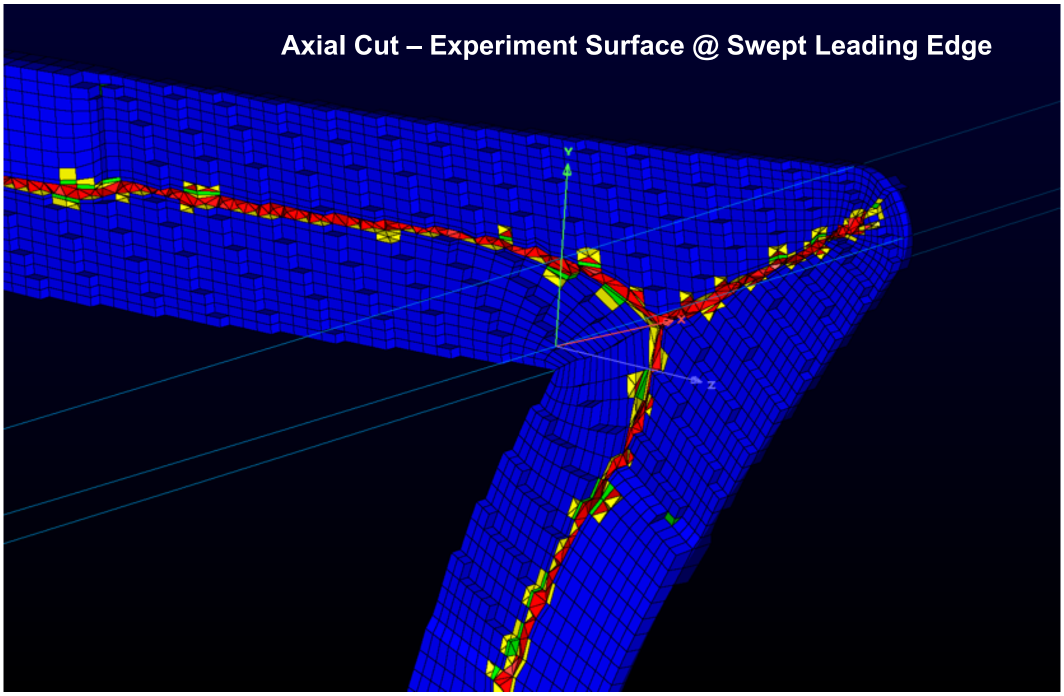
Axial Cut – Experiment Surface @ Swept Leading Edge

Thermal Grid Images

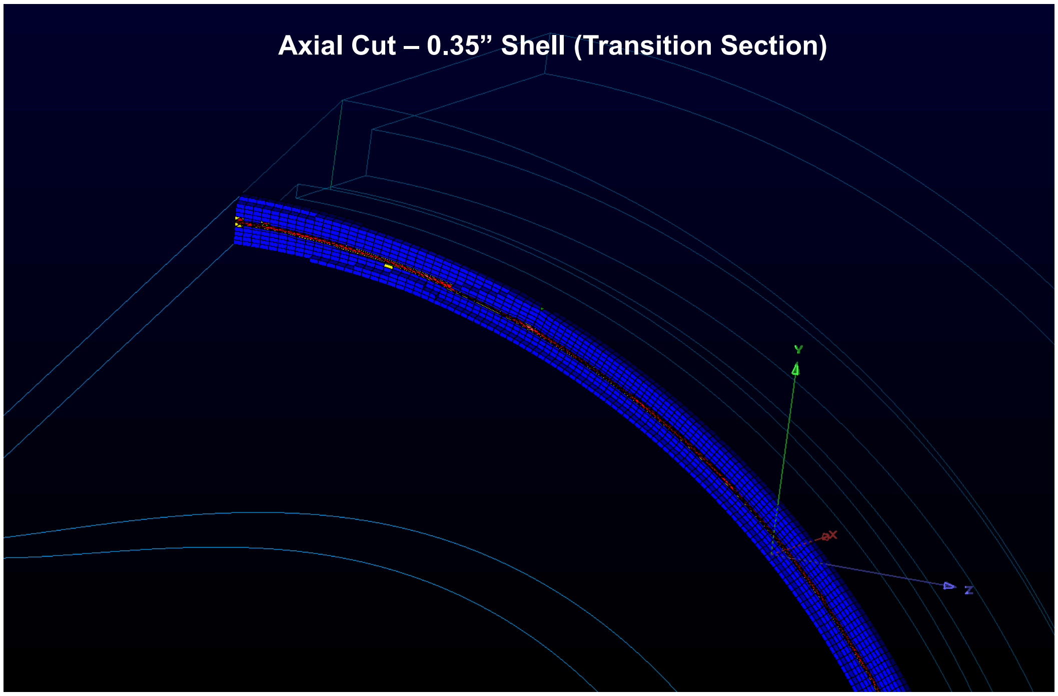

Thermal Grid Pointwise Defaults Used

- All dimensions gridded in SI units (meters)
- Connectors
  - Average Δs = 0.001
  - Monotonic Rational Quadratic Spline (MRQS) distribution functions
- Domains (for surface meshes)
  - Advancing Front Ortho algorithm, with triangles and quads
- Blocks (for volume meshes)
  - T-rex solver defaults:
    - Max layers 99, full layers 99 (ensures full layer creation deep into volume)
    - Cell types “All and Reduce Pyramids”
    - Push attributes to domains
  - Delauney algorithm for isotropic meshing
  - Volume wall spacing and clustering:
    - Nosetip = 0.0005 initial spacing, 1.05 growth rate
    - Frustum = 0.001 initial spacing, 1.05 growth rate
    - Transition and booster = 0.001 initial spacing, 1.005 growth rate (to achieve ~8-10 cells through thin shell thickness)
  - T-rex BC’s
    - “Wall” with above parameters for flow surface and part/part connections
    - “Match” for symmetry planes

Thermal Grid Cell Count and Size

- Total cells 7.3M
- Large size compared to typical finite element grids
  - No time was available for a grid convergence study
  - Aim point was < 8.0M cells for achievable turnaround time for the transient analysis computation
  - 2.9M hex cells, which are desired for efficiency and numerical results and dominate the volume
  - Majority of cells are Tets, inefficient for filling volumes, but limited to interior regions

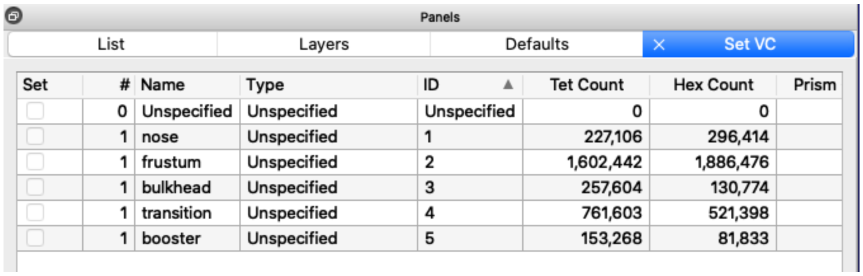

Set	#	Name	Type	ID ▲	Tet Count	Hex Count	Prism
☐	0	Unspecified	Unspecified	Unspecified	0	0	
☐	1	nose	Unspecified	1	227,106	296,414	
☐	1	frustum	Unspecified	2	1,602,442	1,886,476	
☐	1	bulkhead	Unspecified	3	257,604	130,774	
☐	1	transition	Unspecified	4	761,603	521,398	
☐	1	booster	Unspecified	5	153,268	81,833	

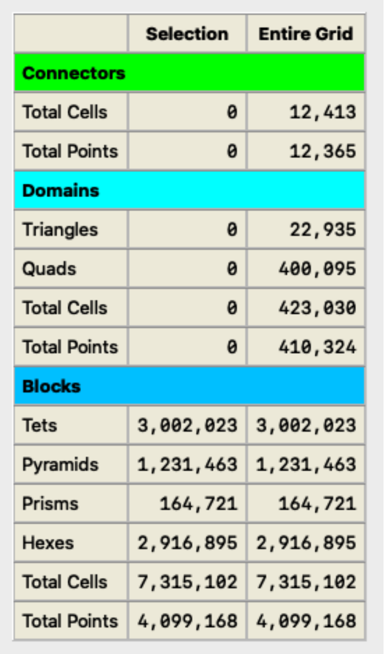

	Selection	Entire Grid
Connectors		
Total Cells	0	12,413
Total Points	0	12,365
Domains		
Triangles	0	22,935
Quads	0	400,095
Total Cells	0	423,030
Total Points	0	410,324
Blocks		
Tets	3,002,023	3,002,023
Pyramids	1,231,463	1,231,463
Prisms	164,721	164,721
Hexes	2,916,895	2,916,895
Total Cells	7,315,102	7,315,102
Total Points	4,099,168	4,099,168

Thermal Grid Boundary Conditions

- Volume and boundary conditions set in Pointwise for direct export to CFD++ format
- Care was taken to sort connectors, domains, and blocks for each part into a separate view layer, which aided identification of domains for boundary conditions
- Domain/domain “connection BC’s” also tagged representing connections between parts
- Table to right shows all boundary conditions (surface and interior part-to-part connections)

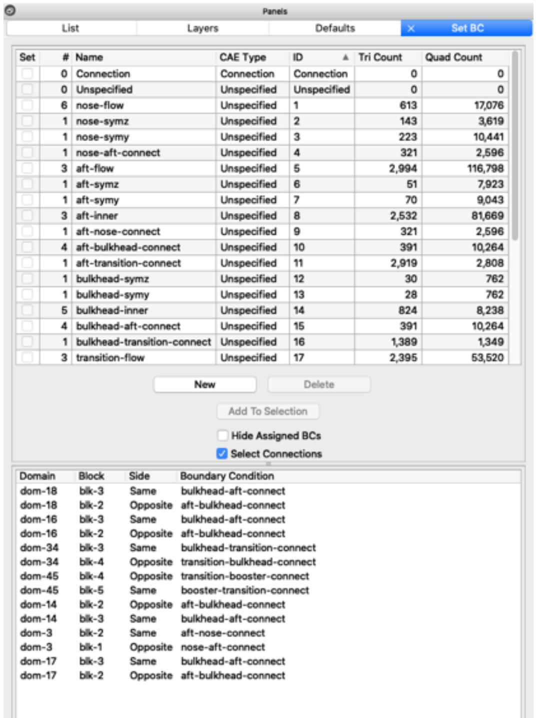

Set	#	Name	CAE Type	ID ▲	Tri Count	Quad Count
☐	0	Connection	Connection	Connection	0	0
☐	0	Unspecified	Unspecified	Unspecified	0	0
☐	6	nose-flow	Unspecified	1	613	17,076
☐	1	nose-symz	Unspecified	2	143	3,619
☐	1	nose-symy	Unspecified	3	223	10,441
☐	1	nose-aft-connect	Unspecified	4	321	2,596
☐	3	aft-flow	Unspecified	5	2,994	116,798
☐	1	aft-symz	Unspecified	6	51	7,923
☐	1	aft-symy	Unspecified	7	70	9,043
☐	3	aft-inner	Unspecified	8	2,532	81,669
☐	1	aft-nose-connect	Unspecified	9	321	2,596
☐	4	aft-bulkhead-connect	Unspecified	10	391	10,264
☐	1	aft-transition-connect	Unspecified	11	2,919	2,808
☐	1	bulkhead-symz	Unspecified	12	30	762
☐	1	bulkhead-symy	Unspecified	13	28	762
☐	5	bulkhead-inner	Unspecified	14	824	8,238
☐	4	bulkhead-aft-connect	Unspecified	15	391	10,264
☐	1	bulkhead-transition-connect	Unspecified	16	1,389	1,349
☐	3	transition-flow	Unspecified	17	2,395	53,520

☐ Hide Assigned BCs

☑ Select Connections

Domain	Block	Side	Boundary Condition
dom-18	blk-3	Same	bulkhead-aft-connect
dom-18	blk-2	Opposite	aft-bulkhead-connect
dom-16	blk-3	Same	bulkhead-aft-connect
dom-16	blk-2	Opposite	aft-bulkhead-connect
dom-34	blk-3	Same	bulkhead-transition-connect
dom-34	blk-4	Opposite	transition-bulkhead-connect
dom-45	blk-4	Opposite	transition-booster-connect
dom-45	blk-5	Same	booster-transition-connect
dom-14	blk-2	Opposite	aft-bulkhead-connect
dom-14	blk-3	Same	bulkhead-aft-connect
dom-3	blk-2	Same	aft-nose-connect
dom-3	blk-1	Opposite	nose-aft-connect
dom-17	blk-3	Same	bulkhead-aft-connect
dom-17	blk-2	Opposite	aft-bulkhead-connect

Pointwise to CFD++ Export

- In order for CFD++ to recognize the internal domains (“part to part connections”) as external boundary conditions, the individual parts must all be exported from Pointwise separately
- Procedure:
  - Create a copy of the master Pointwise file with all properly tagged BC’s
  - For each part, delete all blocks except the block you want to export (corresponding to one part)
  - Perform “File → Export CAE” to CFD++ format for each individual part into a separate subdirectory (i.e. “1”, “2”, “3”, etc.)
  - Reassemble all the CFD++ grid files using CFD++ “Concatenate using Subdirectories” command
  - Reassembled CFD++ files are then loaded into the GUI for problem setup

Thermal Analysis Methodology

Equations

1. Calculation of Heat Transfer Coefficient (HTC) from CFD solutions:

Safety margin

Cold-wall heat flux from 300K isothermal wall CFD solution

$$HTC(x,y,z,t) = 1.2\,\frac{q_{wall}(x,y,z,t)}{T_r(x,y,z,t) - T_{wall}}$$

300K

Recovery temperature from adiabatic CFD solution

2. Calculation of Thermal Response:

Actual transient wall temperature

Actual transient heat flux at wall

$$q_{wall}(x,y,z,t) = HTC(x,y,z,t)[T_r(x,y,z,t) - T_{wall}(x,y,z,t)]$$

Fixed HTC and recovery temperature, interpolated linearly in time

Aluminum 6061 Properties File

Number of lines

Specific Heat (J/kg-K)

Conductivity (W/m-K, x-direction)

Density (kg/m^3)

Conductivity (W/m-K, y-direction)

Temperature (K)

Conductivity (W/m-K, z-direction

```
14
0.56    2700    456.2791656 101.30  0   0   101.30  0   101.30
111.11  2700    653.7298424 122.35  0   0   122.35  0   122.35
166.67  2700    770.3361513 137.78  0   0   137.78  0   137.78
222.22  2700    856.8306831 149.08  0   0   149.08  0   149.08
277.78  2700    911.5335789 156.43  0   0   156.43  0   156.43
333.33  2700    950.8837646 163.54  0   0   163.54  0   163.54
388.89  2700    980.2827538 169.64  0   0   169.64  0   169.64
444.44  2700    1005.87417  174.18  0   0   174.18  0   174.18
500.00  2700    1027.930109 177.33  0   0   177.33  0   177.33
555.56  2700    1046.913573 179.09  0   0   179.09  0   179.09
611.11  2700    1064.733383 178.21  0   0   178.21  0   178.21
666.67  2700    1064.733383 178.21  0   0   178.21  0   178.21
805.56  2700    1131.474659 167.97  0   0   167.97  0   167.97
1111.11 2700    1131.474659 167.97  0   0   167.97  0   167.97
```

Aluminum 6061 data digitized from MIL5-HDBK-5 handbook

Nickel 201 Properties File

Number of lines

Density (kg/m³)

Specific Heat (J/kg-K)

Conductivity (W/m-K, x-direction)

Conductivity (W/m-K, y-direction)

Temperature (K)

Conductivity (W/m-K, z-direction

```
26
73.15   8900    150.000 93.000  0   0   93.000  0   93.000
89.15   8900    188.406 92.306  0   0   92.306  0   92.306
144.15  8900    318.197 90.864  0   0   90.864  0   90.864
173.15  8900    355.000 87.000  0   0   87.000  0   87.000
200.15  8900    380.999 85.094  0   0   85.094  0   85.094
273.15  8900    426.000 81.000  0   0   81.000  0   81.000
293.15  8900    456.000 79.000  0   0   79.000  0   79.000
366.15  8900    473.108 73.556  0   0   73.556  0   73.556
373.15  8900    475.000 73.000  0   0   73.000  0   73.000
473.15  8900    500.000 67.000  0   0   67.000  0   67.000
477.15  8900    552.658 66.345  0   0   66.345  0   66.345
573.15  8900    570.000 60.000  0   0   60.000  0   60.000
589.15  8900    581.965 59.133  0   0   59.133  0   59.133
673.15  8900    530.000 57.000  0   0   57.000  0   57.000
700.15  8900    519.163 56.249  0   0   56.249  0   56.249
773.15  8900    525.000 58.500  0   0   58.500  0   58.500
811.15  8900    535.910 59.133  0   0   59.133  0   59.133
873.15  8900    535.000 61.000  0   0   61.000  0   61.000
922.15  8900    544.284 62.018  0   0   62.018  0   62.018
973.15  8900    550.000 63.000  0   0   63.000  0   63.000
1033.15 8900    556.844 64.181  0   0   64.181  0   64.181
1073.15 8900    565.000 65.500  0   0   65.500  0   65.500
1144.15 8900    573.592 67.066  0   0   67.066  0   67.066
1173.15 8900    580.000 68.000  0   0   68.000  0   68.000
1255.15 8900    602.899 69.229  0   0   69.229  0   69.229
1273.15 8900    590.000 70.500  0   0   70.500  0   70.500
```

Nickel 201 properties provided by Aaron Dufrene

Stainless Steel 410 Properties File

Number of lines

Density (kg/m³)

Specific Heat (J/kg-K)

Conductivity (W/m-K, x-direction)

Conductivity (W/m-K, y-direction)

Temperature (K)

Conductivity (W/m-K, z-direction

```
30
293.15  7860   460.548 24.60   0   0   24.60   0   24.60
323.15  7860   460.548 24.70   0   0   24.70   0   24.70
348.15  7860   460.548 24.70   0   0   24.70   0   24.70
373.15  7860   460.548 24.80   0   0   24.80   0   24.80
398.15  7860   460.548 24.90   0   0   24.90   0   24.90
423.15  7860   460.548 24.90   0   0   24.90   0   24.90
448.15  7860   460.548 25.00   0   0   25.00   0   25.00
473.15  7860   460.548 25.00   0   0   25.00   0   25.00
498.15  7860   460.548 25.10   0   0   25.10   0   25.10
523.15  7860   460.548 25.10   0   0   25.10   0   25.10
548.15  7860   460.548 25.20   0   0   25.20   0   25.20
573.15  7860   460.548 25.20   0   0   25.20   0   25.20
598.15  7860   460.548 25.20   0   0   25.20   0   25.20
623.15  7860   460.548 25.30   0   0   25.30   0   25.30
648.15  7860   460.548 25.30   0   0   25.30   0   25.30
673.15  7860   460.548 25.30   0   0   25.30   0   25.30
698.15  7860   460.548 25.40   0   0   25.40   0   25.40
723.15  7860   460.548 25.40   0   0   25.40   0   25.40
748.15  7860   460.548 25.40   0   0   25.40   0   25.40
773.15  7860   460.548 25.40   0   0   25.40   0   25.40
798.15  7860   460.548 25.50   0   0   25.50   0   25.50
823.15  7860   460.548 25.50   0   0   25.50   0   25.50
848.15  7860   460.548 25.50   0   0   25.50   0   25.50
873.15  7860   460.548 25.50   0   0   25.50   0   25.50
898.15  7860   460.548 25.50   0   0   25.50   0   25.50
923.15  7860   460.548 25.60   0   0   25.60   0   25.60
948.15  7860   460.548 25.60   0   0   25.60   0   25.60
973.15  7860   460.548 25.60   0   0   25.60   0   25.60
998.15  7860   460.548 25.60   0   0   25.60   0   25.60
1023.15 7860   460.548 25.60   0   0   25.60   0   25.60
```

Constant specific heat used for SS410 due to time constraints and lack of easily accessible temperature-dependent data

CFD Interpolation of HTC and Recovery Temperature to Thermal Grid

---

CFD to Thermal Grid Interpolation

- CFD and thermal grids are not point-matched at the surfaces
  - Interpolation of HTC and recovery temperature is required from fluid solution to nodes on thermal grid
  - Otherwise, CFD++ uses a nearest node lookup and the spatial distribution of heating would not be representative of the fluid solution
- Tecplot used to perform interpolation
  - Tecplot macro created to perform the interpolation, then executed for all CFD cases
  - Tecplot ”Kriging” interpolation method previously found to provide the best spatial matching of quantities, although with additional computational time
    - Setting “Drift” to ”Linear” and changing “Zero Value” from default zero to “0.001” found to work well for this grid
  - Interpolations spot checked for a few cases, examples to follow
  - Macro then writes out an ASCII point-format data file containing the variable “X”, “Y”, “Z”, “HTC”, and “T_r”
  - A separate script converts this ASCII file into a plain text file, then runs the CFD++ conversion tool “convert12” to generate a CFD++ binary profile file used directly by the solver for the time-accurate transient thermal solution

Interpolation Spot Check

- Performed using the production Tecplot macro
- Example shown to the right for heat transfer coefficient (HTC)

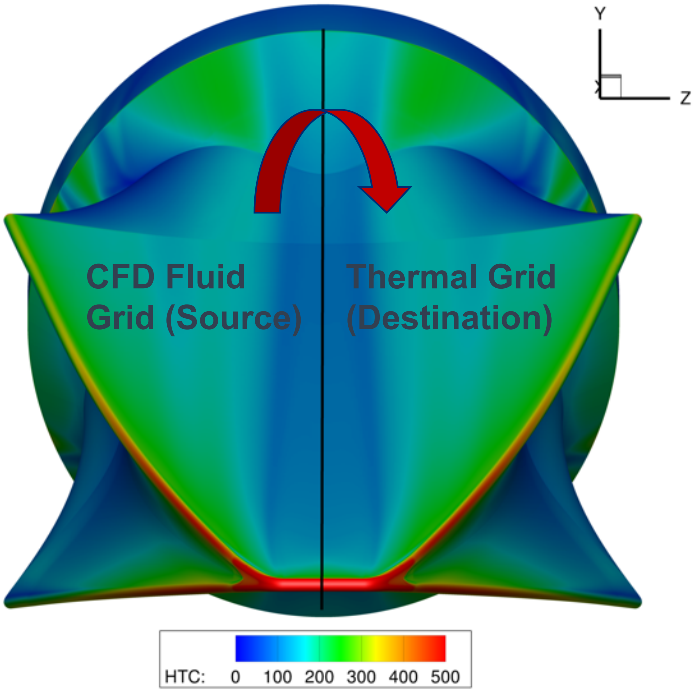

Interpolation Spot Check

- Performed using the production Tecplot macro
- Example shown to the right for heat transfer coefficient (HTC)
- Close up view of nose

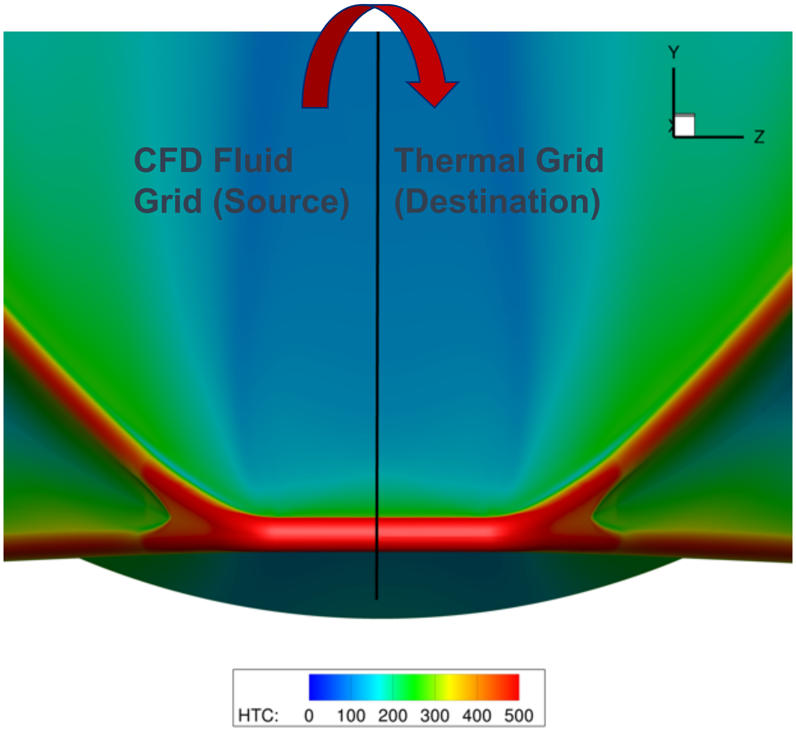

Interpolation Spot Check

- Performed using the production Tecplot macro
- Example shown to the right for heat transfer coefficient (HTC)
- Close up view of nose
- Nose view with respective surface meshes shown

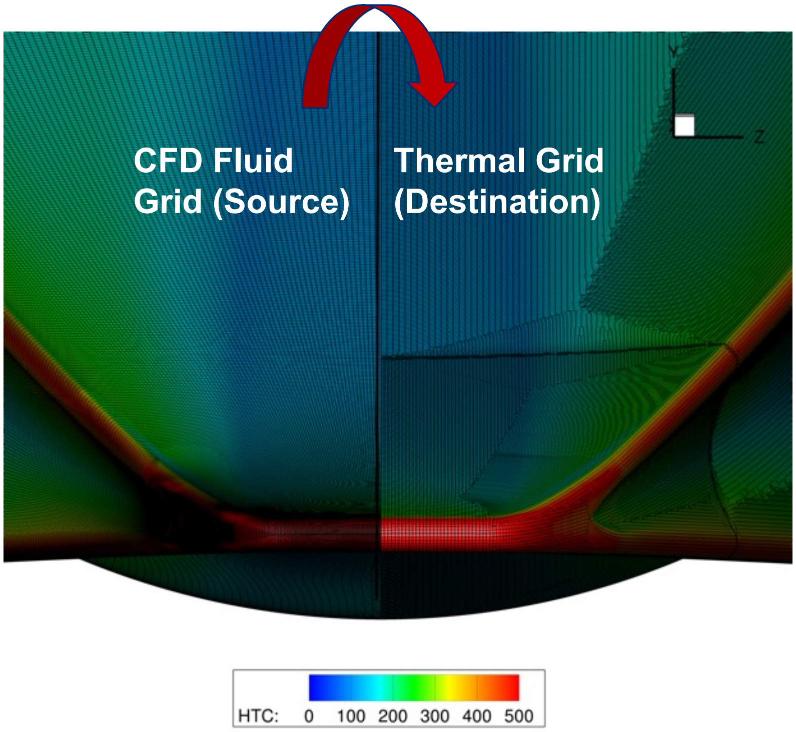

Interpolation Spot Check

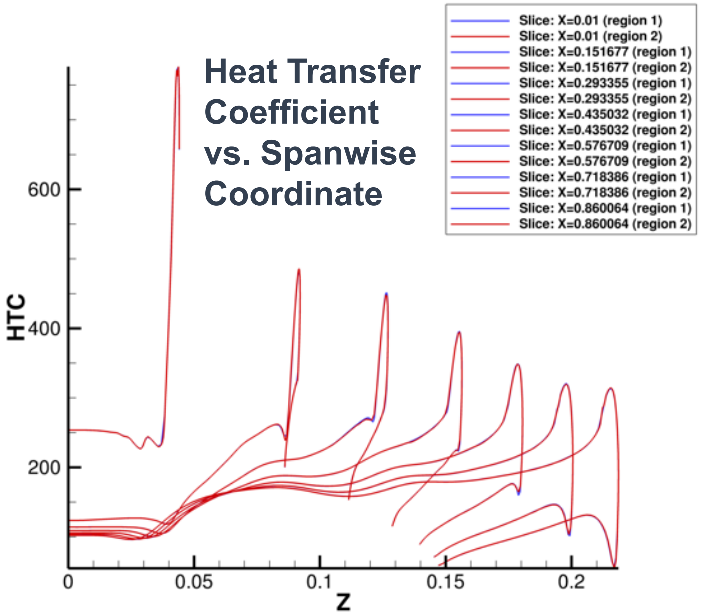
Heat Transfer Coefficient vs. Spanwise Coordinate

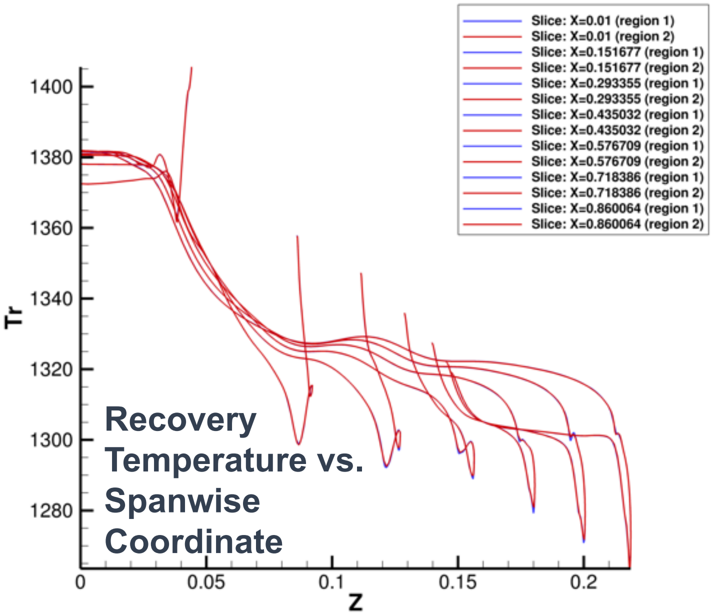
Recovery Temperature vs. Spanwise Coordinate

- Axial slices of original CFD solution (blue) and interpolated thermal grid (red)
- Kriging interpolation captures distribution well, except for some negligible smearing near peaks

Example HTC/Recovery Temperature Profile File

Example from previous APL CFD++ analysis with BOLT

User can generate a profile file for the boundary condition, at each time, in ASCII format that gets converted to CFD++ binary file.

Number of lines

Number of variables (x, y, z, HTC, T_r)

x y z HTC T_r

```
163460 5
 8.659968376E-01 1.231149510E-01 2.194209844E-01 1.034310017E+03 1.950816895E+03
 8.660027981E-01 1.240846887E-01 2.193435878E-01 1.254448822E+03 1.981439819E+03
 8.660022020E-01 1.250216663E-01 2.190793902E-01 1.461258377E+03 2.002134399E+03
 8.660016656E-01 1.258891076E-01 2.186375260E-01 1.633609543E+03 2.010651123E+03
 8.660011292E-01 1.266528070E-01 2.180338651E-01 1.749038283E+03 2.010318481E+03
 8.660005927E-01 1.272824705E-01 2.172914594E-01 1.827109501E+03 1.998643677E+03
 8.660001159E-01 1.277534217E-01 2.164394855E-01 1.860720736E+03 1.980074951E+03
 8.659995198E-01 1.280479580E-01 2.155116051E-01 1.815945869E+03 1.952036743E+03
 8.659989834E-01 1.281560808E-01 2.145441025E-01 1.709050914E+03 1.923475098E+03
 8.659983873E-01 1.280754954E-01 2.135738879E-01 1.548835755E+03 1.890838501E+03

. . .

(16340 total lines)
```

Profile Lookup File for BOLT2 Current Analysis

For time and spatially varying heat flux problems, a user must provide a lookup file to tell CFD++ which profile binary files to use at which time. In between times, the profile files are linearly interpolated at each XYZ location.

Number of lines

Profile file name (*.bin)

Solution time (s)

```
15
0.0 0.0s.bin
5.9 5.9s-2.2km-m2.3.bin
7.0 7.0s-3.0km-m2.2.bin
9.0 9.0s-4.4km-m2.0.bin
12.0 12.0s-6.2km-m1.8.bin
15.1 15.1s-7.9km-m1.6.bin
18.8 18.8s-10.2km-m2.6.bin
22.4 22.4s-13.8km-m4.2.bin
24.5 24.5s-16.6km-m5.3.bin
26.0 26.0s-19.1km-m6.1.bin
26.5 26.5s-20.0km-m6.1.bin
28.0 28.0s-22.6km-m5.9.bin
30.0 30.0s-26.0km-m5.8.bin
32.0 32.0s-29.4km-m5.6.bin
33.5 33.5s-31.9km-m5.5.bin
40.0 40.0s.bin
```

ASCENT

```
9
370.0 370.0s.bin
385.5 385.5s-31.8km-m5.3.bin
390.0 390.0s-24.5km-m5.5.bin
392.0 392.0s-21.2km-m5.6.bin
394.0 394.0s-18.0km-m5.6.bin
396.0 396.0s-14.8km-m5.5.bin
398.0 398.0s-11.8km-m5.1.bin
399.0 399.0s-10.3km-m4.8.bin
400.0 400.0s-8.9km-m4.4.bin
```

DESCENT

Extrapolated Portions of Trajectory!

- In between CFD "anchor points" in time, CFD++ will linearly interpolate (in time) the spatial profiles to vary HTC and T_r at every surface location
- What about regions outside of the CFD anchor points?
  - These regions are extrapolated!
  - Profile file at t=0s manually created:
    - Set HTC to that of the first CFD point (5.9s)
    - Set T_r to 300K
    - This causes heating to slowly build between t=0s and t=5.9s in a representatively physical manner, in the absence of separate subsonic and transonic CFD solutions
  - Profile file at t=40s manually created:
    - Set HTC to zero everywhere
    - Used T_r of previous CFD point (33.5s), since spot check of T_r using flat plate equations showed similar values in this portion of the trajectory
    - Causes slow ramp down of heating after ascent, but this is of course extrapolated
  - Profile file at t=370s manually created:
    - Set HTC to zero everywhere
    - Set T_r equal to first descent point (385.5s)
    - Causes slow buildup of heating ahead of first reentry CFD anchor point
  - The goal with extrapolation is to only do it in LOW heating regions of the flight!
- Exoatmospheric phase (40s to 370s) modeled as pure adiabatic on the outer surfaces to allow for thermal soak throughout the parts

---

CFD++ Transient Solver Setup and Run Procedures

CFD++ Thermal Boundary Conditions

- All part exterior boundaries shown
- Each boundary tagged as specific numerical boundary condition for the thermal solver

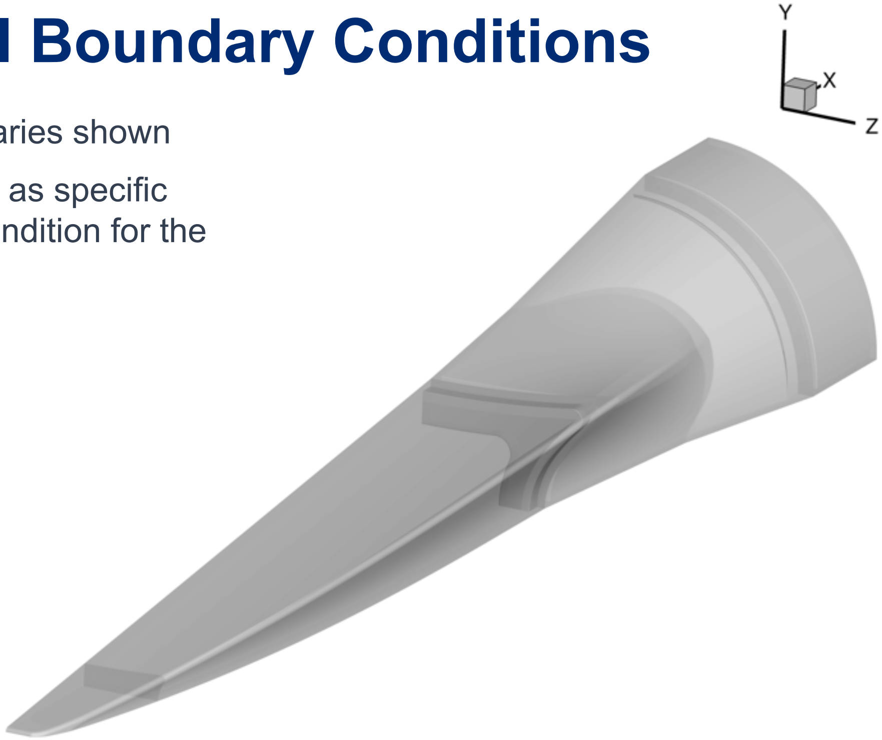

CFD++ Thermal Boundary Conditions

- Exterior flow surfaces (blue)
- For ascent and descent phases, these are set to the HTC/T_r time and spatially dependent profiles from CFD
- For the exoatmopheric phase (40s to 370s), these are set to adiabatic
- No radiation is currently modeled

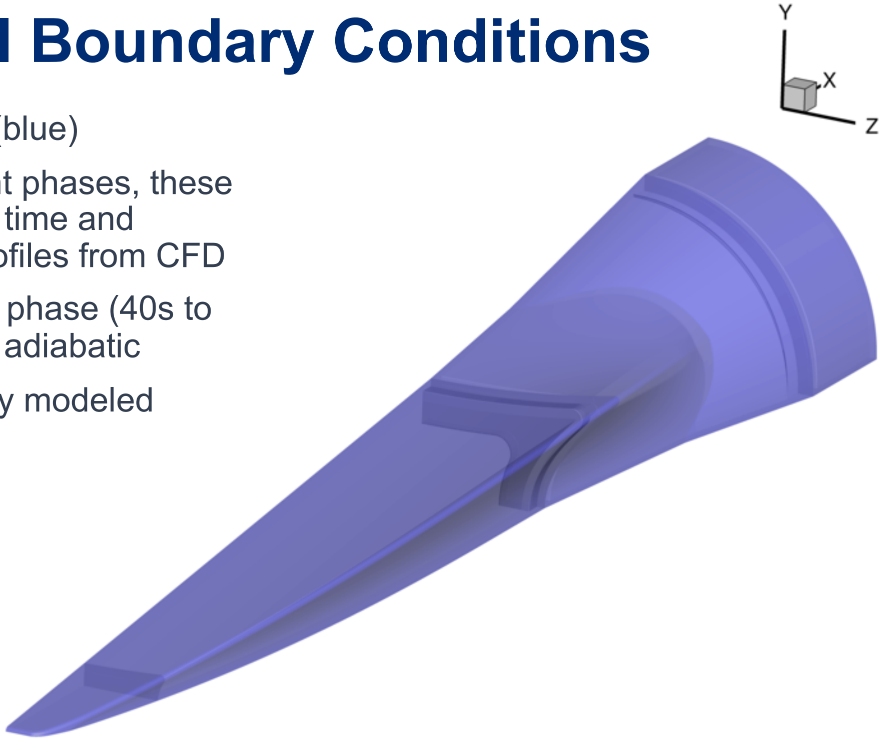

CFD++ Thermal Boundary Conditions

- Symmetry planes and aft boundary at end of booster section (green)
- These are set to adiabatic

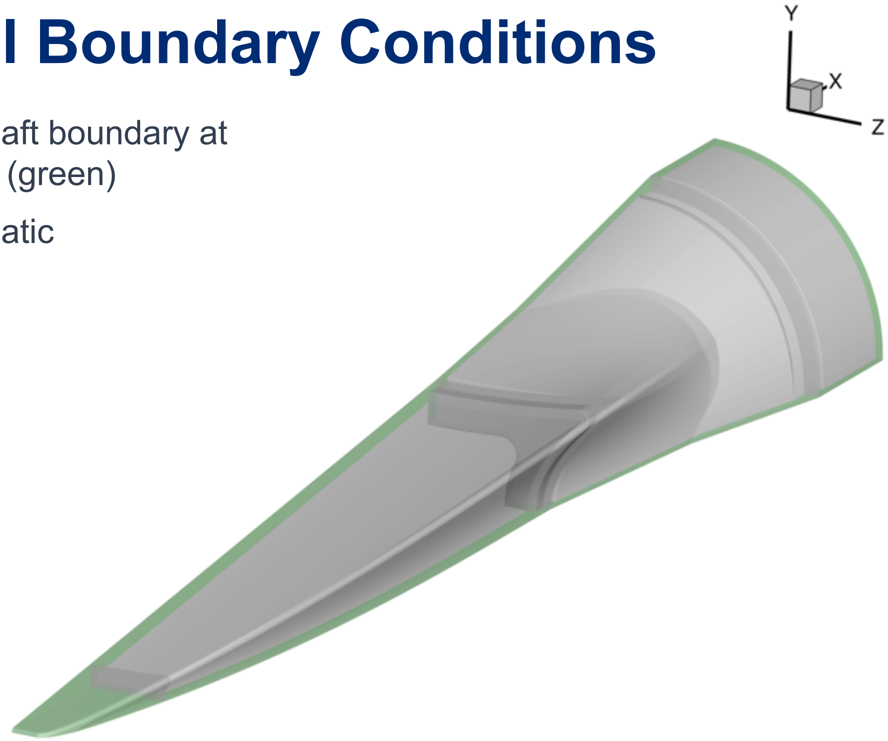

CFD++ Thermal Boundary Conditions

- Part to part contacting surfaces (Red)
- These are set to a CFD++ “zonal boundary condition” “Conjugate Heat Transfer”
- Allows conduction between parts
- Only perfect conduction is available, as no contact resistance term is available, however the surfaces can be set to adiabatic in a separate simulation to understand the effects on part temperatures of no conduction

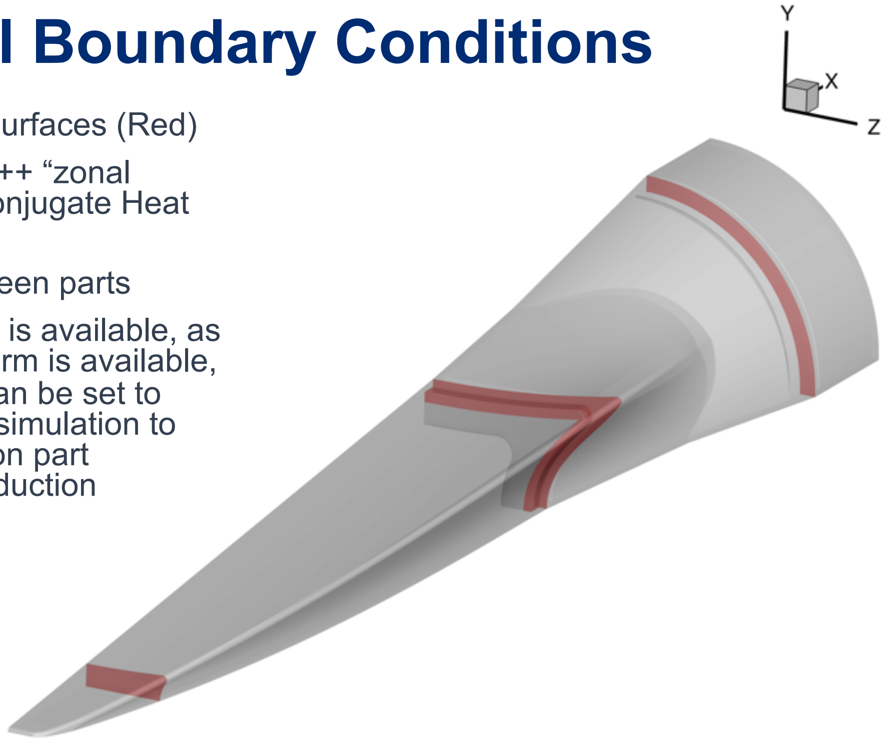

Testing Materials Assignment

- Initial test case run in CFD++ to verify proper materials assignment
- Thermal conductivity “Kappa” plotted
- Parts verified:
  - Nickel 201 (green)
  - Stainless Steel 410 (blue)
  - Aluminum 6061 (red)

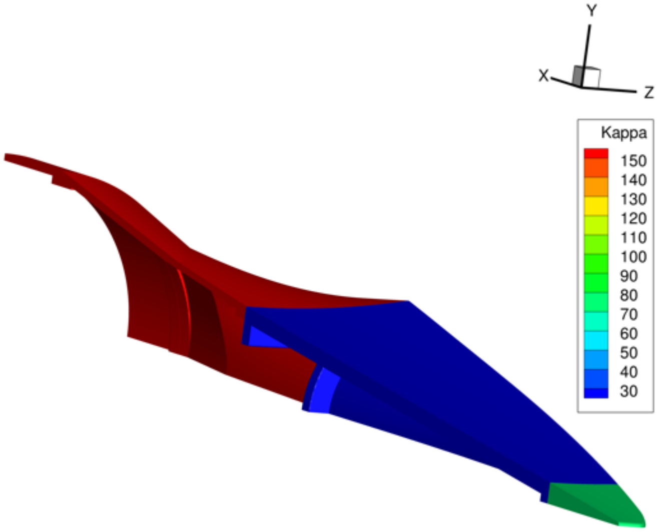

Thermal Solver Run Procedures

- Set initial temperature to 300K at t = 0.0s
- Global time step:
  - 0.001 s (0 < t < 40 s, ascent phase)
  - 0.01 s (40 < t < 370 s, thermal soak phase)
    - More aggressive timestep since only the thermal soak conduction is of interest
  - 0.001s (370 < t < 400 s, descent phase)
- Outputs:
  - ASCII files with min/max/volume-averaged temperatures of each component
  - ASCII files with min/max/volume-averaged temperatures of joint interface planes and outer surfaces
  - Tecplot full volume solutions
    - Every 200 iterations (0.2 seconds) for ascent/descent portions
    - Every 1000 iterations (10 seconds) for thermal soak

Export of Temperatures to CUBRC for ANSYS Structural Analysis

- Temperature point clouds exported for different cases and solution times to CUBRC for incorporation into structural analysis
- Point cloud data:
  - Quarter geometry
  - Thermal solution ends at x = 65 inches
  - XYZ in meters, temperature in Kelvin
- Process for export (scripted):
  - Load CFD++ output Tecplot file for given case and time combination
  - Export first zone “BRICK_CELLS” (volume data) into Tecplot ASCII point format, with only variables X,Y,Z,T
  - Convert to CSV file at command line, assuming the Tecplot ASCII file is called ‘test.dat’:

    -
      ```
      cat test.dat | grep "E[+/-]" | sed 's/^ *//g' | sed 's/ /,/g' > test.csv
      ```
    - Grabs only the numerical data, removes leading zeros on each line, adds commas
    - Exports to new CSV file ‘test.csv’
  - Compress csv file into gzipped tarball for lower file size to enable transfer

Initial Cases Run for BOLT2 PDR

- 3D Baseline configurations (no cork TPS added to transition and booster)
  - Nickel nose
  - SS410 nose
- 3D Cork TPS
  - Nickel nose, 1/8” thick cork added to transition and booster sections. Cork modeled as conduction only, may not be physically representative!
- Cork 1D case
  - Simple 1D solution using peak temperature location on transition section

CFD-Based Thermal Results (PDR)

Baseline 3D Cases (No Cork TPS)

Temperature Statistics By Component – Full Trajectory

- Nosetip
    - Nickel 201 nose peaks at ~850K (~1070 ºF) during ascent, ~980K (~1300 ºF) at end of flight
    - SS410 nose peaks at ~1040K (~1400 ºF) during ascent, ~1120K (~1560 ºF) at end of flight
- Remaining components largely unaffected by nosetip choice (axial conduction through SS410 frustum low)
- SS410 frustum experiment surface reaches high temperatures ~1000 ºF on leading edge at end of flight, but bulk temperatures remain low
- SS410 bulkhead, structural component, remains at reasonable temperatures throughout flight
- AL6061 transition and booster sections, without TPS, reach temperatures at which aluminum retains little strength:
    - ~540K (~510 ºF) bulk temperature at end of flight for transition section
    - TPS likely required for the current configuration to protect the aft aluminum sections

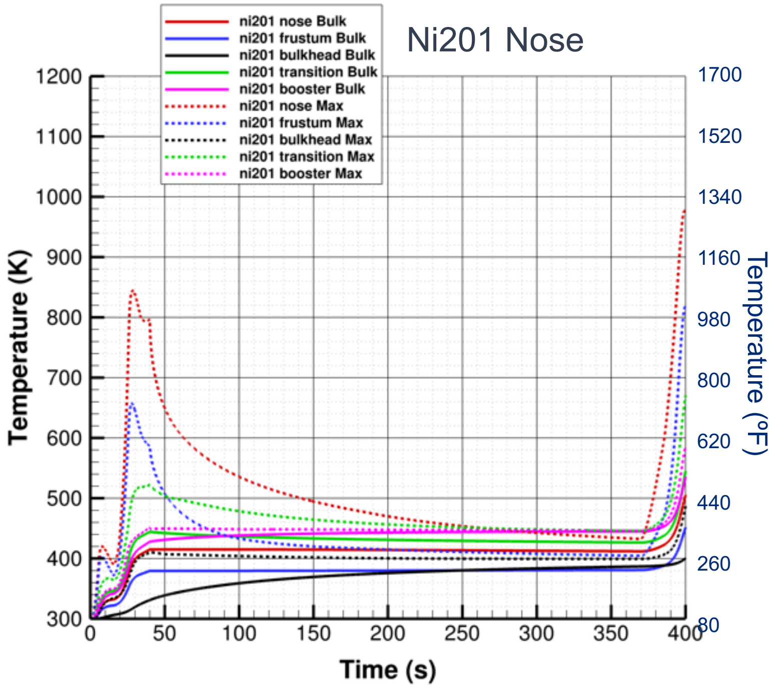

Temperature Statistics By Component – Full Trajectory

- Nosetip
    - Nickel 201 nose peaks at ~850K (~1070 ºF) during ascent, ~980K (~1300 ºF) at end of flight
    - SS410 nose peaks at ~1040K (~1400 ºF) during ascent, ~1120K (~1560 ºF) at end of flight
- Remaining components largely unaffected by nosetip choice (axial conduction through SS410 frustum low)
- SS410 frustum experiment surface reaches high temperatures ~1000 ºF on leading edge at end of flight, but bulk temperatures remain low
- SS410 bulkhead, structural component, remains at reasonable temperatures throughout flight
- AL6061 transition and booster sections, without TPS, reach temperatures at which aluminum retains little strength:
    - ~540K (~510 ºF) bulk temperature at end of flight for transition section
    - TPS likely required for the current configuration to protect the aft aluminum sections

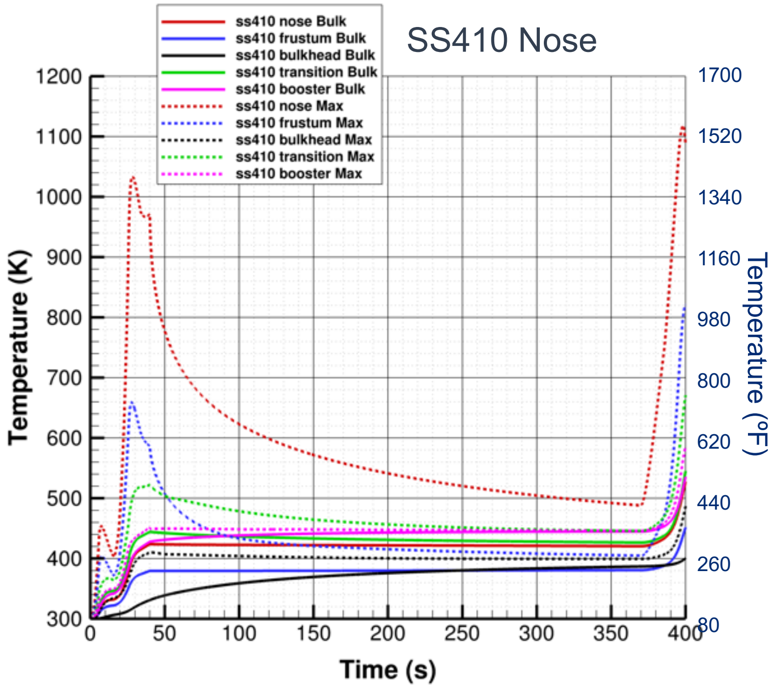

Temperature Statistics By Component – Ascent

- Nosetip
  - Nickel 201 nose peaks at ~850K (~1070 ºF) during ascent, ~980K (~1300 ºF) at end of flight
  - SS410 nose peaks at ~1040K (~1400 ºF) during ascent, ~1120K (~1560 ºF) at end of flight
- Remaining components largely unaffected by nosetip choice (axial conduction through SS410 frustum low)
- SS410 frustum experiment surface reaches high temperatures ~1000 ºF on leading edge at end of flight, but bulk temperatures remain low
- SS410 bulkhead, structural component, remains at reasonable temperatures throughout flight
- AL6061 transition and booster sections, without TPS, reach temperatures at which aluminum retains little strength:
  - ~540K (~510 ºF) bulk temperature at end of flight for transition section
  - TPS likely required for the current configuration to protect the aft aluminum sections

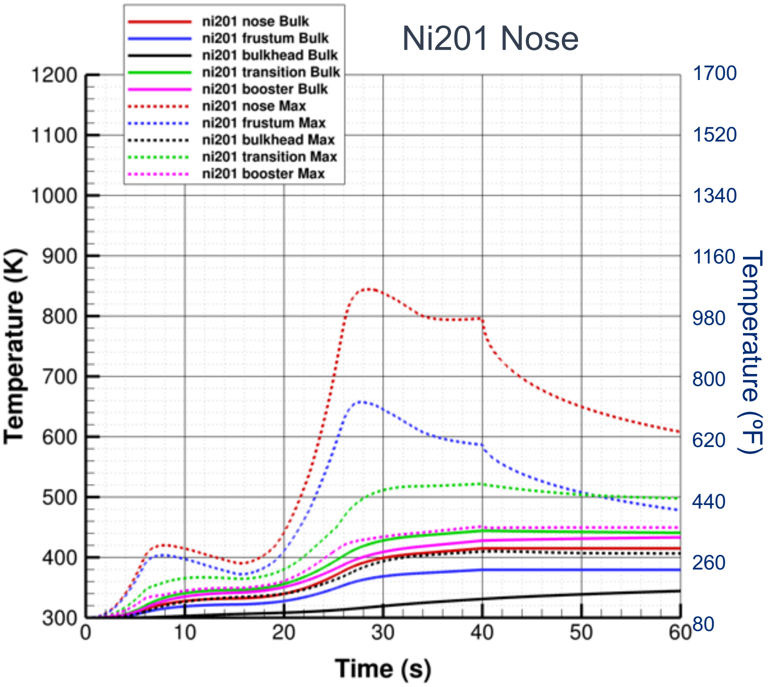

Temperature Statistics By Component – Ascent

- Nosetip
  - Nickel 201 nose peaks at ~850K (~1070 ºF) during ascent, ~980K (~1300 ºF) at end of flight
  - SS410 nose peaks at ~1040K (~1400 ºF) during ascent, ~1120K (~1560 ºF) at end of flight
- Remaining components largely unaffected by nosetip choice (axial conduction through SS410 frustum low)
- SS410 frustum experiment surface reaches high temperatures ~1000 ºF on leading edge at end of flight, but bulk temperatures remain low
- SS410 bulkhead, structural component, remains at reasonable temperatures throughout flight
- AL6061 transition and booster sections, without TPS, reach temperatures at which aluminum retains little strength:
  - ~540K (~510 ºF) bulk temperature at end of flight for transition section
  - TPS likely required for the current configuration to protect the aft aluminum sections

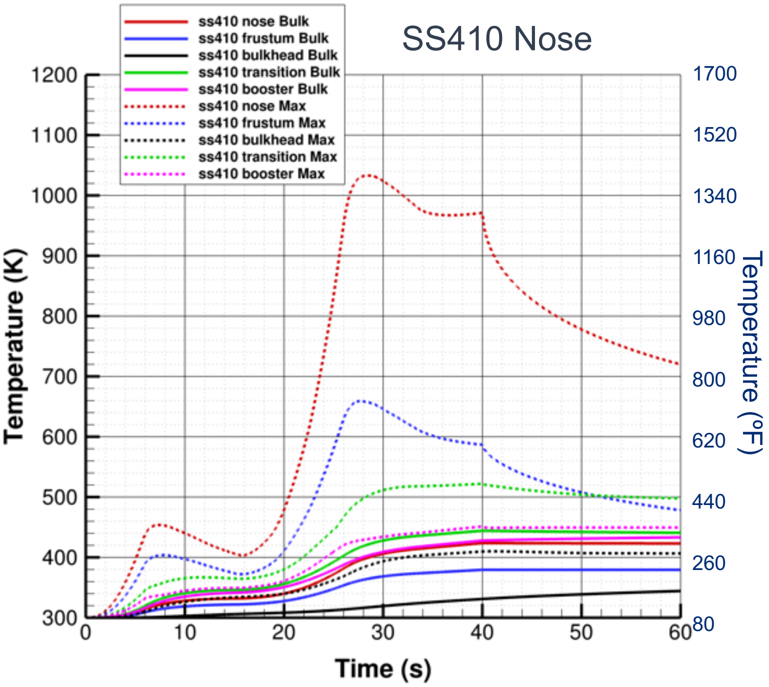

Temperature Statistics By Component – Descent

- Nosetip
  - Nickel 201 nose peaks at ~850K (~1070 ºF) during ascent, ~980K (~1300 ºF) at end of flight
  - SS410 nose peaks at ~1040K (~1400 ºF) during ascent, ~1120K (~1560 ºF) at end of flight
- Remaining components largely unaffected by nosetip choice (axial conduction through SS410 frustum low)
- SS410 frustum experiment surface reaches high temperatures ~1000 ºF on leading edge at end of flight, but bulk temperatures remain low
- SS410 bulkhead, structural component, remains at reasonable temperatures throughout flight
- AL6061 transition and booster sections, without TPS, reach temperatures at which aluminum retains little strength:
  - ~540K (~510 ºF) bulk temperature at end of flight for transition section
  - TPS likely required for the current configuration to protect the aft aluminum sections

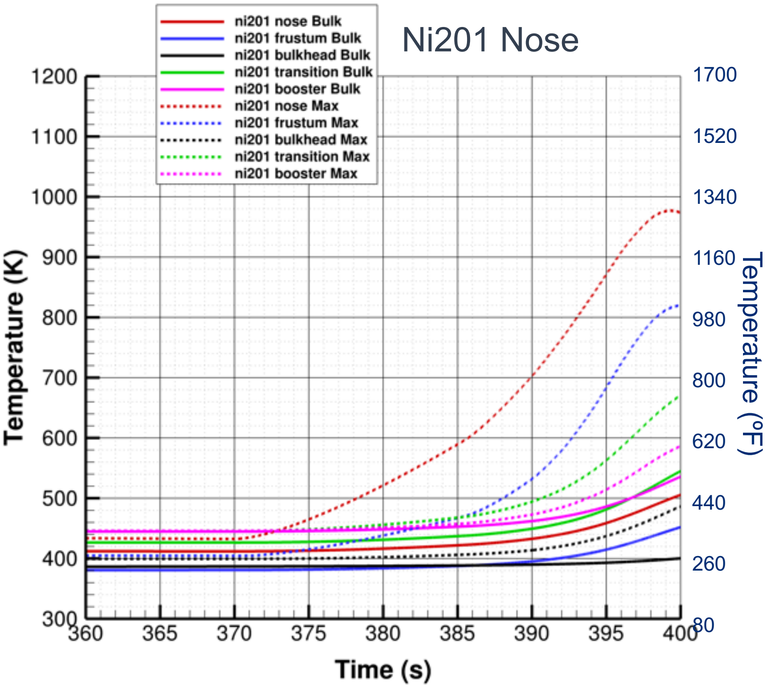

Temperature Statistics By Component – Descent

- Nosetip
  - Nickel 201 nose peaks at ~850K (~1070 ºF) during ascent, ~980K (~1300 ºF) at end of flight
  - SS410 nose peaks at ~1040K (~1400 ºF) during ascent, ~1120K (~1560 ºF) at end of flight
- Remaining components largely unaffected by nosetip choice (axial conduction through SS410 frustum low)
- SS410 frustum experiment surface reaches high temperatures ~1000 ºF on leading edge at end of flight, but bulk temperatures remain low
- SS410 bulkhead, structural component, remains at reasonable temperatures throughout flight
- AL6061 transition and booster sections, without TPS, reach temperatures at which aluminum retains little strength:
  - ~540K (~510 ºF) bulk temperature at end of flight for transition section
  - TPS likely required for the current configuration to protect the aft aluminum sections

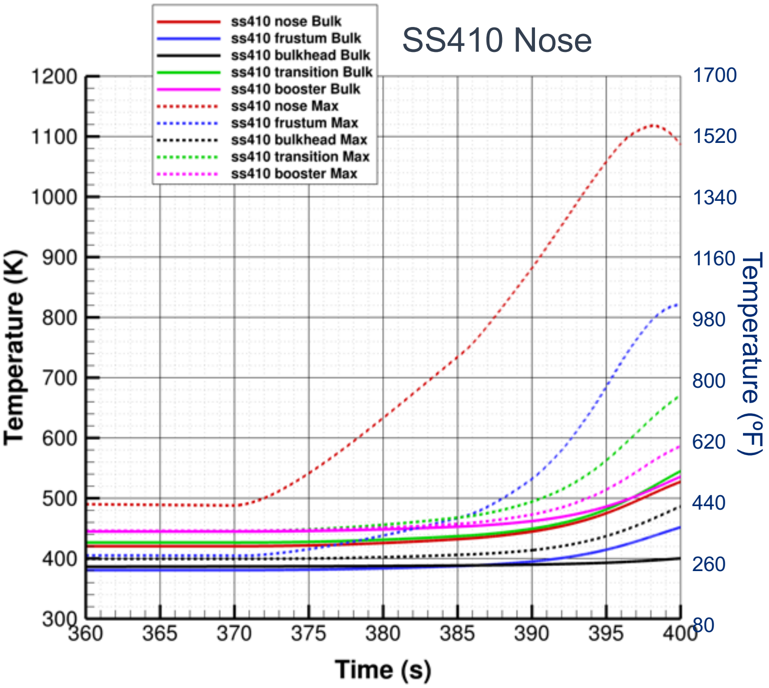

Video – Nickel Nose (Ascent)

- Ascent peak temperatures experiences around 28-30 s
- Major substructures of steel components remain cool, like BOLT heating is highest at the swept leading edges

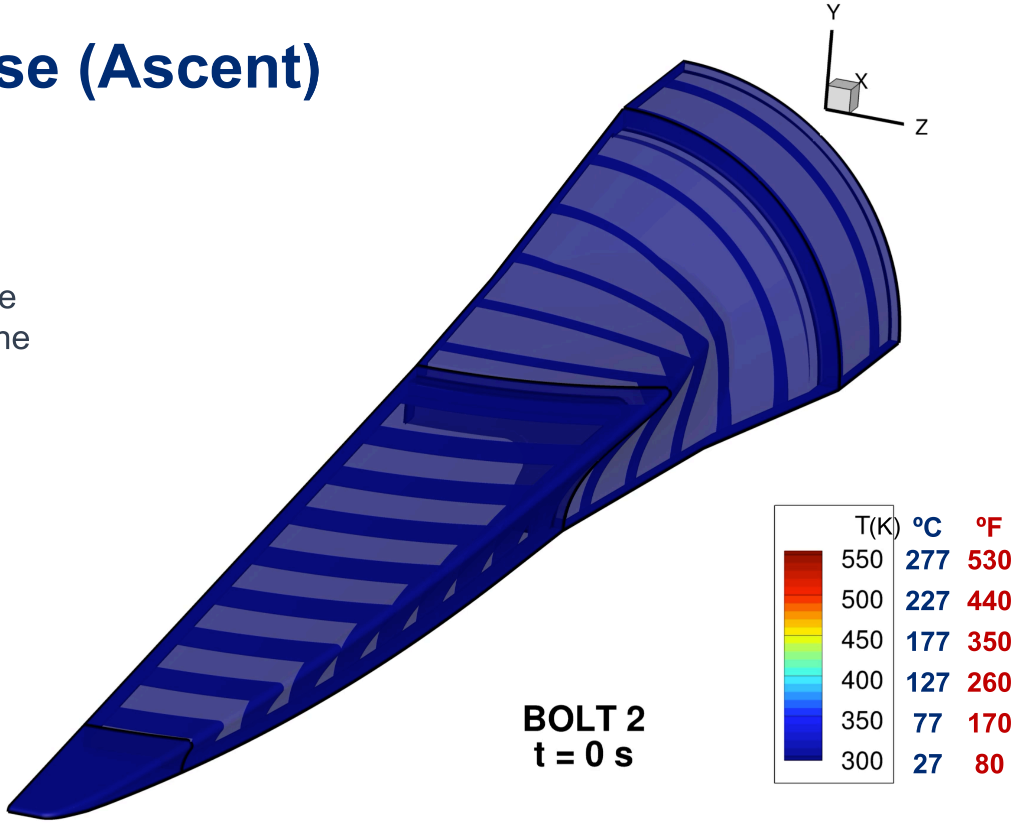

Video – Nickel Nose (Exo)

- Video shows long thermal soak during exoatmospheric phase, prior to reentry
- Steel experiment surface does not reach relative equilibrium prior to descent

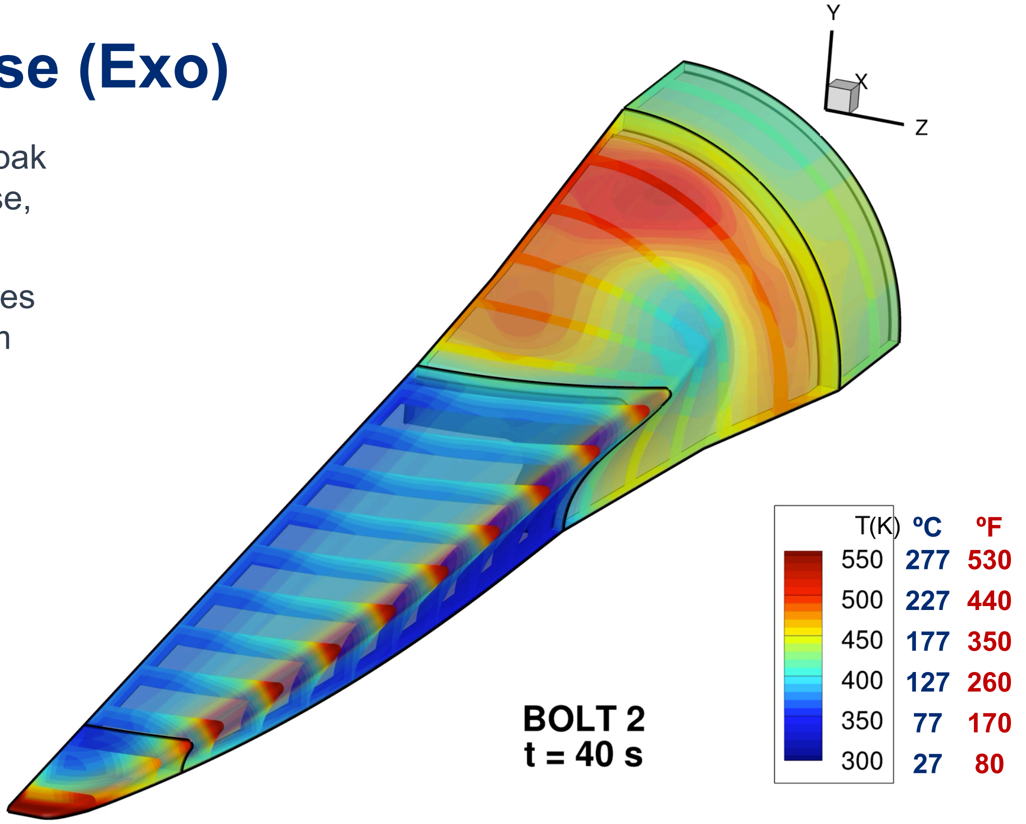

Video – Nickel Nose (Descent)

- Descent phase of experiment
- At end of flight, experiment surface sees fairly high temperatures but bulk/interior remains at lower temperatures
- This video shows the high levels of heating throughout the aluminum transition section when TPS is not used. High temperatures are throughout the bulk of the aluminum aeroshell.

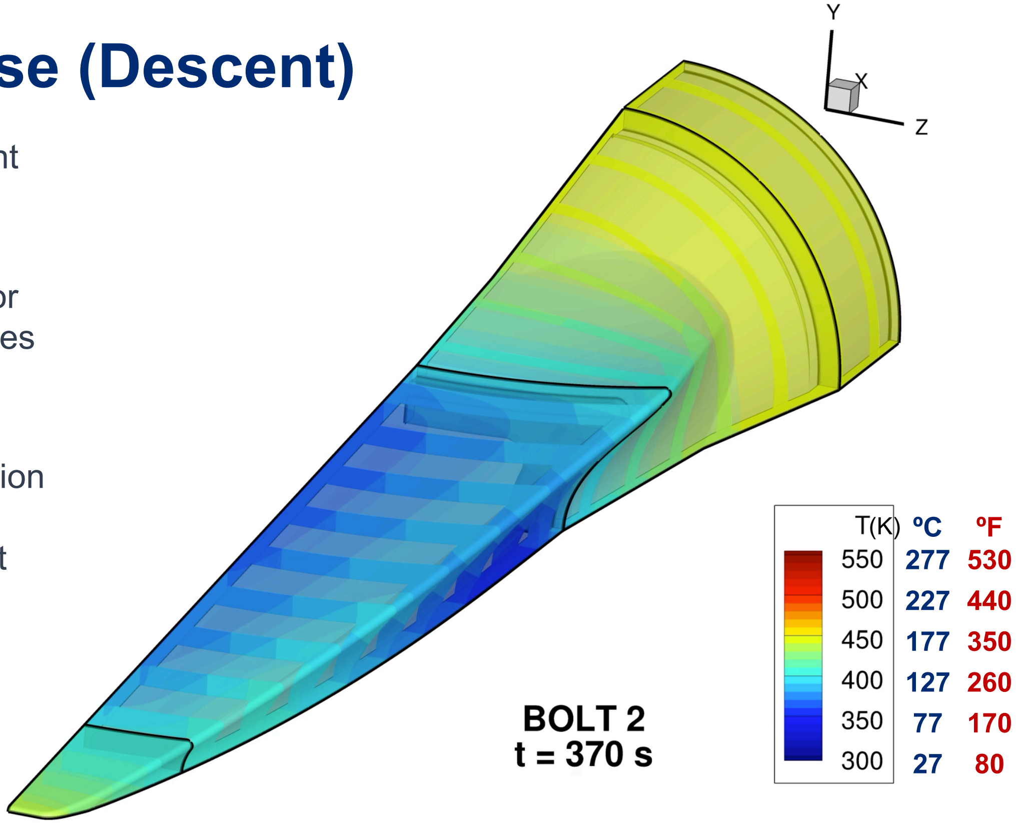

Cork 1D Simulation

- Performed a quick look at a 1/8” cork protective layer over a 0.35” aluminum aeroshell, using HTC and T_r from the transition section peak temperature location
  - x = 1.403539181E+00 , y = 1.830397099E-01, z = 7.794038206E-02 (meters)
- This analysis models pure conduction only!
  - Not representative of ablation or charring
  - Temperatures at the surface of the cork are quite high as a result of the low thermal conductivity of cork → may result in much lower heating entering the substructure due to the use of a Heat Transfer Coefficient
- Thermal properties of Amorim P50 cork used (ref: website)
  - Density = 480 kg/m^3
  - Specific Heat = 2100 J/kg-K
  - Conductivity = 0.07 W/m-K

Preliminary Cork 1D Case Results

- Red = min/max/average temperature of 1/8” cork layer on outer flow surface
- Blue = min/max/average temperature of 0.35” thick AL6061 aeroshell beneath cork
- Preliminary findings (with caveats on modeling only pure conductivity) are much lower temperatures of aeroshell:
  - Bulk temperature of aeroshell reduced from ~540K (~510 ºF) at end of flight to ~350K (~170 ºF)
  - Proper modeling of cork TPS physics via CHAR is planned by CUBRC
- Preliminary findings suggest Cork TPS will need to be applied to the conical transition section, and perhaps to other aluminum sections, but will likely keep temperatures at acceptable levels
- APL is currently running a full 3D case modeling cork TPS, but also the effects of inter-part conduction on the bulk temperatures of the aluminum sections

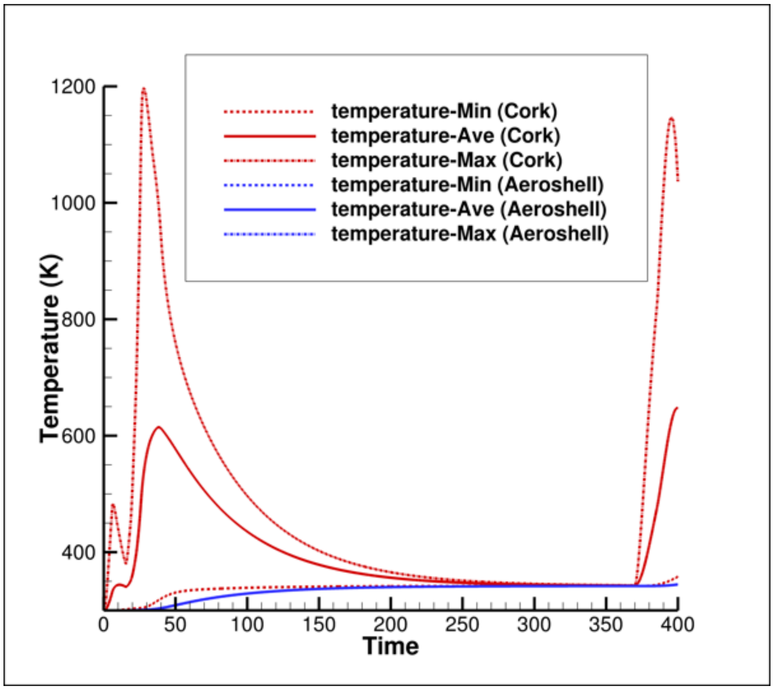

Potential Future Work

Future Work → Transition to TAMU/CUBRC

- Support transition of final pre-CDR thermal analysis to BOLT2 team
- Support BOLT2 team in conducting independent comparisons to the present results

---

Potential Future Checks

- Additional cases with no safety factor on HTC
- Additional cases including radiative heat transfer during trajectory (exploring impact on exoatmospheric leg)
- Compute new flow solutions varying isothermal wall temperature on computed HTC (how does HTC vary with temperature, is 300K-based HTC the best choice?

Continued Development Tasks

- New transient thermal runs with more aggressive global time step (0.01s or 0.1s)
  - Compare against 0.001s timestep and possibly save computation time on future analyses
  - Compare temperature convergence of 0.01s and 0.01s timestep cases to 0.001s baseline (potentially run a 0.0001s case as well)
- Additional cases using only theoretical recovery temperature instead of adiabatic CFD based recovery temperature
  - Would potentially eliminate 50% of CFD solutions needed, dramatically cutting analysis cost

---

JOHNS HOPKINS
APPLIED PHYSICS LABORATORY

A.3. BOLT II Independent Fin Heating CFD Analysis

The following appendix contains details comparisons of CFD heating to the correlation-based heat transfer rates predicted by Northop Grumman on the BOLT II second stage fin. Overall, good agreement was obtained, providing confidence in the Northrop Grumman thermal results.

This work was supported by the Air Force Office of Scientific Research under award number FA9550-20-1-0043 (PO: Dr. Sarah Popkin). Any opinions, finding, and conclusions or recommendations expressed in this material are those of the author(s) and do not necessarily reflect the views of the United States Air Force.

Fin Heating on BOLT2

Computational comparisons

Greg McKiernan, Ph.D.
11/09/20
gregory.mckiernan@jhuapl.edu

Introduction

- MSLRAD and CFD++ computations were completed by JHUAPL for comparison to Northrup-Grumman (NG) heating estimates on the BOLT 2 booster fin.
- Comparisons of the three techniques were made and are presented
  - MSLRAD and NG data were digitized and compared to laminar and turbulent CFD++ data
  - MSLRAD results were not a single line of data due to the way the edge conditions were calculated at the thermal nodes.
    - Instead presented as 5 strips (from root to tip) of thermal nodes from the four fins.
    - An approximate average of the multiple strips of thermal nodes were used for comparison.
  - All NG fin side heating data is from their Colburn Reynolds analogy calculation.

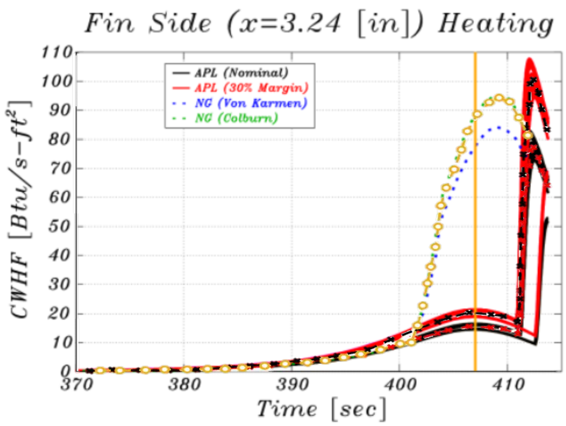

Sample case of the digitization of MSLRAD and NG results. Lines are the MSLRAD output. Symbols are the MATLAB digitization.

Introduction – CFD++

- CFD++ solutions were completed at individual times
  - For simplicity, fin was modeled on a flat plate.
  - t = 19, 27, 32, 399, 406, and 409 s
  - Trajectories from 46027_Heat.txt
  - 1976 Standard atmosphere
  - T_{wall} = 294 K (70° F)
  - Fully laminar and fully turbulent solutions were completed (1-equation SA turbulence model)
  - Surface heat transfer rates were used to compare to MSLRAD and NG

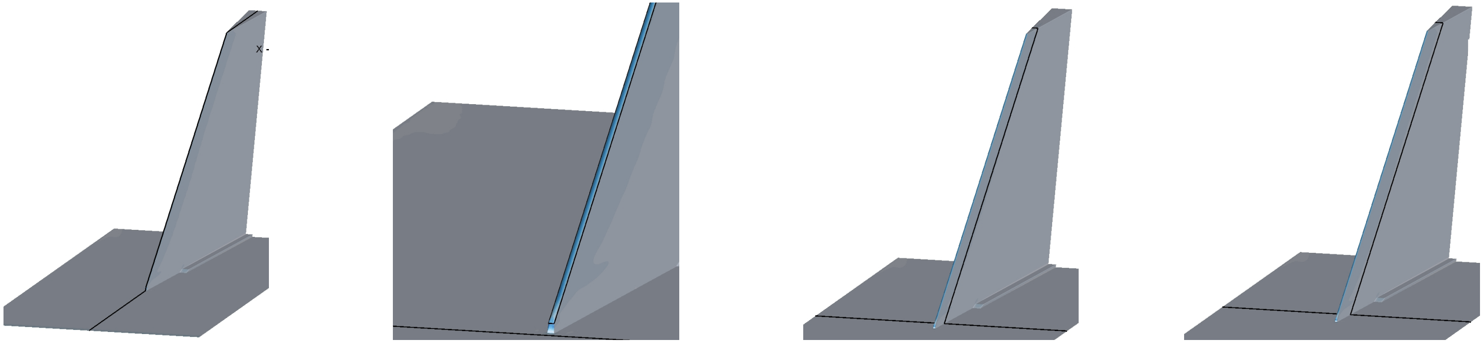

Leading edge (Y=0) Tangency point (X=0.062") Fin side (X=2.15") Fin side (X=3.24")

Data extraction locations

CFD++ Grid

- Hybrid grid was created for CFD++ analysis
- 5e-8 wall spacing was used to adequately resolve the leading edge
  - For lower Reynolds numbers cases a 1e-7 wall spacing was used.
- ~70 anisotropic hex cells were placed near the wall surface to resolve the boundary layer.
- Isotropic tetrahedral cells were used further from the wall.
- A y+ < 1 was desired for the fin.
  - Difficult near the leading edge
  - y+ near 1 on the leading edge
  - y+ < 0.1 off leading edge

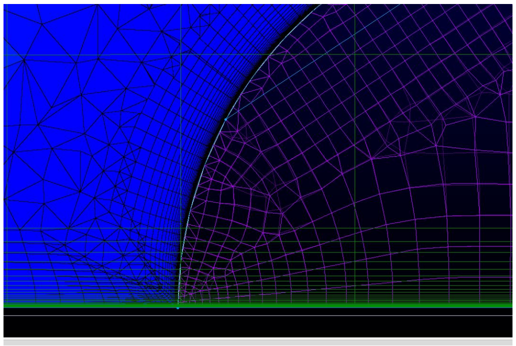

Nosetip surface and volume grid

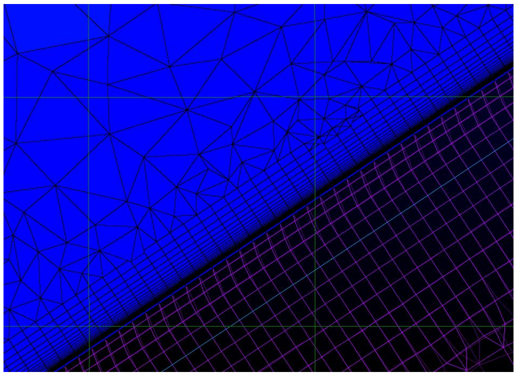

Leading edge surface and volume grid

Boundary Conditions

- In-flow conditions matched the freestream conditions at a given time during the trajectory.
- Flat plate and fin were given an isothermal wall boundary condition.
  - T_{wall} = 294 K (~70° F)
- Side walls have a characteristic-based BC.
  - Set at freestream conditions.
  - Allows for inflow or outflow depending on local velocity vectors
- Supersonic outflow

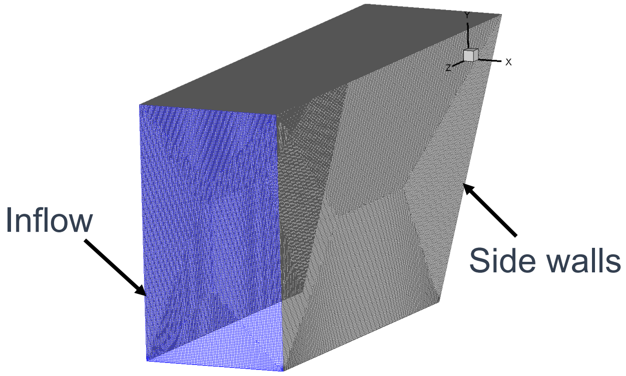

Nosetip surface and volume grid

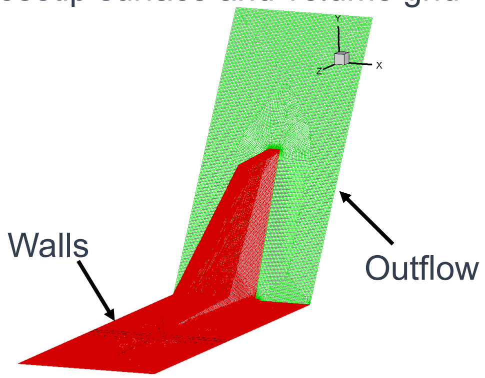

Leading edge surface and volume grid

Leading edge heating comparisons

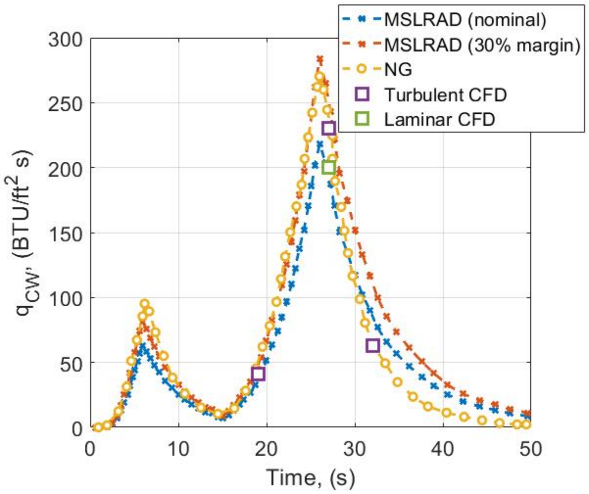

Ascent

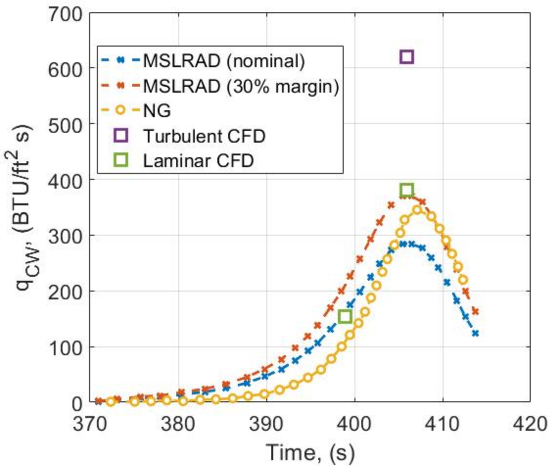

Descent

- Good agreement between methods for leading edge heating.
  - Leading edge flow is anticipated to be laminar, so turbulent CFD data points are shown for reference only

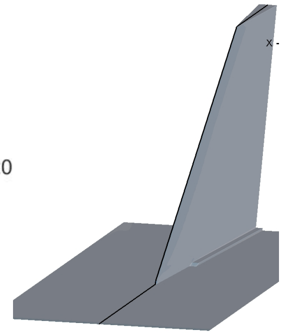

Leading edge definition

Tangency point (x = 0.62 in.) heating comparisons

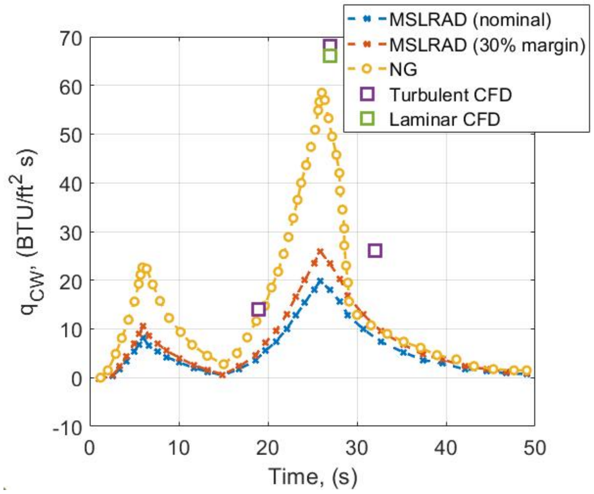

Ascent

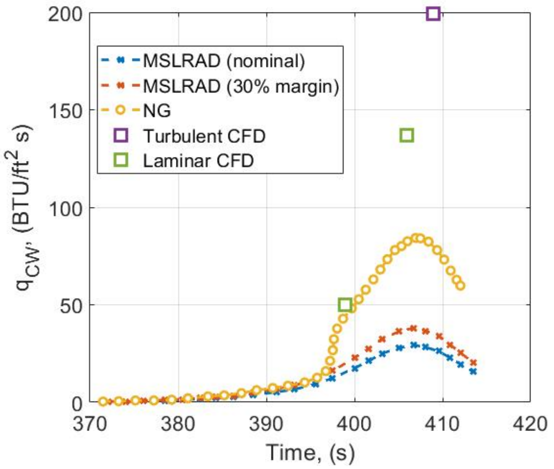

Descent

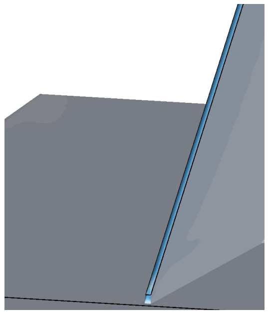

Cut location

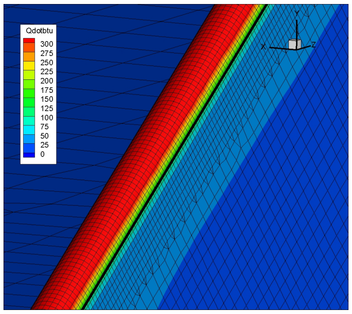

Cut location with mesh and laminar surface heating

- Significant differences between MSLRAD, NG, and CFD++ at this fin location
- CFD++ solutions saw largest discrepancy from MSLRAD and NG at this location.
  - CFD++ solution is ~1.25x the NG correlation during the ascent window (t = 27 s)
  - CFD++ solution is ~1.6x the NG correlation during the descent window (t = 406 s)

Fin side (x = 2.15 in.) heating comparisons

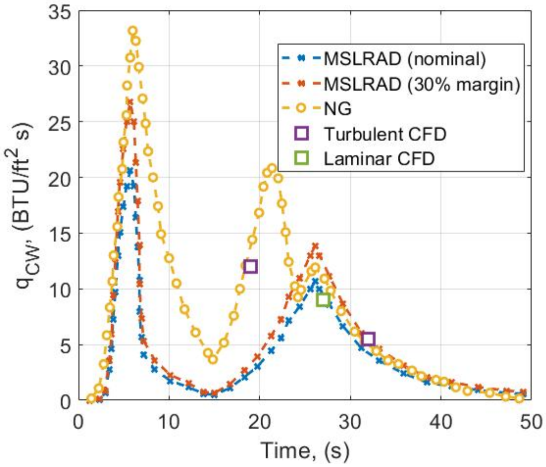

Ascent

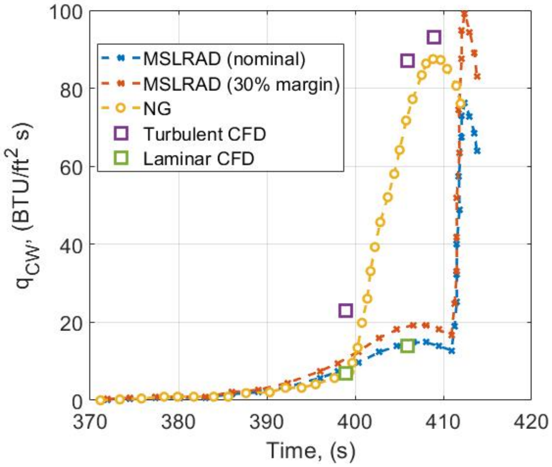

Descent

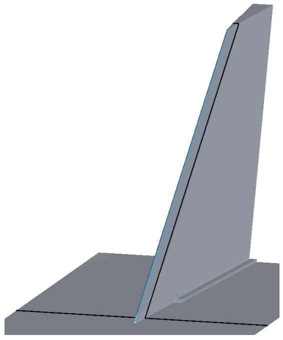

X=2.15”

- Significant differences between MSLRAD, NG correlations
- CFD++ solutions agree with both correlations
  - Turbulent heating agrees with NG heating
  - Laminar heating agrees with MSLRAD heating

Fin side (x = 3.24 in.) heating comparisons

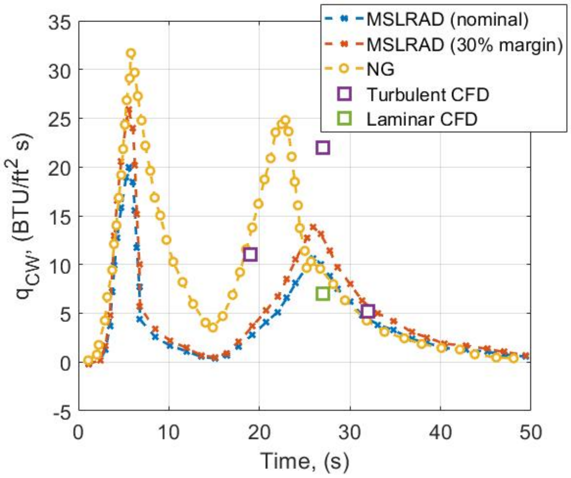

Ascent

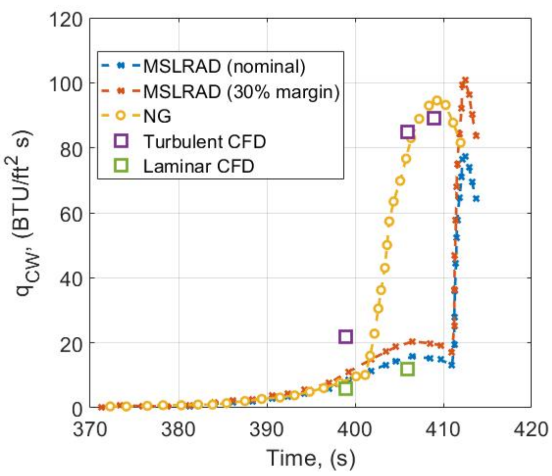

Descent

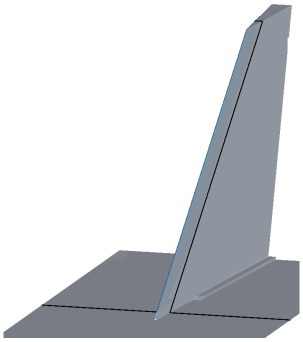

X=3.24”

- Significant differences between MSLRAD, NG correlations
- CFD++ solutions agree with both correlations
  - Turbulent heating agrees with NG heating
  - Laminar heating agrees with MSLRAD heating

JOHNS HOPKINS
APPLIED PHYSICS LABORATORY

B. Year 2 Interim Report (Archived Copy)

The following pages of this appendix section contain an archived copy of the previously-submitted interim/annual report for the second year of this grant. Inclusion of this report supplements the final performance report with a copy of any previously-referenced analysis.

JOHNS HOPKINS
APPLIED PHYSICS LABORATORY

FA9550-20-1-0043 Year 2 Annual Report
10 March 2022
JHU/APL Project Number FGX75

To: Dr. Sarah Popkin
Program Officer - High Speed Aerodynamics
AFOSR/RTA
875 N. Randolph St., Suite 325, Room 3112
Arlington, VA 22203-1768

From: Dr. Bradley M. Wheaton (Principal Investigator)
Dr. Daniel B. Araya (Co-Investigator)
Dr. Dennis C. Berridge (Co-Investigator)
Dr. Cameron S. Butler
Dr. Gregory R. McKiernan
Mr. Prasad M. Kutty
Mr. Jim B. Fortier
Dr. John T. Melcher
Mr. Eliott J. Radcliffe
Mr. David M. Gers
Mr. Ryan L. Eby
Ms. Lauren D. Ashby (Financial Manager)
Mr. Justin R. Smith (Program Manager)

Subject: Boundary Layer Transition (BOLT) Post-Flight Research and BOLT II Flight Test Support (Grant FA9550-20-1-0043, period 11 March 2021 through
10 March 2022)

This report summarizes the second year of research efforts by the Johns Hopkins University Applied Physics Laboratory (JHU/APL) under grant number FA9550-20-1-0043 from the Air Force Office of Scientific Research (AFOSR), consisting of research to analyze the flight data from the Boundary Layer Transition (BOLT) flight experiment as well as to support the execution of BOLT-2: The Holden Mission.

Major activities from this year included post-flight research to investigate the behavior of the BOLT flight experiment via a collaborative investigation with DLR and AFRL partners (Section 2), post-flight six degree of freedom modeling of the BOLT vehicle behavior (Section 3), modeling of the aeroelastic effects that coupled into the flight vehicle dynamics (Section 4), scientific analysis of supersonic transition data measured during the as-flown BOLT trajectory (Section 5), and support of the BOLT-2 preflight preparations including incorporating modeling lessons learned from the BOLT flight to ensure a successful experiment for the follow-on BOLT-2 flight (Section 6).

Contents

1 Introduction 4

1.1 Description of Research 4
1.2 Year 2 Major Activities 4

2 BOLT Postflight Investigation 6

2.1 Investigation Structure and Partners 6
2.2 Summary of Observed Flight Behavior 6
2.3 Noncontributing Factors 6
2.4 Investigation Finding: Flight Deviation via Pitch Roll Coupling and Static Margin Reduction 7
  2.4.1 Rigid Body Aerodynamics Cannot Explain Reduced Stability 8
  2.4.2 Flexible Body Aerodynamics Can Explain Reduced Stability 9
2.5 Investigation Outcomes and Lessons Learned 10
  2.5.1 Flight Systems Were Not Causal to the Flight Behavior 10
  2.5.2 Preflight Analysis Was Consistent with Previous HIFiRE Flights 10
  2.5.3 Modeling Angle of Attack Divergence Near the Resonance Condition 11
  2.5.4 Trajectory Simulation Pedigree and Prediction of Pitch Roll Coupling 12
  2.5.5 Program Execution and Structure 12
  2.5.6 Lessons Learned and Recommendations 13

3 BOLT Postflight 6DOF Modeling 15

3.1 Description of Flight Behavior 15
3.2 Aerodynamic Modeling 17
3.3 Rigid Body 6DOF Simulation Studies 19
  3.3.1 Rigid Body Nominal Modeling 20
  3.3.2 Rigid Body Monte Carlo Modeling 23
3.4 Aeroelastic 6DOF Simulation Studies 24
  3.4.1 Simple Aeroelastic Model 25
  3.4.2 High Fidelity Aeroelastic Modeling 26
3.5 Potential Mitigations 30
3.6 Summary and Future Work 33

4 BOLT Postflight Aeroelastic Modeling 35

4.1 Flight Deviations from Planned Mission 35
4.2 Model of a Slender Asymmetric Flexible Spinning Airframe 36
  4.2.1 Linearized Dynamics Model 37
  4.2.2 Quasistatic Analysis 39

4.2.3 Distributed Model Parameters 40
4.2.4 Flexible Fin Model 40
4.3 Flight Stability at Stage Separation 42
4.4 6-DOF Flight Simulation 44
4.5 Conclusions 46

5 Supersonic Transition Analysis from the BOLT Flight **47**
5.1 BOLT Flight Payload and Vehicle 47
5.2 Flight Trajectory and Experiment Conditions 47
5.2.1 Best Estimate Trajectory 49
5.2.2 Flight Dynamics Axis Definitions 49
5.2.3 Surface Pressure Attitude Reconstruction 50
5.2.4 Vehicle Attitude 51
5.3 Analysis of Descent Transition Measurements 53
5.3.1 Scientific Experiment Coordinate System 53
5.3.2 Data Processing Methods 56
5.3.3 Primary Surface Windward 57
5.3.4 Primary Surface Leeward 60
5.4 Computational Studies 61
5.4.1 Mean Flow Computations 61
5.4.2 Flight Comparisons 65
5.4.3 Stability Analysis 69
5.5 Summary and Recommended Future Work 73

6 BOLT-2 Support **77**
6.1 6DOF Monte Carlo Stressors Based on BOLT Investigation 77
6.2 Postflight Investigation of Drag Modeling 77
6.3 Future Work 78

A Investigation Fault Tree **81**

B Rigid Body Aerodynamics Check on BOLT 2nd Stage **83**

1. Introduction

1.1. Description of Research

Prediction of hypersonic boundary-layer physics is critical to optimize the design of hypersonic vehicles for maximum range, thermal survivability, and controllability. Physics-based prediction methods are under development that have the potential to improve the ability of hypersonic vehicle designers to estimate transition and turbulent flow effects. These methods require extensive validation with ground and flight test data that is often not available for the geometry of interest. To date, much of the available validation data are on simple conical geometries. The Johns Hopkins University Applied Physics Laboratory (APL) proposed this Boundary Layer Transition (BOLT) Post-Flight Research and BOLT II Flight Test Support to assist the Air Force Office of Scientific Research (AFOSR) and university researchers in obtaining and analyzing critical hypersonic boundary layer physics validation data in the flight environment. The proposed research will be conducted within a three-year project period with a requested total funding of $825K ($275K/year).

The primary objective of this research was to continue to utilize the BOLT boundary-layer transition flight test data that was to be obtained in a previous grant (AFOSR Award Number FA9550-17-2-0001) to discover and document the salient physics of the laminar-to-turbulent transition process observed during the flight test, as well as to disseminate the findings and test data at the direction of the AFOSR to other investigators within the AFOSR portfolio.

The secondary objective of this project was to strengthen the development of the planned Texas A&M and CUBRC BOLT II: The Holden Mission flight test to study turbulent flow phenomena by leveraging the expertise and significant experience of the APL team who led the BOLT flight experiment. APL performed independent aerodynamic and thermal analyses to ensure the BOLT II flight experiment would be delivered at the desired experimental conditions and that the experiment hardware would survive through the flight environment. APL also plans to assist the BOLT II team in post-processing the flight data.

1.2. Year 2 Major Activities

The majority of the Year 1 activities on this grant were focused on support of the BOLT II flight experiment via independent analysis in the aerodynamics and thermal analysis areas. Additional support has been given in the knowledge transfer and advisory of BOLT information to the BOLT II team.

Year 2 of this grant's research encompassed the BOLT flight experiment in June 2021. Unfortunately, the BOLT experiment exhibited unexpected flight behavior and did not reach its intended hypersonic flight conditions. As a result, much of the planned post flight research was redirected in consultation with the AFOSR PO to conducting a post flight investigation of the BOLT flight such that a cause could be determined and the results used to ensure that the follow-on BOLT-2 flight would be successful. A summary of the investgation findings appears in Section 2 with the details of the supporting analyses covered in Sections 3 and 4. Following the investigation, the focus of the research turned to analysis of the supersonic transition data from the flight and the in progress research is summarized in Section 5. Concurrently, APL staff worked together with NASA Wallops to incorporate lessons learned from the BOLT investigation into the final modeling ahead of the BOLT-2 flight. APL's efforts to support BOLT-2 are summarized in Section 6.

2. BOLT Postflight Investigation

Supported by funding from this grant, APL lead a post flight analysis (investigation) of the BOLT flight unexpected behavior from the June 2021 flight event. The investigation was a collaborative effort with flight partners AFRL/RQ and DLR and was conducted with full participation of the AFOSR Program Officer Dr. Popkin.

2.1. Investigation Structure and Partners

Within the budgetary and schedule constraints of the BOLT program, a small advisory committee was formed to investigate the flight behavior. The committee consisted of members of the BOLT team from AFRL, DLR, and APL. In addition, a small number of additional staff from APL and Sandia National Laboratory were brought in as Subject Matter Experts to assist with particular aspects of the investigation. The investigation initiated in August 2021, and results were briefed to AFOSR at two reviews: (1) an interim investigation review on 20 September 2021 as well as (2) a final review on 19 November 2021. APL published four AIAA papers documenting the post flight research phase as seen in Wheaton et al. [1] from SciTech 2022, as well as three papers for AVIATION 2022 (Butler et al. [2], Kutty et al. [3], and Melcher et al. [4]). The advisory committee developed a fault tree to guide the investigation efforts, which appears in Appendix A.

2.2. Summary of Observed Flight Behavior

The BOLT experiment was launched under benign observable meteorological conditions. After an apparent nominal first stage flight, the S31 first stage separated at the expected flight conditions. However, immediately after the Stage 1 separation at around 11 s into flight, the Stage 2 vehicle began to develop a coning motion with an increasing angle of attack, opening up to approximately 7 deg cone half-angle magnitude at the point of Improved Orion ignition, which occurred at the expected time. Upon ignition of the Improved Orion, the angle of attack diverged further, exceeding 25 deg by the time of Improved Orion burn out. The high angle of attack resulted in misdirection of the rocket motor thrust, and increased drag, both of which contributed to a significant loss of vehicle performance in terms of achieved altitude and velocity.

Upon examination of the flight data, it was quickly noted that although the roll rate appeared to be within expected values up through a couple of seconds into the coast period, at about 13 s, the roll rate deviated sharply from the established trend. Furthermore, the windward meridian, or azimuthal ray of the vehicle that is directly exposed to the impinging free stream, locked in to a single value. This is an indication of the phenomenon known as pitch-roll coupling, wherein a resonance occurs between the natural pitching frequency and roll rate of the vehicle. Further analysis of the flight data indicated that the pitch-roll coupling persisted from 13 s through Improved Orion burn. In addition, pitch-roll coupling was observed during portions of the descent phase of the flight.

2.3. Noncontributing Factors

Many possible contributors were exonerated in the course of the investigation, as shown in the fault tree. A brief summary of the major areas deemed to be not contributing to the anomaly is given below:

- **Environmental/Meteorological**: Weather conditions were benign at the launch site. Standard practices for weather condition monitoring were used. There was no indication of adverse temperatures, winds, or wind shear during the flight.
- **Staging anomaly:** There was no apparent anomaly in the staging event which separated the spent S31 first stage from the Stage 2 flight configuration. Staging occurred at the expected time, within the nominal range of flight conditions. No unexpected accelerations or rates were imparted to the vehicle of an impulsive nature that would indicate any kind of separation hang-up or recontact.
- **Fin cant setting error or fin separation:** The roll rate achieved during Stage 1 was close to the preflight nominal prediction, and well within expected variations. Furthermore, upon separation of the S31 stage, the roll rate of the Stage 2 configuration initially increased to a higher value, as expected. There was nothing observed in the roll rate history up until the onset of pitch-roll coupling at 13 s, that would point to a fault of the fins.
- **Vehicle breakup or demise:** With the exception of a small subset of surface instrumentation that failed to be transmitted, all instrumentation on the vehicle functioned as expected and was transmitted by telemetry until shortly before impact. This included instrumentation in the forward experimental payload section as well as that located aft of the experimental portion. There was no indication of loss of any instrumentation due to a vehicle demise. Aerodynamic and thermal loading prior to the angle of attack divergence were within predictions and were not excessive. Instrumentation from the nosetip and other vehicle components remained functioning throughout the event. Postflight analysis exploring potential loss of an aerodynamic fairing indicated this would have had a negligible effect on the vehicle aerodynamics.
- **Pre-launch mechanical damage:** There was no indication of damage to the fin panels, leading edges, or other vehicle structure prior to launch, that would have contributed to the behavior. Stage 1 portion of flight appeared to be nominal. In addition, during the descent phase, upon breaking out of the pitch-roll coupling which occurred at the higher descent altitudes, the vehicle took on a very nominal motion profile, with the angle of attack converging to very small values as the vehicle descended to low altitude.

2.4. Investigation Finding: Flight Deviation via Pitch Roll Coupling and Static Margin Reduction

The occurrence of pitch-roll coupling, which appears to be definitive for the BOLT flight, is indicative of a much lower static margin achieved in flight than was predicted pre-flight. During pitch-roll coupling, the roll rate locks in to the vehicle natural pitching frequency. For the BOLT vehicle, which has an asymmetric front payload section, the natural pitching frequency is a function of the plane of the pitching motion, being most distinct between the vehicle pitch and yaw planes, as defined by the body coordinate system. The natural pitching frequency may be predicted, but it is difficult to measure it directly from the flight data. However, the body roll rate is easily measured by the vehicle IMU(s) with high confidence. During pitch-roll coupling, the aerodynamic pitching frequency must be equal to the body roll rate. By knowing the pitching frequency during pitch-roll coupling, the vehicle static margin may be calculated. These calculations show up to a 40–50% reduction in static margin compared to preflight predictions.

Preflight predictions showed an expected range of natural pitching frequencies significantly higher than the expected vehicle roll rate during the coast phase. Moreover, upon ignition of the Improved Orion, the vehicle roll rate was predicted to increase sharply, and transition through the region of critical pitching frequencies quite rapidly. This showed a good design of the vehicle roll rate following common sounding rocket practices. However, the flight showed that the actual critical pitching frequencies were much lower, very close to the coasting vehicle roll rate.

The preliminary cause of the observed flight deviation was a significant reduction in the second stage aerodynamic static stability relative to preflight predictions. As a result of reduced stability, the critical pitch frequency was in close proximity to the roll rate during the initial portion of the coast phase following separation of the first stage ($t > 11$ s) enabling roll resonance “lock-in” (roll rate locks-into the critical pitch frequency). Roll resonance “lock-in” caused exponential growth in the vehicle angle of attack. The primary contributor was aeroelastic flexure of the 2nd stage during the coast phase exacerbated by high dynamic pressure and the significant lift produced by the forebody in the pitch plane. Aeroelastic flexure was also expected to create a large divergence of the pitch plane and yaw plane critical frequencies, caused by the asymmetric shape of the vehicle outer mold line, and exacerbated by a loss of static margin due to significant aeroelastic effects. The divergence of the pitch plane and yaw plane critical frequencies also expanded the region in which the vehicle was susceptible to entering roll-pitch coupling.

2.4.1. Rigid Body Aerodynamics Cannot Explain Reduced Stability

It was shown during the investigation that rigid-body aerodynamics cannot explain the reduced aerodynamic static stability observed during flight. Extensive post-flight aerodynamics work showed that the preflight rigid-body vehicle aerodynamics were predicted within normal uncertainties utilizing the same methods used for previous HIFiRE flights. Pitch roll coupling was not expected at $t = 11$ s with estimates that are consistent with methods used in previous HIFiRE flights.

The aerodynamic database used for the pre-flight trajectory predictions was developed by AFRL/RQ using a combination of the CART3D inviscid CFD prediction tool and the Missile DATCOM. Preflight predictions incorporated the asymmetric payload shape, and resulted in characteristics that reflected distinct differences in static margin and natural pitching frequencies for the vehicle pitch and yaw planes. The Stage 2 configuration was predicted to have 10–12% body length static margin at $t = 11$ s. The static margin for the yaw plane was larger than that for the pitch plane, so the vehicle stability was deemed sufficient for the BOLT mission. The rigid body center of pressure was independently verified by APL during the post flight investigation and was similar to preflight predictions performed by AFRL/RQ. The vehicle gravimetrics and center of gravity were well characterized from preflight measurements and were reproduced independently by the team during the post-flight investigation. The static margin difference cannot be attributed to incorrect vehicle gravimetrics buildup or incorrect rigid body aerodynamic predictions.

Postflight six degree of freedom (6DOF) trajectory analysis was performed by APL to predict the effects of differences in the 2nd stage pitch and yaw rigid-body aerodynamic stability due to the highly asymmetric forebody. This analysis shows a high propensity for angle of attack amplification during roll resonance crossing but does not explain the dramatic reduction in 2nd stage aerodynamic stability observed during flight.

Since post-flight it was known or strongly suspected that the static margin was different than that obtained by predictions, additional investigations were conducted to determine whether some aerodynamic effect had been overlooked, or whether the static margin reduction could be explained by a change to the vehicle configuration in flight.

The results of all the post-flight aerodynamic investigations were a corroboration of the original rigid body predictions. Since all post-flight analysis indicated the validity of the original rigid body aerodynamic predictions, the team began to posit aeroelastic effects as being a potential cause of the observed static margin reduction.

2.4.2. Flexible Body Aerodynamics Can Explain Reduced Stability

The investigation identified aeroelasticity as the most probable cause of the static margin reduction which led to the onset of pitch-roll coupling in the BOLT flight. There are three threads of analysis that led to this conclusion:

- Lack of any other probable cause
- Apparent correlation between static margin reduction and dynamic pressure (larger static margin loss as indicated by roll rate occurred at highest dynamic pressure, and as dynamic pressure descreased during ascent the apparent static margin loss also decreased)
- Flight vehicle structural compliance in tandem with the unique lift distribution generated by the BOLT shape was later shown to result in large static margin reduction under expected flight loads

It was found that flexible body aerodynamics could explain the reduced aerodynamic static stability observed during flight. The lack of other likely cause has been addressed above, and is shown in the fault tree. While some elements in the fault tree cannot be ruled out completely, the investigation found that these other possible contributors are not likely, and further analysis has indicated aeroelastic effects as being a likely contributor, as will be shown below.

The investigation determined that only plausible explanation for the reduced aerodynamic static stability observed during second stage coast ($t > 11$ s) is flexible body aerodynamic effects. During roll resonance lock-in ($t = 13$ s), the 2nd stage static margin can be measured from the roll rate (critical pitch frequency is equal to roll rate). Postflight static margin was 5.4% body length which is approximately 50% of the preflight static margin prediction based on rigid body aerodynamics of 10–12% body length. The primary candidate for reduced stability is aeroelastic flexure of the vehicle. Aeroelastic analysis of the second stage has shown a static margin reduction of 6% at $t = 11$ s. This reduction was shown to be proportional to freestream dynamic pressure. The separation altitude of 6km for BOLT resulted in a dynamic pressure of 5700 psf which was approximately five times higher than for a previous asymmetric payload (HIFiRE-5) on the same second stage (Improved Orion). This high dynamic pressure would have exacerbated aeroelastic effects for BOLT. Postflight trajectory reconstruction simulations have been run with a simple representation of the aeroelastic dependency on dynamic pressure (Section 3) and have shown to reproduce similar behavior to that observed in the flight. Structural modeling of the BOLT flight vehicle with representative mechanical properties shows a potential reduction of pitch plane static margin of about 6% body length, at the point of Stage 1 separation. Compliance of the vehicle structure, vehicle section joints, and fins are included in this analysis, and all combine to result in a predicted significantly lower static margin, when aeroelasticity is accounted for. Section 4 shows the aeroelastic modeling performed by APL.

It is important to note that while the structural prediction shows a large reduction of static margin compared to the rigid body calculation, the structural analysis does not indicate a failure in flight, or an inherent design weakness or deficiency in any particular element of the vehicle structural design. Rather, the result indicates that the vehicle has a certain inherent compliance, and when subject to the aerodynamic loading expected in flight with the unique BOLT shape, that compliance will reduce the static margin to atypically lower values. It should be noted that the BOLT forebody shape provides large lifting surfaces that generate significantly larger normal forces on the forward payload section than would be experienced for a more traditional front end geometry. For the BOLT flight, the reduction in static margin caused the natural pitching frequencies to be much lower than predicted, and resulted in the observed angle of attack divergence and pitch-roll coupling.

2.5. Investigation Outcomes and Lessons Learned

2.5.1. Flight Systems Were Not Causal to the Flight Behavior

The malfunction of any particular flight system does not appear causal to the flight behavior. DLR, AFRL, and APL vehicle electronic systems appeared to function per design. The exception was the failure of 1 of 12 AFRL flight computers resulting in loss of 32 of 350+ scientific instrument channels (not causal to the flight behavior, but only resulting in a minor loss of science data channels). Factoring inoperative sensors and the flight computer loss, over 86% of all 350 sensor data channels were functioning. Data from onboard sensors in various portions of the vehicle (payload, service modules) were received throughout the flight, indicating that the vehicle and payload remained structurally intact. A review of preflight procedures was conducted to verify that the assembly of the vehicle and setting of desired fin cant angles were correctly conducted, to rule out vehicle misalignment from incorrect assembly procedures.

2.5.2. Preflight Analysis Was Consistent with Previous HIFiRE Flights

The preflight analysis of the vehicle performance was conducted consistent with standard practice techniques for very low cost scientific flight experiments utilized in previous AFRL flight tests such as the HIFiRE program. The investigation found that the rigid-body aerodynamic force and moment predictions were correct and consistent with best practice for scientific flight mission planning. Likely contributing to the flight behavior was the larger than typical aerodynamic asymmetry of the BOLT forebody shape and overall vehicle. This asymmetry has been shown to amplify angle of attack significantly at times when the roll rate is in the vicinity of natural vehicle dynamics frequencies (pitch and yaw eigenfrequencies). The preflight trajectory simulations utilized a tool that assumed rotationally symmetric aerodynamics, an assumption that was later found to mask the BOLT vehicle's susceptibility to pitch-roll coupling during resonance crossing periods. Postflight trajectory simulations with nominal rigid body aerodynamic and vehicle mass properties show a tendency of the vehicle to exhibit similar angle of attack growth and pitch-roll coupling several seconds into the Improved Orion burn, albeit at a time of 7–8 seconds later than was actually observed in flight. This result indicates that the BOLT flight vehicle has a tendency to exhibit pitch-roll coupling. The postflight trajectory simulations also indicate that there must have been some mechanism acting which reduced the vehicle static margin and natural pitching frequencies below the nominal preflight predicted values (as noted above), to cause the initiation of the instability to occur at 11s into flight, prior to Stage 2 ignition. A preflight 6DOF Monte Carlo analysis was not performed by the team, nor was a preflight assessment of flexible body static margin performed. Neither 6DOF Monte Carlo analysis nor flexible static margin have historically been performed during previous HIFiRE flight preparations.

2.5.3. Modeling Angle of Attack Divergence Near the Resonance Condition

Angle of attack divergence of a rolling vehicle as the roll rate approaches the critical pitching frequency has been described in the literature [5, 6], and is based mainly upon analytical modeling of reentry vehicles. During a postflight literature search, it was found that the angle of attack divergence observed during the BOLT flight appears to be described qualitatively by the existing resonance theories.

This theory predicts an amplification of the trim angle of attack that will occur as the roll rate approaches the critical pitching frequency. According to this theory, the larger the trim angle of attack (prior to resonance), the larger the angle of attack divergence at the resonance point. The theory shows that angle of attack amplification is much greater for asymmetric configurations, with the magnitude of amplification increasing with vehicle asymmetry. The BOLT Stage 2 configuration aerodynamic asymmetry was shown to be greater than that in the previous similar HIFiRE-5 flight vehicle, contributing to a likely increase in susceptibility to trim angle of attack amplification during resonance crossings. The trim angle of attack amplification is a dynamic phenomena, that required postflight 6DOF modeling with roll-dependent aerodynamics to reproduce.

During the course of the postflight aerodynamic model investigation, it was discovered that a pristine aerodynamic model that had identically zero trim angle of attack, was incapable of predicting the pitch-roll coupling and attendant angle of attack divergence. However, an aerodynamic model with small trim angles of attack (numerical artifacts at zero angle of attack for the APL database) was capable of predicting the pitch-roll coupling and angle of attack divergence. The observation correlates with theory from literature, and a lesson learned is that preflight 6DOF Monte Carlo analysis should incorporate terms (such as pitch and yaw moment biases) that induce small trim angles of attack within the MC analysis for proper dynamic behavior predictions.

Using the aero database with non-zero trim angles of attack, pitch-roll coupling was predicted for the BOLT flight to occur a few seconds after Improved Orion ignition. These results show that allowing for non-zero trim angle of attack in the aerodynamic database and preflight modeling for the BOLT vehicle is imperative in order to capture the likelihood of large angle of attack divergence at the pitch-roll coupling condition.

2.5.4. Trajectory Simulation Pedigree and Prediction of Pitch Roll Coupling

While aeroelasticity has been identified as the major probable contributor to the flight behavior as observed, there is another important aspect regarding the trajectory modeling which must be considered as part of the investigation.

The trajectory simulation code used for the preflight analysis does not support the modeling of the pitch/yaw plane aerodynamic asymmetries. For the preflight predictions, aerodynamics were alternately set to the pitch plane models, and then the yaw plane models. Acceptable performance was shown with each set of aerodynamics, and the determination was made that vehicle performance was acceptable. Static margin for both planes was shown to be well above the minimum required. The rigid body aerodynamic models predicted natural frequencies well above the roll rates expected during coast phase, as noted previously.

However, what the preflight trajectory analysis missed was the large region of potential critical pitching frequencies that exists between the pitch plane values, and the yaw plane values. In reality, this large region of possible critical frequencies means that the potential for pitch-roll coupling is in fact much greater than the preflight analysis suggested.

Using the independent aerodynamic model generated post-flight, the investigation has shown that the BOLT vehicle exhibits a tendency for pitch-roll coupling at a slightly later point in the flight, even with rigid body aerodynamic models.

The significance of this finding is twofold:

(1) For the BOLT, pitch-roll coupling and associated angle of attack divergence and likely mission failure would be expected even for a perfectly rigid vehicle configuration. The only difference from the observed flight anomaly is that the onset of resonance would be expected to occur about 5 s later than observed.

(2) For any future flight experiment involving an asymmetric payload geometry, or any other vehicle property which would tend to drive pitch-roll coupling, the use of a trajectory simulation that captures all the relevant asymmetries is essential. In addition, a full Monte Carlo analysis which varies critical vehicle parameters throughout their possible ranges is critical to assessing the viability of the flight configuration.

2.5.5. Program Execution and Structure

BOLT was a low-cost scientific flight experiment, and not a major program. Consistent with keeping costs low, a larger than typical acceptance of risk is carried, risks that are otherwise reduced with additional requirements, higher fidelity analysis, and independent evaluation which all would have otherwise lead to increased cost and schedule. BOLT heavily leveraged existing HIFiRE program experience to reduce costs that included a vehicle and payload similar to the successful HIFiRE-5b boundary layer transition flight experiment. The BOLT payload and APL/AFRL systems underwent program CoDR (Feb 2018), PDR (Oct 2018), and CDR (March 2019) design reviews . Similarly the DLR vehicle underwent program design reviews including vehicle Critical Design Review (Apr 2019) as well as separate design reviews for the Attitude Control System development (April 2019 and May 2019). Consistent with low cost programs, robust independent analysis by multiple parties for aerodynamics, etc. was largely not performed.

2.5.6. Lessons Learned and Recommendations

The BOLT investigation provided valuable lessons learned for sounding rocket flight experiments with complex three-dimensional shapes that are aerodynamically asymmetric Corrective actions to be applied to future scientific flight experiments should be targeted to addressing the phenomena observed in this investigation, without drastically increasing the costs that are consistent with risk-tolerant scientific flight testing.

Major lessons learned include:

- Assessment of vehicle aerodynamic asymmetry and recognition of the increased unstable behavior of asymmetric vehicles near pitch-roll frequency crossings
- The ratio of vehicle C_{m_α} and C_{n_β} derivatives can be compared as in Hodapp [5] for a quick assessment of vehicle asymmetry as an indicator of the potential for trim angle of attack amplification at resonance crossings
- For future flights with vehicles expected to have significant aerodynamic asymmetry, 6DOF Monte Carlo analysis should be performed to understand the flight dynamics at resonance crossings. This modeling should include roll-dependent vehicle aerodynamics. Preferably, the aerodynamic coefficients should be a function of angle of attack when assessing resonance behavior, as the coefficients at higher angles of attack may be slightly nonlinear.
- The Monte Carlo parameters used to examine flight dynamics of asymmetric vehicles should include reasonable C_m and C_n moment biases at zero angle of attack, as well as lateral CG offsets, thrust misalignments, and other parameters known to cause pre-crossing trim angle of attack that can be excited by resonance crossings
- 6DOF Monte Carlo analysis should be performed for the rigid body aerodynamics as well as for the reduced static margin aerodynamics, if able, with uncertainties applied in the analysis
- Robust center of pressure variation should be explored early in effort to understand flight dynamic uncertainty (+/-5% body length movement)
- Robust center of gravity variations, longitudinal and lateral, should be explored early in effort to understand flight dynamic uncertainty
- The following recommendations can be considered based on individual, project based, priority and risk dependent decisions, as a balance between risk reduction and resource prioritization:

- If the science experiment program budget permits, independent analysis of aerodynamics and flight dynamics is recommended for further reduction of risk
- Inclusion of additional sounding rocket subject matter experts at design reviews for science flights when support is available
- Duplicate analysis of critical flight items (aerodynamics, trajectory, structural) by at least two parties for flight configurations that deviate significantly from the established standard and proven flight heritage

3. BOLT Postflight 6DOF Modeling

This section summarizes APL's 6DOF investigations of the off-nominal flight performance experienced during the BOLT flight experiment, while the scientific research gained from the experiment are shown in Section 5. The work in this study specifically seeks to understand the vehicle dynamics, identified as roll-pitch coupling, and how this particular phenomenology was induced during flight. In addition to understanding what occurred, a goal of this section is to reproduce the as-flown performance through high-fidelity 6 Degree of Freedom (6DOF) trajectory simulation. Section 3.1 describes the flight behavior in more detail. As much of the simulation work relies heavily on understanding and modifying the vehicle aerodynamics, development of the aerodynamic database is described in Section 3.2. Section 3.3 and Section 3.4 present the 6DOF simulation studies, including initial approaches and more complex modeling that incorporate aeroelastic effects. Finally, Section 3.5 and Section 3.6 use the lessons learned from the preceding analysis to explore approaches that mitigate the unwanted dynamics and present areas for potential future study. The fundamental knowledge of these dynamics is important for effectively utilizing low-cost sounding rockets for basic science experiments in hypersonics, where shrouding the payload is not feasible, and complex payload geometries that are not aerodynamically symmetric are of interest.

3.1. Description of Flight Behavior

The BOLT vehicle experienced an unexpected flight event immediately after separation of the Improved Orion from the S31 motor, which occurred 11.3 seconds after launch. This event was characterized by a divergence of the roll rate from its intended steady state condition, the initiation of a coning motion, and associated increase in angle of attack which persisted after ignition of the S31 motor. The behavior of coning could specifically be classified as lunar motion, signified by the roughly constant windward meridian angle (the radial orientation of the angle of attack vector) of 180°. Figure 1 show the total angle of attack, roll rate, windward meridian, and lateral rate (root sum square of body y-axis and z-axis inertial angular rate) from the BET.

Based on the vehicle telemetry and further corroborated by cell phone video of the launch taken by a ground observer [1], it was clear that the vehicle had entered an unstable condition that resulted in an inability to fly the nominal flight profile. In addition to the period of lunar motion at 11-12 seconds into the flight, the behavior of the roll rate led to the conclusion that the vehicle was experiencing roll-pitch coupling. Instead of continuing to increase at Stage 2 ignition (15 seconds) via the canted fins of the Improved Orion motor, the roll rate signal took a precipitous drop to a steady state of 1.3 Hz and then continued to descend starting at 16 seconds. This is indicative of roll-pitch coupling where the roll rate locks into a critical frequency from which the vehicle cannot recover. This phenomenon is accompanied by an amplification of the vehicle angle of attack as it enters resonance (roll rate approaches the vehicle critical frequencies), which is precisely the behavior observed in Figure 1.

The post-flight investigation considered several potential causes of this instability including re-contact of the first and second stages, damage to the exterior of the vehicle body during handling and transportation, or substantial breakage of vehicle components (such as the fins) during the Stage 1 burn. These were eventually ruled out as unlikely based on detailed fault tree analysis conducted by the program. Ultimately, it was determined that the most probable explanation for

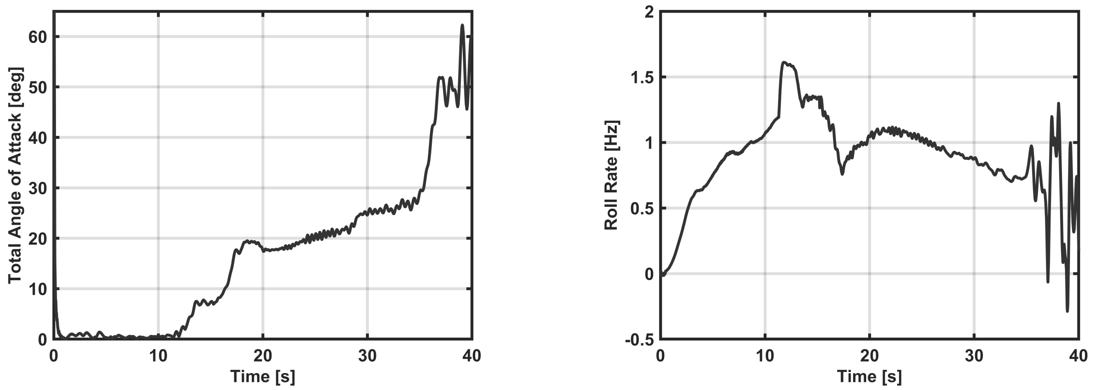

(a) Total Angle of Attack

(b) Roll Rate

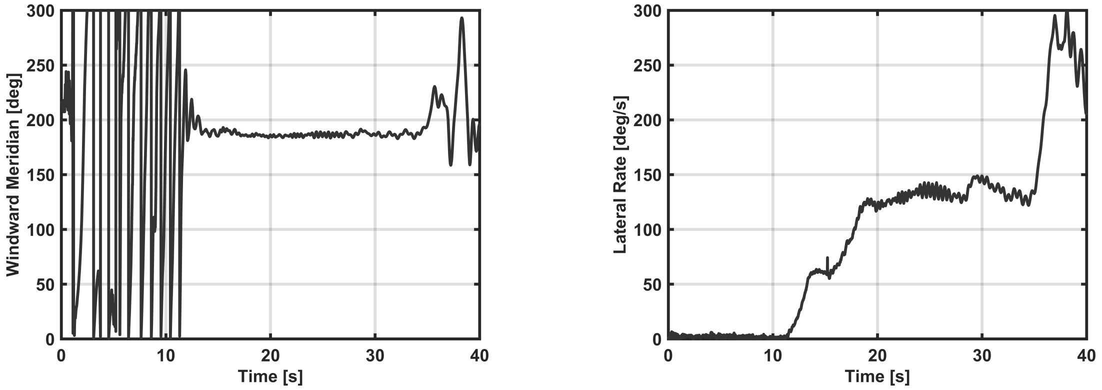

(c) Windward Meridian

(d) Lateral Rate

Figure 1. Flight Performance: Best Estimated Trajectory

the instability was a superposition of effects from aeroelastic deformation of the vehicle and the asymmetric aerodynamics of the BOLT forebody. Hodapp [5] presents an analytical formulation for the motion of a spinning vehicle with asymmetric aerodynamic coefficients. Their findings show that asymmetry has the effect of dramatically amplifying the trim angle of attack when the vehicle spin rate lies within the so-called "resonance region" bounded by the critical pitch and yaw frequencies. These frequencies may be computed as:

$$\Omega_{pitch} = \sqrt{\frac{-C_{m_\alpha}}{I_{zz} - I_{xx}}} \tag{1}$$

$$\Omega_{yaw} = \sqrt{\frac{C_{n_\beta}}{I_{yy} - I_{xx}}} \tag{2}$$

where C_{m_α} and C_{n_β} refer to the pitch and yaw moment slope coefficients (moments with respect to α and β, respectively), and I_{xx}, I_{yy}, and I_{zz} are the moments of inertia about the x, y, and z body axes.

Aeroelasticity has the effect of not only reducing C_m and C_n, but reducing them asymmetrically. This results in a vehicle with lower static margin and also a widened resonance region, as the critical frequencies lie further apart. Additionally, aeroelasticity moves the vehicle center of pressure (CP) forward, which changes the moment slopes and the resulting critical frequencies. While some allowance for flexure was considered in pre-flight analysis, the extent of this behavior was likely underestimated. A thorough examination of aeroelasticity based on the vehicle's flexural rigidity is presented in Section4, the results of which are used in this study to implement an aerodynamic model with aeroelastic contributions. That analysis is described in Section 3.4 and utilized to reproduce the BOLT flight behavior.

3.2. Aerodynamic Modeling

An aerodynamic database was generated post-flight by APL to support these simulations as well as to verify pre-flight estimates of the characteristic pitching and yawing frequencies and static margin. This database was compiled predominantly using Cart3D, an inviscid flow solver developed by NASA which emphasizes automation and scalability. Simulations were performed for Mach numbers of 2, 2.5, 3, 4, 6, and 8, with the vehicle total angle of attack, α_T, swept from 0-10° in 2.5° increments. The vehicle roll orientation, ϕ, was varied from 0-180° in 5° increments.

The Cart3D solutions were compared to viscous simulations performed using Metacomp CFD++ to assure their efficacy. The primary motivation for conducting the CFD++ simulations was to capture vortex effects and determine their impact on the vehicle aerodynamics. Figure 2 shows vorticity contours on the BOLT vehicle painted by static pressure for a simulation performed at $\alpha_T = 5^\circ$ and $\phi = 15^\circ$. Vortices are shed at each of the fairings and propagate downstream to the fins, however, the vortices dissipate and remain small relative to the fins.

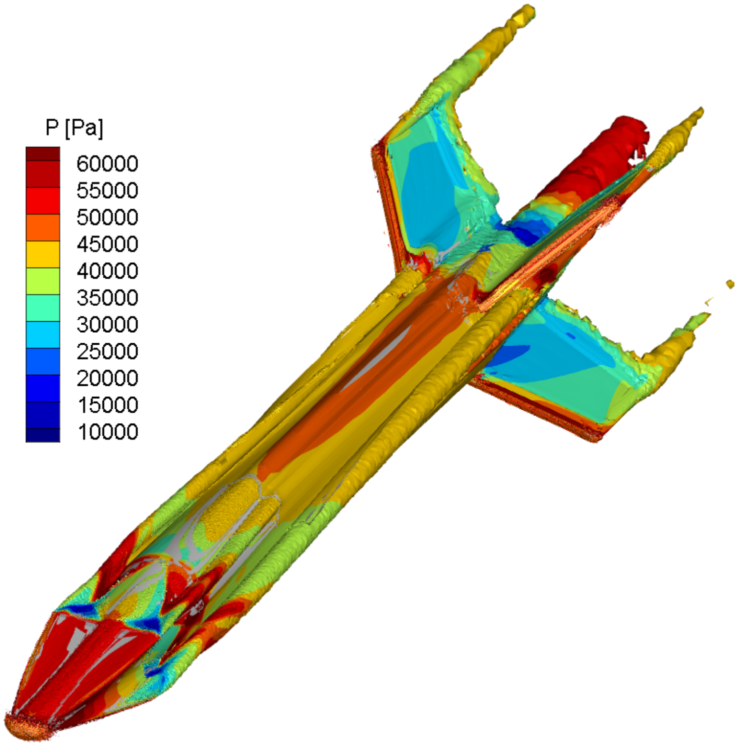

Figure 2. Vorticity contours overlaid with pressure for $\alpha_T = 5°$, $\phi = 15°$

The aerodynamic moment coefficients computed with each solver are compared in Figure 3, where C_m refers to the body-fixed pitching moment and C_n is the body-fixed yawing moment, both about the center of gravity (CG). The results show excellent agreement despite the lack of vortex effects in the Cart3D simulations, demonstrating that they do not substantially alter the vehicle aerodynamics. This lends confidence that the aerodynamic trends for the nominal Stage 2 geometry are captured by the Cart3D simulations and that the resulting aerodynamic database is sufficient for 6DOF trajectory simulations.

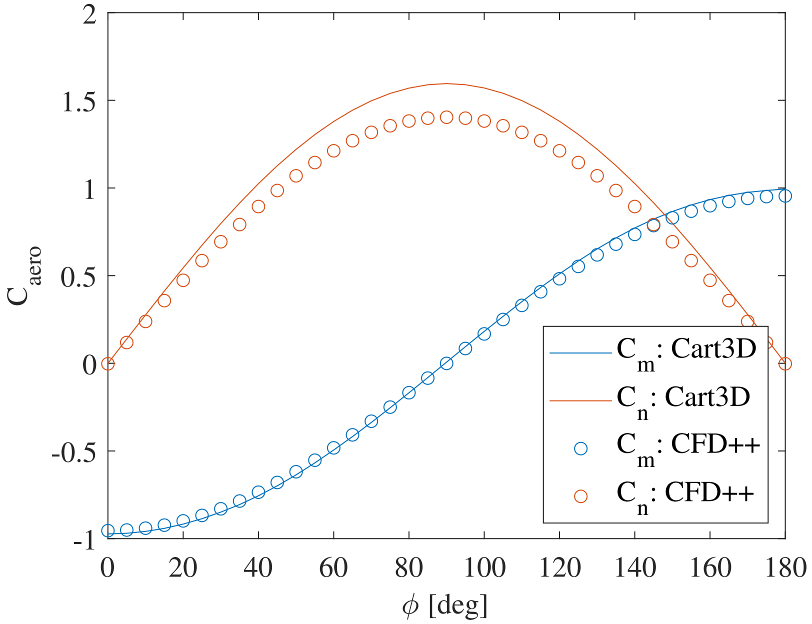

Figure 3. Aerodynamic moment coefficients computed using Cart3D and CFD++

3.3. Rigid Body 6DOF Simulation Studies

After development of the aerodynamic database was complete, a 6DOF trajectory simulation of the BOLT vehicle was assembled in order to better understand and model the unexpected aerodynamic behavior during the experiment and reproduce the as-flown performance. In addition to aerodynamics, simulation input models for mass properties and propulsion were also constructed, and initial conditions were obtained from the flight data. The goal in the early stages of the post-flight investigation was to focus the analysis on understanding the instability and the work presented in the following sections evaluate only the Improved Orion trajectory with that aim in mind.

Simulation analysis was performed using the Trajectory Analysis and Optimization Software (TAOS), a general purpose trajectory modeling tool developed by Sandia National Laboratories. TAOS is an industry standard simulation environment commonly used for modeling high speed vehicles like sounding rockets and ballistic missiles. The TAOS platform takes the initial conditions, mass properties, and forces acting on the vehicle to determine a resulting trajectory. In addition to nominal trajectory modeling, TAOS has capability to run parametric surveys and Monte Carlo studies to understand performance sensitivities and conduct error analysis.

This section describes the performance of the rigid body 6DOF simulation based on the aerodynamic model outlined in the previous section. Nominal modeling was first conducted to understand the expected performance of the vehicle under ideal conditions. Off-nominal modeling was then performed to include variations on vehicle properties representing error in the known vehicle characteristics that might trigger the dynamic instability, even for a rigid body formulation of the aerodynamic database. Fundamentally, TAOS is meant to express rigid body performance of a vehicle in flight. However, as will be shown in Section 3.4, the simulation can be utilized to characterize aeroelastic effects by manipulating the form of the rigid body aerodynamic model.

3.3.1. Rigid Body Nominal Modeling

As a first step, a nominal 6DOF model of the BOLT vehicle was developed by APL using the aerodynamic database described in Section 3.2. Both the measured mass properties and propulsion model (vacuum thrust and mass flow rate) were delivered by AFRL. Initial conditions were obtained from flight data, and because the unexpected flight behavior occurred after separation of the first stage, modeling activities began by initializing the 6DOF simulation at this separation condition. Table 1 shows the flight conditions used to initiate the 6DOF simulation at the separation condition of the Improved Orion motor from the S31 motor.

Table 1. IO Separation Flight Conditions

State	Flight Condition
Altitude	5682.79 km
Geodetic Latitude	67.8954°
Longitude	21.1036
Velocity	905.5 m/s
Flight Path Angle	87.46°
Azimuth	-5.33°
Body x-axis Inertial Angular Rate (roll rate)	428.41°/s
Body y-axis Inertial Angular Rate (pitch rate)	1.87°/s
Body z-axis Inertial Angular Rate (yaw rate)	1.96°/s

Keeping in mind that the aim of the initial modeling efforts was to induce the roll-pitch coupling phenomenon, an initial study with nominal rigid body aerodynamics examined the effects of small perturbations to the pristine aerodynamic database. This database nominally assumed trim pitch and yaw moments at a $\alpha_T = 0°$. The corresponding tables for lateral force and moment coefficients had values of numerical zero when queried at $\alpha_T = 0°$. With this aerodynamic treatment, the resulting vehicle trajectory reflected a stable rigid body profile reaching the desired steady state roll rate and experiencing no lateral rate or angle of attack excursion during second stage flight. Plots of these three parameters with nominal rigid body implementation are shown in Figure 4. Added to the roll rate plot in Figure 4 are the time varying critical pitch and yaw frequencies from which the roll rates must depart in order to avoid the dynamic instability observed during the BOLT flight experiment. That is clearly the case here as roll rate quickly exceeds the expected rigid body critical frequencies and avoids approaching this region of resonance for any significant period of time.

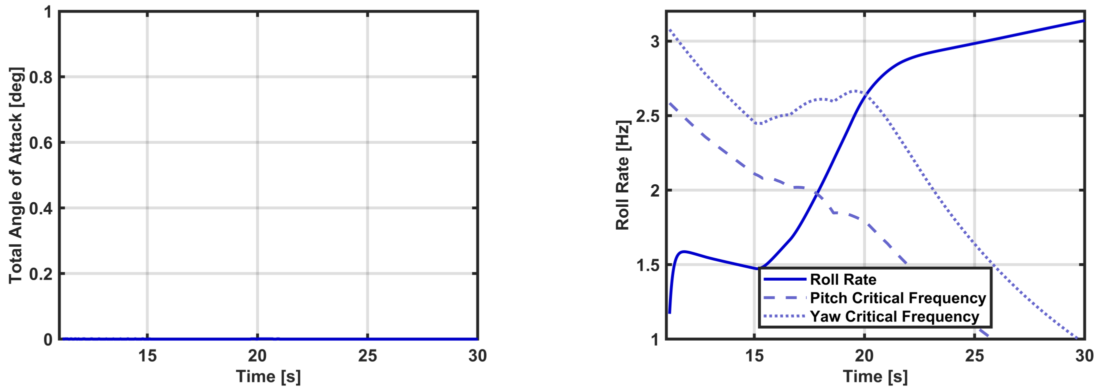

(a) Total Angle of Attack

(b) Roll Rate

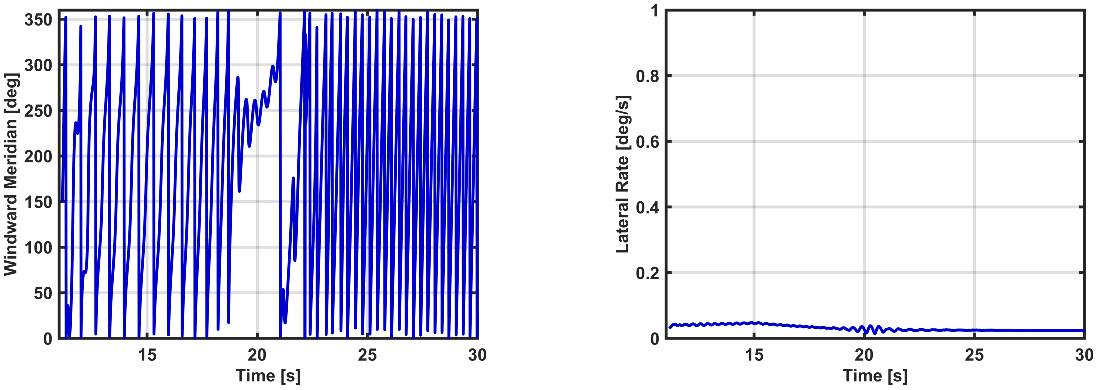

(c) Windward Meridian

(d) Lateral Rate

Figure 4. Flight Performance: Nominal Rigid Body Model

Next, this pristine version of the aerodynamics was modified slightly by adding non-zero offsets (on the order of tenths of a unit) to the lateral force and moment coefficients at the $\alpha_T = 0°$ grid point. This perturbed treatment of the nominal rigid body aerodynamics was being used to increase the vehicle asymmetry and probe for stability sensitivities. Interestingly, the result was an instantiation of roll-pitch coupling at 17 seconds, which was a promising finding although not at the exact flight time of 11.3 seconds. As can be seen in Figure 5, all four of the parameters in Figure 5 display noticeable divergences from the nominal rigid body results when using the non-zero perturbations.

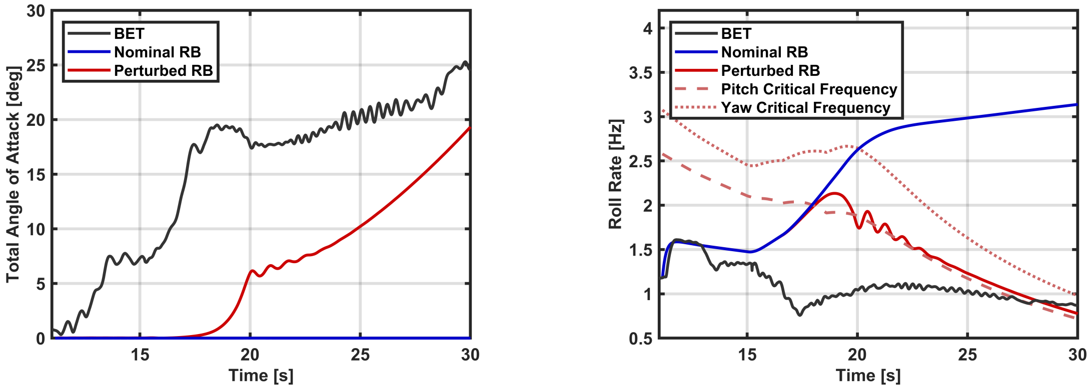

(a) Total Angle of Attack

(b) Roll Rate

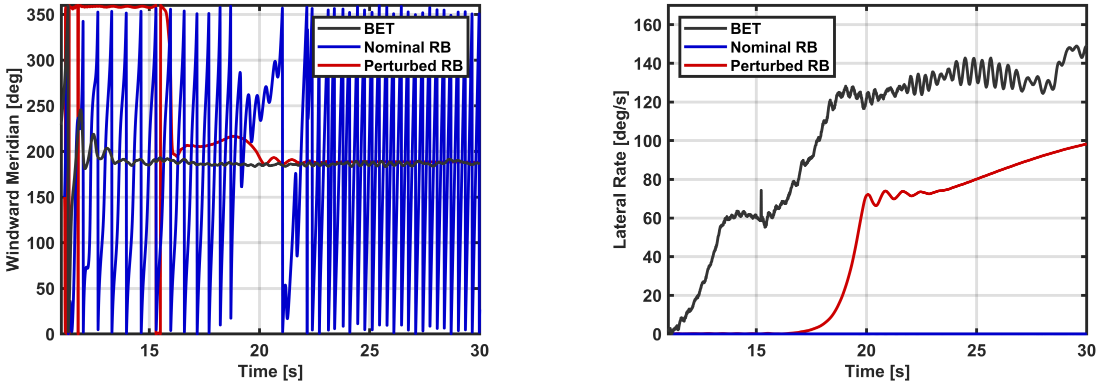

(c) Windward Meridian

(d) Lateral Rate

Figure 5. Flight Performance: Perturbed Rigid Body Model with BET and Nominal

Similar to Figure 4, Figure 5 presents the critical frequencies for the perturbed run. The contrast between how these two runs behave relative to their critical frequencies is noticeable. Instead of avoiding resonance, the perturbed run locks into the pitch critical frequency and its roll rate holds that value to produce the dynamic instability.

This first analysis, while simple to produce, provided a very powerful result: with only the slightest modification to the rigid body aerodynamics, the conditions for roll-pitch coupling were planted. It should be noted that the study above does not exactly replicate the performance observed during the BOLT flight. Specifically, the timing of the unexpected behavior (at the onset of stage separation) is not consistent with the results shown in this section, which occur soon after the Improved Orion motor ignites (17-18 seconds). However, the goal of 6DOF modeling at this stage in the investigation was to better understand the factors that induced the resonance before a more precise replication of the flight was undertaken. Knowing that the trim values of force and moment coefficients played a crucial role in inciting this mode of instability served to inform the follow-on studies in the ensuing sections where more complex techniques for capturing aeroelastic effects were utilized.

3.3.2. Rigid Body Monte Carlo Modeling

Further investigation of the vehicle performance using Monte Carlo simulation methods was conducted to understand how closely the rigid body aerodynamics, under the influence of off-nominal dispersions, could approximate the flight instability. An initial 200 run Monte Carlo trajectory set was generated with variations, as shown in Table 2, applied to the trim moment offsets, center of gravity, and initial conditions. Errors in the estimation of these parameters were expected to be the driving contributors to roll-pitch coupling, motivating their sole inclusion at this stage of off-nominal modeling.

Table 2. Rigid Body Monte Carlo Parameters

Parameter	Distribution	Mean	3σ	Min	Max
C_m Bias	Normal	0	0.1	-	-
C_n Bias	Normal	0	0.1	-	-
x_{CG} Error [m]	Normal	0	0.25	-	-
y_{CG} Error [m]	Normal	0	0.019	-	-
z_{CG} Error [m]	Normal	0	0.019	-	-
Initial Pitch Rate [°/s]	Normal	0	6	-	-
Initial Yaw Rate [°/s]	Normal	0	6	-	-
Initial α_T [°]	Uniform	-	-	0	10
Initial ϕ [°]	Uniform	-	-	0	360

The results of this preliminary Monte Carlo trajectory set are shown in Figure 6. Similar to the perturbed runs in the previous section, this MC set shows a significant number of runs that deviate in roll rate, total angle of attack, and lateral rate representing the resonance associated with roll-pitch coupling. Also comparable to the results in Section 3.3 3.3.1 are the presentation of the instability a few seconds into burn, instead of at separation. Through these studies, it became clear that in order to attain the true flight-like behavior of the BOLT experiment, added fidelity to the modeling approach was required. In particular, a more precise handling of aeroelastic effects needed to be considered leading to the studies in Section 3.4.

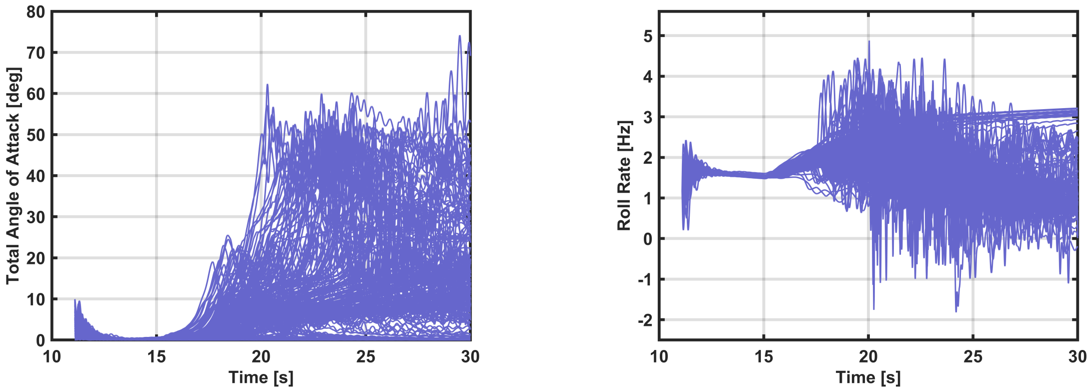

(a) Total Angle of Attack

(b) Roll Rate

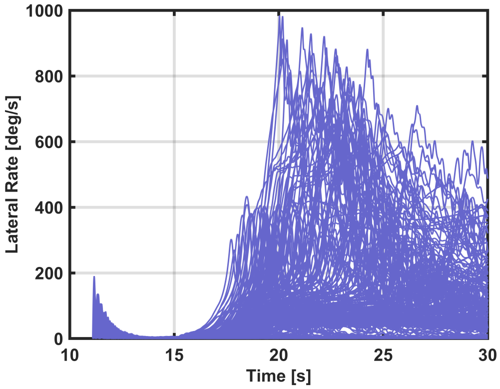

(c) Lateral Rate

Figure 6. Flight Performance: Rigid Body Monte Carlo

3.4. Aeroelastic 6DOF Simulation Studies

It became evident over the course of the post-flight investigation modeling that a large divergence of the pitch plane and yaw plane critical frequencies must have occurred, caused by the asymmetric shape of the vehicle outer mold line, and exacerbated by a loss of static margin due to aeroelastic effects. Vehicle aeroelasticity was found to be correlated to the freestream dynamic pressure, which was at a maximum near the stage separation event. The divergence of the pitch plane and yaw plane critical frequencies resulted in a wider range of potential roll rates where the vehicle was susceptible to entering roll-pitch coupling, and were investigated as a potential primary contributor to the unanticipated behavior shortly after stage separation. The BOLT post-flight investigation team performed extensive mechanical and structural analysis to predict the vehicle deformation and corresponding aerodynamic effects. The culmination of this analysis was to capture these effects in the 6DOF simulation to reproduce the flight performance and verify the predicted root cause.

As an initial approach to modeling aeroelastic effects, a simple augmentation of the aerodynamic model was implemented to manipulate static margin based on dynamic pressure. That analysis and corresponding comparison to the BET is shown in Section 3.4 3.4.1. A more complex treatment of aeroelasticity was also employed in the 6DOF simulation. This higher fidelity model, developed through analysis of the vehicle mass properties and flexural rigidity, was effectively an update to the original rigid body aerodynamics. This new model provided the necessary contribution of aeroelasticity to reduce stability margin as observed during the BOLT experiment. The results of this study and comparison to the BET is shown in Section 3.4 3.4.2.

3.4.1. Simple Aeroelastic Model

The first attempt to notionally model aeroelasticity in the 6DOF simulation utilized a straightforward, empirical approach. This simple model sought to reduce static margin by modifying the vehicle center of pressure as a function of dynamic pressure. Effectively, the model presumed a linear relationship between vehicle flexibility and the dynamic pressure through which the vehicle flew. As such, the maximum flexure was prescribed to occur at the occurrence of peak dynamic pressure, which corresponds to the separation of the two stages. Figure 7 presents the vehicle dynamic pressure starting just prior to separation through the Improved Orion burn phase.

Movement of the vehicle's center of pressure was mechanized through the location of the aerodynamic moment reference point (MRP), which is nominally set at the vehicle's nose. A linear scaling of the MRP x-axis location was implemented to move this location in proportion to dynamic pressure, with a maximum movement selected conservatively at 10% of the second stage body length (5035 mm). This maximum shift occurred at vehicle staging, and amounts to a change of 0.53 meters. The form of this scaling is shown in Eq. 3:

$$x_{MRP} = \frac{x_{MRP_{max}} q_{\infty}}{q_{\infty_{max}}} \tag{3}$$

In Eq. 3, $x_{MRP_{max}}$ represents the maximum movement at the peak dynamic pressure represented by $q_{\infty_{max}}$. From this expression, as dynamic pressure decreases towards 0 Pa with increasing vehicle altitude, the MRP location returns to its ideal rigid body value of 0 meters. For the BOLT aerodynamic database formulation, the nominal rigid body MRP location is at the vehicle nose and forward movement (reduced static margin) is a positive increment. Note that this formulation to represent aeroelasticity does not account for potential dependency on Mach number, and only dynamic pressure is used to model the flexible effects.

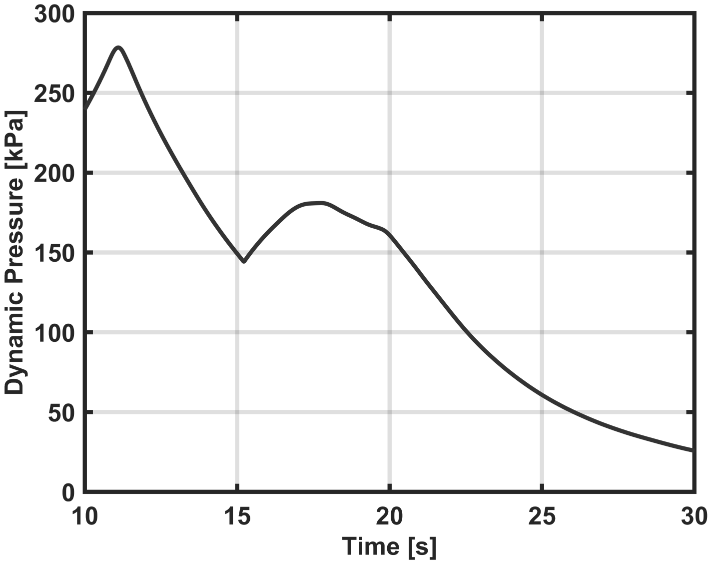

Figure 7. Stage 2 BET Dynamic Pressure

Figure 8 show the effects of the CP adjustment compared to the as-flown performance. Using the simple, dynamic pressure-based aeroelastic model, the roll rate agrees quite well with the BET, almost immediately tracking the pitch critical frequency and locking into resonance soon after separation occurs. Total angle of attack also deviates immediately from a trimmed state and reaches a value of 20°as soon as 3 seconds into burn. Additionally, the second significant rise in angle of attack experienced during the BOLT flight at 35 seconds is also well captured by the simple aeroelastic model reaching a steady state value of roughly 50°.

The windward meridian is also shown in Figure 8. Here again the simple aeroelastic model closely resembles the flight data such that a majority of the second stage burn period is locked into a 0°meridian, indicating the lunar motion that accompanies roll pitch coupling.

3.4.2. High Fidelity Aeroelastic Modeling

A second, more complex aerodynamic model was implemented in the 6DOF simulation to characterize the aeroelastic effects with greater fidelity. This model was informed through analysis of a linearized flexible-body dynamics model of the full second stage (IO and BOLT payload) based on prior work for slender spinning vehicles [7]. The analysis is described in Section 4 and demonstrates the potential for CP shifts up to 5.7% of the vehicle body length and peak dynamic pressure, with an associated static margin reduction of over 50% from the rigid body value.

The approach taken for the higher fidelity aeroelastic model was to modify the rigid body aerodynamics by reducing the lateral force and moment coefficients by a factor predicted by the aeroe-

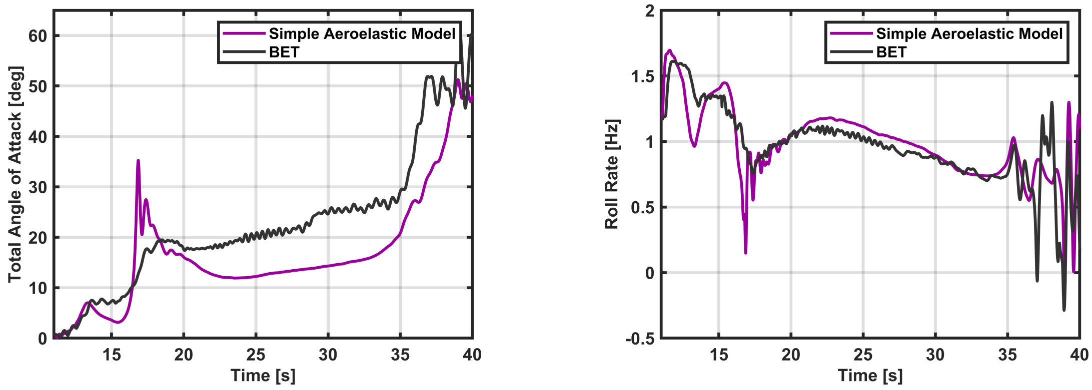

(a) Total Angle of Attack (b) Roll Rate

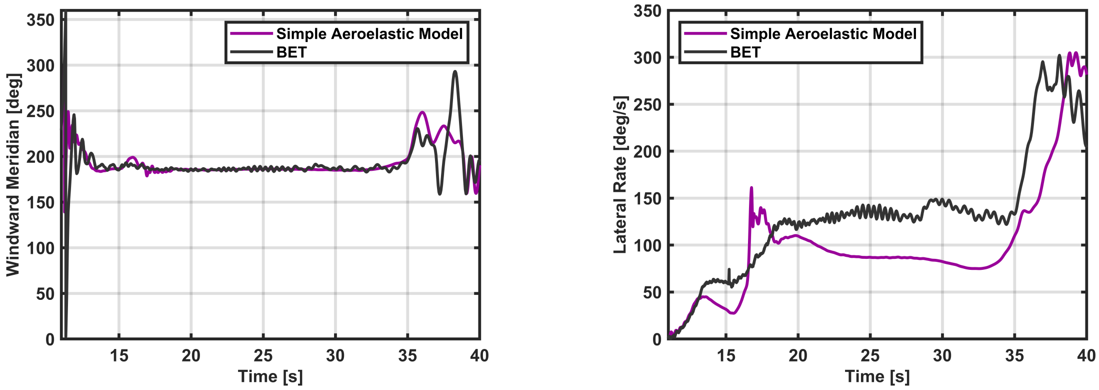

(c) Windward Meridian (d) Lateral Rate

Figure 8. Flight Performance: Simple Aeroelastic Model

lastic structural analysis. The rigid body aerodynamic database was developed in the form of body axis force and moment coefficients. Accordingly, the predicted reduction factors were applied to the pitch and yaw body axis moment coefficients (C_m, C_n) and the y and z body axis force coefficients (C_Y and C_Z). Similar to the simple aeroelastic model, these reduction factors were functionally dependent on dynamic pressure in addition to their rigid body dependencies on angle of attack, angle of sideslip, and Mach number. Its important to note that unlike the simple aeroelastic model, the reductions here are based on the vehicle structural properties. An update to the rigid body aerodynamic tables was thus produced to capture these changes, allowing the 6DOF simulation results to represent the estimated aeroelastic effects.

In addition to the rigid body aerodynamic coefficient corrections, a non-zero trim moment coefficient was also determined to be crucial to reproducing the flight instability consistent with theory for vehicles with asymmetric stability characteristics such as BOLT [5]. This moment coefficient component at $\alpha_T = 0°$ (C_{m_0}) generates a trim total angle of attack condition before the roll rate crosses the vehicle critical frequencies. That trim total angle of attack is then amplified during the frequency crossings as the vehicle goes into resonance. Several values of C_{m_0} were applied to understand the stability sensitivity and find a value that yielded a good match to the as flown performance. This trim offset to the moment coefficient was fundamental to seeding the roll pitch coupling instability.

Two last modifications were made to the aerodynamic model treatment to further stress the vehicle dynamics. The first, similar to the simple aeroelastic model described in Section 3.4 3.4.1, was the location of the MRP. Because the high fidelity aeroelastic model utilized reduction factors to the rigid body aerodynamics as a function of dynamic pressure, an extra shift of the MRP was treated as a constant bias in terms of the body length of the second stage configuration. The second additional aerodynamic parameter tuned in the aerodynamic model was the multiplier on the pitch and yaw moment stability derivatives, C_{m_q} and C_{n_r}. For 6DOF modeling of missiles and sounding rockets, these moment coefficients usually carry a significant amount of uncertainty, and for this analysis, they were reduced by as much as 50%. These two parameters (MRP location and lateral moment stability derivatives) were varied for the analysis here in order to best match the flight data.

Table 3 describes the parameters that were varied in the 6DOF simulation that were used to influence the aeroelasticity of the vehicle. These parameters were surveyed parametrically to produce a trajectory for every combination of values. Note that the %BL (percent of the overall body length) for the MRP location refers to the Improved Orion, which has a total length of 5035 mm.

Table 3. Aeroelastic Modeling Parameters Varied in 6DOF

Parameter	Minimum	Maximum	Increment
C_{m_0}	0.005	0.05	0.005
MRP Location	2.0%BL	3.5%BL	0.5%BL
C_{m_q}, C_{n_r} Multiplier	0.5	1.0	0.1

The aeroelastic modeling treatment described above (updated force and moment coefficients, shift in MRP, and tuning of C_{m_q},C_{n_r}) was then employed to generate a parametric survey of 6DOF trajectories to find comparable performance to the BOLT flight. A trajectory set of 240 runs was created to sweep through these specific parameters and assess the resulting performance. Figure 9 presents the roll rate, total angle of attack and lateral rate for the trajectory set compared against the resulting trajectory using the simple aeroelastic model and the BET.

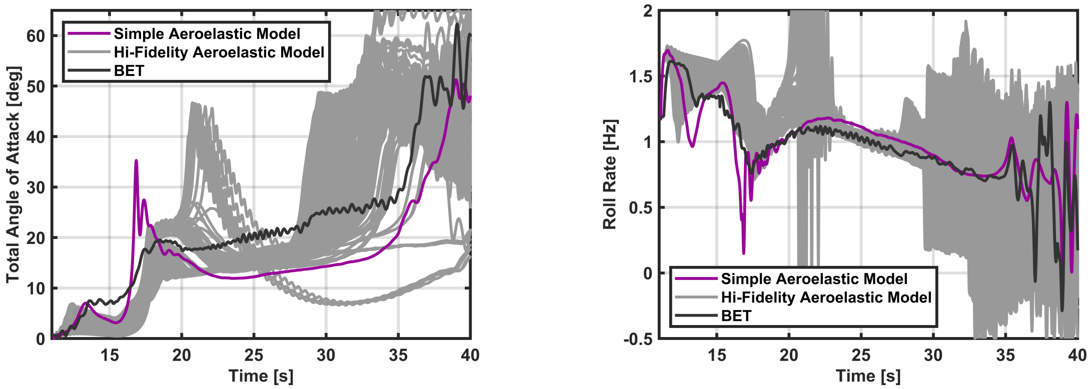

(a) Total Angle of Attack

(b) Roll Rate

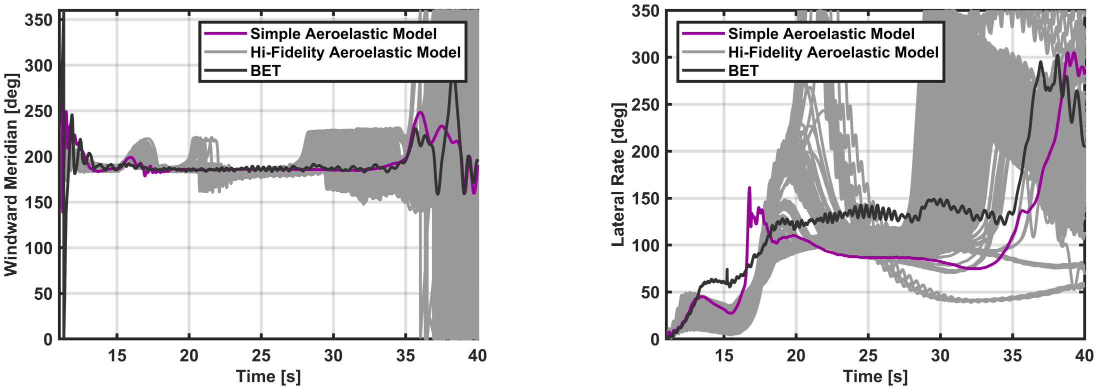

(c) Windward Meridian

(d) Lateral Rate

Figure 9. Flight Performance: Comparison of Aeroelastic Models with BET

From a broad evaluation of these trajectories, there appear to be many runs that track reasonably well with the BET performance. The immediate divergence in the flight α_T is captured by the simulation as well as the first and second steady state values of roughly 7°and 20°. The rise in α_T at the end of burn experienced in flight at 35 seconds is also experienced across much of the trajectory data, although not quite matching in timing. It also appears that every run experiences lock-in of the roll rate with the critical frequencies and very large divergences in lateral rate, both indicative of the instability that affected the BOLT experiment. Windward meridian for every run shows significant periods that hold at a constant 180°value, a tell-tale sign of lunar motion.

After evaluating the full trajectory set, a single run with the aeroelastic parameter settings presented in Table 4 was identified as the best match to the BET performance. The selected candidate trajectory is shown in comparison with the BET and the simple aeroelastic simulation run in Figure 10.

Table 4. Candidate Trajectory Modeling Parameters

Parameter	Candidate Value
C_{m_0}	0.005
MRP Location	3.5%BL
C_{m_q}, C_{n_r} Multiplier	0.5

3.5. Potential Mitigations

As a final element of this study, the BOLT team investigated ways in which the vehicle could have successfully operated in its BOLT configuration. A comprehensive list of potential mitigation strategies was assembled, and two of the strategies were explored with high fidelity analysis. The strategies that were not selected were either deemed to be insufficiently effective in avoiding dynamic instability or required significant changes to the design of the vehicle. The two approaches described in this section were assessed using the previously described 6DOF simulation to explore the parameter space and sensitivities outside of the BOLT flight regime which could have resulted in flight stability.

The first method to mitigate the effects of aeroelastic bending was to increase the achieved roll rate of the Improved Orion during burn. The goal of this approach is to quickly attain a high enough roll rate that prevents the vehicle from flying near the critical frequencies for a prolonged period of time. This is a common methodology used in sounding rocket flight performance analysis, but here the aeroelasticity is captured in the vehicle aerodynamics to produce the reduced critical frequencies expected for this vehicle.

For this analysis, the roll rate was modified through a multiplier on the roll moment coefficient (C_l), effectively resembling an increase in the cant of the Improved Orion fins. A survey of multipliers values was applied to understand the increase in roll moment (and thereby spin rate) needed to avoid the instability. These values varied from nominal (multiplier of 1) to a 50% increase in roll moment (multiplier of 1.5). Shown in Figure 11b is the resulting roll rate behavior for each run that was generated. Above a roughly 33% increase in roll moment, the vehicle maintains stability through the burn phase, avoiding significant time near the critical frequencies. Figure 11a presents the resulting total angle of attack, which shows that multiplier values below 1.33 produce significant amplification from the trim value.

The mitigation to increase the achieved second stage roll rate provides a potential solution from

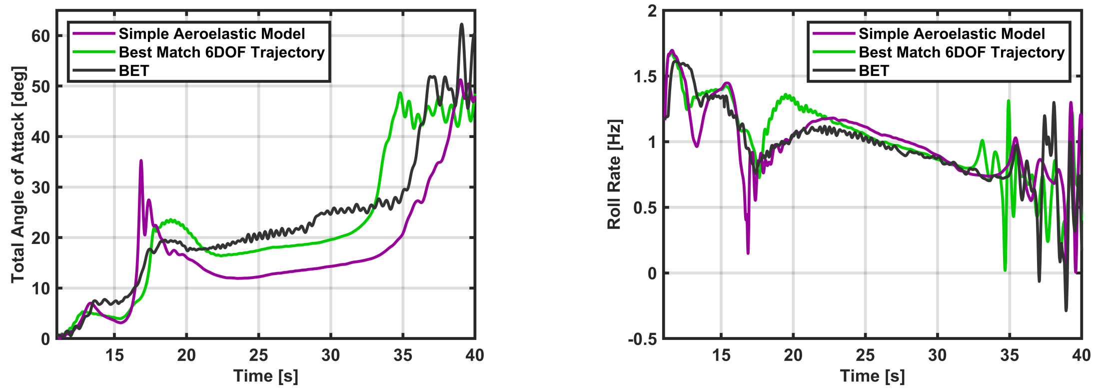

(a) Total Angle of Attack

(b) Roll Rate

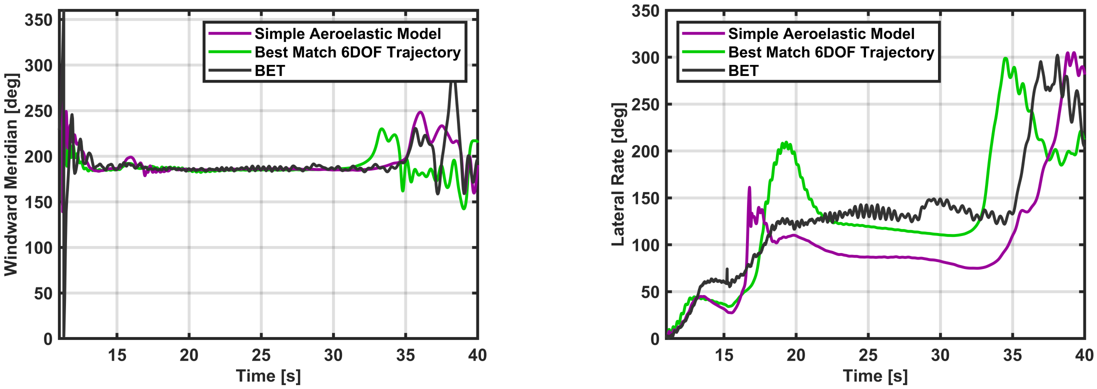

(c) Windward Meridian

(d) Lateral Rate

Figure 10. Flight Performance: Comparison of Candidate Trajectory with BET

a flight dynamics perspective, but further refinement of this study inside of a full Monte Carlo treatment would be needed to accurately assign the appropriate fin cant. Additionally, Figure 11b shows a resulting burnout roll rate of almost 2000 °/s (5.6 Hz), which might be higher than can be feasibly flown for the Improved Orion. Additional assessment is needed to determine a maximum possible roll rate that can be flown for this vehicle in order to finalize a fin cant setting.

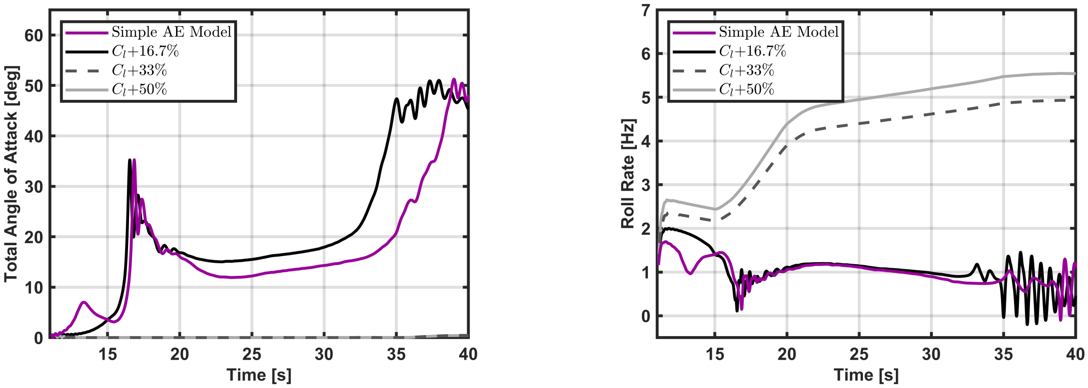

(a) Total Angle of Attack

(b) Roll Rate

Figure 11. Mitigation 1 Performance: Increased Roll Rate

The second option to escape resonance is to separate the Improved Orion vehicle at a higher altitude than the nominal BOLT mission design. Because the vehicle experiences maximum dynamic pressure at separation, raising the altitude of that condition allows the second stage burn to occur at lower dynamic pressures, thereby lessening the associated aeroeleastic forces. Two options are available for increasing separation altitude: (1) replacing the first stage with a higher impulse motor or (2) allowing the unseparated vehicle to coast to the desired altitude. Both options would require some level of vehicle redesign, with the former requiring a wholesale change of the lower stage and the latter requiring an active separation system (as opposed to the drag separated strategy of the BOLT mission).

For the purposes of exploring this mitigation approach, such a redesign was not selected and developed. Instead, the simulation was used simply to understand the effectiveness of the approach by initiating the model at separation. The BOLT mission was nominally designed to separate at 5.6 km with a dynamic pressure of 273 kPa (5700 psf). For this mitigation analysis, that altitude was raised to 17 km for a corresponding dynamic pressure of 52 kPa (1100 psf), which was selected based on the HIFiRE-5b mission [8] that used an S30 lower stage motor. This change provides a fivefold decrease in dynamic pressure that significantly changes the critical frequency profile during burn.

Figure 12 shows the effect of the reduced dynamic pressure, with critical frequencies both lowered and closer together. This trajectory design presents a smaller resonance region through which the vehicle could travel, minimizing the risk of entering roll-pitch coupling. Trim angle of attack amplification does not occur because the vehicle quickly departs from its pitch and yaw critical frequencies.

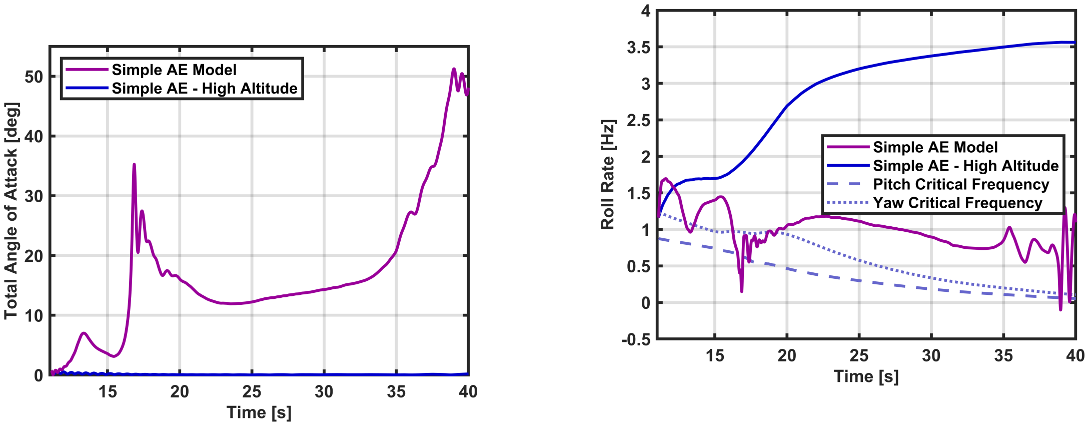

(a) Total Angle of Attack

(b) Roll Rate

Figure 12. Mitigation 2 Performance: Increased Separation Altitude

3.6. Summary and Future Work

The BOLT flight experiment presented an opportunity to investigate the unique mode of instability that the vehicle experienced. While unable to attain its desired flight performance for hypersonic scientific research, the post-flight analysis team was able to explore the root cause conditions that resulted in the vehicle entering roll-pitching coupling. The complex, asymmetric geometry of the flight payload led to substantial aeroelastic forces and a large reduction in static margin. Through these factors, the vehicle reached a resonance condition wherein the roll rate locked into the critical frequencies, and the angle of attack began a period of amplification. The as-flown performance was recreated through a high fidelity 6DOF trajectory simulation that captured aeroelasticity through an innovative treatment of the rigid body aerodynamics. For details of this treatment, see Section 4. Flight performance was modeled using the original rigid body aerodynamic database and compared against the new aeroelastic model. Several parameters were tuned in the aeroelastic model to match the experiment trajectory profile, and a final candidate trajectory was selected. Finally, two approaches to mitigate the aeroelastic effects were evaluated and described.

Several areas of future research were identified by the BOLT post-flight analysis team. While the intent of this initial effort was to explain and reproduce the unexpected flight behavior using a 6DOF modeling environment, an exact match to the experiment performance was not obtained. Further refinement of the aeroelastic treatment could be carried out to improve the mission matching exercise. A more robust treatment of capturing the trim moment offsets (C_{m_0}, C_{n_0}) could be applied in which those offsets are calculated via flight calculated derivatives of the moment coefficients with respect to the wind angles (C_{m_α}, C_{n_β}). A full scale Monte Carlo analysis could be implemented with a complete set of parameter variations including other contributors to asymmetric effects that could induce unstable behavior. Those parameters would include lateral CG variations, thrust misalignment, and additional aerodynamic model uncertainties. Finally, an additional mitigation technique could be considered that reduces the vehicle roll rate such that critical frequency crossings occur much later in flight when dynamic pressure is lower, minimizing aeroelastic effects. This approach would have to be analyzed thoroughly to understand the tradeoff between improvements in stability characteristics versus the resulting diminishment of dispersions in the aimpoint accuracy.

The post-flight investigation of the BOLT experiment has helped the analysis team better understand the underlying causes behind the in-flight performance. By understanding those factors, mitigations have been identified that could be useful for others in the development of asymmetric vehicle configurations.

4. BOLT Postflight Aeroelastic Modeling

This section summarizes the investigation of the contribution of aeroelasticity to a reduction in stability margin, pitch and yaw frequencies, and ultimately flight behavior. Equations of motion for a rolling hypersonic vehicle are developed using an approach similar to [7], but accounting for payload asymmetries in the pitch and yaw planes. Implementation on the BOLT vehicle requires various supporting analyses to obtain model parameters including mass properties and flexural rigidity of the airframe, forward payload, tail can and fins. The model predicts that the combined effects of these flexible-body elements contribute a -5.7% (of body length) shift in the center of pressure (CP) and results in a reduction of the pitch frequency from 2.58 to 1.68 Hz at stage separation. Analysis of the flight data suggests the CP shift is closer to -9.2% with a pitch frequency of 1.3 Hz. The difference is attributed to uncertainty in the aerodynamics model and vehicle structural model.

4.1. Flight Deviations from Planned Mission

Figure 13 depicts altitude and Mach number for the pre-flight prediction for a nominal flight trajectory, and a best estimate of trajectory (BET), reconstructed post-flight using GPS after the mission was conducted on 23 June 2021. The nominal trajectory predicts a total flight time of 500 seconds prior to payload ejection, with an apogee at 267 km altitude, while the BET indicates the vehicle reached an apogee of 78 km, impacted the ground at roughly 270 seconds, and did not separate the payload prior to impact. A primary objective of the BOLT mission was to reach hypersonic speeds between Mach 5 and 7 during both ascent and descent phases, the BET indicates that the actual maximum of Mach 3.9 was reached at about 20 seconds into ascent.

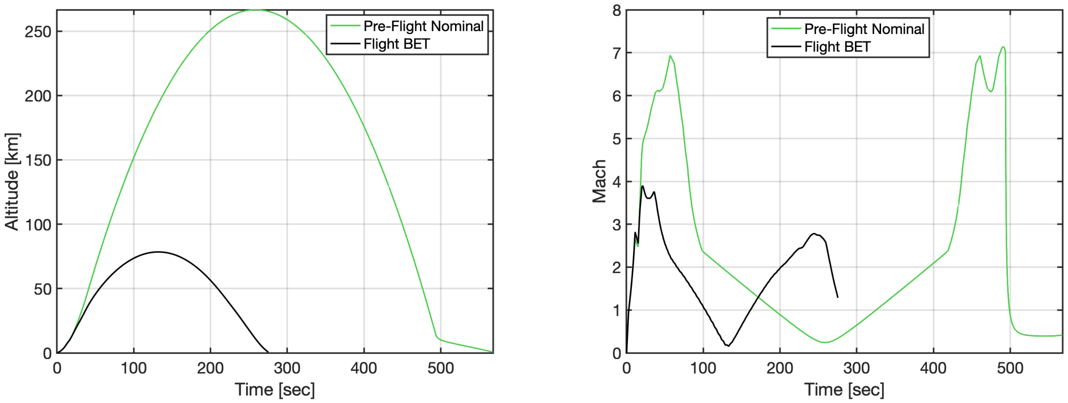

Figure 13. Flight Trajectory

Deviations in the BET from nominal predictions are attributable to angle of attack divergence beginning shortly after separation of the S31 stage, 11.2 seconds into flight. Total angle of attack (root-sum-squared of pitch angle α and sideslip angle β) is reconstructed from IMU data, and depicted in Figure 14a. Total angle of attack grows exponentially between approximately 11.5 sec and 13.5 sec, during which time the roll rate is close to 1.6 Hz (Figure 14b). Predicted angle of attack (not shown) is near zero at the same time period, consistent with a mission objective of maintaining angle of attack < 5 deg [9], and the intent of reducing dispersions. The angle of attack divergence resulted in coning motion of the flight vehicle on ascent (observed on video taken from the ground), deviations in intended flight path, increased drag on the flight vehicle, and ultimately the inability to achieve mission objectives for Mach and Reynold's number.

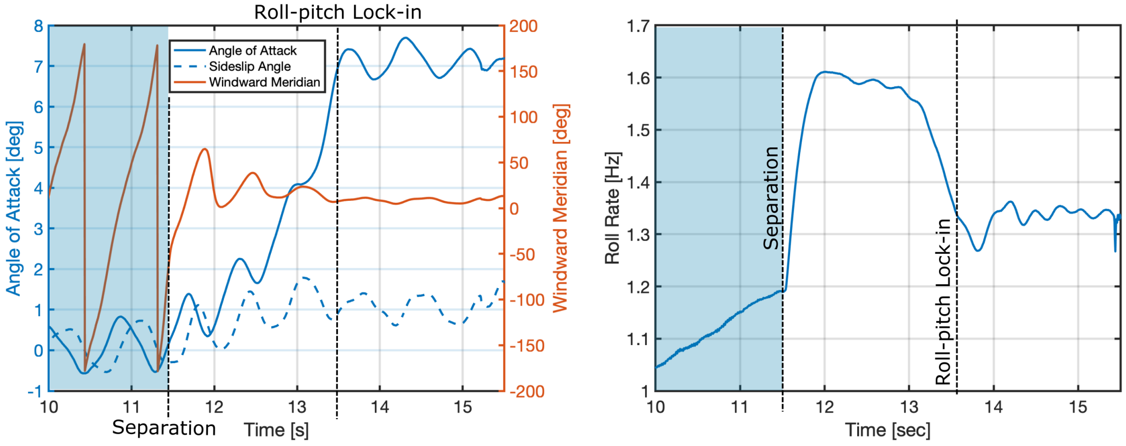

(a) Angle-of-attack

(b) Roll Rate

Figure 14. BET Flight Conditions Following Stage 1 Separation

Angle of attack divergence is commonly associated with vehicle instability, which was not predicted in the flight configuration based on preflight analysis. Various candidates for root cause have been considered, such as off-nominal performance of the booster stages, off-nominal construction of vehicle components affecting gravimetrics, structural failure of vehicle joints, and environmental effects such as wind shear. The preflight pitch and yaw frequencies were estimated using standard practice of assuming a rigid body and investigations have confirmed that the rigid-body frequencies were estimated consistent with standard practice. A focus of the investigation described in this section is a reduction in static stability of the vehicle caused by a deviation in the CP from rigid-body predictions. Subsequent portions of this section discuss how this deviation can be attributed to a reduction of pitch and yaw critical frequencies from the rigid-body values due to aeroelasticity from combined flexibility of various segments of the vehicle. The asymmetric shape of the forebody further contributed to a wider range of potential roll rates where the vehicle was susceptible to entering roll-pitch coupling. None of the other possible root causes currently explain the relatively large shift in CP that is estimated from flight data.

4.2. Model of a Slender Asymmetric Flexible Spinning Airframe

This section describes the development of a linearized flexible-body dynamics model of the second stage BOLT vehicle. Prior work on slender spinning vehicles, such as Platus [7] and others [10, 11], have developed the equations in the body-fixed frame attached to the rigid-body motion or mean motion. This approach yields equations capable of simulating the full duration of flight despite large rotations of the vehicle. However, for the purpose of evaluating stability of a given flight condition, a simpler linearized model can be derived in a spinning frame that follows the roll motion of the vehicle, but does not pitch or yaw. This formulation is typical for gyroscopic systems [10].

The linearized equations of motion for the slender vehicle are derived with the following assumptions:

- Flexure of the vehicle is modeled Euler-Bernoulli beam theory
- Axial forces (thrust, drag) are neglected
- Rotational inertia of the beam cross-section is neglected
- Vehicle roll rate is constant
- Vehicle is not axisymmetric but does have 2-fold (180 deg) rotational symmetry. This assumption applies to both the aerodynamic loads and the flexural stiffness

The intent of the present modeling effort is to evaluate the stability of the equilibrium at zero angle of attack as the roll rate is varied. An unstable equilibrium provides one explanation for the angle of attack divergence observed in the flight data. However, the linear analysis cannot assess global stability or predict nonlinear roll-pitch coupling.

4.2.1. Linearized Dynamics Model

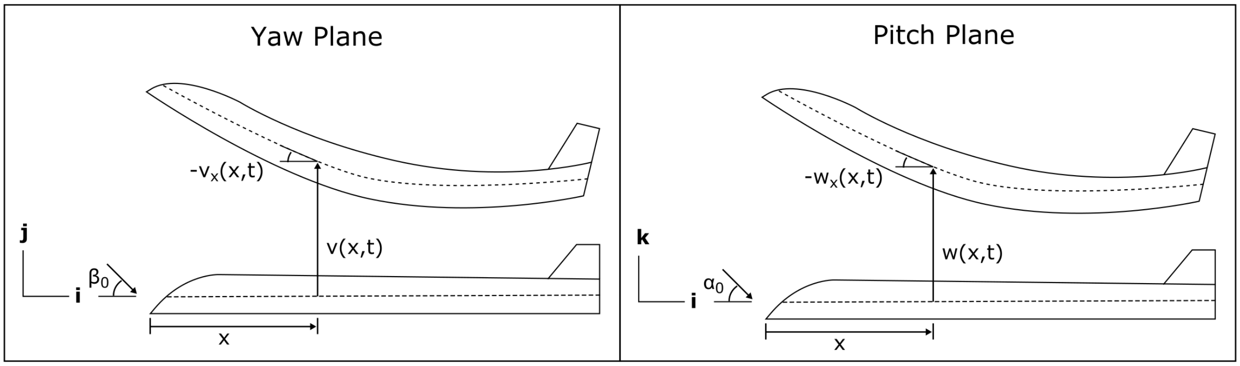

Figure 15. Schematic of Flexible Spinning Airframe

Figure 15 shows a schematic of the flexible airframe in the $\mathbf{i}-\mathbf{j}-\mathbf{k}$ frame that spins about $\mathbf{i}$ with constant rate Ω corresponding to the roll rate of airframe. The velocity of a point on the airframe centerline is given by

$$\mathbf{v} = [\dot{v}(x,t) - \Omega w(x,t)]\mathbf{j} + [\dot{w}(x,t) + \Omega v(x,t)]\mathbf{k}. \tag{4}$$

The linearized equations of motion are derived from Hamilton's extended theorem. which states

$$\int_{t_1}^{t_2} (\delta T - \delta V + \delta W)\mathrm{d}t = 0, \tag{5}$$

where δ is the variational operator, and T and V and the kinetic and potential energy, respectively, and W is the virtual work. The integration bounds t_1 and t_2 are arbitrary, requiring the integrand in Equation 5 to be zero at all time. The kinetic energy is

$$\begin{aligned} T &= \frac{1}{2}\int_0^L \rho A(x)\mathbf{v}^T\mathbf{v}\mathrm{d}x \qquad (6)\\ &= \frac{1}{2}\int_0^T \rho A(x)\left\{[(\dot{v}(x,t) - \Omega w(x,t)]^2 + [\dot{w}(x,t) + \Omega v(x,t)]^2\right\}\mathrm{d}x. \qquad (7)\end{aligned}$$

The potential energy, which exclude rotational inertia, is given by

$$V = \frac{1}{2}\int_0^L \left[EI_{zz}(x)v_{xx}(x,t)^2 + EI_{yy}(x)w_{xx}(x,t)^2\right]\mathrm{d}x. \tag{8}$$

The virtual work is given by

$$\delta W = \int_0^L [f_y(x,y)\delta v(x,t) + f_z(x,y)\delta w(x,t)]\,\mathrm{d}x, \tag{9}$$

where

$$\begin{aligned} f_y(x,t) &= -L_\beta(x,t)\beta(x,t), \qquad (10)\\ f_z(x,t) &= -L_\alpha(x,t)\alpha(x,t), \qquad (11)\end{aligned}$$

are linearized distributed aerodynamic loads and the angle of attack and sideslip angle, respectively, are given by

$$\begin{aligned} \alpha(x,t) &= \alpha_0 + w_x(x,t), \qquad (12)\\ \beta(x,t) &= \beta_0 + v_x(x,t). \qquad (13)\end{aligned}$$

A N-element discretization using finite element (FE) method with Hermite cubics transforms the continuous $v(x,t)$ to a $2(N+1)\times 1$ vector of nodal displacements and rotation $\mathbf{y}$ in the vertical direction. Likewise, $w(x,t)$ is transformed into $2(N+1)\times 1$ vector $\mathbf{z}$ of nodal displacements and rotations spanwise. The discretized equations governing the dynamics of the flexible, asymmetric, spinning missile are given by

$$\begin{aligned} \mathbf{M}\ddot{\mathbf{y}} + (\mathbf{K}_y + \mathbf{H}_y - \Omega^2\mathbf{M})\mathbf{y} - 2\Omega\mathbf{M}\dot{\mathbf{z}} &= \mathbf{F}_y \qquad (14)\\ \mathbf{M}\ddot{\mathbf{z}} + (\mathbf{K}_z + \mathbf{H}_z - \Omega^2\mathbf{M})\mathbf{z} + 2\Omega\mathbf{M}\dot{\mathbf{y}} &= \mathbf{F}_z,\end{aligned}$$

where $\mathbf{M}$ is a symmetric, positive definite mass matrix, $\mathbf{K}_y$ and $\mathbf{K}_z$ are symmetric, non-negative stiffness matrices related to the missile flexural response, and $\mathbf{F}_y$ and $\mathbf{F}_z$ are external forces from aerodynamic loads for β_0 and α_0. Finally, $\mathbf{H}_y$ and $\mathbf{H}_z$ are asymmetric aerodynamic matrices that include the effects of the vehicle flexure $v_x(x,t)$ and $w_x(x,t)$, respectively. These matrices can be decomposed additively into a symmetric stiffness matrix and a skew-symmetric circulatory matrix. Equation 14 is recast as a single system of equations given by

$$\mathbf{M}^*\ddot{\mathbf{x}}+\mathbf{G}^*\dot{\mathbf{x}}+(\mathbf{K}^*+\mathbf{H}^*)\mathbf{x}=\mathbf{F}^*, \tag{15}$$

where

$$\mathbf{x}=\begin{pmatrix}\mathbf{y}\\ \mathbf{z}\end{pmatrix}, \qquad \mathbf{M}^*=\begin{bmatrix}\mathbf{M} & \mathbf{0}\\ \mathbf{0} & \mathbf{M}\end{bmatrix} \qquad \mathbf{G}^*=\begin{bmatrix}\mathbf{0} & -2\Omega\mathbf{M}\\ 2\Omega\mathbf{M} & \mathbf{0}\end{bmatrix}$$
$$\mathbf{K}^*=\begin{bmatrix}\mathbf{K}_y-\Omega^2\mathbf{M} & \mathbf{0}\\ \mathbf{0} & \mathbf{K}_z-\Omega^2\mathbf{M}\end{bmatrix} \qquad \mathbf{H}^*=\begin{bmatrix}\mathbf{H}_y & \mathbf{0}\\ \mathbf{0} & \mathbf{H}_z\end{bmatrix}, \; \mathbf{F}^*=\begin{bmatrix}\mathbf{F}_y\\ \mathbf{F}_z\end{bmatrix},$$

and $\mathbf{G}^*$ is skew-symmetric gyroscopic matrix.

Equation 15 is essentially a linear conservative gyroscopic system, however, the asymmetry of $\mathbf{H}^*$ is an added complication that breaks the symmetry of the eigenvalue problem. This finding is consistent with finding by Platus [7], however, the present model extends to non-uniform, asymmetric vehicles.

By inspection of $\mathbf{K}^*$, it is clear that as Ω is increased, the stiffness matrix will eventually produce a negative eigenvalue and the system will become unstable. Increasing Ω further eventually achieves gyroscopic stabilization through $\mathbf{G}^*$.

4.2.2. Quasistatic Analysis

Equation 15 provides the framework necessary for a full linear stability analysis of the vehicle. This could include, for example, aeroelastic flutter in the fins. However, if it can be assumed that the flexure of the airframe and fins respond quasistatically to the time-varying flight conditions, a simpler analysis may be appropriate. The quasistatic assumption means that the sole effect of aeroelasticity is to reduce the 6 degree of freedom (6-DOF) aerodynamics coefficients. The modified aerodynamics coefficients can be implemented in the 6-DOF dynamics model to account for aeroelasticity as long as this assumption is valid.

The static analysis is performed by first substituting $\ddot{\mathbf{x}}=\dot{\mathbf{x}}=\mathbf{0}$ and $\Omega=0$ into Equation 15. Next, the rigid-body modes are removed from $\mathbf{x}$ by substituting $\mathbf{x}=\mathbf{V}\mathbf{q}$, where $\mathbf{V}$ represents all the normal modes of the vehicle defined by the $(\mathbf{M}^*,\mathbf{K}^*)$ eigenvalue problem, except the rigid-body modes, and $\mathbf{q}$ are the generalized coordinates. Premultiplying Equation 15 by $\mathbf{V}^T$ yields a linear set linear of equations

$$\mathbf{V}^T\left(\mathbf{K}^*+\mathbf{H}^*\right)\mathbf{V}\mathbf{q}=\mathbf{V}^T\mathbf{F}^*. \tag{16}$$

Equation 16 has a positive-definite stiffness matrix, $\mathbf{V}^T(\mathbf{K}^*+\mathbf{H}^*)\mathbf{V}$, that can be inverted to solve for $\mathbf{q}$. The aerodynamic load $\mathbf{F}^*$ that depends on the original angle of attack α_0 and original side slip angle β_0, is reduced to $\mathbf{F}_R^*=\mathbf{F}^*-\mathbf{H}^*\mathbf{V}\mathbf{q}$ because of the flexure of the vehicle. By evaluating $\mathbf{F}_R^*$ at the grid of points (Mach, angle of attack, side slip angle, etc.) in addition to a range to dynamic pressures, it is possible to construct a modified aerodynamic coefficients table that incorporates the effects of aeroelasticity under the quasistatic assumption into the 6-DOF dynamics model.

4.2.3. Distributed Model Parameters

Distributed model parameters for the second stage vehicle were derived from the vehicle Computer Aided Design (CAD) and six degree of freedom (6-DOF) aerodynamics model. Figure 16a shows the flexural stiffnessess $EI_{yy}(x)$ and $EI_{zz}(x)$ vs. x. Figure 16b shows the linear mass density $\rho A(x)$ vs. x. The center of gravity (CG) of the distributed mass model is 2.92 m from the aft tip of the vehicle, and in good agreement with the measured flight vehicle (2.89 m).

An aerodynamic database was generated primarily using Cart3D, an inviscid solver, with a limited set of comparisons to the viscous solver CFD++. The linearized distributed aerodynamic loads were determined by numerically differentiating the total normal/lateral loads first with respect to x and, second with respect to α/β. Figure 17 shows the linearized distributed aerodynamic loads predicted by CFD++ at stage 1 separation.

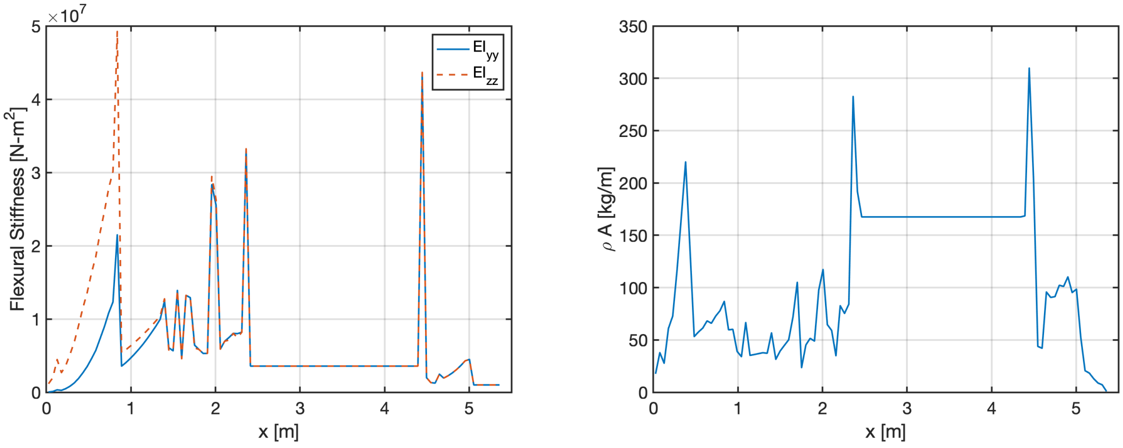

(a) Flexural stiffness (b) Linear mass density

Figure 16. Distributed Stage 2 Structural Parameters

4.2.4. Flexible Fin Model

Flexibility of the tail can and fins on the aft of the IO stage can also cause a reduction stability margin. Since these are the aft-most components of the second stage, any reduction in normal force in this spatial region can cause a significant shift forward in the vehicle CP, and reduction in stability margin. A finite element (FE) model of the fin is generated in Abaqus, and used to predict effective overall stiffness of the fins.

A modal frequency analysis step with the fins fixed in all translational and rotational degrees of freedom at its interface with the tail can is used to obtain the dominant fin bending and torsional modes. The first two modes predicted by the FE model are shown in Figure 18; a bending mode at 39.3 Hz (left), and a torsional mode at 115 Hz (right). Contours reflect modal displacement magnitudes relative to their undeformed position.

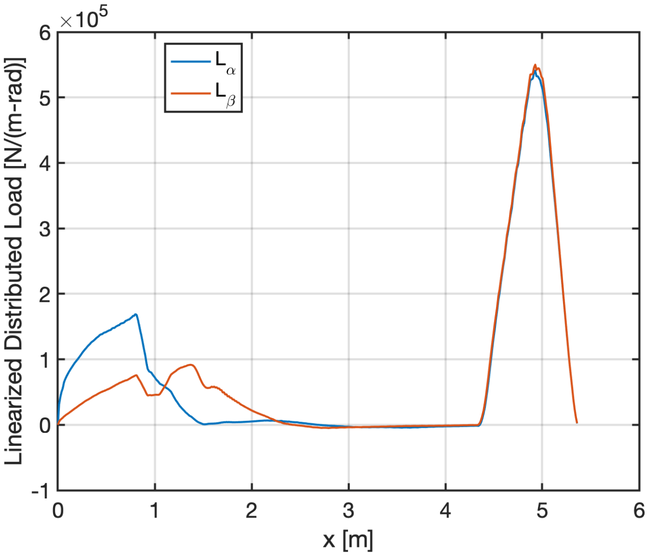

Figure 17. Linearized Distributed Stage 2 Aerodynamic Loads (Mach=2.8, q=274.5 kPa)

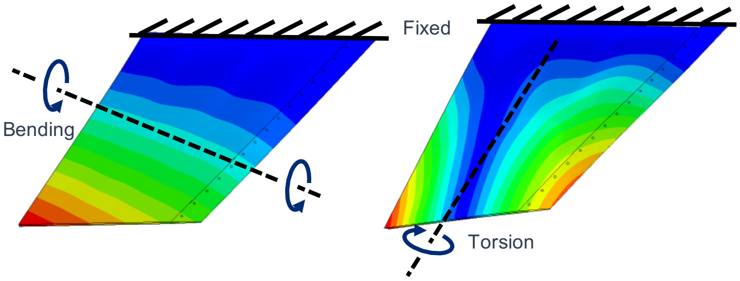

Figure 18. Predicted Bending and Torsional Modes of the IO Fins

Data derived from the FE model are used to obtain parameters for a reduced order representation of the fin and tail can for implementation in the linearized vehicle aeroelasticity model. A schematic describing this reduced order implementation is shown in Figure 19. The fin and tail can are assumed to be a small segment of the vehicle that hangs off the aft of the airframe, attached by a spring with rotational stiffness (K_{Fin}). As the aerodynamics exerts a force F_{Fin} at some point aft of this interface, there will be a corresponding angular deflection of the fin and tail can section, which introduces a balancing moment (M_{Fin}). Because of this angular deflection, F_{Fin} will be reduced relative to its undeflected case.

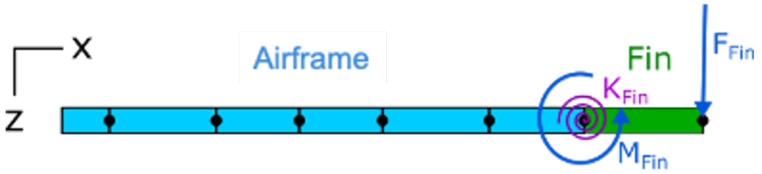

Figure 19. Implementation of the Flexible Fin Model

The effective stiffness K_{Fin} is estimated from the FE analysis by equating pitching rotation determined in the FE model to the rotation of a simple paddle such that the influence on pitching moment is the same. This is accomplished by first applying a pressure loading step, where CFD pressure solution is applied to the sheet and leading edge on one side of the fin (other side is unloaded), and the resultant nodal displacement angle $\theta(x,y,z)$ is determined at each node of the model. A weighted average fin displacement angle, $\hat{\theta}$ is then determined from

$$\hat{\theta} = \frac{1}{I}\int_A \theta(x,y,z)(\mathbf{p}(x,y,z)\cdot\mathbf{k})(x - x_{CG})\mathrm{d}A \tag{17}$$
$$I = \int_A (\mathbf{p}(x,y,z)\cdot\mathbf{k})(x - x_{CG})\mathrm{d}A$$

where $\mathbf{p}(x,y,z)\cdot\mathbf{k}$ represents the projection of pressure in the surface normal directions into a vector expressed in the vehicle $\mathbf{k}$ axis, and both integrals are carried out over the area A. With $\hat{\theta}$ known the effective stiffness K_{Fin} can be determined from

$$F_{\text{Fin}}L_{\text{Fin}} = K_{\text{Fin}}\hat{\theta} \tag{18}$$

where L_{Fin} is a length of the fin paddle segment in the vehicle aeroelasticity model.

4.3. Flight Stability at Stage Separation

This section presents results on the reduction in static margins caused by aeroelasticity as well as linear stability analysis. The results of the linear stability analysis are compared to classic results for an asymmetric rigid-body vehicle [5].

Table 5 shows the original CPs in the pitch and yaw plane, as well as the reduced values that incorporate the effects of aeroelasticity. While the shift in CP is only a small fraction of the total

Table 5. Effects of Aeroelasticity on Static Margins (t=11.2 sec, q=274.5 kPa, Mach=2.8)

	Pitch Plane	**Yaw Plane**
Original CP (m)	3.51	3.88
Reduced CP (m)	3.20	3.67
CP Shift ($\Delta L/L$)	-5.7%	-4.2%
Original Static Margin (m)	0.588	0.958
Reduced Static Margin (m)	0.303	0.747
Original Pitch/Yaw Freq. (Hz)	2.54	3.15
Reduced Pitch/Yaw Freq. (Hz)	1.68	2.58

length of the second stage, the reduction in the static margin is more significant. This reduction in turn causes a significant reduction, in particular, in the pitch frequency from 2.54 Hz to 1.68 Hz.

Figure 20 shows the first eight eigenvalues $\lambda_j = \sigma_j + i\omega_j$, $j = 1, 2, \ldots, 8$ of the linearized flexible-body dynamics model separated into real Re(λ_j) = σ_j and imaginary Im(λ_j) = ω_j components vs. the roll rate. At $\Omega = 0$ there are four zero eigenvalues, corresponding to the rigid-body translation in y- and z-directions, followed by two imaginary roots at $\omega_{5,6} = \pm 10.6$ rad/s (1.68 Hz), corresponding to the pitch frequency, and two imaginary roots at $\omega_{7,8} = \pm 16.2$ rad/s (2.58 Hz), corresponding to the yaw frequency.

As Ω is increased, the pair of imaginary eigenvalues belonging to the pitching mode begin to converge as mode exhibits whirling motion in the yz-plane. These eigenvalues coalesce at Ω equal to the pitch frequency, giving rise to two real eigenvalues, one positive, unstable eigenvalue (purple curve in Figure 20b) and one negative, stable eigenvalue (green curve in Figure 20b). The unstable eigenvalue belongs to a pure pitching mode the will cause exponential growth in the angle of attack without affecting the sideslip angle. This behavior is precisely what is seen in the flight data in Figure 14a. Increasing Ω beyond the pitch frequency, the real eigenvalues eventually coalesce at Ω equal to the yaw frequency producing two imaginary eigenvalues (gyroscopic stabilization). However, the pitching mode is unstable when the roll rate is in between the pitch and yaw frequencies.

The results presented in Figure 20 are found to be in good agreement with prior work by Hodapp [5] on rigid asymmetric vehicles, once aeroelasticity is incorporated in the 6-DOF aerodynamics model, which is accomplished using the methodology outlined in Section 4.2.2. Figure 21 shows all four eigenvalues of Hodapp's fourth-order model applied to the second-stage BOLT vehicle at the separation flight condition as the roll rate is varied parametrically. Qualitatively, the results are similar, except that the lateral translation modes are not included in Hodapp's model which describes the angle of attack and side slip dynamics directly. Quantitatively, the pitch (1.69 Hz) and yaw (2.56 Hz) frequencies are in close agreement with the flexible-body model because the aeroelastic effects have been incorporated in the 6-DOF aerodynamics coefficients. The additional aerodynamic damping terms included in Hodapp's model cause the system to be strictly stable (eigenvalues have a negative real component) rather than marginally stable for roll rates outside the pitch and yaw frequencies. For roll rates in between the pitch and yaw frequencies,

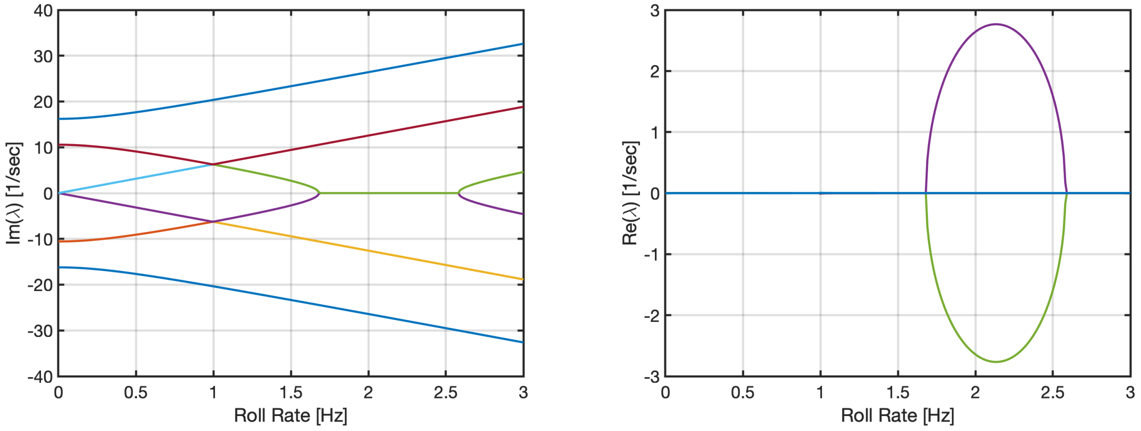

(a) Imaginary (b) Real

Figure 20. Eigenvalues of Linearized Flexible-body Dynamics Model

stability is only lost for the portion of the red curve in Figure 21b that is positive as opposed to the full range.

4.4. 6-DOF Flight Simulation

Key features of the BET can be reproduced by the BOLT 6-DOF model once aeroelasticity is incorporated. As with the analysis of Hodapp's model, this is accomplished using the methodology outlined in Section 4.2.2 to incorporate aeroelasticity in the 6-DOF aerodynamics model. While comparing the BET to the 6-DOF model predictions, it was determined that an additional -3.5% body-length shift in the CP was required to reproduce the flight behavior. The additional -3.5% is within the uncertainty estimated for the aerodyanmics model but could also be related to uncertainty in the vehicle structural model, particularly vehicle joint and fin compliance. For additional details, see Section3.

Figure 22 shows the post-flight 6-DOF model predictions for roll rate and angle of attack compared to the BET. Figure 22a also includes the pitch and yaw frequencies for both the original rigid-body model and the post-flight model that includes aeroelasticity. The 6-DOF model predicts lock-in to the pitch frequency, starting shortly after stage separation and persisting for the majority of ascent. While the roll-rate remains locked to the pitch frequency, the angle of attack is stable. Brief excursions into the unstable region in between the pitch and yaw frequencies are accompanied by abrupt, exponential growth in angle of attack (Fig. 22b). These excursions occur following stage separation, following IO ignition at 15.5 sec, and later on in ascent, around 33 seconds, where dynamic pressure is low.

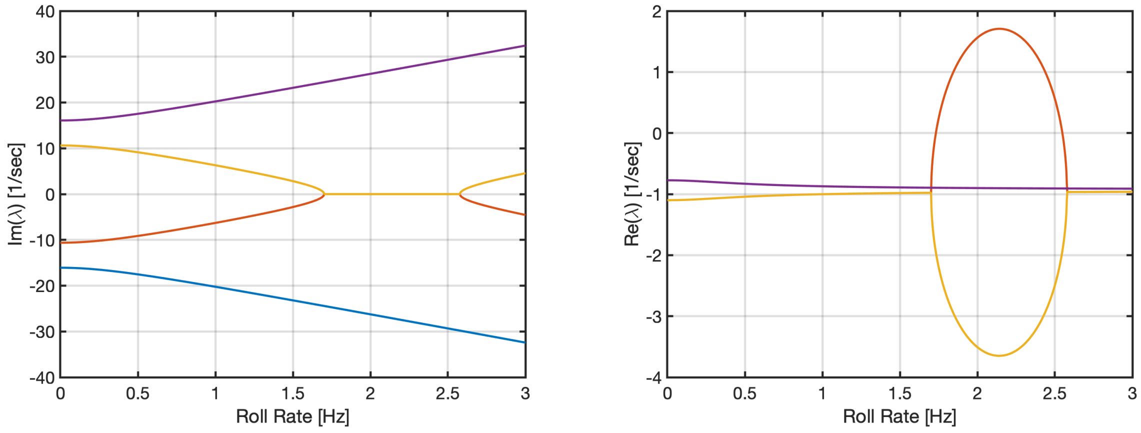

(a) Imaginary (b) Real

Figure 21. Eigenvalues of Hodapp's Model with Aeroelasticity Included

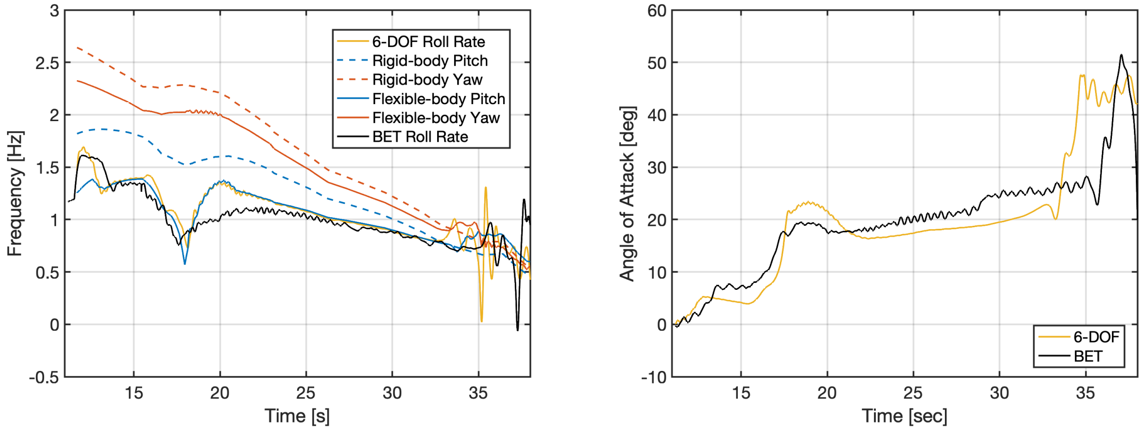

(a) Roll Rate (b) Angle of Attack

Figure 22. Post-flight 6-DOF Simulation

4.5. Conclusions

The unexpected flight behavior in the 23 June 2021 BOLT flight was ultimately caused by aeroelastic effects that were neglected in the preflight analysis and resulted in a significant reduction in static margin. The BOLT flight geometry deviates from typical sounding rocket payloads in two significant ways: (i) the asymmetry that causes the pitching and yawing frequencies to separate, and, (ii) the large acreage of the forebody increases the bending load on the airframe, making aeroelastic effects more pronounced. The present aeroelastic model for the BOLT research vehicle predicts -5.7% body length reduction in the pitch plane static margin at the separation flight condition. Analysis of the BOLT flight data suggests that the total reduction in static margin from preflight estimates is closer to -9.2% body length, the difference is attributed to uncertainty in the aerodynamics model and the vehicle structural model.

Understanding the 23 June 2021 BOLT flight dynamics is essential to developing a mitigation strategy for potential future flights involving complex, asymmetric payloads. One approach is to design the roll-rate to stay below the critical frequencies for the majority of ascent until dynamic pressure has decreased and the pitch and yaw frequencies have converged. This strategy, however, comes at the cost of increased downrange/cross-range dispersions.

5. Supersonic Transition Analysis from the BOLT Flight

Although the BOLT experiment did not reach its intended Mach 5–7 conditions in flight, the experiment did gather boundary-layer transition measurements at supersonic conditions (Mach ≈ 3) during the descent phase of flight. Unfortunately, reentry to the atmosphere occurred several minutes sooner than anticipated due to the much lower apogee, resulting in only one of the three scientific data telemetry streams being active during the descent phase. Thus, a limited number of instrument data on the order of 90 channels were received during the BOLT descent. This section will present an analysis of this data and the boundary-layer transition events which may be inferred at various points during the supersonic descent. This analysis is coupled with a computational investigation performed for the flight conditions, allowing for direct comparisons of surface heat flux. These computations are also leveraged to conduct preliminary stability analyses meant to identify potential transition mechanisms encountered in flight.

5.1. BOLT Flight Payload and Vehicle

The BOLT payload (or "Flight Geometry") contained a scientific experiment designed with a unique shape provided by AFOSR for study in this research effort. Figure 23a shows the Flight Geometry outer mold line, the complex geometry that serves as the subject of the scientific research. Figure 23b shows the completed flight hardware including the Flight Geometry, as well as the Transition Support Module (TSM) and Payload Support Module (PSM sections). Additional details of the experiment design are summarized in [9]. The Flight Geometry contained an extensive suite of surface instrumentation (thermocouples, pressure sensors, and heat transfer gauges) at 226 discrete locations providing a total of 344 scientific measurements.

Figure 24 shows the overall BOLT Flight Research Vehicle, with dimensions in millimeters. The image shows the 866 mm Flight Geometry along with the PSM and TSM, the cold gas system (CGS) and attitude control system / service module (ACS/SM) which will reorient the vehicle ahead of reentry for the descent experiment, and the motor adapter (MA). The first stage consists of the S31 solid rocket booster from the Brazilian Aeronautics and Space Institute (IAE) of the Department of Aerospace Science and Technology (DCTA) and the second stage consists of an Improved Orion motor. The two stages were selected with the intent to deliver the BOLT Flight Geometry to conditions to make measurements within the hypersonic regime (Mach 5 to 7) for measurements of transition on both ascent and descent. Further details are provided in Hörschgen-Eggers et al. [12].

5.2. Flight Trajectory and Experiment Conditions

This section describes the actual vehicle behavior during the BOLT flight utilizing the "best estimate trajectory" (BET) from the vehicle Inertial Measurement Unit (IMU) and Global Position System (GPS) receivers. The BET was provided by AFRL. The "best estimate atmosphere" (BEA) was provided by the U.S. Air Force Weather Agency based on global weather model anchored with discrete weather balloon soundings at the range. The DLR roll-stabilized IMU saturated due to the unexpectedly high angular rates during ascent, meaning that the IMU provided by AFRL/RQ was relied upon for reconstructing the attitude through descent. This IMU is not roll-stabilized and

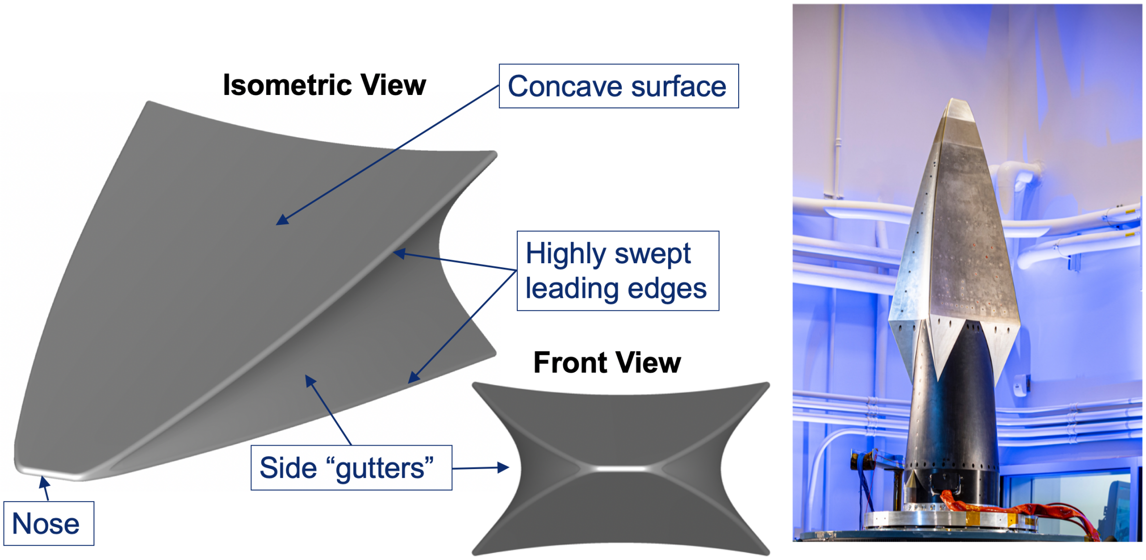

(a) Flight Geometry

(b) Completed Flight Experiment

Figure 23. BOLT Flight Geometry

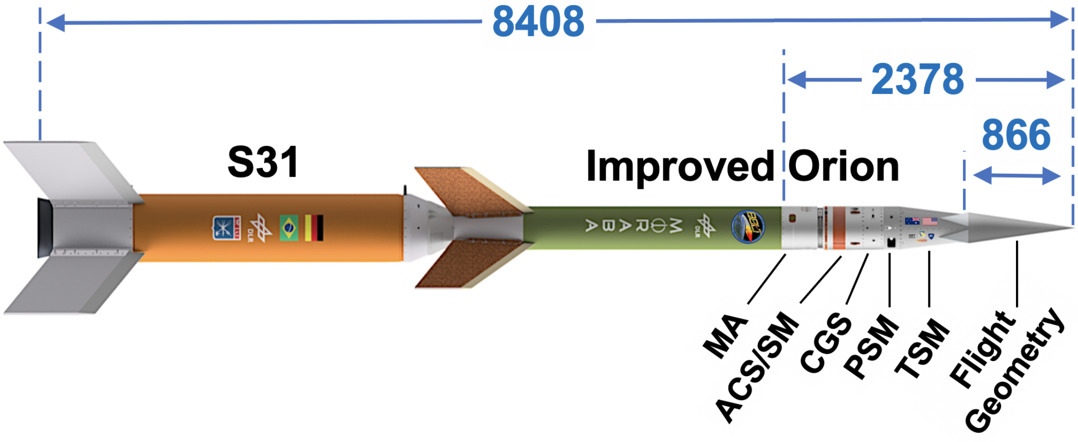

Figure 24. BOLT Flight Research Vehicle (dimensions in mm). Image provided by DLR MORABA.

thus susceptible to the buildup of small errors and drift. These errors were mitigated applying an extended Kalman filter (EKF) to the integration, leveraging the available GPS data. A check on the IMU attitude solution is provided by measurements of the mean surface pressure on the BOLT forebody made throughout flight with eight Kulite pressure transducers.

5.2.1. Best Estimate Trajectory

The final BET is shown in Figure 25. Maximum dynamic pressure occurred during stage separation at 11.1 s at an altitude of 5.6 km, at which point a divergence of the vehicle from the nominal trajectory occurred. The flight continued as planned with the payload remaining attached to the second stage Improved Orion (IO) motor, however due to the increased drag from the unexpected behavior the maximum Mach number achieved on ascent was 3.9 instead of 7.0 and 2.7 on descent.

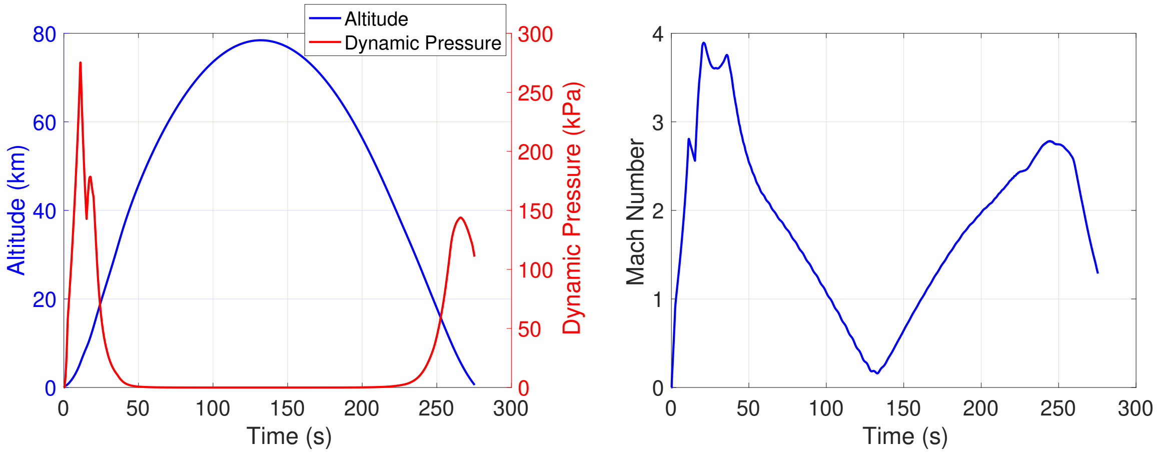

(a) Altitude and Dynamic Pressure

(b) Mach Number

Figure 25. Best Estimated Trajectory (BET)

5.2.2. Flight Dynamics Axis Definitions

Descriptions of the vehicle motion are provided relative to a flight dynamics axis reference system shown in Figure 26, viewed from the front of the vehicle. The axes are body fixed with an origin at the vehicle center of gravity. The X (roll) axis points forward, with the lateral axes Y and Z describing pitch and yaw motion, respectively. A positive angle of attack (α) is achieved by a positive rotation about the Y (pitch) axis, and a positive sideslip angle (β) is achieved by a positive rotation about the Z (yaw) axis. The total angle of attack (α_T) is defined as the included angle between the vehicle X axis and the incoming wind vector, and represents the magnitude of both α and β by the relation:

$$\tan^2(\alpha_t) = \tan^2(\alpha) + \tan^2(\beta) \tag{19}$$

Rays of the vehicle are denoted 0–360° in Figure 26 and will be used to report the windward meridian angle of the flow. The windward meridian is the vehicle azimuthal angle that is windward with respect to the incoming velocity vector. The windward meridian is 0° when the primary experiment surface is windward and 180° when the secondary experiment surface is windward.

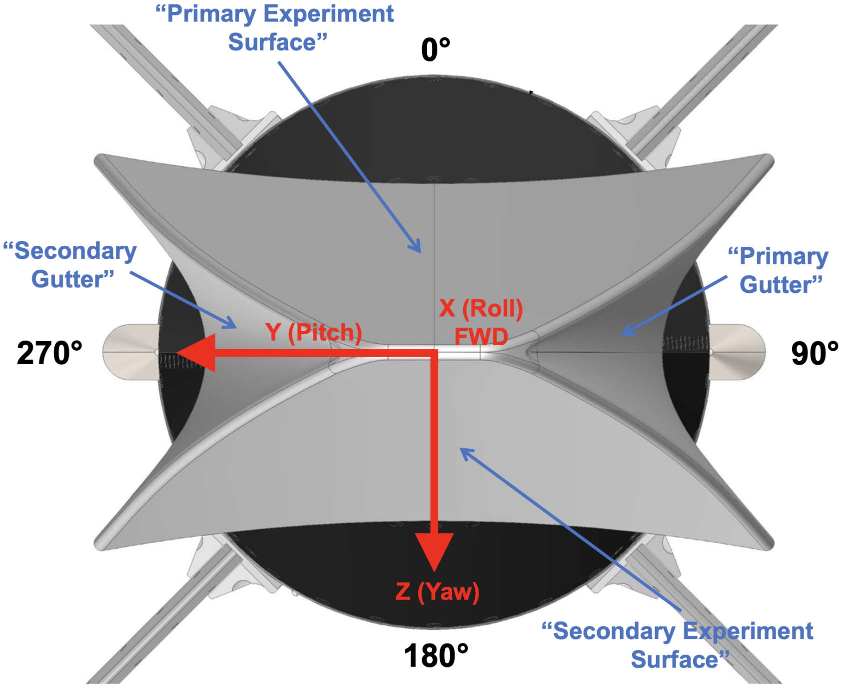

Figure 26. Axis definitions for descriptions of flight dynamics (view forward looking aft).

5.2.3. Surface Pressure Attitude Reconstruction

As mentioned previously, the BOLT forebody was instrumented with 8 Kulite pressure transducers for measuring the surface static pressure. These measurements were originally intended to capture the changes in pressure due to the vehicle rolling at a small angle of attack. The vehicle attitude may be reconstructed by minimizing the rms difference between the flight measurements and a computed surface pressure database, similar to Jewell et al. [13]. The rms difference was defined as

$$p_{RMS} = \frac{1}{p_\infty}\left[\frac{1}{8}\sum_{i=1}^{8}(p_{CFD}(\alpha_t,\phi,M_\infty) - p_F)_i^2\right]^{0.5}, \tag{20}$$

where p_∞ refers to the freestream pressure given by the GPS altitude, the subscript i denotes the sensor, p_{CFD} is the pressure predicted at the sensor location as a function of total angle of attack and aerodynamic roll angle, and p_F is the measured surface pressure. The database used for p_{CFD} was generated with CART3D, a high-fidelity inviscid CFD package with a fully integrated adjoint-driven mesh adaption. The database spanned the range of α_t, ϕ (aerodynamic roll angle), and Mach number for the scientifically-relevant portions of the flight, detailed in Table 6. For every time step, the database was interpolated to the correct Mach number and then interpolated again to a finer resolution of α_t and ϕ. The rms difference was then calculated and minimized to find the correct α_t and ϕ. Figure 27 shows an example of the resulting p_{RMS} for a given point in flight, with the determined attitude given by the minimum at $(\phi \approx 75^\circ, \alpha_t \approx 15^\circ)$.

Table 6. Range of conditions for CART3D CFD database

Variable	Range	Increment
α_t	0–25°	0.5°
ϕ	0–360°	10°
M	1.5–4.5	0.5

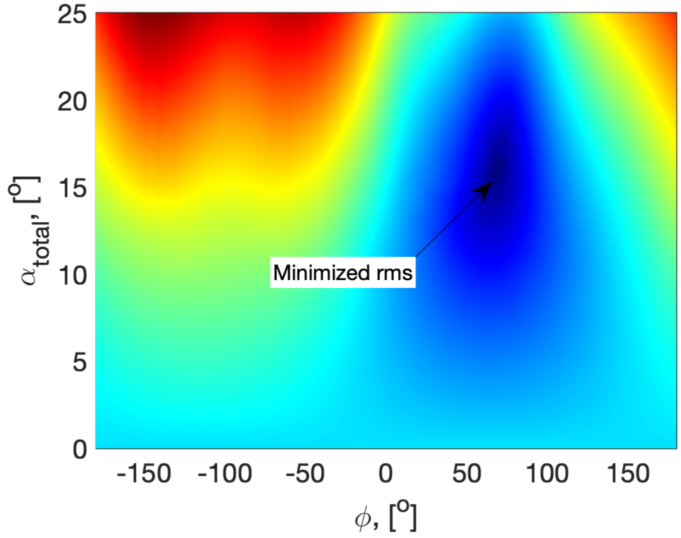

Figure 27. Example of rms differences for a given Mach number.

5.2.4. Vehicle Attitude

The vehicle attitude solutions derived from IMU integration and the forebody pressure reconstruction are shown in Figure 28 for the ascent phase from 10 s (just prior to stage separation) until 45 s. The length of the BOLT Flight Geometry (0.866 m) was used in determining a length Reynolds number (Re_L), which is employed as a secondary abscissa. Shortly after stage separation, the vehicle experienced a positive pitching motion nearly entirely about the Y axis which resulted in growth of total angle of attack from small values less than 0.5° to 7–7.5° in just a few seconds. The vehicle became locked into the flow with a windward meridian angle near the 180° ray (secondary surface experiment windward). The ignition of the IO motor occurred at 15.1 s at $\alpha_t = 7^\circ$, after which a further angle of attack increase occurred to values of α_t near 20°. Data suggests that the vehicle entered into pitch-roll coupling at a rate of approximately 500°/s shortly after 11 s and remained in this state throughout most of the ascent. The lock-in of the windward meridian during this time can be described as “lunar motion,” in which the vehicle rotates about the wind vector but the same side of the vehicle is facing the incoming wind vector.

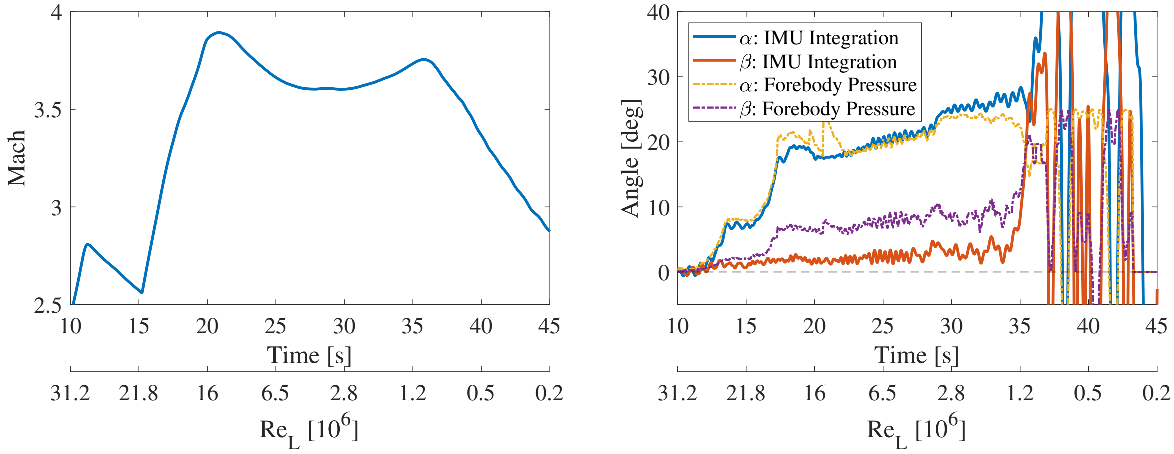

(a) Mach Number

(b) Alpha/Beta

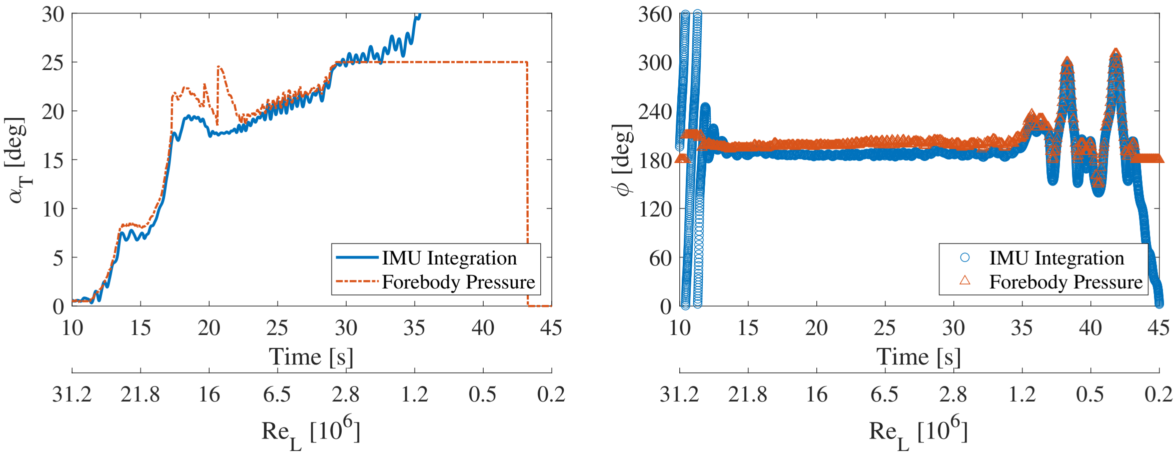

(c) Total Angle of Attack

(d) Windward Meridian Angle

Figure 28. Ascent phase experiment conditions from 10 s to 45.0 s, plotted against the length Reynolds number of the BOLT Flight Geometry (0.866 m)

The BOLT descent phase dynamics from $220-270$ s are shown in Figure 29. The vehicle appears to have entered the atmosphere with large oscillations in attitude due to the lack of a reorientation maneuver (as originally was planned for nominal flight). These oscillations gradually diminish as the vehicle attitude becomes aligned with the flight path vector. The IMU and forebody pressure attitude solutions agree well for the entirety of descent, though the IMU solution shows significant oscillations in α_t and ϕ after ≈ 255 s which are not present in the pressure-derived solution. Both methods indicate that the vehicle re-entered lunar motion around this point in the trajectory with the secondary side windward for the majority of the descent phase, although at a much lower total angle of attack (2-3°) than that of the ascent. The low angle of attack coupled with a fairly consistent windward meridian angle makes this region of potential interest for scientific analysis and will be explored further in the section. Notably, there also exists a brief period from $248-252$ s ($Re_L \approx 4-6\times 10^6$) during which the vehicle became somewhat locked-in to lunar motion with the primary surface windward and the angle of attack at $4-8°$. This region is thus also of interest for scientific analysis.

The original BOLT experiment Reynolds number of interest were $Re_L = 0\text{–}20\times 10^6$, during which it was expected to achieve natural transition. Although transition Reynolds number typically varies with Mach number, no pre-flight ground testing or analysis was performed at supersonic conditions, and it is assumed that transition onset should still occur within this relatively broad range of Re_L. Examination of Figure 28 shows that the majority of flight conditions with $Re_L = 0-20\times 10^6$ during ascent occurred at relatively large angles of attack in the range of 17-30°. In addition, the secondary side of the experiment was windward with respect to the incoming velocity vector during this entire period. The primary side was thus leeward to the flow, and unfortunately it contained the majority of the flight experiment sensors. For these reasons, the remainder of this transition-focused assessment will focus on the descent phase of flight. Future efforts may seek to extract useful turbulent heating data from the ascent phase of flight.

5.3. Analysis of Descent Transition Measurements

This section will document the analyses to date of the supersonic transition measurements during the descent phase of the BOLT flight. Unfortunately, only a single telemetry (TM) stream was received throughout descent, limiting analysis to approximately 90 of the 344 data channels. This single TM stream was due to a pre-planned and time-based shutoff of two of the three TM streams carrying the scientific data during the BOLT nominal trajectory to alleviate thermal concerns from the transmitters during exoatmospheric flight. The sensors available during the BOLT descent phase are demarcated with red, blue, and black dots in Figure 30 with the sensors not received shown as small white dots. Note that not all front-face thermocouples had a back-face counterpart, rendering those unusable for heat flux calculations.

5.3.1. Scientific Experiment Coordinate System

For the remainder of the section, a new coordinate system will be used in an experiment-focused reference plane as in Figure 30. In this new coordinate system, designated with x,y, and z, the coordinate x is the axial coordinate beginning at the experiment nosetip and z is a spanwise coordinate. The variable ψ may be used in place of z to locate the sensors in the spanwise direction,

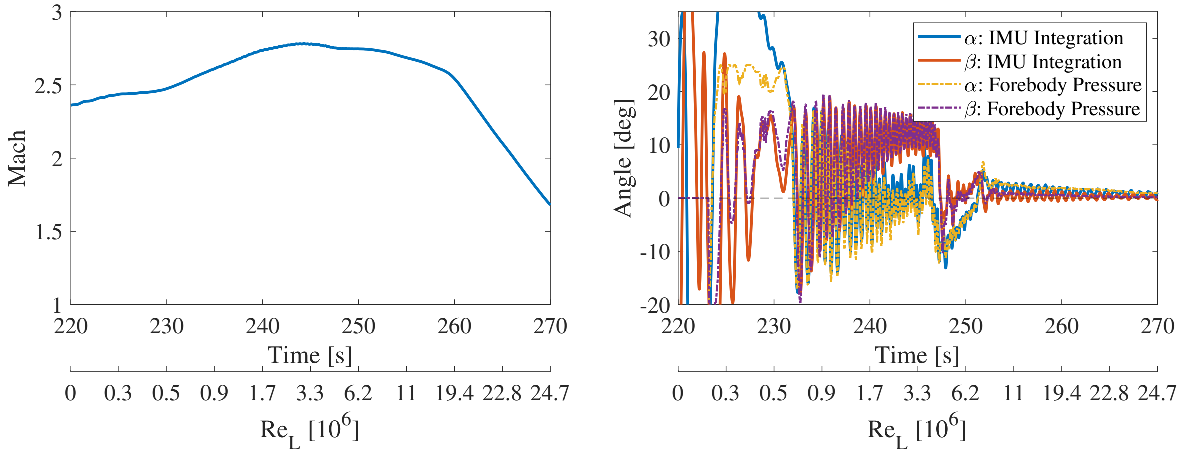

(a) Mach Number

(b) Alpha/Beta

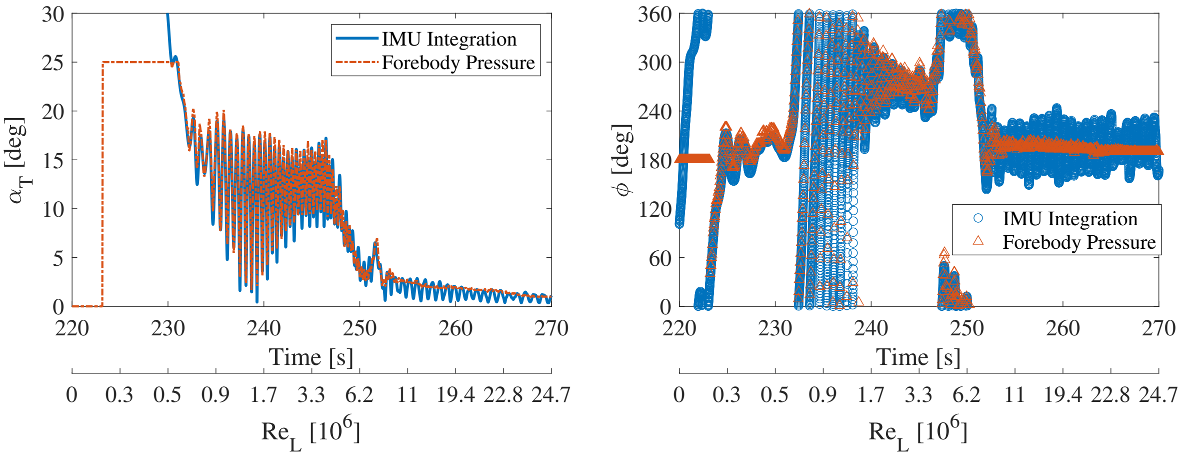

(c) Total Angle of Attack

(d) Windward Meridian Angle

Figure 29. Descent phase experiment conditions from 220 s to end of flight, plotted against the length Reynolds number of the BOLT Flight Geometry (0.866 m)

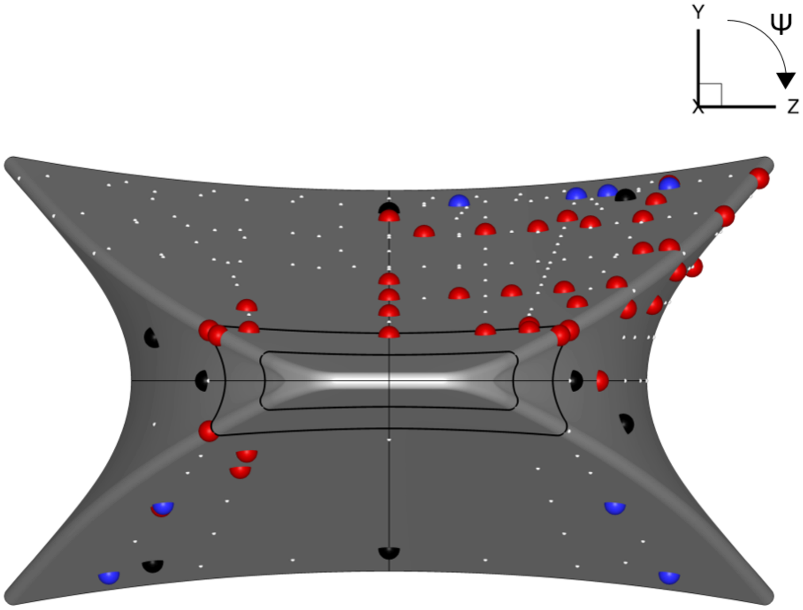

Figure 30. Sensor feeds transmitted during descent: (red) thermocouples, (black) mean pressure sensors, and (blue) fluctuating pressure sensors.

with $\psi = 0°$ referring to the Flight Geometry main surface centerline and $\psi = 90°$ referring to the gutter centerline. The leading edge is located at approximately $\psi = 55 - 65°$, however the precise angle depends on the axial station.

5.3.2. Data Processing Methods

Medtherm coaxial thermocouples were leveraged as the primary means of transition front detection. A marked increase in surface heat transfer at a given sensor location may be interpreted as the onset of transition. Previous HIFiRE transition flights have been able to utilize a one-dimensional inverse heat transfer analysis method to convert Medtherm temperature data into local discrete heat transfer rate histories (see Juliano et al. [14, 15]). As in these works, heat transfer calculations throughout this study were performed using a MATLAB implementation of QCALC provided by Prof. Tom Juliano at the University of Notre Dame which, given the temperature on the inner and outer surface of the vehicle, uses a second-order Euler-explicit finite-differencing scheme to solve for the temperature profile through the aeroshell. The heat flux is then given by a second-order approximation to the temperature derivative at the wall [16]. Note that this 1D inverse heat transfer method assumes that axial and spanwise conduction is negligible relative to conduction in the wall-normal direction. This assumption is expected to remain valid in the vicinity of the BOLT centerline, but becomes questionable near the swept leading edges, where spanwise conduction effects are known to be substantial. As such, results near the leading edges should be treated with some skepticism.

Prior to the heat flux calculations within QCALC, the temperature time histories were processed with a 10 Hz low-pass filter. As described by Juliano et al. [14], the thermocouples are also susceptible to drift which can produce spurious offsets in the computed heat transfer later in flight. To mitigate these effects, a temperature shift was applied to all back-face thermocouples at 190 s such that the front and back face temperatures are identical and thus the computed heat transfer is zero. This time was chosen to occur prior to the descent phase when the only expected heat transfer would correspond to axial and spanwise conduction through the aeroshell. The analysis herein focuses on the centerline ray and the spanwise slices at the 350 mm and 650 mm stations of the primary surface, as these locations remained sufficiently instrumented despite the telemetry shutdown. Conclusions regarding transition on the secondary surface are limited in scope, as telemetry was only received for four of these sensors.

Eight of the original 32 Kulite XCEL-100-5A pressure transducers were available throughout descent and were sampled at relatively high frequencies of either 15 kHz or 70 kHz. These medium bandwidth pressure (PMBW) sensor measurements provide an alternative avenue for detecting transitional and turbulent flow. As indicated by the blue circles in Figure 30, the four operating PMBW sensors on the primary experiment surface were all located in the same quadrant along a spanwise ray at $x = 790\,\text{mm}$. The precise coordinates of each sensor are given in Table 7.

In general, the PMBW measurements may indicate transition with a rise in the surface RMS fluctuations, $\tilde{P}$. For proper interpretation of the measurements and assessment of transition, the fluctuations must be normalized by the time-varying mean pressure at the surface, P. This nondimensionalization is accomplished by interpolating from the CART3D database described in section III. 5.2.3 onto each PMBW station, assuming the vehicle attitude and freestream conditions of the

PMBW	1	2	3	4	5	6	7	8
x [mm]	490	490	790	790	790	790	790	790
y [mm]	-70.5	-70.5	-110.4	-110.4	100.4	104.5	106.3	110.4
z [mm]	-129	129	-160	160	40	107	125	160
ψ [deg]	-119	119	-125	125	21.7	45.7	49.6	55.4
F_s [kHz]	70	15	15	15	70	15	15	15

Table 7. Descent PMBW locations and sampling rates.

IMU trajectory to reflect the true flight conditions.

5.3.3. Primary Surface Windward

Heat transfer traces computed for stations along the experiment main surface centerline over the full descent window are shown in Figure 31a along with the variation in α_T. From the beginning of descent up to Re_L 4×10^6, transition is indicated for all sensors downstream of $x = 275\,\text{mm}$ by intermittent spikes in the heat transfer. Unfortunately, as demonstrated by the attitude solution in Figure 29, these transition events correspond to a time at which the vehicle is locked into an orientation of almost pure sideslip, with the windward meridian aligned with one of the gutters, and occur as the vehicle oscillates between positive and negative α. To clarify the measurements of interest, Figure 31b shows these same centerline traces, but with symbols denoting times at which the primary surface was nearly windward ($\phi = 0 \pm 1^\circ$). This limits our focus essentially to two experimental windows: one which occurs from the beginning of flight up until Re_L 1×10^6 and another which spans Re_L $4-7\times10^6$. The first window is extremely limited in the magnitude of Re_L and all sensors appear to remain laminar during this time. The second window, however, appears to contain measurement of natural supersonic transition. A close-up of this time period is presented in Figure 32. The heat transfer for station $x = 725\,\text{mm}$ spikes suddenly at $Re_L = 5.5\times10^6$, presenting a transition Reynolds number for the centerline at Mach 2.75. The angle of attack during this window decreases from approximately 8° to 4°.

This transitional behavior may be further characterized by examining the heat transfer along the spanwise arrays. Again, these traces were computed assuming 1D heat conduction through the Flight Geometry wall, and are thus subject to some uncertainty. The 350 mm slice, shown in Figure 32b, has a single midspan sensor at $\psi = 40^\circ$ which shows no signs of transitioning. At $X = 650\,\text{mm}$ (Figure 32c), however, transition is observed around the same $Re_L = 5.5\times10^6$ established previously. Transition is first seen near the centerline at $\psi = 14^\circ$ and quickly spreads outboard to encompass $\psi = 33^\circ$, while the outboard sensors near the leading edge show no evidence of transition. This lack of outboard transition holds for the $\psi = 56^\circ$ sensor at $X = 725\,\text{mm}$ in Figure 32d.

The normalized RMS fluctuations for the PMBW sensors are shown over this same descent window of interest for $\phi = 0^\circ$ in Figure 33. On the primary surface, transition is first evident at $\psi = 22^\circ$ around $Re_L = 5.2\times10^6$ as the surface fluctuations suddenly spike over an order of magnitude. Note

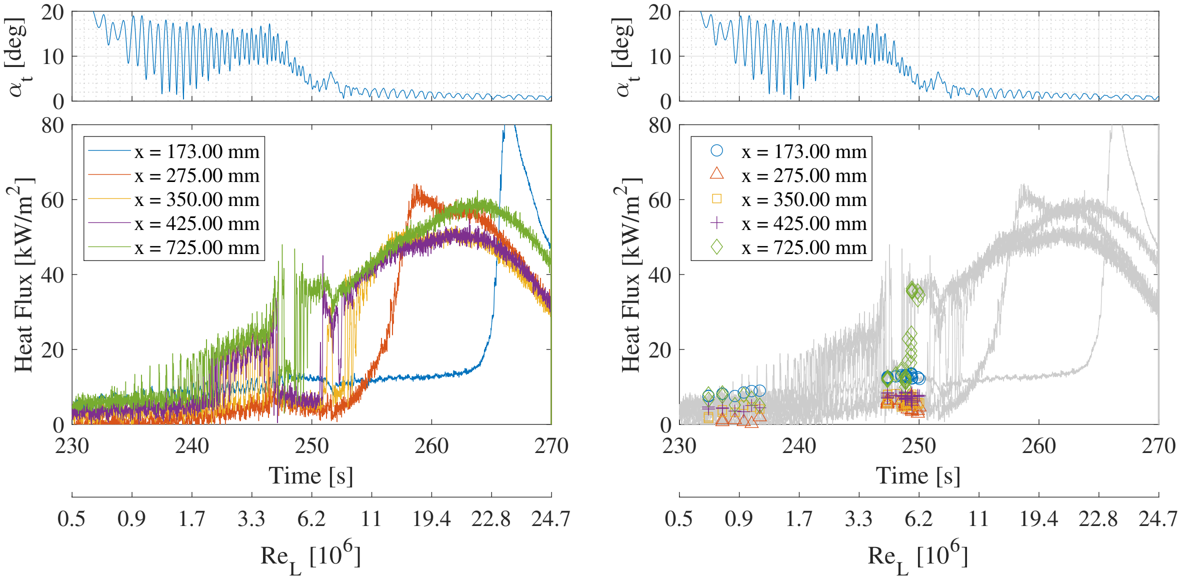

(a) Centerline heat transfer over full descent window.

(b) Centerline heat transfer with symbols to denote $\phi = 0 \pm 1°$.

Figure 31. Heat transfer computed for various thermocouple rays with the primary experimental surface windward during descent.

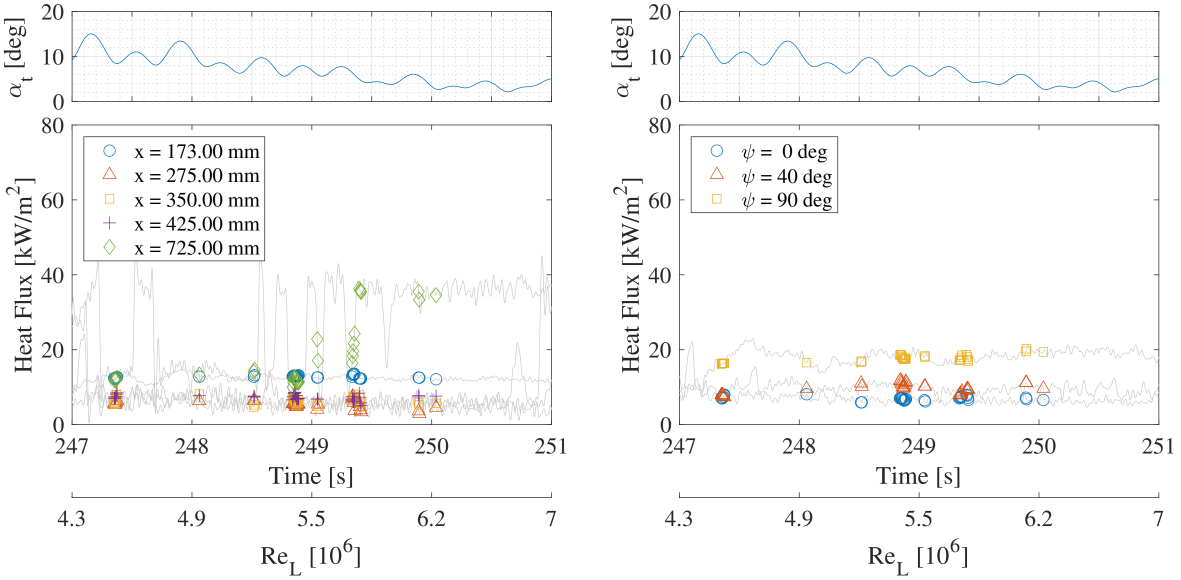

(a) Centerline heat transfer

(b) Heat transfer at 350 mm

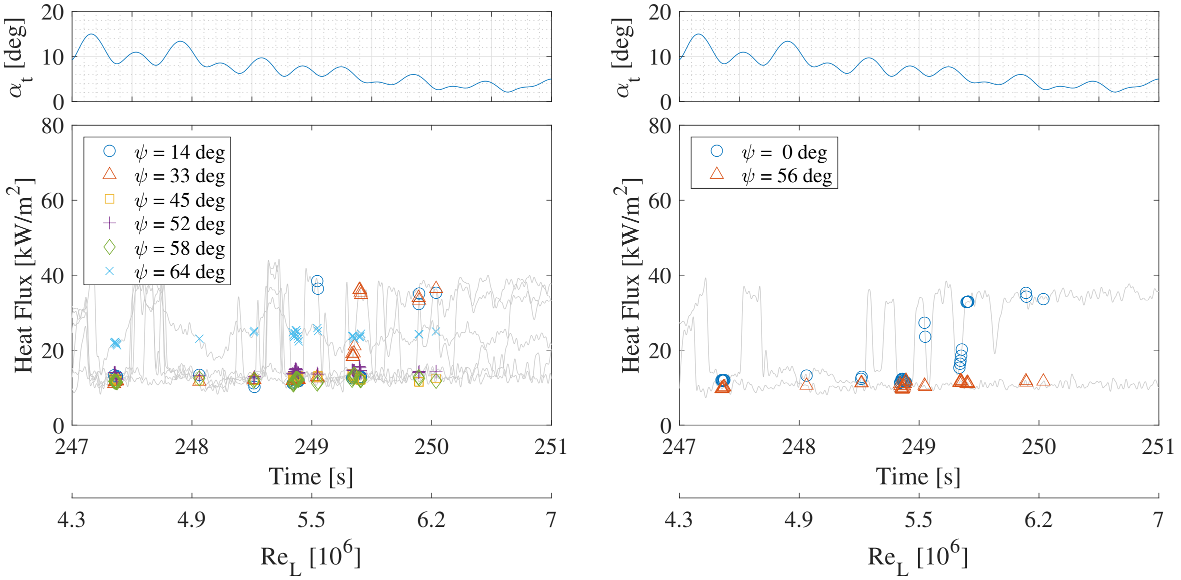

(c) Heat transfer at 650 mm

(d) Heat transfer at 725 mm

Figure 32. Heat transfer computed for various thermocouple rays with the primary experimental surface windward during descent.

that this occurs slightly earlier in flight than the centerline transition at $X = 725\,\mathrm{mm}$ indicated by the thermocouple data. The transition front then spreads outboard, as was seen along the 650 mm slice. All four sensors are clearly transitional by $Re_L = 6.2 \times 10^6$, though it is not clear that the boundary layer has become fully turbulent at $\psi = 55°$. As an aside, Figure 33b plots the fluctuations experienced by the secondary surface sensors during this time period and suggests consistently turbulent behavior.

Taken together, the PMBW and thermocouple measurements are inconclusive as to whether transition originates along the centerline or slightly outboard. That said, the earlier appearance of transition in the PMBW signal at $\psi = 22°$ is noteworthy. In order for this transition front to originate along the centerline, it would have to occur just downstream of 725 mm, implying a spreading half-angle of at least 32°. This would be substantially higher than spreading angles typically reported in literature. It thus seems more likely that transition initiates off-centerline. Additional measurements supporting this interpretation will be presented in the next section.

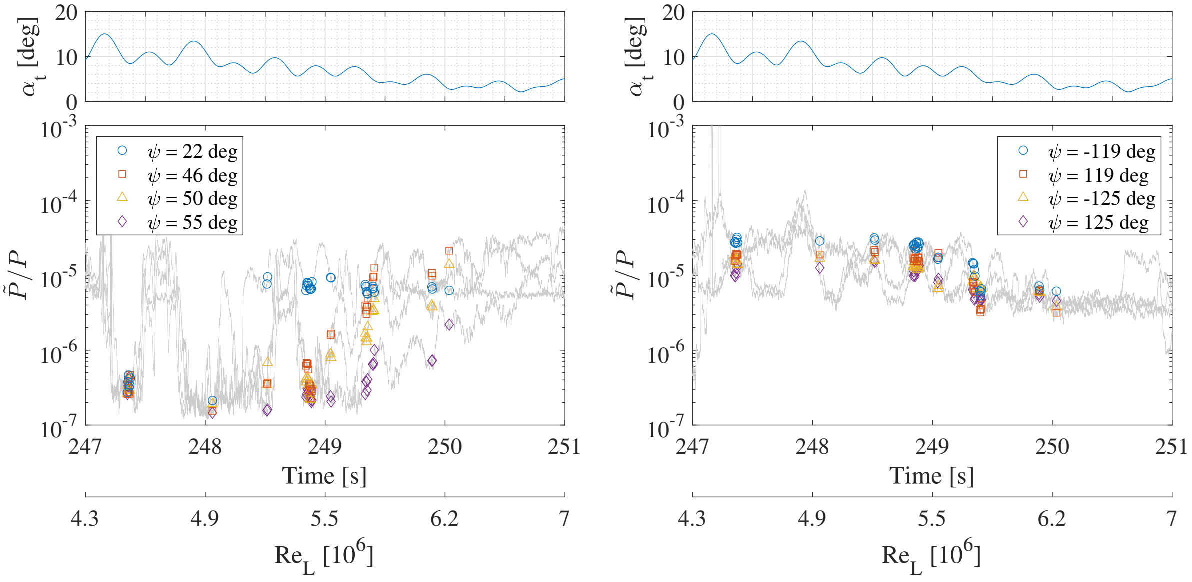

(a) Primary surface PMBW's. $\phi = 0°$.

(b) Secondary surface PMBW's. $\phi = 0°$.

Figure 33. Normalized RMS pressure fluctuations for the PMBW stations where symbols denote times with the primary surface windward.

5.3.4. Primary Surface Leeward

Later in flight, we have established that the vehicle becomes locked into an orientation with the secondary surface windward. Figure 34 depicts the heat transfer traces on the primary surface during this window, but with symbols now denoting points at which the windward meridian angle is $180 \pm 1°$. From these centerline traces (Figure 34a), we observe a gradual forward motion of the transition front from $Re_L = 8 - 20 \times 10^6$, providing a large sweep of Re_L at approximately constant

Mach number of 2.7. Three specific conditions were selected for further computational analysis and are denoted with vertical, dashed lines. The $X = 425\,\mathrm{mm}$ station seems to experience transition almost as soon as the experimental window begins around $Re_L = 7.9 \times 10^6$ and is quickly followed by the 350 mm and 275 mm stations, respectively. By $Re_L = 11 \times 10^6$, all thermocouple stations appear transitional/turbulent with the exception of the forward-most location at $X = 173\,\mathrm{mm}$. The spanwise slice at $X = 350\,\mathrm{mm}$ (Figure 34b) presents experimental confirmation of transition initiating off-centerline. This is demonstrated by the elevated heat flux levels at $\psi = 40^\circ$ relative to the centerline at the beginning of the experimental window. The spanwise stations at 650 mm and 725 mm (Figure 34c,d) demonstrate that the boundary layer is uniformly turbulent across the entire span for the entirety of this experimental window.

Figure 35 again illustrates the RMS fluctuations for the primary and secondary surface PMBW's, respectively, but now with symbols corresponding to times with $\phi = 180^\circ$. The normalized pressure fluctuations maintain a constant amplitude for the primary surface array, again demonstrating the same turbulent behavior observed in the thermocouple data. The secondary surface PMBW's mimic this turbulent behavior with the exception of station $\psi = 119^\circ$, which appears to transition up from $Re_L = 7 - 10 \times 10^6$. The fact that this behavior is not mirrored at $\psi = -119^\circ$ suggests some degree of nonzero sideslip, as was suggested by the pressure-reconstructed attitude solution. That said, the pressure reconstruction shows this sideslip to be less than 1° in magnitude throughout this period and thus sideslip effects were considered to be outside the scope of this study.

5.4. Computational Studies

5.4.1. Mean Flow Computations

APL has previously developed and implemented numerous analysis techniques for both the design of the flight experiment hardware and also the understanding of the fluid physics phenomena on the BOLT Flight Geometry [9]. Naturally, these analyses were all carried out for the hypersonic conditions expected during the nominal experimental windows and are of little applicability for the supersonic conditions experienced during flight. A computational study was thus conducted to better characterize the flow topology for the flight conditions of interest and to better understand potential underlying transition mechanisms. The precise simulated freestream conditions are given in Table 8. Condition 1 was chosen to match the primary surface transition event identified at $Re_L = 5.5 \times 10^6$ with $\phi = 0^\circ$, while Conditions 2A-C target the transitional behavior observed from $Re_L = 7 - 20 \times 10^6$ when the primary surface was leeward ($\phi = 180^\circ$). Note that the wall was modeled as isothermal at 298 K throughout this work, ignoring the temperature rise experienced throughout flight. Furthermore, as described in Berry et al. [17], the experiment was designed with rear-facing steps located at $X = 0.0845\,\mathrm{m}$ and $0.1841\,\mathrm{m}$ intended to equalize during the nominal flight experiment window. Because the flight was shortened and the vehicle only received heating associated with supersonic (rather than hypersonic) flight, the actual transition measurements are likely occurring with rear-facing steps at the upstream joints. However, the geometry modeled throughout this computational effort did not include these steps.

All mean flow computations were carried out with US3D, an unstructured, finite-volume, compressible, Navier-Stokes solver developed by Candler et al. at the University of Minnesota. First-order implicit time integration with the data-parallel line relaxation method was used to march

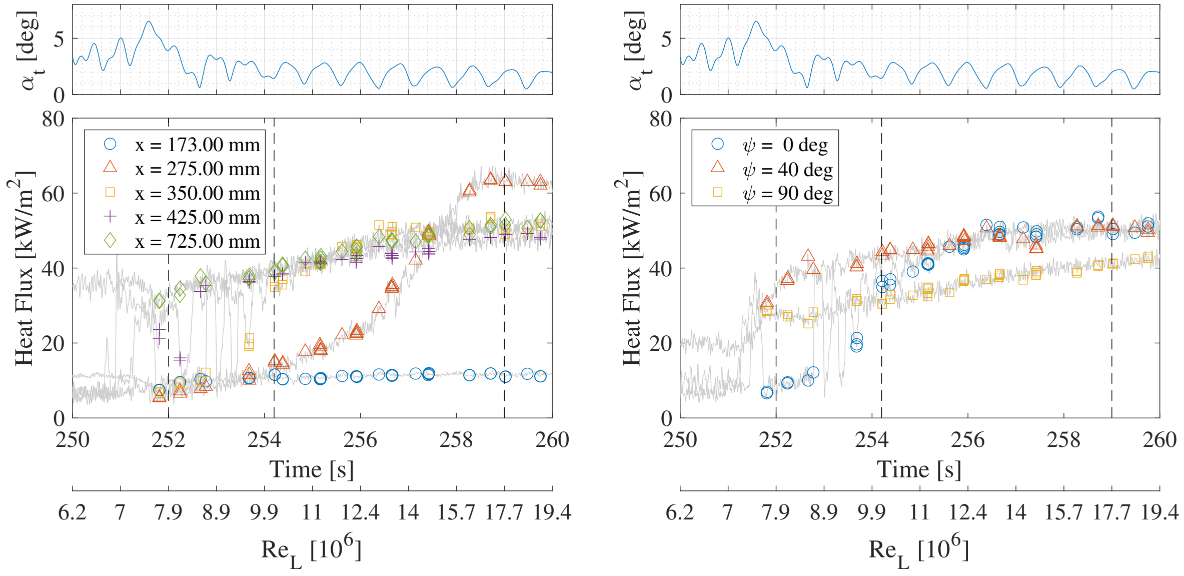

(a) Centerline heat transfer (b) Heat transfer at 350 mm

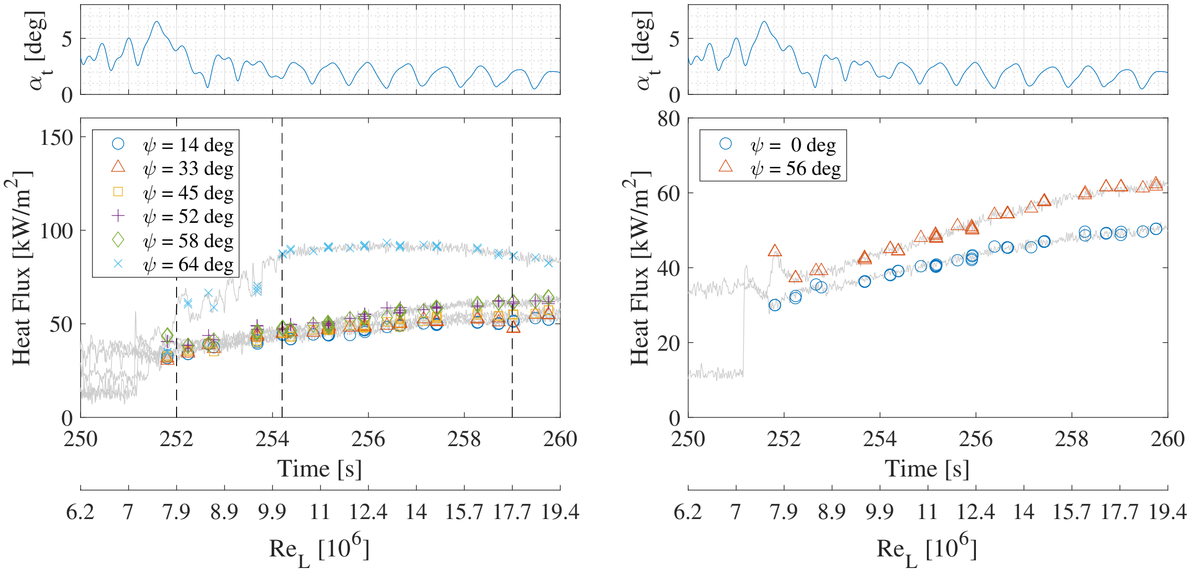

(c) Heat transfer at 650 mm (d) Heat transfer at 725 mm

Figure 34. Heat transfer computed for various thermocouple rays with the secondary experimental surface windward during descent.

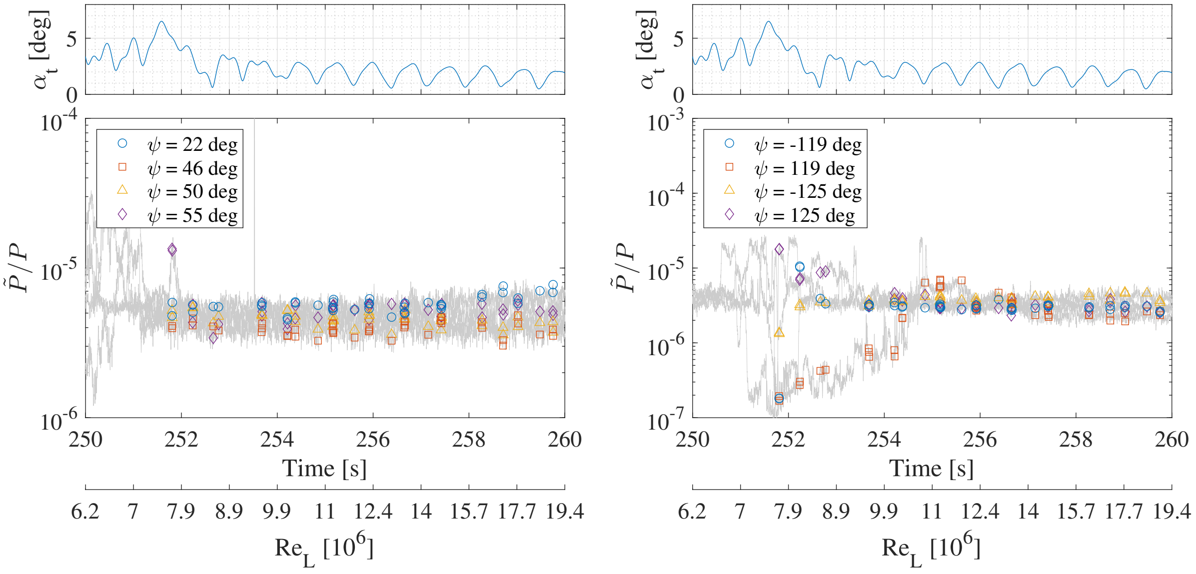

(a) Secondary surface PMBW's. $\phi = 180°$.

(b) Secondary surface PMBW's. $\phi = 180°$.

Figure 35. Normalized RMS pressure fluctuations for the PMBW stations where symbols denote times with the secondary surface windward.

the solution to steady state. Inviscid fluxes were evaluated using a second-order, low-dissipation, kinetic energy consistent scheme with a Mach dissipation switch. While the bulk of the simulations performed were laminar base flows, a limited set of turbulent RANS simulations were carried out at each condition to bound the expected heat flux. These simulations employed the negative Spalart-Allmaras turbulence model.

Condition	Mach	$Re_L[\times 10^6]$	$\alpha[^\circ]$	$\beta[^\circ]$	$P_\infty[kPa]$	$T_\infty[K]$	$U_\infty[m/s]$	$\rho_\infty[kg/m^3]$	$P_0[bar]$	$T_0[K]$
1	2.75	5.5	8.0	0	7.23	224	825	0.113	1.82	563
2A	2.7	8.0	-4.0	0	10.6	225	823	0.163	2.46	554
2B	2.7	10.0	-2.5	0	13.9	228	817	0.211	3.22	559
2C	2.6	17.5	-2.0	0	25.7	223	778	0.383	5.12	525

Table 8. Freestream conditions for computational studies.

A grid convergence study was carried out using 4 grids of varying streamwise and spanwise resolution to ensure all relevant flow features are captured. These fully-structured grids were generated using a combination of the GoHypersonic LINK-3D and Cadence Design Systems (formerly Pointwise) mesh generation tools and the details regarding the various resolutions are given in Table 9. The lowest-resolution Grid A was generated with uniform azimuthal spacing, while all others employed some degree of clustering near the geometry centerline. Note that all grids employed were half-symmetry domains.

Grid	Type	Cells $[\times 10^6]$	Streamwise Nodes	Azimuthal Nodes	Wall-normal Nodes
A	Full	34	436	105	251
B	Full	90	985	138	206
C	Full	215	2,411	127	174
D	Full	210	1,308	184	274

Table 9. Grid parameters used in convergence study.

Figure 36 presents flow visualization obtained for Condition 1 with Grid D. The primary experimental surface (windward) is shown painted by heat flux (in W/m^2) on the right and pressure (in Pa) on the left with contours of Mach number shown at the exit plane. The windward surface at these conditions is characterized by a thick centerline boundary layer which thins downstream. The surface heat flux has a local maximum along the centerline and an additional peak further outboard where the centerline boundary layer rapidly diminishes. This contrasts sharply with the centerline vortex roll-up characteristic of hypersonic conditions (see, for instance, [18] and [19]). This difference in behavior can be explained by the relative absence of crossflow for the current conditions. This is primarily attributable to the reduced Mach number, which substantially alters the shock shape along the leading edge, reducing the spanwise pressure gradient.

Grid independence for this condition was assessed based on slices of surface heat flux. The surface heating predicted along the centerline of the primary surface for the each mean flow solution is plotted in Figure 37a. The agreement between the Grid A and Grid D solutions demonstrates a

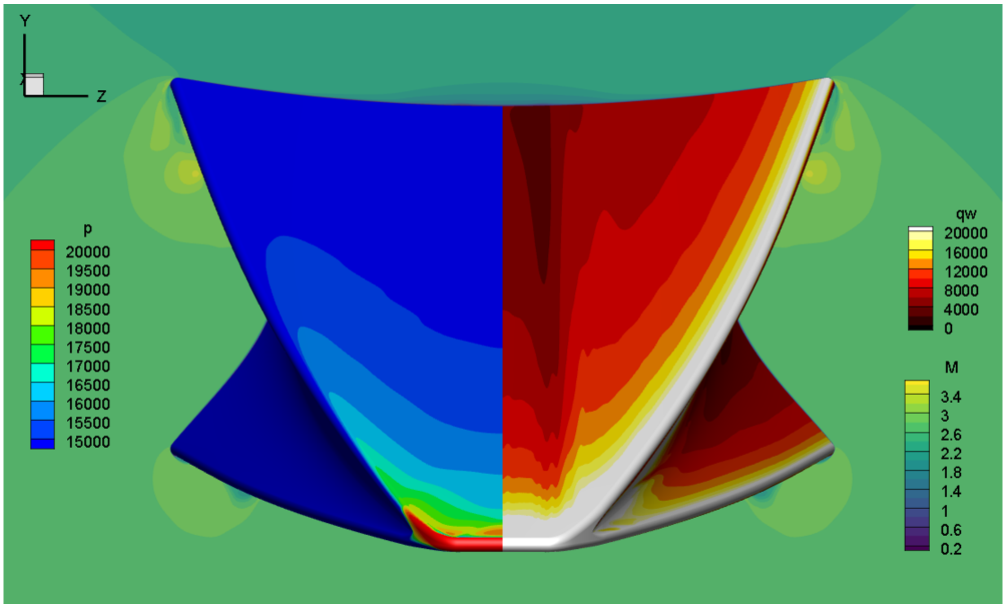

Figure 36. Flow visualization for Condition 1. Heat flux is given in W/m^2 and pressure in Pa.

high degree of grid insensitivity along the centerline. Figure 37b,c present spanwise comparisons at axial stations of 350 mm and 650 mm. From these figures, it is apparent that higher grid resolutions resolve additional features away from the centerline, as the Grid D solution includes spanwise oscillations not observed at lower grid resolutions. That said, these oscillations remain fairly low in magnitude, and the Grid D solutions were thus considered sufficiently resolved for the purposes of this preliminary study.

5.4.2. Flight Comparisons

The same heat flux slices from the previous section for Grid D are plotted against data from the flight experiment in Figure 38 along with a turbulent heating prediction computed with Grid B. The experimental data points correspond to averages over small windows extracted from the points plotted in Figure 32 where $\phi = 0 \pm 1^\circ$. The computational trace agrees well with the experimental data up until $X = 725$ mm, where even the data from earlier times periods is elevated above the laminar prediction. It is currently unclear if this is due to transitional behavior or uncertainty in the experimental measurements. Nonetheless, at 249 s the experimental heat flux rapidly rises to three times its earlier value, indicative of transition. Spanwise comparisons are given in the bottom two images of Figure 38 at $X = 350$ mm and $X = 650$ mm. The 350 mm slice demonstrates good agreement between the flight measurement and CFD prediction even at the midspan station ($\psi \approx 40^\circ$), though the results suggest the gutter ($\psi = 90^\circ$) may be turbulent. At 650 mm, decent agreement is observed towards the leading edge, but further inboard we see a significant underprediction relative to the flight data. This is most pronounced at $\psi = 14^\circ$ and $\psi = 33^\circ$ and mimics the centerline observation at 725 mm. While the cause for the discrepancy remains unclear, it may again be evidence of transitional behavior. As discussed previously, transition is clearly seen for $\psi = 14^\circ$ at 249 s and shortly thereafter at $\psi = 33^\circ$, demonstrating the outboard spread of the transition front.

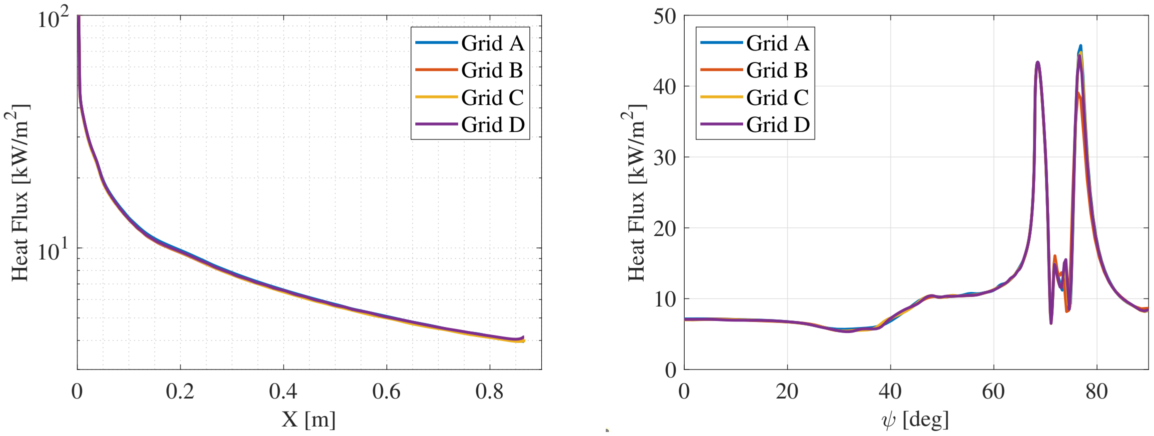

(a) Centerline heat transfer

(b) Heat transfer at 350 mm

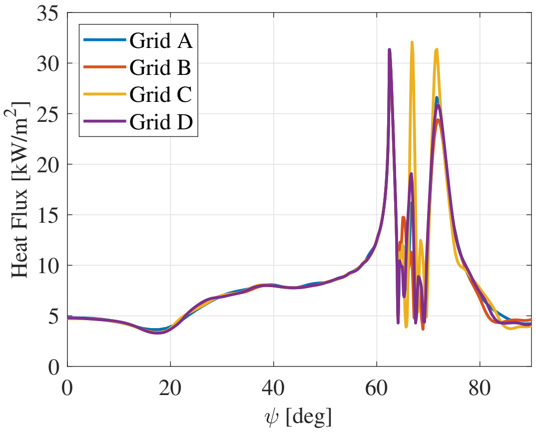

(c) Heat transfer at 650 mm

Figure 37. Slices of computed laminar heat flux for the Condition 1 grid resolution study.

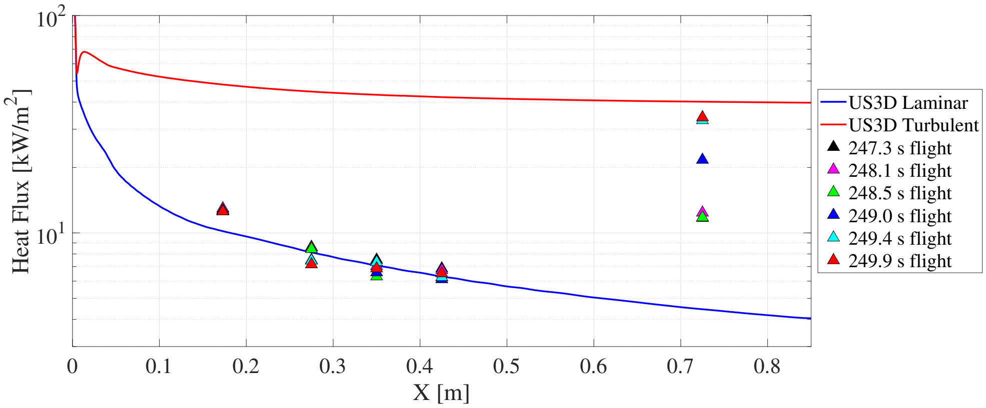

(a) Centerline slice.

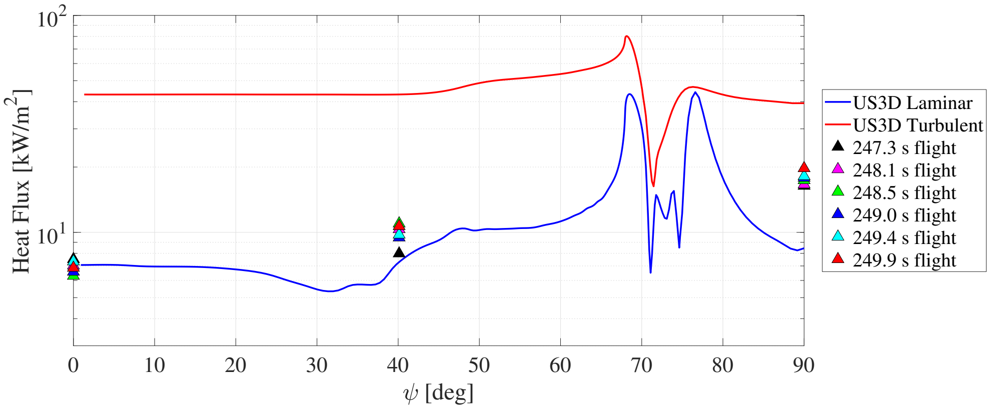

(b) $X = 350\,\text{mm}$ slice.

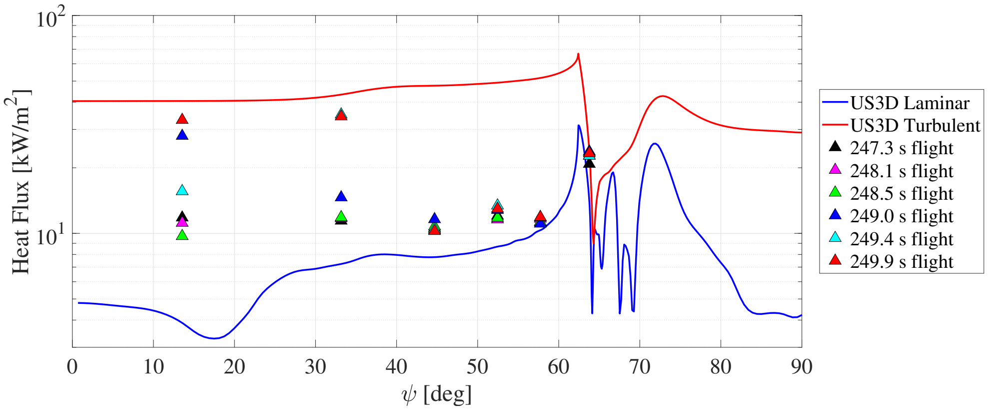

(c) $X = 650\,\text{mm}$ slice.

Figure 38. Heat flux comparisons for Conditions 1.

Base flow visualizations of the primary experimental surface (now leeward) for Conditions 2A-C are presented in Figure 39. These visualization demonstrate significant topological differences relative to Condition 1, most notably the formation of distinct heating streaks. The furthest inboard of these streaks clearly bend towards the centerline downstream, suggestive of enhanced crossflow. This increased crossflow may be attributed to the leeward orientation, which produces a far different shock shape along the leading edge relative to Condition 1. As Re_L increases and α_T decreases between Conditions 2A and 2C, the flow topology becomes more complex, with additional streaks appearing and persisting further downstream. Another notable feature which arises due to the leeward orientation at these conditions is the vortex formed by the leading edge. This vortex creates a region of low heat flux slightly inboard of the leading edge as well as a large spike where the vortex reattaches.

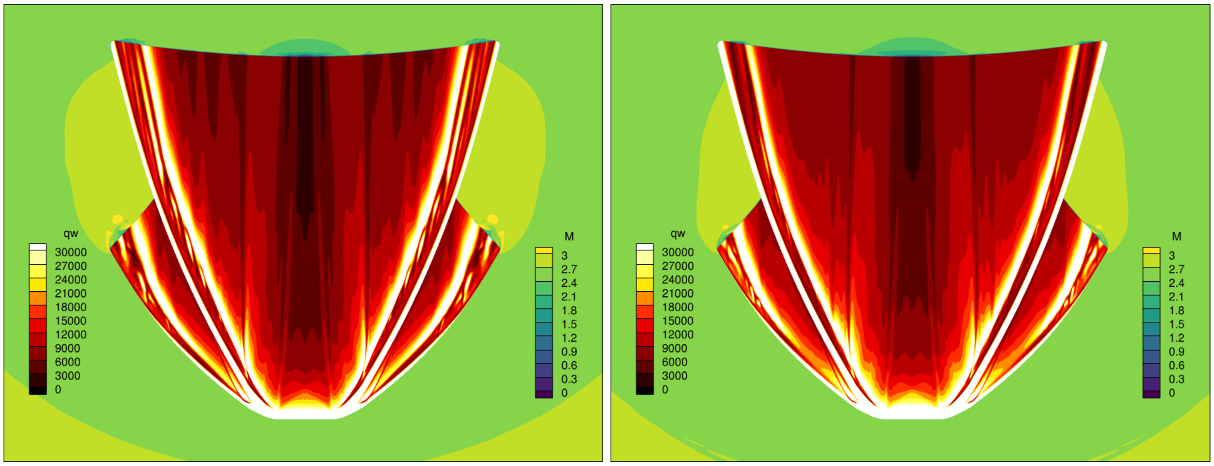

(a) Condition 2A

(b) Condition 2B

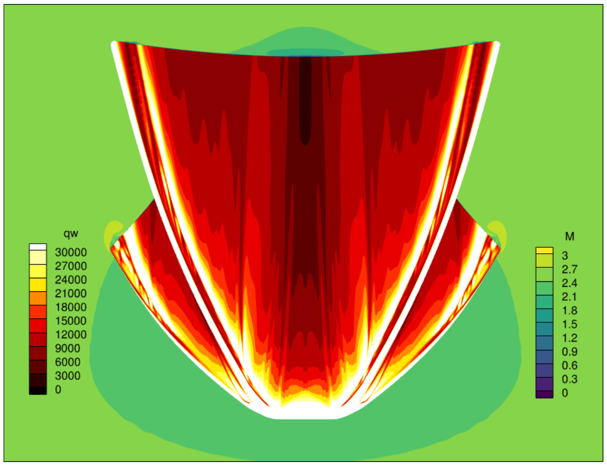

(c) Condition 2C

Figure 39. Flow visualization for Conditions 2A-C showing primary experimental surface (leeward).

Comparisons between the flight data and computations are presented in Figure 40 for Condition 2. Note that the solid lines correspond to the US3D solutions for Condition 2A, while the 2C solutions are given by the upper boundary of the shaded regions. The prediction for Condition 2B thus lies within the shaded region. Along the centerline (Figure 40a), we see the laminar solution slightly underpredicts the heat flux across all conditions for the presumably laminar station at $X = 0.173\,\mathrm{m}$. Further downstream, we see the flight-measured heat flux increases to lie between the laminar and turbulent predictions, suggestive of transitional behavior. This transition process is accelerated between Condition 2A, where the boundary layer likely reaches a fully turbulent state in the vicinity of 0.425 m, and Condition 2C, where even the second station at 0.275 m appears fully turbulent. We generally see excellent agreement between the flight data and the turbulent CFD predictions.

Examining the 0.35 m slice in Figure 40b, we see from the flight data that the centerline is laminar or early-transitional at Condition 2A, but fully turbulent at 2B. The heat flux recorded by the sensor at $\psi = 40°$, on the other hand, reads turbulent levels even at condition 2A. This provides strong evidence that transition initiates off-centerline and has already enveloped this midspan sensor while the centerline is still in a transitional state. As seen along the centerline, the RANS heating predictions very nearly match the flight data across the vehicle span. The 0.65 m slice demonstrates similar levels of agreement with a greater sensor density, suggesting the acreage is fully enveloped by turbulence at this axial station for all studied flight conditions.

5.4.3. Stability Analysis

Preliminary stability analyses of the above baseflows were carried out with LASTRAC (Langley Stability and Transition Analysis Code) to identify potential instability mechanisms at each flight condition. LASTRAC is a transition-prediction code developed by NASA which offers computations based on either quasi-parellel linear stability theory (LST) or the parabolized stability equations (PSE). The PSE formulation is implemented in both linear (LPSE) and nonlinear variants. All formulations are based on a decomposition of the Navier Stokes equations into mean and fluctuating components. A full description of the governing equations and numerical formulation of LASTRAC are given in the user manual. This effort primarily utilized LASTRAC's LST implementation. Note that this effort is meant to be a first look at the potential stability characteristics for these flight conditions and not an authoritative assessment of the dominant instabilities. The LASTRAC analysis is naturally limited by the inherent assumption of spanwise homogeneity in the flow, an assumption that may not apply to the BOLT flowfield in many cases.

All stability analyses were performed on the Grid D base flows with inviscid edge streamlines extracted for use as marching paths. The boundary-layer edge used for computing these streamlines was identified as the wall-normal distance at which the total enthalpy reached 99.5% of its freestream value. The influence of different marching paths on disturbance growth was not examined in this work, but is expected to be small given the minimal amount of crossflow present across all conditions. Separate LST surveys were conducted to examine the growth of 2-D disturbances as well as oblique disturbances, such as first mode and stationary and traveling crossflow (SCF and TCF). The 2-D analysis considered disturbances from 2 kHz up to 800 kHz in increments of 2 kHz. The oblique disturbance analysis considered disturbances from 0 kHz (stationary crossflow) up to 100 kHz in increments of 2 kHz with fixed spanwise wavelengths of $0.5, 1, 2, 3, 5, 7.5, 10$ and

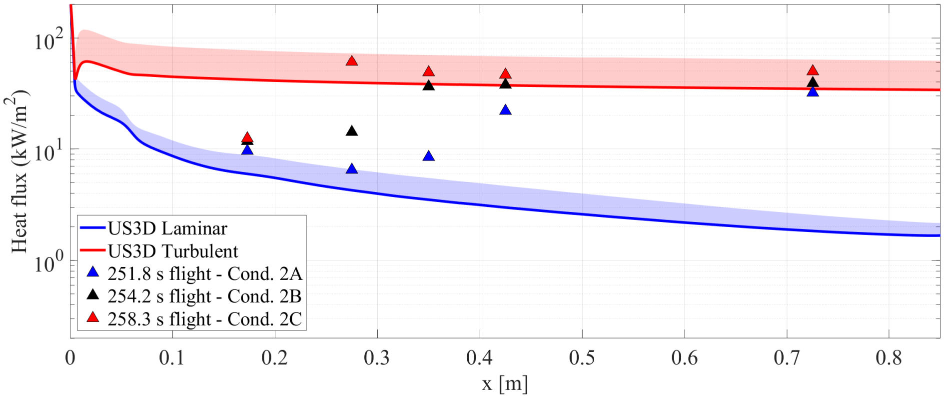

(a) Centerline slice.

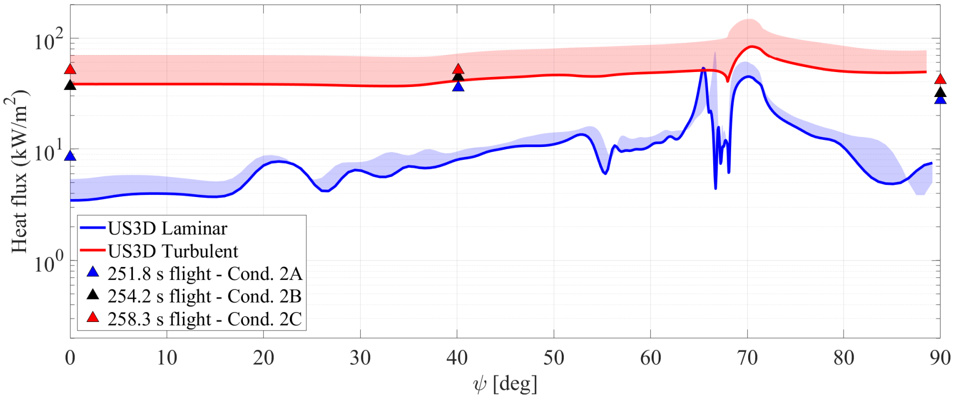

(b) $X = 350\,\text{mm}$ slice.

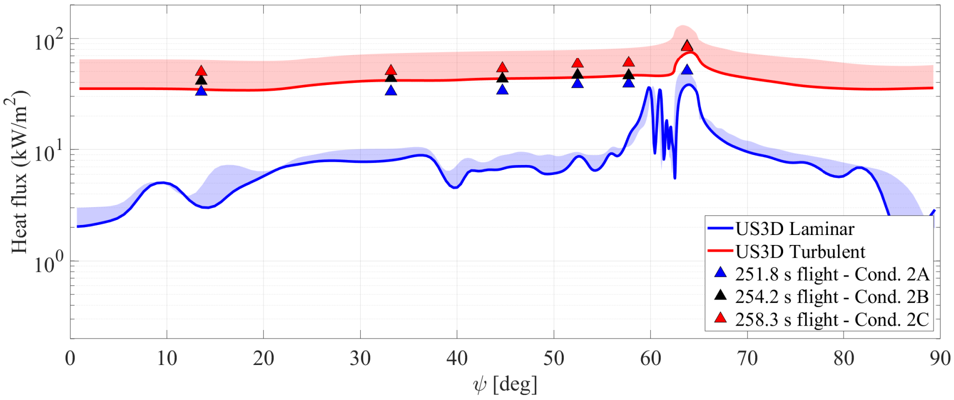

(c) $X = 650\,\text{mm}$ slice.

Figure 40. Heat flux comparisons for Conditions 2A-C.

15 mm.

Surface distributions of maximum N factors obtained along each streamline from the LST analysis of Condition 1 are presented in Figure 41 for 2-D disturbances and stationary crossflow. The black circles towards the rear of the surface denote the locations of the PMBW sensors while black lines are included to denote the locations of the aforementioned joint steps. LASTRAC predicts only limited growth of 2D disturbances, with a maximum N factor of ≈ 0.4. The greatest amplification is observed along a streak slightly off-centerline for frequencies in the range of $8-12$ kHz. The exceedingly low N factors make it unlikely these disturbances would be the cause of transition observed in flight.

Stationary crossflow (left half of Figure 41) appears along this same streak, nearly coincident with the near-centerline PMBW sensor, and undergoes far greater amplification. The most amplified stationary crossflow disturbances reach a peak N factor of ≈ 3 and have a spanwise wavelength of 5 mm. Although these N factors would still be generally considered too low to cause transition, stationary crossflow is highly susceptible to nonlinear secondary instabilities which would not be captured by linear analysis techniques. Furthermore, the backward-facing steps could interact with these disturbances. It is not immediately clear what impact the presence of such a surface discontinuity may have on the developing boundary-layer disturbances, though prior work by Balakumar et al. and Hildebrand et al. suggest it may have a destabilizing effect.

Note that traveling oblique disturbances have been excluded for this condition due to the lack of amplification identified by this analysis. The only such disturbances found to be unstable in this analysis were at frequencies below 2 kHz and had lower amplifications than the stationary crossflow disturbances along the same streamlines.

The streamline with the greatest amplification of stationary crossflow was extracted for further analysis using PSE, and the resulting comparison between LST and PSE N factors is given in Figure 42. The PSE computations predict the neutral stability point for this disturbance to lie slightly upstream of its location in the LST analysis, and the disturbance undergoes far greater amplification over the length of the body, reaching an N factor of approximately 4 by 650 mm, where transition was observed in flight. The non-parallel effects included in the PSE methodology are thus shown to be of significant importance for the accurate assessment of disturbance amplification. This is a shortcoming for the remainder of the results presented herein, which are based entirely on LST. A full analysis of this flowfield with LPSE is recommended for future exploration.

Maximum LST N factors for conditions 2A-C are presented in Figure 43 over the vehicle surface. Although stationary crossflow still appears as a strongly amplified disturbance, we now observe significant amplification for 2-D disturbances and traveling oblique disturbances. These disturbances all appear within the same region near the vehicle centerline. For all conditions, the growth of traveling oblique disturbances exceeds that of the stationary crossflow. The maximum N factor reached increases from approximately 5.7 at condition 2A to 10 at condition 2C. The 2-D disturbances reach similar N factors, but appear only along a few streamlines. This highly-localized behavior may be indicative of errors in the LASTRAC computations. These N factors represent a substantial increase over Condition 1, but are still somewhat low for transition in flight. However, the coexistence of several instability modes enhances the potential for nonlinear transition mecha-

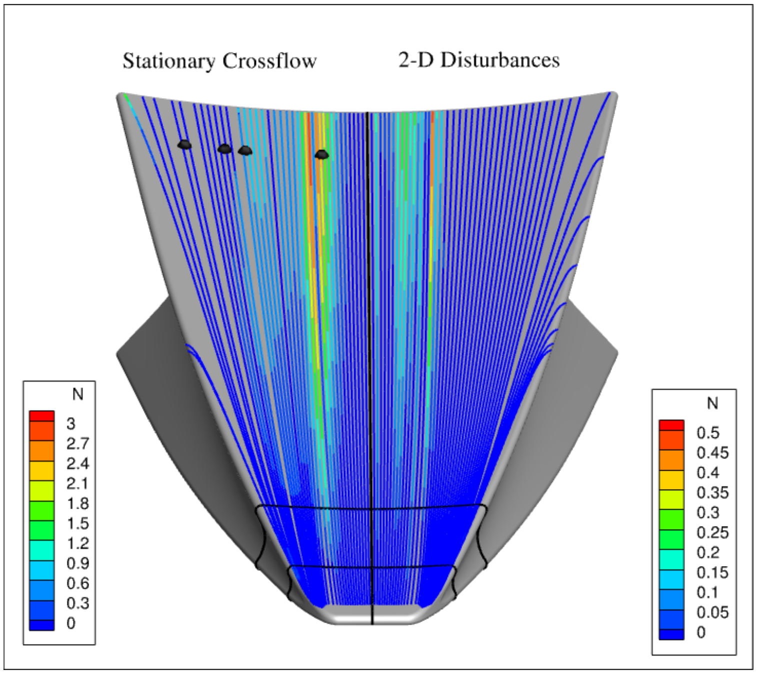

Figure 41. Maximum 2-D and stationary crossflow N factors for Condition 1 on Grid D.

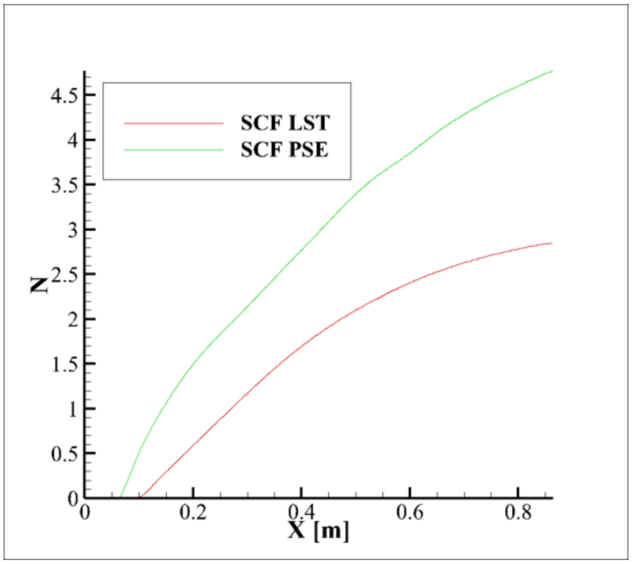

Figure 42. A comparison between LST and PSE N factors for stationary crossflow at Condition 1.

nisms to accelerate breakdown.

In order to better characterize the unsteady disturbances, two streamlines (shown in Figure 44a) were extracted which display significant growth of oblique disturbances across all conditions. N factor envelopes along these streamlines for various frequencies and spanwise wavelengths are presented in figures 44b-e. At condition 2A, streamline 1 (Figure 44b) shows the greatest amplification for 8.5 kHz disturbances with a spanwise wavelength of 7.5 mm from $X = 0.07 - 0.6$ m. At $X = 0.3$ m, a band of high-frequency disturbances begins to develop, with a peak frequency of 60 kHz. We see that growth over this frequency band is maximized for 2-D disturbances. Streamline 1 displays this same behavior at conditions 2B and 2C (not pictured), whereby upstream growth is concentrated within low-frequency oblique disturbances with high-frequency, 2-D disturbances developing further downstream.

N-factor envelopes for conditions 2A-C are presented along streamline 2 in figures 44c-e. It is along this streamline that the highest N factors are observed. All streamlines show similar behavior, where the greatest amplification is attained by low-frequency disturbances from $2.5 - 8.5$ kHz and spanwise wavelengths of $3 - 5$ mm.

5.5. Summary and Recommended Future Work

While the BOLT experiment did not reach its intended Mach 5–7 conditions in flight, the experiment did gather potentially useful boundary-layer transition measurements at supersonic conditions (Mach ≈ 2.7). This section has presented a characterization of the vehicle attitude solution for the as-flown trajectory, allowing for the identification of time periods during which the vehicle orientation was well-characterized and thus conducive to meaningful scientific analysis. It was quickly determined that the high angle of attack ($> 15°$) sustained throughout ascent precluded the study of transition physics and the focus for this effort was placed on the descent phase. Unfortunately, reentry to the atmosphere occurred several minutes sooner than anticipated due to the much lower apogee, resulting in only one of the three scientific data telemetry streams being active during the descent phase and a severely limited post-flight data set on the order of 90 channels. This data primarily consisted of thermocouples which could be used to compute surface heat flux, but also included a small number of surface pressure transducers and was concentrated almost entirely on the primary experimental surface of the vehicle.

Despite this limited data set, synthesis of the attitude solution and flight data resulted in the identification of two distinct periods of flight where transition could be observed on the primary surface with the vehicle in a reasonable orientation. The first of these occurred at a $Re_L \approx 5.5 \times 10^6$ when the vehicle was at an angle of attack of $5 - 8°$ with the primary surface windward. Although it could not be concluded from the flight data whether transition initiated along the centerline or slightly off-centerline, the transition front was seen to spread outboard with increasing Re_L. The second period of interest spanned $Re_L = 8 - 17.5 \times 10^6$ where the angle of attack remained below $4°$ but the primary surface remained leeward to the flow. During this portion of flight transition was clearly observed to originate away from the centerline.

Laminar and turbulent CFD computations were performed at the identified flight conditions of interest to characterize the flow topology at the flown Mach numbers and allow for direct compar-

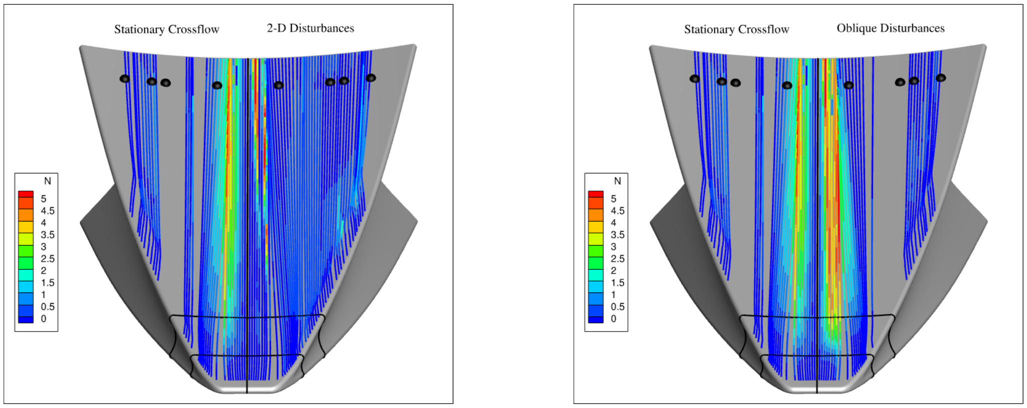

(a) SCF and 2-D N factors at Condition 2A. (b) SCF and oblique N factors at Condition 2A.

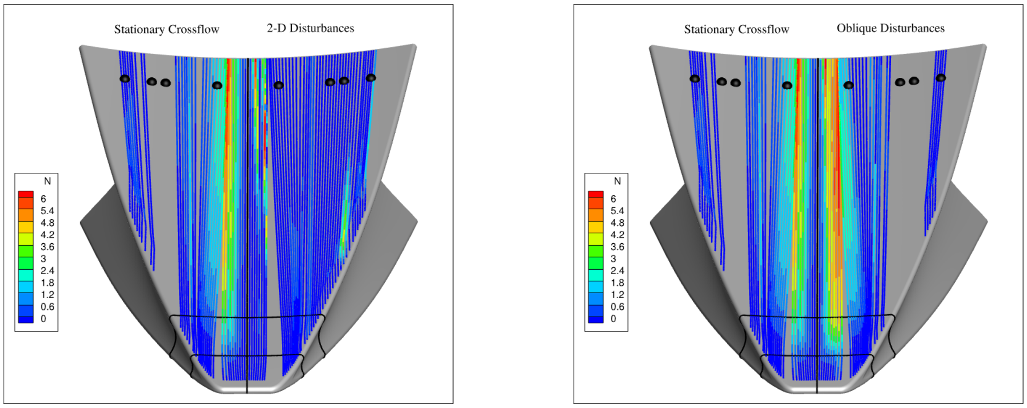

(c) SCF and 2-D N factors at Condition 2B. (d) SCF and oblique N factors at Condition 2B.

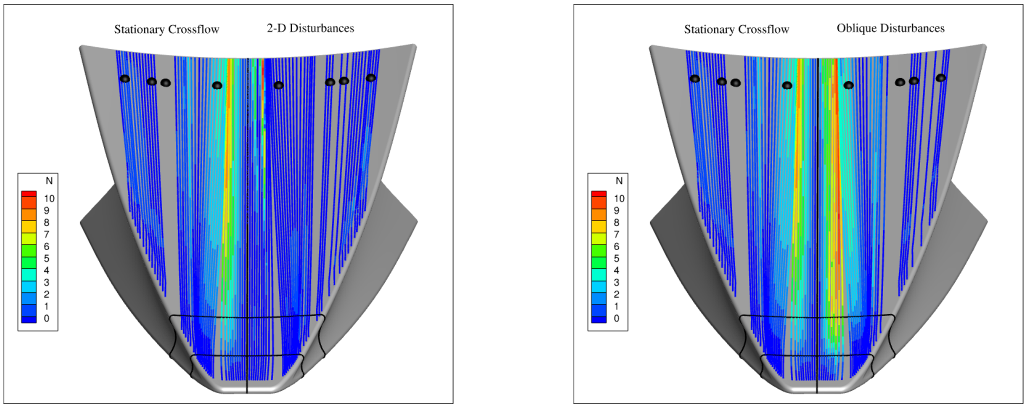

(e) SCF and 2-D N factors at Condition 2C. (f) SCF and oblique N factors at Condition 2C.

Figure 43. Maximum N factors for LST computations at Conditions 2A-C.

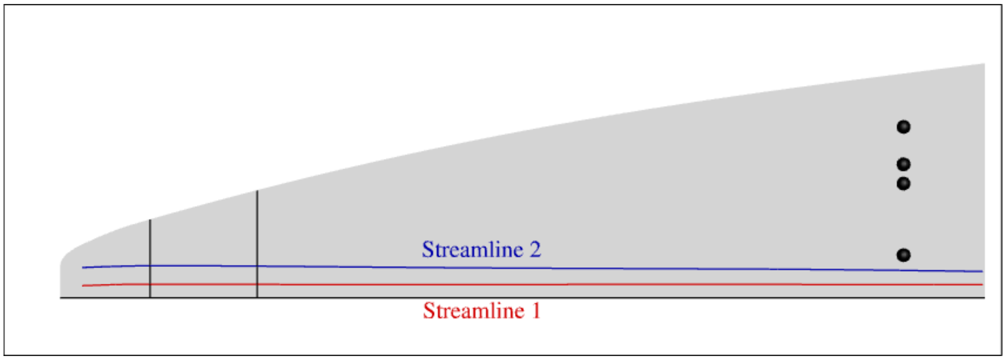

(a) Streamlines considered for further analysis.

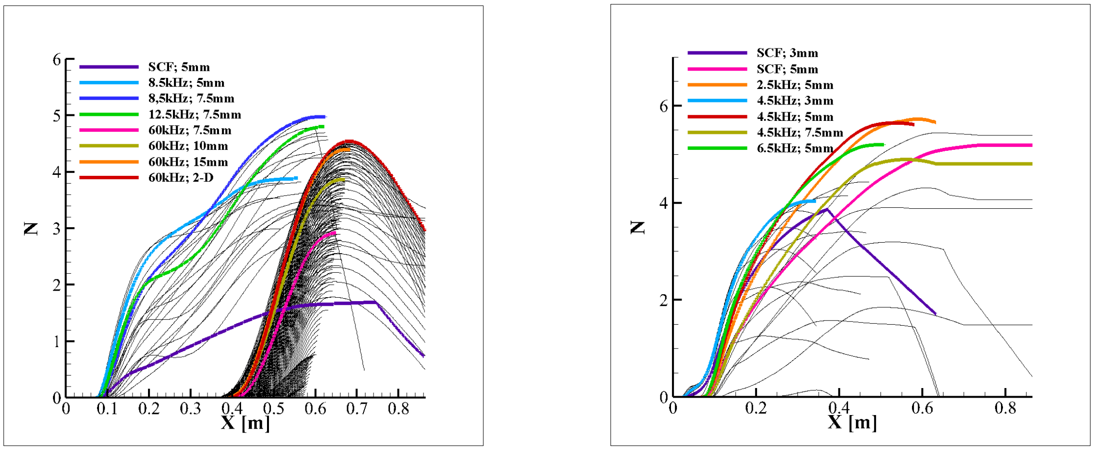

(b) Condition 2A; streamline 1.

(c) Condition 2A; streamline 2.

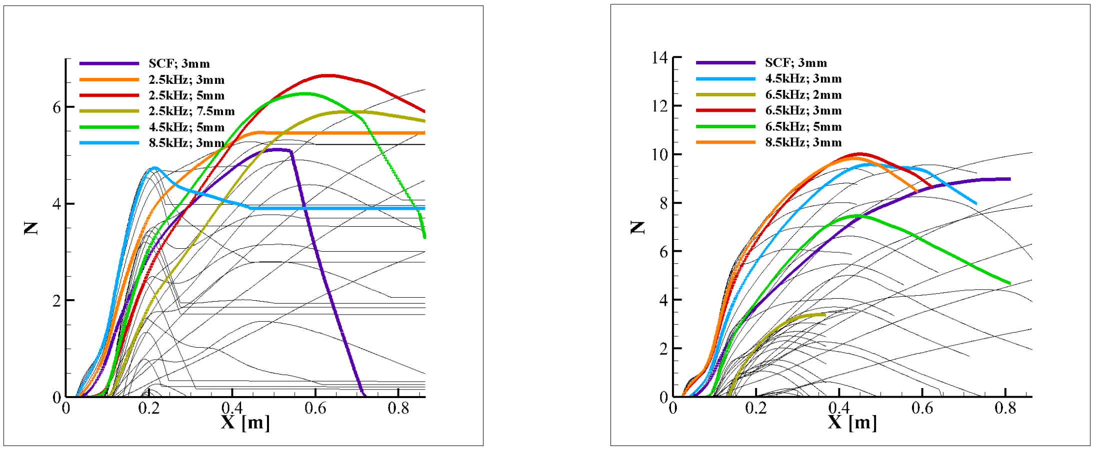

(d) Condition 2B; streamline 2.

(e) Condition 2C; streamline 2.

Figure 44. LST N-factor envelopes for select streamlines.

isons against the flight data. At the earliest studied flight condition, the high angle of attack and low Mach number combined to substantially reduce the spanwise pressure gradient and centerline vortex roll-up relative to pre-flight predictions for hypersonic conditions. Later in flight, with the primary surface leeward and Re_L increased, multiple heating streaks were seen forming over the vehicle acreage. In general, good agreement was achieved between both laminar and turbulent CFD predictions and the flight data along the centerline and several spanwise slices.

Initial stability analyses were carried out with LASTRAC, primarily leveraging LST, to identify potential instability mechanisms at the flight transition conditions. These assessments identified substantial growth of stationary crossflow off-centerline across all flight conditions. At low angles of attack, 2-D and traveling oblique disturbances were identified which experienced greater amplification than stationary crossflow. All disturbances were shown to develop slightly off-centerline, correlating well with the location of flight instrumentation which first identified transition. That said, the transition N factors were found to be somewhat low. The influence of rear-facing joint steps that were likely present in the actual flight should be considered as a contributor to the observed transition behavior, and offer a potential explanation for the low transition N-factors calculated with LASTRAC.

Future work regarding this flight data should seek to expand upon the preliminary stability analyses presented herein. Specifically, the impact of the wall temperature and joint steps should be assessed, particularly as it pertains to the development of crossflow disturbances. The analysis could also be improved by leveraging PSE and application of higher-fidelity stability analysis techniques such as BiGlobal analysis which may resolve instability mechanisms not captured in the present study. Furthermore, the development of multiple instability mechanisms within the same region of the vehicle suggests that proper transition prediction may require methodologies which allow for nonlinear energy exchange between disturbances.

6. BOLT-2 Support

Following the BOLT investigation summarized in Sections 2 through 4, APL assisted AFOSR and NASA Wallops in incorporating lessons learned to evaluate the BOLT-2 preflight work and ensure that the planned experiment was robust to the instability modes observed in the BOLT flight.

6.1. 6DOF Monte Carlo Stressors Based on BOLT Investigation

The BOLT investigation concluded in November 2021, leaving only four months between the conclusion of the investigation and the expected launch of the BOLT-2 experiment. Following the BOLT investigation, APL worked with NASA Wallops to evaluate the Wallops TAOS trajectory modeling for BOLT-2 and provide an independent analysis of the 6DOF modeling to ensure that terms found to be important to the BOLT pitch roll coupling behavior were incorporated adequately into the BOLT-2 modeling.

APL obtained the BOLT-2 TAOS model from NASA Wallops in late January 2022 as well as a description of the modeled Monte Carlo parameters in the simulation. Due to the unknown sensitivity of the models, results are not plotted here but were provided separately to NASA and AFOSR. On initial receipt of the TAOS model, APL noted that the Wallops modeling did not include a blanket uncertainty on center of pressure. APL typically recommends a 5% body length uncertainty on center of pressure. APL performed independent simulations of the BOLT-2 trajectory with Monte Carlo parameters that included a 5% and 10% (unrealistic but stressing) body length center of pressure uncertainty. In addition, knowing from the BOLT investigation that the moment bias terms provide the initial seeding for angle of attack amplification, APL performed additional simulations with a 3X multiplier on the Wallops tailcan misalignment term (the term responsible for providing these moment biases).

The results showed that the BOLT-2 vehicle was much more robust to these terms due to the selection of a low roll rate that avoided pitch-roll crossings at high dynamic pressures. APL presented the results to Wallops in January 2022. The analysis was deemed a complete check of the phenomena from the BOLT investigation and satisfied the Wallops team that the preflight analysis did not miss any unexpected behavior. BOLT-2 had a successful launch in late March 2022.

6.2. Postflight Investigation of Drag Modeling

The BOLT-2 vehicle preliminary trajectory indicates a greater than anticipated velocity was achieved, as well as a greater than anticipated downrange distance. APL had noted in Year 1 of this project a potential drag estimate discrepancy, which potentially could explain the over-performance of the flight. APL is currently working with NASA Wallops to investigate and quantify the contributions of anticipated drag disagreements on the trajectory, which could better inform drag prediction and buildup for future sounding rocket flights with complex geometries.

6.3. Future Work

APL is working on a postflight analysis of the BOLT-2 transition data in cooperation with CUBRC and Texas A&M. APL has applied its postflight tools developed originally for the BOLT experiment (Section 5) on the BOLT-2 instrumentation. The results have been shared with the rest of the science team.

APL is working on computational meshing for a postflight simulation of BOLT-2 utilizing spatial biglobal and planar marching parabolized stability equations. APL has submitted an abstract to AIAA SciTech 2023 for the BOLT-2 special session to present the analysis.

APL is also working on a postflight thermal analysis of the BOLT-2 flight experiment as part of a second abstract for AIAA SciTech 2023. Because APL performed the preflight thermal analysis for BOLT-2, a postflight run can assess the conservatism inherent in the modeling and inform modeling of temperatures for future flights. The postflight thermal analysis has involved a RANS based database of laminar and turbulent CFD simulations that have been completed. A preliminary thermal run has compared the temperatures from ascent to an all-turbulent transient thermal analysis and indicates significant conservatism in RANS heat transfer predictions based on the flight data. Future work will attempt to model the flight with transitional flow. In addition, the analysis will produce best estimated wall temperature distributions that can be used by other researchers who wish to simulate the BOLT-2 flight boundary conditions. Finally, the analysis will also produce time histories of laminar and turbulent heat flux at all the sensor locations for comparison against the computed heat flux from the sensors. The heat flux histories will be shared with the Texas A&M researchers who are analyzing the flight data.

Acknowledgments

This work was supported by the Air Force Office of Scientific Research under award number FA9550-20-1-0043 (PO: Dr. Sarah Popkin). Any opinions, finding, and conclusions or recommendations expressed in this material are those of the author(s) and do not necessarily reflect the views of the United States Air Force. This work was supported in part by high-performance computer time and resources from the Department of Defense (DoD) High Performance Computing Modernization Program.

References

[1] Wheaton, B. M., Butler, C. S., McKiernan, G. R., and Berridge, D. C., "Initial Results from the BOLT Flight Experiment," *AIAA Paper 2022-0345*, 2022. doi:10.2514/6.2022-0345, URL `https://arc.aiaa.org/doi/10.2514/6.2022-0345`.

[2] Butler, C. S., Araya, D. B., McKiernan, G. R., and Wheaton, B. M., "Supersonic Transition Measurements During the BOLT Flight Experiment Descent Phase," *AIAA Paper 2022-4099*, 2022. doi:10.2514/6.2022-4099, URL `https://arc.aiaa.org/doi/10.2514/6.2022-4099`.

[3] Kutty, P. M., Butler, C. S., Wheaton, B. M., and Fortier, J. B., "6DOF Simulation Analysis for the Post-Flight Investigation of the Boundary Layer Transition (BOLT) Experiment," *AIAA Paper 2022-3884*, 2022. doi:10.2514/6.2022-3884, URL `https://arc.aiaa.org/doi/abs/10.2514/6.2022-3884`.

[4] Melcher, J. T., Radcliffe, E. J., Butler, C. S., and Wheaton, B. M., "Effects of Aeroelasticity on Flight Stability of the Boundary Layer Transition (BOLT) Experiment," *AIAA Paper 2022-3748*, 2022. doi:10.2514/6.2022-3748, URL `https://arc.aiaa.org/doi/10.2514/6.2022-3748`.

[5] Hodapp, A. E., "Effects of Unsymmetrical Stability Derivative Characteristics on Re-Entry Vehicle Trim Angle Behavior," *Journal of Spacecraft and Rockets*, Vol. 11, No. 5, 1974, pp. 300–307. doi:10.2514/3.62067, URL `https://arc.aiaa.org/doi/10.2514/3.62067`.

[6] Hodapp, A. E., "Effects of unsymmetrical stability derivative characteristics on re-entry vehicle transient angular motion," *Journal of Spacecraft and Rockets*, Vol. 13, No. 2, 1976, pp. 82–90. doi:10.2514/3.27887, URL `https://arc.aiaa.org/doi/10.2514/3.27887`.

[7] Platus, D. H., "Aeroelastic stability of slender, spinning missiles," *Journal of Guidance, Control, and Dynamics*, Vol. 15, No. 1, 1992, pp. 144–151. doi:10.2514/3.20812.

[8] Kimmel, R. L., Adamczak, D., Hartley, D., Alesi, H., Frost, M. A., Pietsch, R., Shannon, J. ., and Silvester, T., "HIFiRE-5b Flight Overview," *AIAA Paper 2017-3131*, 2017. doi:10.2514/6.2017-3131, URL `https://arc.aiaa.org/doi/10.2514/6.2017-3131`.

[9] Wheaton, B. M., Berridge, D. C., Wolf, T. D., Araya, D. B., Stevens, R. T., McGrath, B. E., Kemp, B. L., and Adamczak, D. W., "Final Design of the Boundary Layer Transition (BOLT) Flight Experiment," *Journal of Spacecraft and Rockets*, Vol. 58, No. 1,

2021, pp. 6–17. doi:10.2514/1.A34809, URL `https://doi.org/10.2514/1.A34809`.

[10] Meirovitch, L., and Nelson, H. D., "On the high-spin motion of a satellite containing elastic parts," *Journal of Spacecraft and Rockets*, Vol. 3, No. 11, 1966, pp. 1597–1602. doi:10.2514/3.28713.

[11] Li, H., and Ye, Z. Y., "Numerical investigation on aerodynamic and inertial couplings of flexible spinning missile with large slenderness ratio," *Aerospace Science and Technology*, Vol. 99, 2020, p. 105582. doi:10.1016/j.ast.2019.105582, URL `https://doi.org/10.1016/j.ast.2019.105582`.

[12] Hörschgen-Eggers, M., Kirchhartz, R. M., Jung, W., Schoppmann, K., Ettl, J., and Wittkamp, M., "Boundary Layer Transit Flight Experiment: Mission Overview, Launch Vehicle and Payload Subsystems," *Journal of Spacecraft and Rockets*, Vol. 58, No. 1, 2021, pp. 26–37. doi:10.2514/1.A34877, URL `https://arc.aiaa.org/doi/10.2514/1.A34877`.

[13] Jewell, J. S., Kimmel, R. L., Adamczak, D. W., Poggie, J., Porter, K. M., and Juliano, T. J., "HIFiRE-5b Flow Computations and Attitude Determination via Comparison with Flight Data," *Journal of Spacecraft and Rockets*, Vol. 55, No. 6, 2018, pp. 1356–1368. doi:10.2514/1.A34162, URL `https://arc.aiaa.org/doi/10.2514/1.A34162`.

[14] Juliano, T. J., Adamczak, D., and Kimmel, R. L., "HIFiRE-5 Flight Test Heating Analysis," *AIAA Paper 2014-0076*, 2014. doi:10.2514/1.A33142, URL `http://arc.aiaa.org/doi/10.2514/1.A33142`.

[15] Juliano, T. J., Poggie, J., Porter, K. M., Kimmel, R. L., Jewell, J. S., and Adamczak, D. W., "HIFiRE-5b Heat Flux and Boundary-Layer Transition," *AIAA Paper 2017-3134*, 2017. doi:10.2514/6.2017-3134, URL `https://arc.aiaa.org/doi/pdfplus/10.2514/6.2017-3134`.

[16] Boyd, C. F., and Howell, A., "Numerical Investigation of One-Dimensional Heat-Flux Calculations," *Dahlgren Division Naval Surface Warfare Center, TR NSWCDD/TR-94/114*, 1994. URL `https://apps.dtic.mil/sti/citations/ADA286293`.

[17] Berry, S. A., Wheaton, B. M., and Chynoweth, B. C., "Secondary Side Considerations for Boundary Layer Transition Flight Experiment," *Journal of Spacecraft and Rockets*, Vol. 58, No. 1, 2021, pp. 18–25. doi:10.2514/1.A34778, URL `https://doi.org/10.2514/1.A34778`.

[18] Kostak, H. E., and Bowersox, R. D. W., "Preflight Ground Test Analyses of the Boundary Layer Transition (BOLT) Flight Geometry," *Journal of Spacecraft and Rockets*, Vol. 58, No. 1, 2021, pp. 67–77. doi:10.2514/1.A34858, URL `https://doi.org/10.2514/1.A34858`.

[19] Li, F., Choudhari, M. M., and Paredes, P., "Streak Instability Analysis on BOLT Configuration," *AIAA Paper 2020-3028*, American Institute of Aeronautics and Astronautics (AIAA), 2020. doi:10.2514/6.2020-3028, URL `http://arc.aiaa.org`.

A. Investigation Fault Tree

The next page presents the final fault tree developed by DLR, APL, and AFRL ahead of the post flight review meeting held in November 2021.

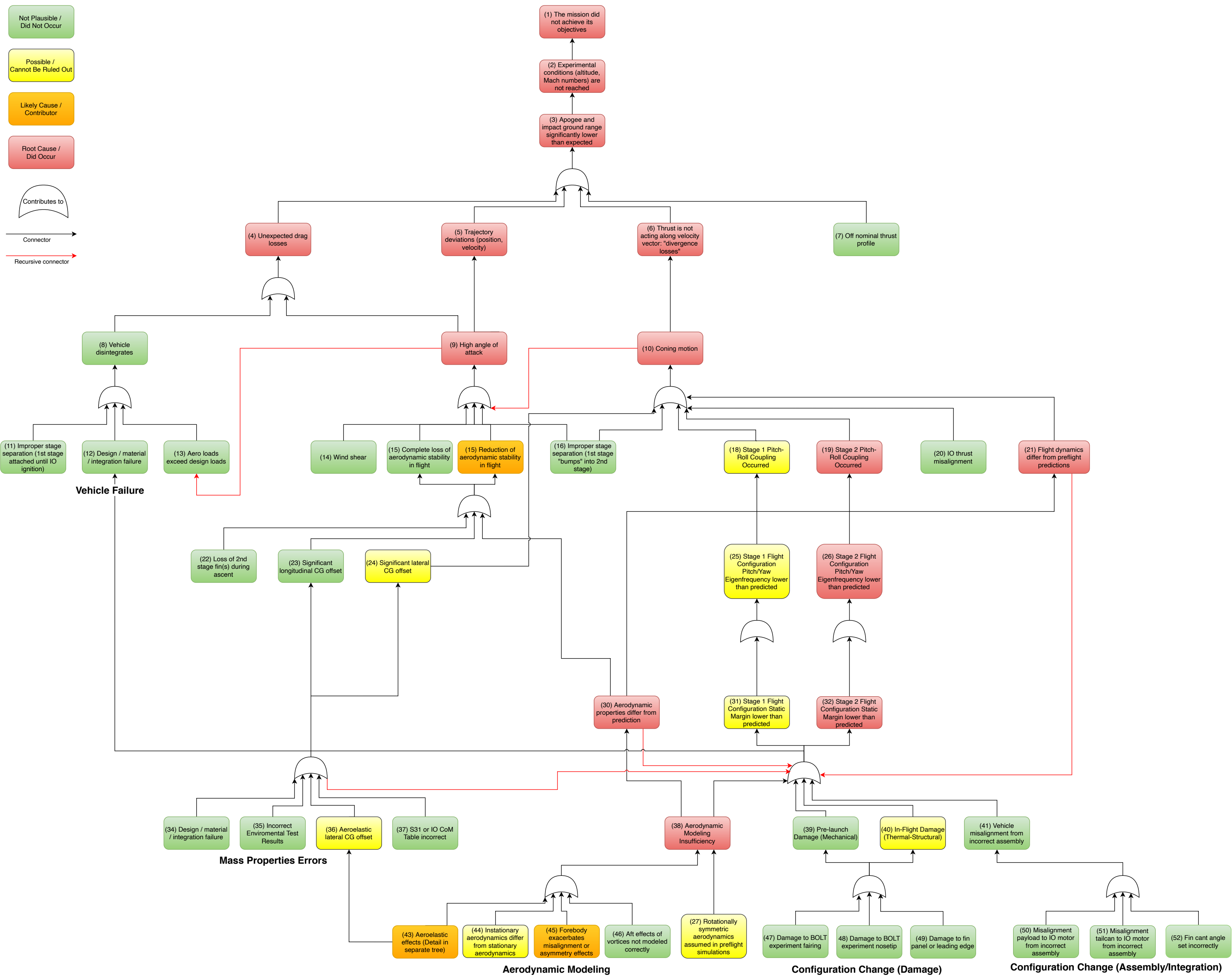

DISTRIBUTION A: Distribution approved for public release.

B. Rigid Body Aerodynamics Check on BOLT 2nd Stage

The following slides document the APL independent confirmation of the BOLT second stage static margin using rigid body estimates. This analysis was important to confirm that the BOLT preflight aerodynamics were predicted correctly when using a rigid body assumption.

JOHNS HOPKINS
APPLIED PHYSICS LABORATORY

11100 Johns Hopkins Road
Laurel, MD 20723-6099

BOLT Second Stage Aerodynamic Assessment

Cameron Butler

This work was supported by the Air Force Office of Scientific Research under award number FA9550-20-1-0043 (PO: Dr. Sarah Popkin). Any opinions, finding, and conclusions or recommendations expressed in this material are those of the author(s) and do not necessarily reflect the views of the United States Air Force.

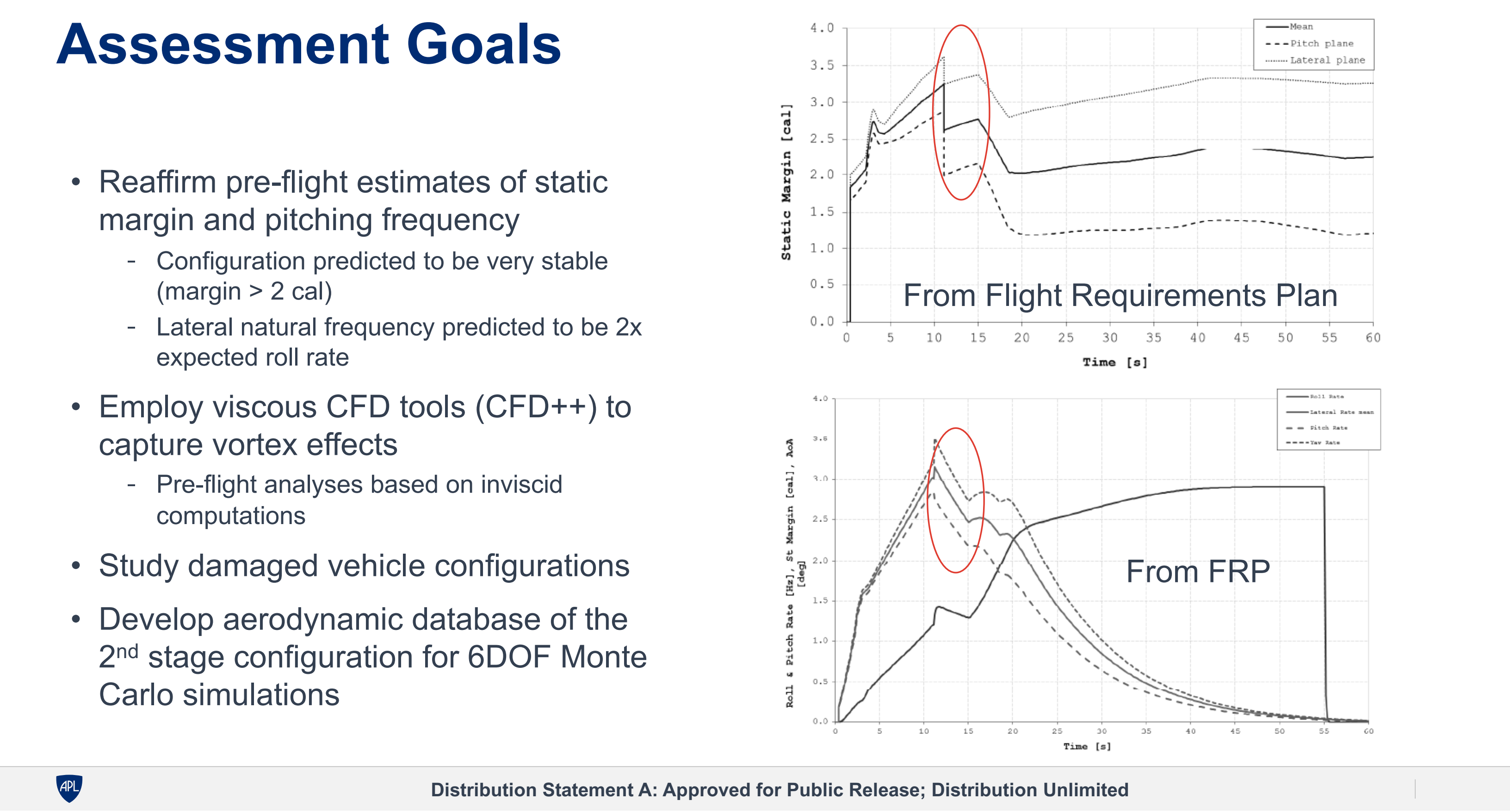

Assessment Goals

- Reaffirm pre-flight estimates of static margin and pitching frequency
  - Configuration predicted to be very stable (margin > 2 cal)
  - Lateral natural frequency predicted to be 2x expected roll rate
- Employ viscous CFD tools (CFD++) to capture vortex effects
  - Pre-flight analyses based on inviscid computations
- Study damaged vehicle configurations
- Develop aerodynamic database of the 2nd stage configuration for 6DOF Monte Carlo simulations

From Flight Requirements Plan

From FRP

Distribution Statement A: Approved for Public Release; Distribution Unlimited

CFD++ Simulation Details

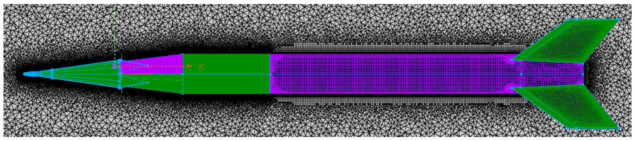

- Emphasis placed on small turnaround time for gridding
  - Initial height = 0.005" (0.13mm)
  - No camera pods
- Focus on separation condition (see table)
- Sweep in α_T and φ (see diagram)
- Can get margin and frequency from aerodynamics

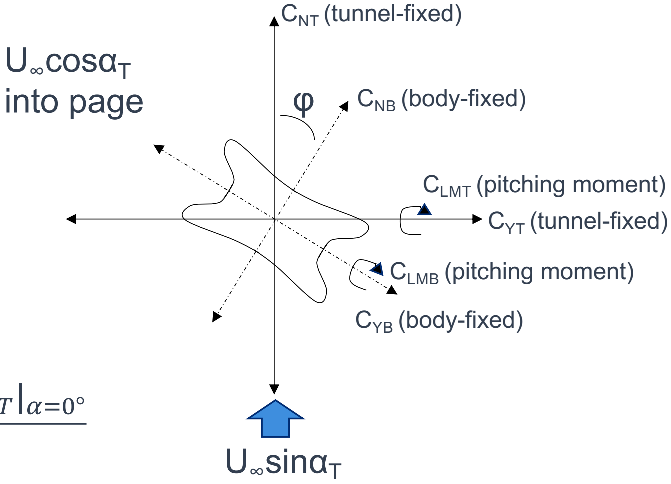

C_{NT} (tunnel-fixed)

$U_\infty \cos\alpha_T$ into page

φ

C_{NB} (body-fixed)

C_{LMT} (pitching moment)

C_{YT} (tunnel-fixed)

C_{LMB} (pitching moment)

C_{YB} (body-fixed)

$U_\infty \sin\alpha_T$

$$Static\ Margin\ (cal) = \frac{X_{CP} - X_{CG}}{L_{ref}} \qquad X_{CP} \approx \frac{C_{LMT}}{C_{NT}}$$

$$\omega_{lat} = \sqrt{{.5\rho_\infty U_\infty^2 A_{ref} C_{m\alpha T}}\Big/{I_{lat}}} \qquad C_{m\alpha T} \approx \frac{C_{LMT}|_{\alpha=2°} - C_{LMT}|_{\alpha=0°}}{2 * {\pi}/{180}}$$

M_∞	P_∞ [kPa]	T_∞ [K]	U_∞ [m/s]	L_{ref} [m]	S_{ref} [m²]	Xcg [m]	I_{lat} [kg/m²]	I_{pol} [kg/m²]
2.8	47.2	249.2	886.3	0.356	0.0995	2.898	976	12.8

Sample Results

- Apparent vortices captured at fairing
- Small relative to fins
- Configurations representative of potential structural failures also considered

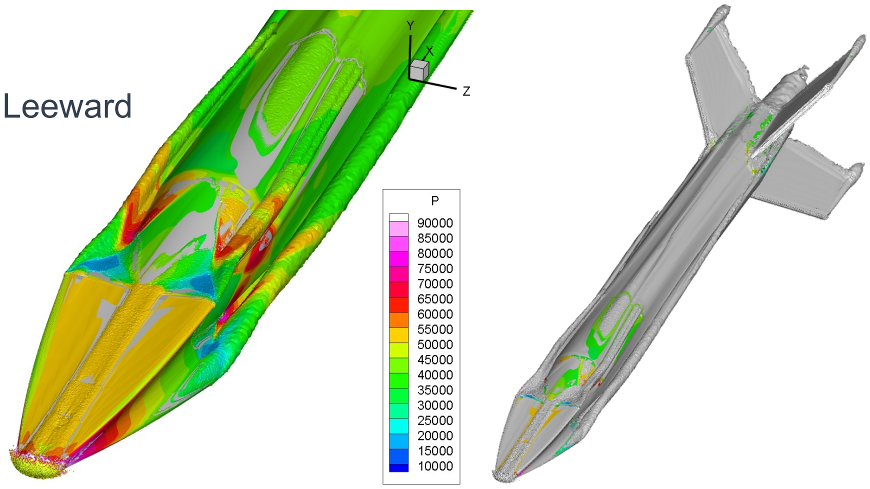

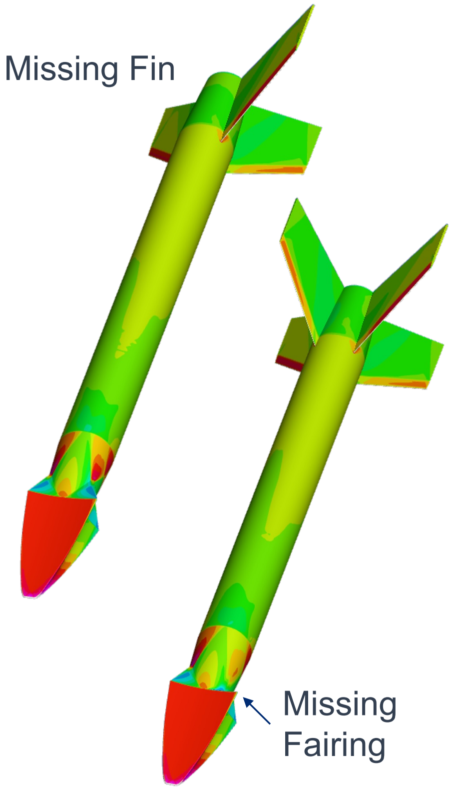

Aerodynamic Stability Metrics ($\alpha_T = 2°$)

- Baseline results show good agreement with preflight estimates at the separation condition (M = 2.8, 6km altitude)
- Missing fairing has minimal impact on vehicle aerodynamics
- Missing fin causes dramatic reduction in static margin
  - Particularly at φ=40°; 210°
- Missing fin causes oscillation in pitching frequency which brackets 1.5Hz

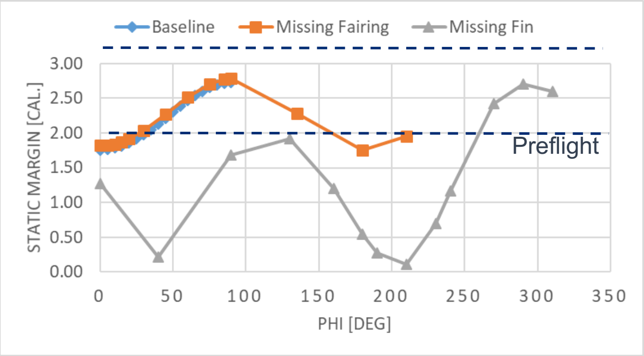

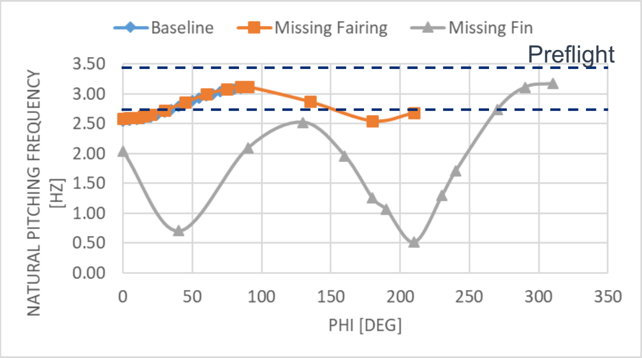

US3D Comparison

- US3D simulations performed by Candler
  - Substantial increase in boundary-layer resolution
  - Inclusion of camera pods and fin supports
  - Better captures shed vortices
- Minimal discrepancy in aerodynamic coefficients from baseline CFD++

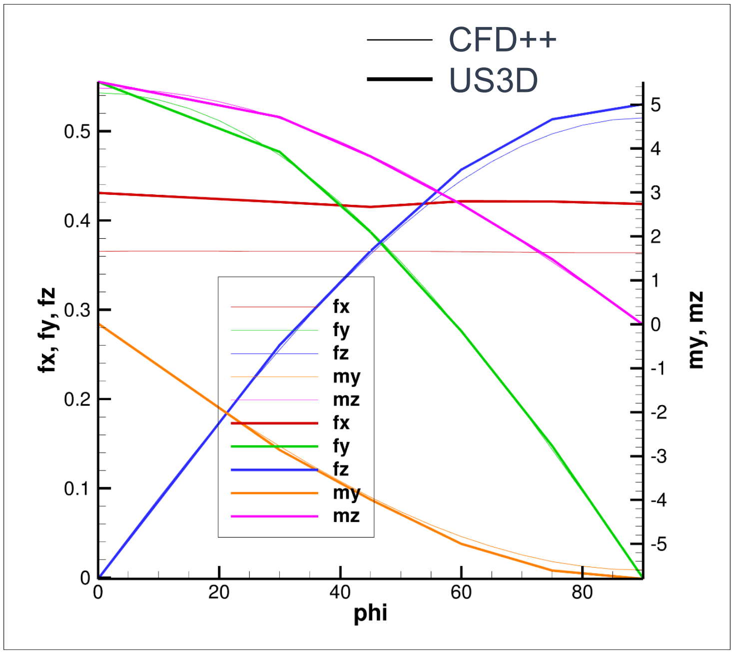

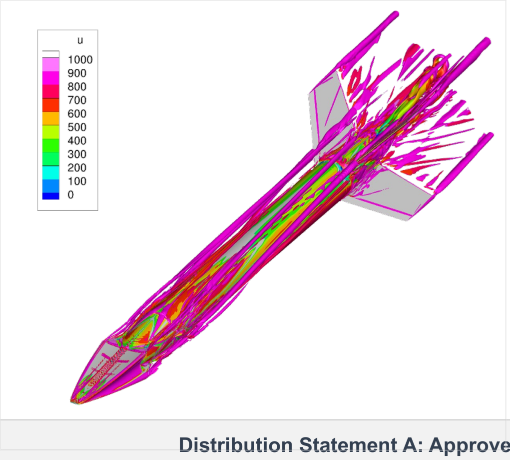

Rolling Effects ($\alpha_T = 2°$)

- CFD++ simulation with vehicle rolling at 1.67Hz about body axis
- Rolling induces small yaw moment about CG
  - Due to slight differences in fin loading and vortex extent

	Cm	Cn
Fixed	-0.95	0.003
Rolling	-1.01	-0.017

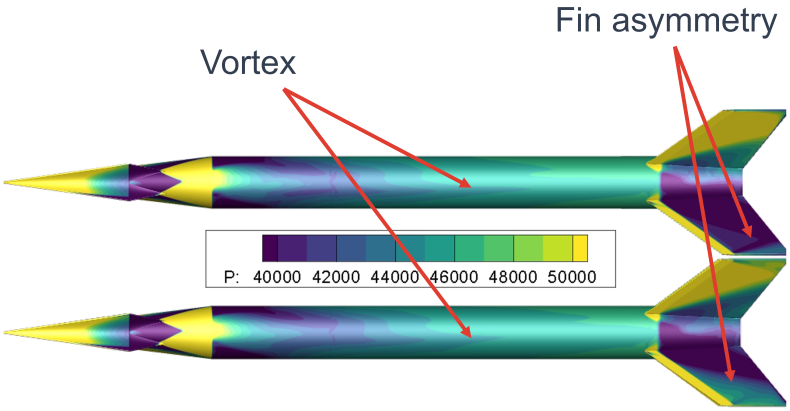

Summary

- Independent viscous CFD confirms pre-flight predictions of 2nd stage configuration at separation conditions:
  - Static margin
  - Natural pitch frequency
- Single missing fairing appears to have minimal impact on vehicle aerodynamics
- Missing fin from 2nd stage would reduce static margin and natural pitch frequency substantially
- Magnus effects on aerodynamics appear minimal and should be appropriately captured in Monte Carlo dispersions

JOHNS HOPKINS
APPLIED PHYSICS LABORATORY

FA9550-20-1-0043 Final Report
10 March 2023
APL Project FGX75

To: Dr. Doug Smith
Acting Program Officer - High Speed Aerodynamics
AFOSR/RTA
875 N. Randolph St., Suite 325, Room 3112
Arlington, VA 22203-1768

From: Dr. Bradley M. Wheaton (Principal Investigator)
Dr. Daniel B. Araya (Co-Investigator)
Dr. Dennis C. Berridge (Co-Investigator)
Dr. Cameron S. Butler
Dr. Gregory R. McKiernan
Mr. Prasad M. Kutty
Mr. Jim B. Fortier
Dr. John T. Melcher
Mr. Eliott J. Radcliffe
Mr. David M. Gers
Mr. Ryan L. Eby
Mr. Thomas D. Wolf
Ms. Deana M. Prosniewski (Financial Manager)
Mr. Rubbel Kumar (Program Manager)

Subject: Final Performance Report for Boundary Layer Transition (BOLT) Post-Flight Research and BOLT II Flight Test Support (Grant FA9550-20-1-0043, period 11 March 2020 through 10 March 2023)

Cover Page Data

- **Federal Agency and Organization Element to Which the Report is Submitted:**
  Air Force Research Laboratory Air Force Office of Scientific Research (AFRL/AFOSR)
- **Federal Grant or Other Identifying Number Assigned by Agency:**
  FA9550-20-1-0043
- **Project Title:**
  Boundary Layer Transition (BOLT) Post-Flight Research and BOLT II Flight Test Support
- **Project Director/Principal Investigator (PD/PI):**
  Dr. Bradley M. Wheaton
  Senior Professional Staff
  Bradley.Wheaton@jhuapl.edu
  +1 240-228-6470
- **Co-Investigator:**
  Dr. Daniel B. Araya
  Senior Professional Staff
  Daniel.Araya@jhuapl.edu
  +1 240-592-2302
- **Co-Investigator:**
  Dr. Dennis C. Berridge
  Senior Professional Staff
  Dennis.Berridge@jhuapl.edu
  +1 240-228-4399
- **Submission Date:**
  10 March 2023
- **Recipient Organization (Name and Address):**
  Johns Hopkins Applied Physics Laboratory
  11100 Johns Hopkins Rd., Laurel, MD 20723
- **Project/Grant Period (Start Date, End Date):**
  11 March 2020 to 10 March 2023
- **Total Funding:**
  $825,000
- **Reporting Period End Date:**
  10 March 2023
- **Report Term or Frequency (annual, semi-annual, quarterly, other)**
  Annual
- **Final Report?**
  Yes

Abstract

This report summarizes the three-year research effort by the Johns Hopkins University Applied Physics Laboratory (APL) under grant number FA9550-20-1-0043 from the Air Force Office of Scientific Research (AFOSR) to conduct postflight analysis of the BOLT flight experiment and to support the development, execution, and analysis of data from BOLT-2: The Holden Mission. Key accomplishments from this research included characterization of supersonic transition flight data received from the BOLT experiment, investigation and identification of the probably cause of unexpected flight behavior that occurred in the BOLT flight, significant independent analysis of the BOLT-2 flight during the pre- and postflight research phases, and new Spatial BiGlobal stability calculations of the BOLT geometry in support of the BOLT-2 flight analysis and a NATO STO-AVT-346 working group activities. The research resulted in seven conference papers with an eighth paper planned. The research led to advances in understanding of supersonic transition, flight dynamics, aeroelastic effects on aerodynamics, thermal analysis methodology for low-cost sounding rocket experiments, and advancements in the use of Spatial BiGlobal stability on the BOLT geometry. APL plans to continue research on many of these topics in a new grant from AFOSR, FA9550-22-1-0357, that will also support a re-flight attempt of the BOLT experiment called BOLT-1B.

Contents

1 Introduction and Research Objectives 5

2 Accomplishments 7

2.1 BOLT Postflight Analysis of Experiment Conditions and Supersonic Transition Data 7
2.2 BOLT Postflight Analysis of Flight Dynamics 8
2.3 BOLT-2 Knowledge Transfer and Advisory Activities 10
2.4 BOLT-2 Independent Analysis 11
  2.4.1 Preflight Aerodynamics Analysis 12
  2.4.2 Preflight Thermal/Structural Analysis 13
  2.4.3 Preflight Trajectory Analysis and Application of BOLT-1 Lessons Learned 15
  2.4.4 BOLT-2 Postflight Data Analysis 17
2.5 BiGlobal Stability Analysis of BOLT and BOLT-2 19
2.6 NATO AVT-346 Working Group Support 20
2.7 Conference Paper and Publications 21

3 Impacts 21

4 Changes/Problems 23

1. Introduction and Research Objectives

Prediction of hypersonic boundary-layer physics is critical to optimize the design of hypersonic vehicles for maximum range, thermal survivability, and controllability. Physics-based prediction methods are under development that have the potential to improve the ability of hypersonic vehicle designers to estimate transition and turbulent flow effects. These methods require extensive validation with ground and flight test data that is often not available for the geometry of interest. To date, much of the available validation data are on simple conical geometries.

The Johns Hopkins University Applied Physics Laboratory (APL) proposed this Boundary Layer Transition (BOLT) Post-Flight Research and BOLT-2 Flight Test Support to assist the Air Force Office of Scientific Research (AFOSR) and university researchers in obtaining and analyzing critical hypersonic boundary layer physics validation data in the flight environment. The research was conducted within a three-year project period with a total funding of $825K ($275K/year). Previous technical contributions have been summarized in detail in the grant annual performance reports from Years 1 and 2 [1, 2].

The primary objective of this research was to continue to utilize the BOLT (also called BOLT-1 in this report) boundary-layer transition flight test data that was to be obtained in a previous grant (AFOSR Award Number FA9550-17-2-0001) to discover and document the salient physics of the laminar-to-turbulent transition process observed during the flight experiment, as well as to disseminate the findings and test data at the direction of the AFOSR to other investigators within the AFOSR portfolio. Although the BOLT experiment, which was conducted in 2021, did not achieve its intended hypersonic conditions, the current grant supported a detailed analysis of supersonic transition data achieved during the flight [3, 4]. In addition the grant supported research into the flight dynamics that led to the unexpected behavior of the BOLT experiment [5, 6].

The secondary objective of this project was to strengthen the development of the Texas A&M and CUBRC BOLT-2: The Holden Mission flight test to study turbulent flow phenomena by leveraging the expertise and significant experience of the APL team who led the BOLT flight experiment. APL performed independent aerodynamic and thermal analyses to ensure the BOLT-2 flight experiment would be delivered at the desired experimental conditions and that the experiment hardware would survive through the flight environment. The success of the BOLT-2 flight offered new validation data for APL spatial BiGlobal and planar-marching Parabolized Stability Equations (PSE) calculations at hypersonic flight conditions [7]. APL assisted the BOLT-2 team in post-processing the flight data and co-authored several papers with members of the BOLT-2 team including CUBRC, NASA Langley, and Texas A&M [8–10].

The research objectives and related activities as originally proposed are shown in Figure 1. The final grant spending versus the original (linear) planned spending profile are shown in Figure 2. Specific accomplishments and impacts from these research activities will be described in this report.

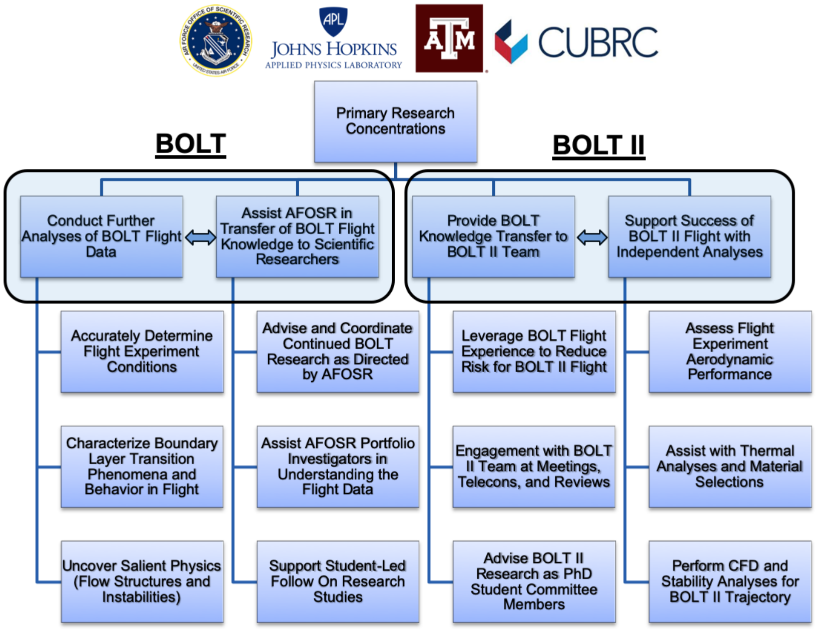

Figure 1. Research objectives and related activities as originally proposed by APL.

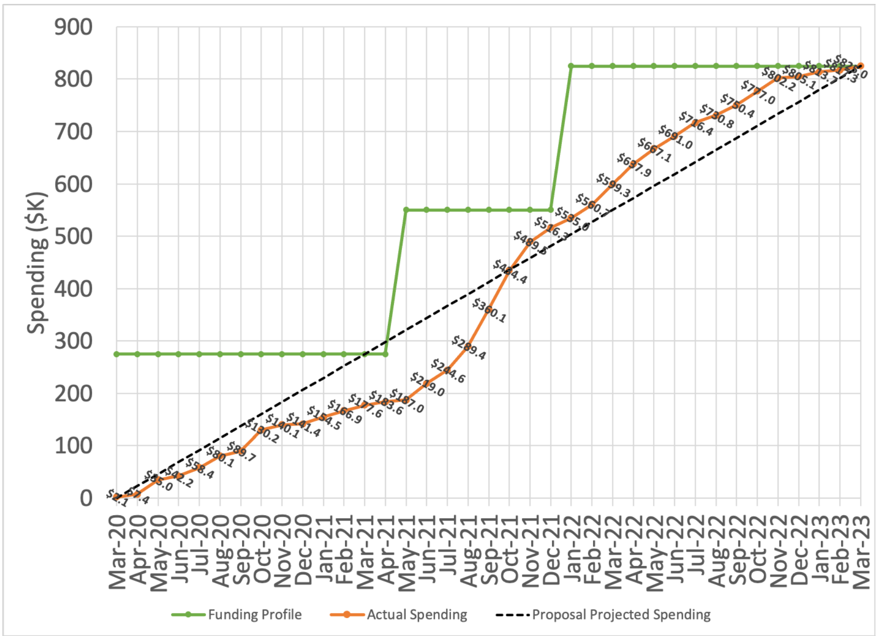

Figure 2. Grant actual spending versus proposed

2. Accomplishments

2.1. BOLT Postflight Analysis of Experiment Conditions and Supersonic Transition Data

Postflight analysis of the BOLT experiment was to be the major focus of the present grant. When this grant was originally awarded in 2020, the BOLT flight had not yet occurred due to delays incurred from the COVID-19 global pandemic. The flight experiment did not occur until Year 2 of this grant in June 2021. Due to expected behavior of the flight vehicle carrying the BOLT experiment, the experiment did not reach its intended Mach 5–7 conditions in flight. The vehicle entered a coning motion and achieved large angles of attack during the ascent phase which complicated the analysis of the experimental data that was ultimately obtained at supersonic conditions (Mach $\approx$ 3) during the descent phase of flight. Unfortunately, reentry to the atmosphere occurred several minutes sooner than anticipated due to the much lower apogee, resulting in only one of the three scientific data telemetry streams being active during the descent phase. Thus, a limited number of instrument data on the order of 90 channels were received during the BOLT descent. APL analyzed the available data to obtain a summary of the boundary-layer transition events which may be inferred at various points during the supersonic descent. This analysis was coupled with a computational investigation performed for the flight conditions, allowing for direct comparisons of surface heat flux. These computations were also leveraged to conduct preliminary stability analyses meant to identify potential transition mechanisms encountered in flight. Initial results from the flight experiment were published in Wheaton et al. [3] while the final analysis of the supersonic data obtained during descent were published in Butler et al. [4]. Full details are described in the Year 2 annual report [2].

The first major task of the BOLT postflight research was to determine the experiment conditions from the flight. APL worked with the Air Force Research Laboratory Aerospace Systems Directorate (AFRL/RQ) as well as the Air Force Weather Agency to obtain a reconstructed estimated atmosphere from the June 2021 flight experiment. The reconstruction of the atmospheric conditions was aided significantly by the AFOSR MURI balloon team that supported the BOLT flight campaign with detailed pressure, temperature, and dew point measurements of the atmosphere. A second major effort included reconstructing the vehicle attitude during the BOLT flight. APL generated a database of inviscid computational fluid dynamics (CFD) solutions that was used along with measured surface pressure sensors on the BOLT forebody to reconstruct an estimated vehicle attitude. The predictions of angle of attack and sideslip angle were then compared against reconstructions of the attitude from the vehicle IMU provided by AFRL/RQ. There were two IMU's on board, however due to the wild trajectory of the vehicle, the DLR DMARS IMU was saturated and not useful during most of the flight. Together, all data sources were compared and used to produce the Best Estimated Trajectory (BET) for the BOLT flight. The BET was version controlled and is stored along with the scientific data for future use by researchers wishing to analyze the BOLT data.

APL developed scripts and processing methods to reduce the measured BOLT surface sensor data to pressure fluctuation magnitude and heat transfer rates for potential identification and characterization of supersonic boundary-layer transition during the flight. It was decided that due to the large angles of attack achieved on the ascent phase, that APL would concentrate analysis of boundary-layer transition to the supersonic descent phase of the experiment. APL also performed new postflight CFD and boundary-layer stability analysis using the NASA LASTRAC code for portions of the descent phase of flight in order to compare against the experimental measurements. Because the BOLT vehicle did not perform a re-pointing maneuver as originally planned, the reentry phase of flight had an erratic attitude. APL worked carefully to compare the vehicle attitude solution to measurements of pressure and transition to make sure that vehicle motion was properly understood. Discrete times were selected for analysis where the vehicle briefly achieved relatively low angle of attack, and these conditions were analyzed with CFD and published in a conference paper [4]. The same paper published the conclusion of transition behavior inferred from the flight measurements during descent. Highlights of the analysis are shown in Figure 3.

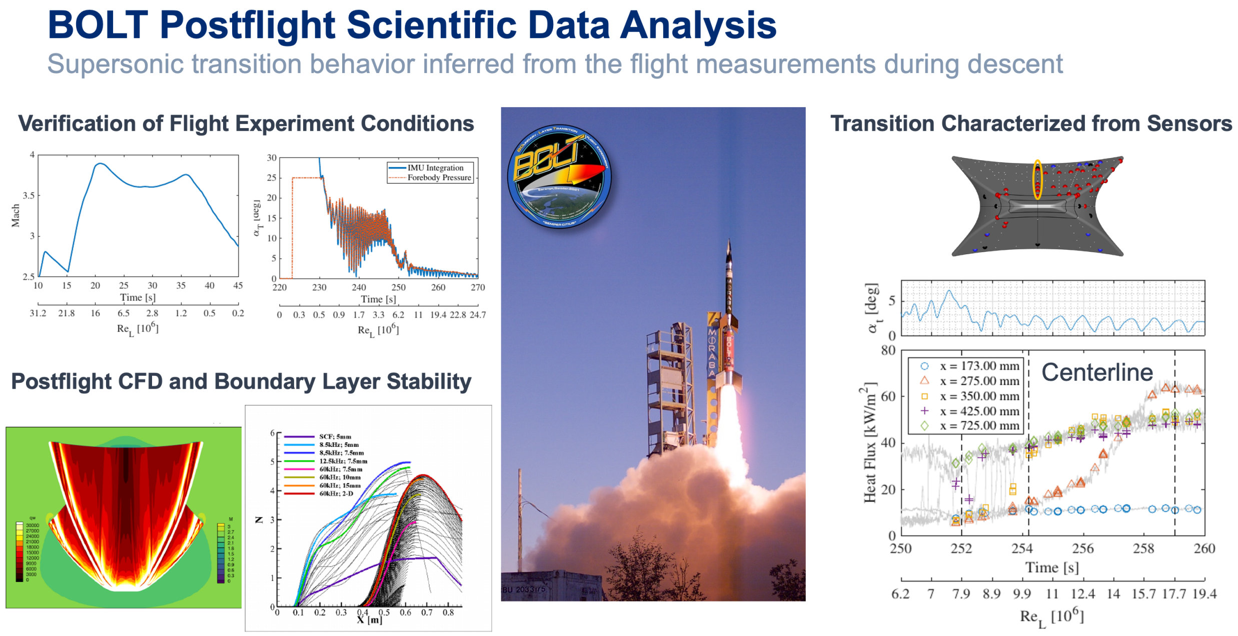

Figure 3. Highlights of postflight supersonic transition analysis of the BOLT flight descent phase.

The postflight scientific data analysis effort was not as extensive as originally proposed, due to the lack of achieving the desired flight experiment conditions and also the limited amount of flight instrument data actually received from the flight (due to a pre-planned telemetry stream shutoff at the actual reentry times). After discussion with the Program Officer, and since both activities were within the scope of the proposed research, it was decided to prioritize assistance in analysis of the BOLT-2 flight data rather than continue further analysis of the BOLT supersonic transition data.

2.2. BOLT Postflight Analysis of Flight Dynamics

Supported by funding from this grant, APL lead a post flight analysis of the BOLT flight unexpected behavior from the June 2021 flight event. The investigation was a collaborative effort with flight partners AFRL/RQ and DLR and was conducted with full participation of the AFOSR Program Officer Dr. Popkin. A small advisory committee was formed to investigate the flight behavior.

The committee consisted of members of the BOLT team from AFRL, DLR, and APL. In addition, a small number of additional staff from APL and Sandia National Laboratory were brought in as Subject Matter Experts to assist with particular aspects of the investigation. The investigation initiated in August 2021, and results were briefed to AFOSR at two reviews: (1) an interim investigation review on 20 September 2021 as well as (2) a final review on 19 November 2021. APL published four AIAA papers documenting the post flight research phase as seen in Wheaton et al. [3] from SciTech 2022, as well as three papers for AVIATION 2022 (Butler et al. [4], Kutty et al. [5], and Melcher et al. [6]). The advisory committee developed a fault tree to guide the investigation efforts.

APL was able to leverage its organizational expertise to simulate flight vehicle trajectories to explore the dynamics of the instability that occurred during the BOLT flight. This included developing a model for the BOLT second stage in the Sandia Trajectory Analysis and Optimization Software (TAOS). Unlike preflight modeling, the new APL model represented the vehicle aerodynamics in an asymmetric manner which was key to uncovering unstable flight behavior. APL led a literature search and found old papers from the 1970's that described the impacts of asymmetric spinning vehicle dynamics on the susceptibility of a vehicle to enter pitch-roll resonance [11, 12]. APL also leveraged subject matter expertise in aeroelastic effects to model the coupled impact of the bending modes of the vehicle with the aerodynamics and flight dynamics. This was the first time at APL that these effects had been combined into a complete vehicle model. Although the aeroelastic effects were simulated for linearized aerodynamic loading valid only at small angles of attack, the aeroelastic model was suitable to recreate the behavior observed in flight. Figure 4 shows the APL postflight 6-DOF modeling (in yellow) against the flight data (in black). The orange and blue lines show the impact of flexible body aerodynamics on the critical pitch and yaw frequencies, which is not typically modeled in standard preflight planning.

It was found that the preliminary cause of the observed flight deviation was a significant reduction in the second stage aerodynamic static stability relative to preflight predictions. As a result of reduced stability, the critical pitch frequency was in close proximity to the roll rate during the initial portion of the coast phase following separation of the first stage ($t > 11$ s) enabling roll resonance "lock-in" (roll rate locks-into the critical pitch frequency). Roll resonance "lock-in" caused exponential growth in the vehicle angle of attack. The primary contributor was aeroelastic flexure of the 2nd stage during the coast phase exacerbated by high dynamic pressure and the significant lift produced by the forebody in the pitch plane. Aeroelastic flexure was also expected to create a large divergence of the pitch plane and yaw plane critical frequencies, caused by the asymmetric shape of the vehicle outer mold line, and exacerbated by a loss of static margin due to significant aeroelastic effects. The divergence of the pitch plane and yaw plane critical frequencies also expanded the region in which the vehicle was susceptible to entering roll-pitch coupling.

The BOLT investigation and resulting lessons learned provided new knowledge and modeling capabilities for determining flight dynamic stability of asymmetric sounding rockets. Full details are described in the Year 2 annual report [2]. The APL team remained in communication with the BOLT-2: The Holden Mission team to ensure that the lessons learned from the BOLT flight were applied ahead of the flight experiment of BOLT-2. The new knowledge is currently being applied by APL in the development of the BOLT-1B experiment that will attempt to re-fly the original BOLT-1 experiment on a new rocket.

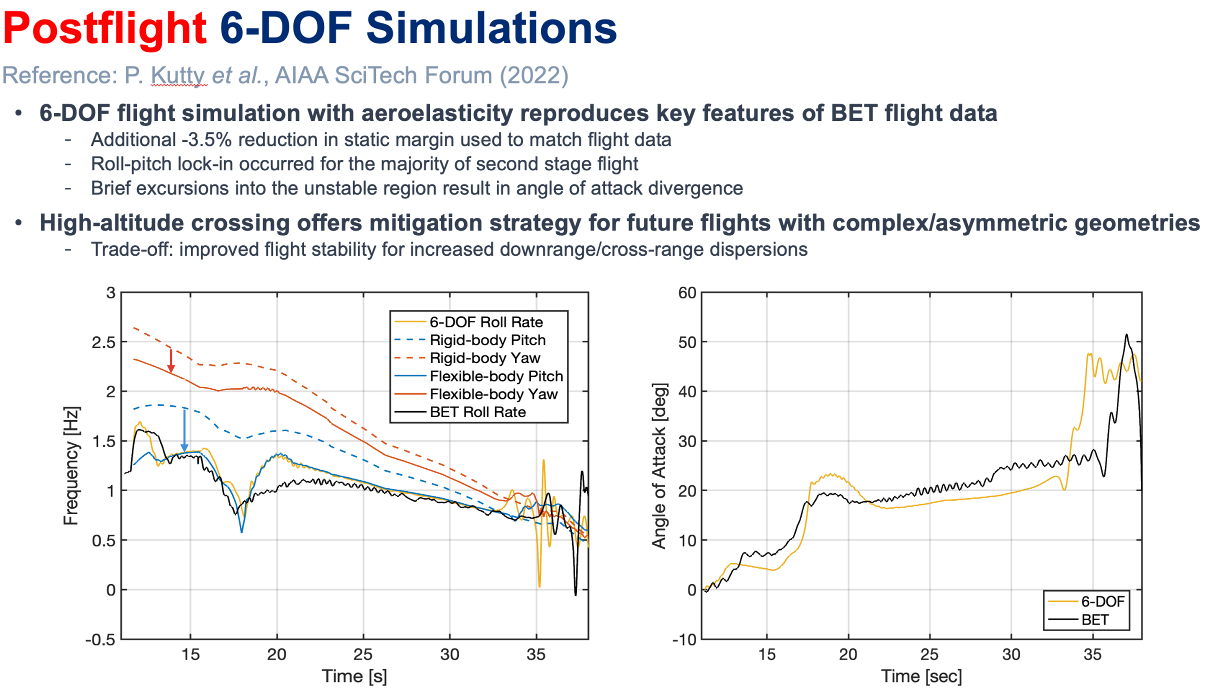

Postflight 6-DOF Simulations

Reference: P. Kutty *et al.*, AIAA SciTech Forum (2022)

- **6-DOF flight simulation with aeroelasticity reproduces key features of BET flight data**
  - Additional -3.5% reduction in static margin used to match flight data
  - Roll-pitch lock-in occurred for the majority of second stage flight
  - Brief excursions into the unstable region result in angle of attack divergence
- **High-altitude crossing offers mitigation strategy for future flights with complex/asymmetric geometries**
  - Trade-off: improved flight stability for increased downrange/cross-range dispersions

Figure 4. APL's final 6-DOF recreation of the BOLT flight behavior (yellow) compared against the flight data (black).

2.3. BOLT-2 Knowledge Transfer and Advisory Activities

A major research focus of this grant, as proposed, was to make available the APL staff members who led the development of the original BOLT flight experiment for transferring experience and knowledge to the follow-on BOLT-2: The Holden Mission team (led by Texas A&M University and CUBRC).

While leading the development of BOLT, APL gained valuable knowledge specific to hypersonic flow over a low-curvature, concave surface with swept leading-edges. Sharing this knowledge and experience helped serve to reduce risk in the design of the BOLT-2 flight experiment. As such, a key component of the activities supported in this grant was for APL to engage in knowledge transfer and advisory activities with the BOLT-2 team. Here "knowledge transfer" is sharing of BOLT design experience and data, while "advisory activities" include all other collaboration with the BOLT-2 team outside of the technical work for independent analysis that will be described later. While this portion of the research did not always produce defined products, the support of the APL BOLT team to engage with the larger BOLT-2 team was integral to developing the follow on flight.

Some of the knowledge transfer and advisory activities to the BOLT-2 team are summarized briefly here. Since March 2020, APL staff supported regular bi-weekly technical discussion phone calls with the BOLT-2 team to observe the current status of experiment design work and related issues.

APL has in most cases conducted follow up communications via e-mail and/or telecons to support the BOLT-2 team researchers and students in various aspects of their research to design their flight experiment. APL provided CAD and other design materials from BOLT-1 directly to the BOLT-2 team and hosted meetings at APL with CUBRC designers and instrumentation specialists to review potential areas for improvement in the design of BOLT-2. Advice and documentation from APL's BOLT experience has been communicated in aspects such as material selection, thermal modeling techniques, detailed mechanical design questions, aerodynamic considerations, experience with designing an aerodynamic fairing, wind-tunnel testing, wind-tunnel results, computational fluid dynamics, instrumentation selection, instrumentation layout considerations, data sampling considerations, version control, flow phenomena, and flight range operations.

APL staff members also supported the BOLT-2 Preliminary Design Review (PDR) and Critical Design Review (CDR) in Year 1 of this research grant, and provided feedback via Requests for Actions (RFA's) in both reviews. APL staff then assisted the BOLT-2 team in responding to the RFA's.

In many instances, APL was encouraged to interact directly with student researchers who were leading aspects of the development of BOLT-2. This allowed the students an outside subject matter expert perspective on their work. Early in the project, APL aerodynamics subject matter experts helped review and assist in the development of the BOLT-2 aerodynamic database that was led by students from Texas A&M. Later in the project, the lessons learned from the design of the BOLT-1 instrumentation layout were communicated to students who were leading the selection of BOLT-2 instrumentation locations. Following the flight experiment, APL staff assisted students analyzing the flight data by suggesting potential analyses and reviewing interim research findings prior to publication.

Throughout the project, APL interacted increasingly with NASA Wallops as details of the BOLT postflight investigation became apparent. APL interacted with NASA Wallops including reviewing latest flight trajectory Monte Carlo studies leading up to the BOLT-2 Mission Readiness Review (MRR) that occurred in the weeks prior to the flight. APL's contributions were highlighted by NASA Wallops / NASA Sounding Rocket Operations Contractor (NSROC) in their official post-flight self-assessment from the Technical Mission Closeout Report (TCMR):

> *The NSROC self-assessment of the 46.027 Holden mission performance is "Excellent". NSROC used recently added TAOS to analyze the non-axisymmetric BOLT 2 payload, working with the SRPO Chief Engineer for TAOS questions, TAMU students running CFD, and APL for an independent review. In addition, NSROC worked with the Exp team to reconfigure an unstable payload to allow the mission to proceed, designed through the pandemic shutdown, and maintained consistency in the team through work being stopped because funding. The results were the first successful sounding rocket flight of a payload with a non-axisymmetric front end.*

2.4. BOLT-2 Independent Analysis

A major set of research activities conducted under this grant included a variety of independent analyses conducted by APL to support the preflight planning and postflight data analysis of BOLT-

2: The Holden Mission. As a University Affiliated Research Center (UARC), APL brings expertise and analysis capabilities not typically found in academia in areas critical to the planning and execution of flight experiments. For the BOLT-2 flight, APL employed these capabilities to assess the vehicle aerodynamics, thermal environment, and structural response of the experiment to the planned flight environment. The analysis was in many cases a “second set of eyes” to check results generated by other members of the BOLT-2 team including students. Contributions of independent analysis to the preflight planning and postflight data analysis will be summarized here. Highlights of some of the APL contributions are shown in Figure 5.

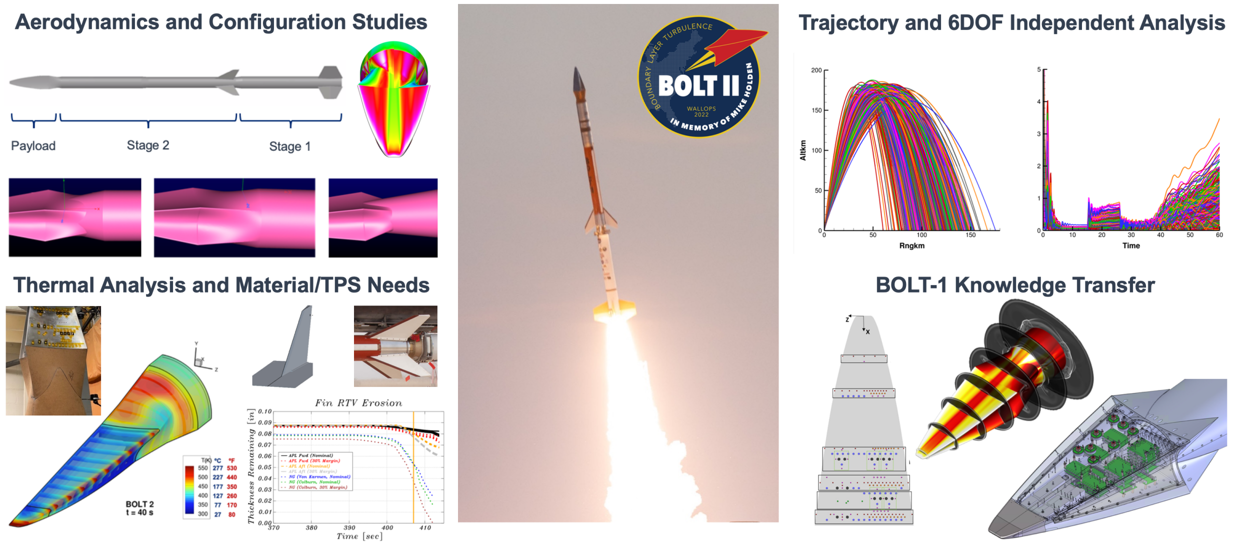

Figure 5. Highlights of APL contributions to BOLT-2: The Holden Mission enabled by this research grant.

2.4.1. Preflight Aerodynamics Analysis

Most of the early independent analysis by APL in this grant was to perform an assessment of the aerodynamic force and moment databases being generated by Texas A&M. APL has significant subject matter expertise in this area and typically supports major hypersonics programs in the generation and validation of aerodynamic databases. As BOLT-2 was the first flight at NASA Wallops of a vehicle with a nonaxisymmetric forebody, NASA required the BOLT-2 team to provide the aerodynamic database as they did not have their own Computational Fluid Dynamics (CFD) capabilities. The primary lead for generation of the BOLT-2 area database was Texas A&M University, and the main data was being generated by graduate students. Because aerodynamic data generated by students would be used directly in preflight predictions by NASA Wallops including vehicle dynamics and range safety, APL’s role under this grant was to support the students and perform verification of the aerodynamic data being generated.

In preparation for the BOLT-2 PDR (held on June 19, 2020), APL conducted a limited set of inviscid and viscous CFD simulations of the BOLT-2 second stage configuration (Payload + Stage 2 rocket motor). This was done to assess the accuracy of the aerodynamic database utilized in the trajectory analysis and to provide feedback for potential improvements to the aerodynamics modeling for future design iterations. Predictions of center of pressure location, X_{cp}, as well as inviscid drag and total drag for total angle of attack = 0° ($CA_{inviscid}$ and CA_0, respectively) were the focus of the assessment. Full details are described in the Year 1 annual report [1]. Generally, good agreement was found between the new APL results and the Texas A&M aerodynamic database for the vehicle center of pressure, a key term in the calculation of static margin to meet the flight requirements. Some small discrepancies in drag terms were noted that prompted further discussions with NASA Wallops about the buildup of drag for their flight modeling.

Following PDR, APL conducted a trade study to examine the stability impacts of three different fairing concepts under consideration by the BOLT-2 team leading up to CDR (held on October 28, 2020). The major conclusions from this analysis were to show that the "short" fairing increased stability and drag, while the "long" fairing decreased both stability and drag relative to the "PDR" fairing design. However, the short fairing was found to have higher local heating. Thus the analysis drove the BOLT-2 team to maintain the fairing outer mold line from PDR for the final flight.

2.4.2. Preflight Thermal/Structural Analysis

Another major accomplishment in this grant was the work by APL to perform preflight thermal analysis that directly supported key design decisions for materials by the BOLT-2 team. The majority of this research was performed in a short time period ahead of the BOLT-2 PDR in 2020. The rapid turnaround of a complete preflight transient thermal analysis to support the PDR was enabled by previous BOLT-1 models and experience developed by APL. Many of the grids, tools, and thermal models were developed under the original BOLT-1 project and available for immediate application to support BOLT-2, with limited modifications//updates to the models required.

The initial support by APL to the BOLT-2 team in the area of thermal modeling utilized correlation-based heating predictions and an existing BOLT-1 model developed previously in the MSLRAD–ATLAS (Missile Radiance/Aerothermal Loads And Stresses) thermal solver developed by APL. MSLRAD–ATLAS is an in-house suite of aerothermal prediction tools developed over many years by APL. It has the powerful capability of rapidly generating correlation-based heating inputs on complex geometries for a given trajectory. APL was provided with a preflight design trajectory generated by NASA Wallops and asked by CUBRC to begin running trade studies of potential materials that were under consideration for the BOLT-2 forebody design. The new BOLT-2 trajectory was less thermally stressing that the original BOLT-1 design trajectory due to an expected lower flight Mach number. APL generated correlation-based heating predictions as well as temperature predictions for the BOLT-2 trajectory using the original material set from BOLT-1 as well as additional materials for BOLT-2. In this early phase of design, the APL results along with close collaboration with CUBRC were critical to identifying and selecting the Nickel 201 nosetip for BOLT-2 along with the 410 stainless steel frustum.

Once the candidate materials had been identified, APL conducted a higher fidelity transient thermal analysis using heating derived from viscous CFD solutions, rather than from empirical correlations. Full details of this analysis are summarized in an AIAA paper that was presented after the flight [8]. Once again, this effort was conducted prior to PDR on a tight schedule and heavily leveraged CFD grids and methods developed under BOLT-1. Because of the longer length of the BOLT-2 forebody, the CFD grids were modified to include the additional length of the BOLT-2 forebody as well as the geometry of the transition module section of the payload. The fluid grid utilized a quarter geometry as the assumption of zero angle of attack was made, and the grid was comprised of 28.5M hexagonal cells (fully structured). Three variations of the grid utilizing the same topology and cell count were generated for different portions of the trajectory. A standard grid was utilized for most of the ascent and descent experiment portions as the outer boundaries were sufficient to capture the outer shock, and the wall spacing remained favorable for the desired $y^+ < 0.5$ condition sought for accurate heat flux. A grid with expanded outer boundaries was utilized early during the supersonic portions of the ascent phase in order to capture the outer shock. Late in the descent phase, a third grid was utilized with a smaller wall spacing to maintain the $y^+ < 0.5$ at higher Reynolds numbers. The transient thermal analysis was completed with a finite volume formulation of the transient heat equation developed within the CFD++ "solids only mode" analysis feature developed by Metacomp. This section describes the use of this capability in CFD++ such that the CFD solutions and resulting thermal response for a simple, short-duration ballistic trajectory such as BOLT-2 can be computed within the same solver. All preflight thermal modeling was completed using the assumption of fully turbulent heating throughout the entire trajectory. In addition, a $C = 1.2$ safety factory was applied to the thermal boundary condition profiles on top of the turbulent heating.

Temperature statistics from each material component were calculated from the transient thermal simulation including the maximum and volume-averaged (bulk) temperatures of each simulated component (nose, frustum, internal bulkhead at the base of the BOLT-2 forebody, the transition section, and the cylindrical booster section). With conservative assumptions, the preflight analysis predicted that the Nickel 201 nose maximum temperature was near 850 K (1070 °F) during ascent and reached a peak value of 980 K (1300 °F) at end of flight. These temperatures were provided to CUBRC for a detailed structural analysis, allowing the final design of the BOLT-2 forebody and transition section to be completed. One other impact of the APL analysis is that relatively high temperatures in the aluminum transition section were noted when a cork thermal protection layer was not modeled. Ultimately, cork was applied on the payload in this region as a result of the APL thermal modeling.

Following PDR, APL also supported several other thermal modeling studies again with the APL MSLRAD–ATLAS code. The MSLRAD–ATLAS code includes the ability to model gas/surface interaction problems such as ablation. APL was asked to perform a trade study to select the thermal protection methods on the BOLT-2 transition section and performed analysis of RTV and cork at various thicknesses in this region. The analysis identified the final thickness of cork that was applied to the TSM. In addition, APL was asked to perform an independent analysis of the RTV thermal protection layer on the second stage Improved Malemute fins. There was concern that the RTV would ablate and expose the fins to high temperatures during the end of flight descent leg, which could have led to fin failure before the end of the BOLT-2 descent phase science experiment window. A primary analysis was being performed by Northrop Grumman in support of NASA Wallops, but APL also performed a MSLRAD/ATLAS analysis showing that the recession of RTV was likely sufficient until the end of flight. APL also performed viscous CFD of the fin geometry at various flight conditions to ensure that the correlation-based heating predictions being used to analyze the fin RTV recession were within expected ranges.

APL supported CUBRC in understanding previously completed structural analysis of the BOLT flight experiment, such that a similar analysis could be completed by CUBRC for the BOLT-2 design. Although BOLT-2 featured different materials than BOLT, the overall design of the interface joints remains common between the two missions. BOLT-2 featured a single joint at the location of the BOLT "downstream isolator/frustum" joint. A potential issue was raised regarding how to model the interaction between differential thermal expansion, pre-flight bolt torque values, and related uncertainties in the initial/pre-flight torque of bolts connecting the parts. APL revisited the BOLT structural analysis with a new ABAQUS structural model that included new details of the bolts within the joints. The new analysis determined that the bolt loads are unlikely to cause failure in flight for the BOLT mission, and remained within acceptable limit loads. The results were shared with the BOLT-2 team and in particular to support the CUBRC structural analysis. It was determined that due to the materials used in BOLT-2, the load environment on the bolts was not of concern and a similar analysis did not need to be completed for BOLT-2. The new analysis helped to verify acceptable levels of risk for the BOLT flight and also allowed both the BOLT and BOLT-2 teams to gain new understanding of the behavior of the joint bolt structural loads through the stressing hypersonic flight environment.

2.4.3. Preflight Trajectory Analysis and Application of BOLT-1 Lessons Learned

APL conducted several preflight reviews of modeling the BOLT-2 trajectory utilizing the Trajectory Analysis and Optimization Software (TAOS) trajectory code and inputs provided by the NASA Wallops team. The first initial review came before the BOLT-2 PDR, very early in the NASA Wallops trajectory modeling process. NASA shared early TAOS modeling directly with APL for an independent review. Along with a general examination of the TAOS input files, four separate cases were considered for analysis: (1) a single nominal trajectory, (2) a single trajectory with reduced stage 2 total drag, (3) a set of 50 Monte Carlo simulations with given dispersions, and (4) a set of 50 Monte Carlo simulations with modified dispersions. The first goal of the trajectory studies was to quantify the potential impact on a reduction in second stage drag, as the initial APL aerodynamic database review noted a potential overprediction of drag by the BOLT-2 team for the second stage. The second goal of the trajectory studies was to explore the flight dynamics associated with NASA's initial scheme for fin cants of the first and second stage, and their corresponding roll rates.

Both the nominal trajectory simulation and simulation with reduced stage 2 total drag remained statically stable (static margin > 2 calibers) for the majority of the flight; only a slight decrease below 2 calibers was noted in the first 30 seconds of flight. It was noted in APL's Year 1 report [1] that the main impact of reduced stage 2 total drag would be a $\sim 10\%$ increase in Mach number on reentry, which could slightly increase heating. It should be noted that in the actual flight the Mach number was higher than anticipated, although it is unclear whether this increase can be attributed entirely to a potential error in calculating the preflight expected drag. Preliminary conversations between APL and NASA Wallops have indicated that there might be other factors associated with the increased Mach number in the actual flight.

The initial APL trajectory modeling highlighted the potential for pitch-roll coupling in the BOLT-2 flight due to the roll rate early in the Stage 2 burn aligning with the expected natural pitch frequency. Without corrections, the first set of Monte Carlo simulations showed a potential for dynamic instability during coast after Stage 1 separation (1 in 50 simulations failed). APL then performed additional Monte Carlo sets with a proposed correction to the fin cant of the second stage that demonstrated improved performance (0 of 50 simulations failed). These results were shared with NASA Wallops. Ultimately, NASA Wallops would go on to devise an even better fin cant and roll rate scheme for BOLT-2 that targeted a CONOPS for extremely low (near zero) roll rate of the second stage to remain below the critical pitch and yaw frequencies.

In retrospect, the susceptibility of the BOLT-2 vehicle to enter pitch-roll coupling for certain roll rate schemes should have highlighted the need to revisit the BOLT-1 mission CONOPS. For BOLT-1, detailed six degree of freedom (6-DOF) Monte Carlo modeling such as employed by APL in this grant and also by NASA Wallops had not been performed before the flight. Instead, other tools had been employed for BOLT-1 that assumed rotationally-symmetric aerodynamics (later found to be insufficient to model the pitch-roll coupling susceptibility of asymmetric spinning vehicles [5, 6]). A detailed 6-DOF Monte Carlo analysis of BOLT-1, which was a completely different vehicle configuration from BOLT-2, was not considered before the flight. The BOLT-1 flight, as mentioned previously, would go on to experience pitch-roll coupling. A major lesson learned from the current grant (from both the BOLT-2 preflight modeling and BOLT-1 postflight investigation modeling) was that a nonaxisymmetric spinning vehicle is inherently susceptible to pitch-roll coupling and must be analyzed with 6-DOF Monte Carlo modeling that considers the asymmetry of the aerodynamics as well as terms that are important to contributing to nonzero trim angle of attack. While this lesson was learned too late to impact the BOLT-1 flight in June 2021, APL was able to complete the BOLT-1 investigation in time to assess the risk of the same issue occurring in the BOLT-2 flight in March 2022.

In the several months before the BOLT-2 flight, APL completed additional trajectory modeling with 6-DOF Monte Carlo methods of the final BOLT-2 flight configuration to determine the risk of pitch-roll coupling occurring in the BOLT-2 flight. The BOLT investigation concluded in November 2021, leaving only four months between the conclusion of the investigation and the expected launch of the BOLT-2 experiment. Following the BOLT investigation, APL worked with NASA Wallops to evaluate the Wallops TAOS trajectory modeling for BOLT-2 and provide an independent analysis of the 6DOF modeling to ensure that terms found to be important to the BOLT pitch roll coupling behavior were incorporated adequately into the BOLT-2 modeling.

APL obtained the BOLT-2 TAOS model from NASA Wallops in late January 2022 as well as a description of the modeled Monte Carlo parameters in the simulation. Due to the unknown sensitivity of the models, results are not plotted here but were provided separately to NASA and AFOSR. On initial receipt of the TAOS model, APL noted that the Wallops modeling did not include a blanket uncertainty on center of pressure. APL typically recommends a 5% body length uncertainty on center of pressure. APL performed independent simulations of the BOLT-2 trajectory with Monte Carlo parameters that included a 5% and 10% (unrealistic but stressing) body length center of pressure uncertainty. In addition, knowing from the BOLT investigation that the moment bias terms provide the initial seeding for angle of attack amplification, APL performed additional simulations with a 3X multiplier on the Wallops tailcan misalignment term (the term responsible for providing these moment biases).

The results showed that the BOLT-2 vehicle was much more robust to these terms due to the selection of a low roll rate that avoided pitch-roll crossings at high dynamic pressures. APL presented the results to Wallops in January 2022. The analysis was deemed a complete check of the phenomena from the BOLT investigation and satisfied the Wallops team that the preflight analysis did not miss any unexpected behavior. BOLT-2 had a successful launch in late March 2022.

2.4.4. BOLT-2 Postflight Data Analysis

Under support from this grant, APL assisted the BOLT-2 team in receiving, post-processing, and understanding portions of the flight data received from the successful experiment. Primary postflight analysis of the BOLT-2 data was led by Texas A&M and CUBRC, but APL contributed to an analysis of a subset of the flight data (from the functioning Medtherm coaxial thermocouples) and also provided a complete set of laminar and turbulent Reynolds Averaged Navier Stokes (RANS) CFD data computed from the as-flown BOLT-2 trajectory. APL coordinated directly with Texas A&M regarding the postflight analysis and also worked directly with one of the Texas A&M students who was leading the postflight analysis. APL discovered that the simple Cook-Felderman [13] analytical solution was likely sufficient to convert the Medtherm temperature data to estimated heat flux in most regions of the BOLT-2 forebody where spanwise conduction effects were low. APL also contributed an initial BiGlobal stability analysis at BOLT-2 flight conditions, described further in the next section. Figure 6 summarizes research highlights from this project that contributed to initial understanding of the BOLT-2 postflight data.

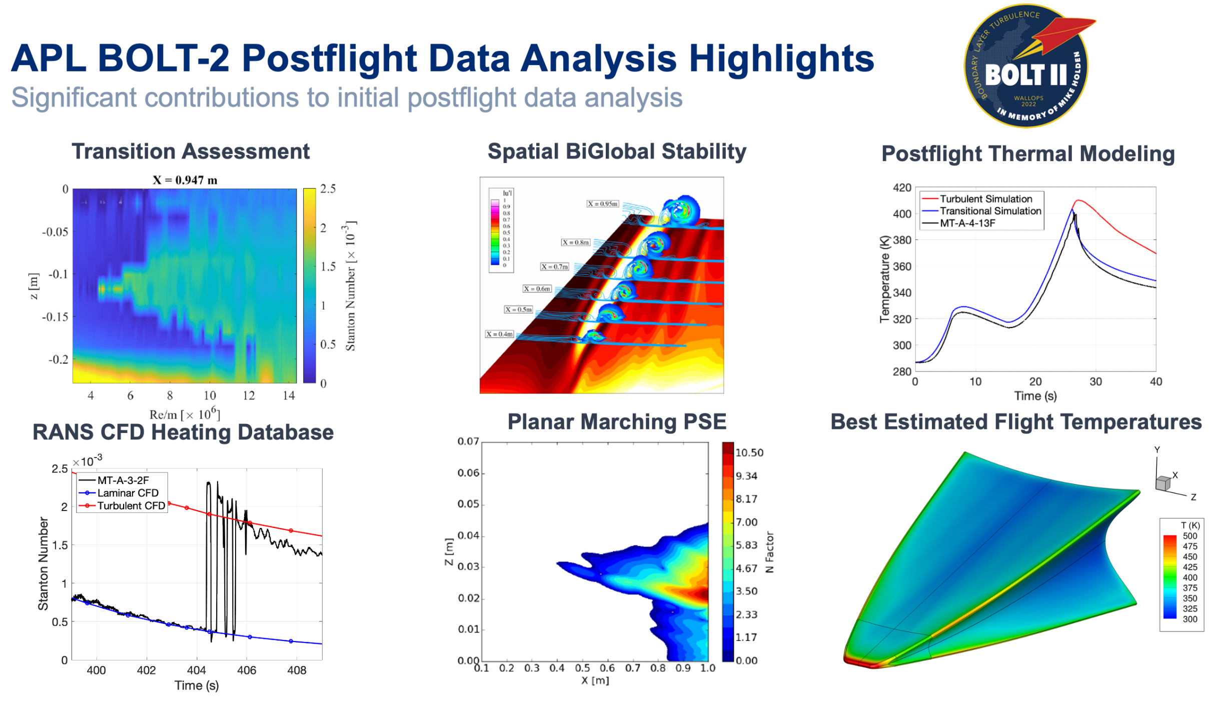
APL BOLT-2 Postflight Data Analysis Highlights

Significant contributions to initial postflight data analysis

Transition Assessment

Spatial BiGlobal Stability

Postflight Thermal Modeling

RANS CFD Heating Database

Planar Marching PSE

Best Estimated Flight Temperatures

Figure 6. Highlights from APL's contributions to the initial BOLT-2 postflight data analysis.

As mentioned, APL focused BOLT-2 experimental data analysis efforts under this grant on analysis of the Medtherm coaxial thermocouples from the flight. The purpose of the APL analysis was to identify suitable transition onset conditions from the BOLT-2 flight for planned postflight

CFD and BiGlobal/Planar Marching PSE stability analysis. In addition, the temperature data from the surface Medtherms represented the final validation of all the APL BOLT-1 and BOLT-2 preflight thermal modeling, and the temperatures were used to compare against a new postflight thermal analysis of the BOLT-2 experiment performed by APL and presented at AIAA SciTech 2023 (Wheaton and Dufrene [8]).

First, a new database of RANS CFD was generated with both laminar and turbulent heating using the same CFD grids and methods from the APL preflight analysis. CFD predictions of laminar and turbulent heat flux, as well as shear stress, were extracted at the BOLT-2 flight sensor coordinates and provided as a database to Texas A&M for further comparison against their postprocessed experimental data. These comparisons will be shown in an upcoming joint AIAA paper at AVIATION 2023 written by Texas A&M and APL [10]. Data were also provided to NASA Langley for the purpose of understanding the Side B experiment of the BOLT-2 flight and resulted in a joint paper led by NASA and contributed to by APL [9]. The APL heating inputs generated by the postflight RANS CFD were critical to understanding the initial boundary layer transition and turbulent flow data on the BOLT-2 flight.

The RANS CFD inputs were then used by APL for a complete postflight thermal analysis using the same methods described earlier for the preflight analysis. The thermal modeling methodology was validated against the flight-measured surface temperatures. The flight data provided the opportunity to assess conservatism in the preflight analysis and to determine best practices for future transient thermal analyses. The temperatures realized in the actual flight were lower than in the preflight analysis, due to conservative assumptions used in the preflight modeling (fully turbulent heating plus a 1.2 safety factor on heat transfer coefficient). It was found that modeling of transitional heating during ascent was crucial to matching the measured ascent surface temperatures. The CFD heating was compared to estimated heat transfer rates from the flight and showed good agreement.

A set of estimated three-dimensional surface temperature distributions were also a product of the postflight thermal modeling, and were found to be a good match to the available flight data. These surface temperature distributions were anchored using measured frustum surface temperatures. APL has made these estimated surface temperature distributions from the BOLT-2 flight available to other researchers who wish to use them as boundary conditions in new simulations, as they offer more accurate temperatures than the assumed constant-temperature isothermal wall condition typically used in CFD analysis.

The postflight best estimated temperature distributions within the nosetip were given to CUBRC and used to estimate the differential thermal expansion at the nosetip/frustum joint interface at the end of flight. Due to the conservatism in the preflight analysis, the differential thermal expansion at the nosetip joint is expected to be smaller than indicated in the preflight analysis.

Overall, the postflight APL thermal analysis and associated CFD database was incredibly impactful to early scientific analysis of the BOLT-2 flight data. Data were generated and shared with relevant BOLT-2 team partners for assistance in understanding the flight data. The postflight thermal modeling will also have a direct impact on the future APL-led BOLT-1B flight experiment as the same methods (now flight validated) can be applied to this future experiment.

2.5. BiGlobal Stability Analysis of BOLT and BOLT-2

The recent success of the BOLT-2 flight experiment has yielded a wealth of hypersonic flight data to compare against computational tools. After discussions with the BOLT-2 team and the AFOSR Program Officer Dr. Sarah Popkin, it was decided that APL should focus some of the final portions of the present grant on detailed boundary-layer stability studies of the BOLT-2 flight conditions using BiGlobal stability analysis. The studies included a computational assessment of boundary-layer instabilities at a single condition in the as-flown trajectory, including comparisons to the flight data. The chosen condition occurs at a Mach number of 6.2 and freestream Reynolds number of $8 \times 10^6/m$, at which point boundary-layer transition is observed in both the near-centerline and outboard regions of the vehicle acreage. The heat flux data collected in flight reveals a transition pattern dominated by two independent fronts in the near-centerline and midspan of the vehicle acreage. The stability analyses conducted for this study focused separately on these two regions.

A limited effort was made to ascertain the degree of grid dependence displayed by the flow topology and resulting stability analysis, though grid convergence is likely not attained in this study. The laminar heating predicted by both grids demonstrated satisfactory agreement with the flight measurements. It also appears that the near-centerline thermocouples capture the motion of heating streaks caused by small variations in vehicle attitude. For both grids employed, the near-centerline region is dominated by the roll-up of two large vortex structures, with increased grid resolution enhancing the degree of roll-up displayed by the outer vortex. Greater grid dependence of the flow resolution was observed in the outboard region where vortex structures are seen developing within the higher-resolution baseflow. It is believed that further increasing the spanwise grid resolution in this region would yield more mature vortex structures.

BiGlobal stability analysis showed the near-centerline region to be dominated by shear instabilities housed within the two vortex structures. Planar-PSE computations show the most-amplified vortex instabilities to initiate within the inner vortex and reach N factors of approximately 16 by the end of the vehicle, regardless of which grid resolution is considered. Although this instability remains confined to the inner vortex with the coarse baseflow, it was shown to spread substantially to the outer vortex for the more highly-resolved baseflow. This instability is believed to precipitate the near-centerline transition observed in flight. Furthermore, it was shown that the enhanced vortex roll-up which accompanies greater resolution of the laminar mean flow produces a new, strongly-amplified instability family within the stem of the outer vortex. This instability was shown to reach N factors in excess of 15, nearly as high as the dominant inner-vortex instability. Significant spatial overlap of the various vortex instabilities is noted as it demonstrates the potential for nonlinear modal interactions, which are outside the scope of this study.

The stability analysis within the outboard region was found to be more susceptible to issues with resolution of the laminar baseflow. Upstream of any significant roll-up, BiGlobal analysis predicts this region to house various families of second-mode instabilities. Planar-PSE marches show these second-mode disturbances amplify substantially downstream as they are modulated by the roll-up predicted by the laminar computations and disturbance energy enters the vortex shear layer. However, the greatest N factors predicted by the Planar-PSE analysis with the highest-resolution grid are approximately 11.5, likely insufficient to cause the transition observed in flight, and occur inboard of the observed transition front.

It is noted that the N factor predictions within this study are meant merely as lower bounds to the actual disturbance amplification, as only a limited number of initial marching locations were surveyed and the neutral points of the various instabilities have yet to be established. Future work in an upcoming grant from AFOSR will seek to remedy this shortcoming in order to yield true maximum N factors. Furthermore, additional effort will be put in to attaining satisfactory grid-convergence of the laminar basic state.

That said, this work provided some quantitative measure of the sensitivity of the BiGlobal/Planar Parabolzed Stability Equations (PPSE) analysis methodology to the resolution of the laminar basic state. Conclusions regarding transition of the near-centerline vortex structure would be largely unimpacted by the choice of grid in this study, and these conclusions are apparently corroborated by the flight data. The same cannot be said for the outboard region, where the in-flight transition behavior was not predicted on either grid, but increased grid resolution produces a significant increase in disturbance amplification. All together, this highlights the need for development of best-practices in grid design and BiGlobal/PPSE stability analysis to avoid incorrect conclusions in studies where experimental data is not available. This work is meant to be a step towards defining these best-practices for the study of complex hypersonic configurations. The results as of the end of this grant were summarized in Butler et al. [7].

2.6. NATO AVT-346 Working Group Support

This grant supported Dr. Bradley Wheaton and Dr. Cameron Butler as members of the North Atlantic Treaty Organization (NATO) Science and Technology Organization (STO) Air Vehicles Technology (AVT-346) working group “Predicting Hypersonic Boundary-Layer Transition on Complex Geometries.” The AVT-346 working group consists of boundary-layer transition subject matter exports from across NATO ally nations to“facilitate an international collaboration of leading experimentalists and numerical simulation experts towards improved hypersonic prediction capabilities.” The simulation approaches will be mechanism-based and the team will use new opportunities for validation in ground facilities.

APL’s involvement in the AVT-346 working group was brought on by the selection of BOLT as a focus geometry for the working group subtask “transition due to the interaction of multiple instability modes.” The BOLT geometry was identified as producing concurrent instability modes (second mode and crossflow) within the same regions of the geometry. APL’s leadership of BOLT and knowledge of available ground test validation data as well as the state of CFD and boundary layer stability surrounding the geometry are extremely beneficial to the working group. Under the working group, new wind tunnel testing of the BOLT geometry are being conducted by the German Aerospace Center (DLR) and the French Aerospace Lab (ONERA) in their wind tunnels. APL is contributing new CFD and BiGlobal analysis of the wind-tunnel cases to the working group. APL, NASA, DLR, and ONERA are working on a chapter together for the AVT-346 final report expected in 2024. The APL support of the AVT-346 working group will continue under a new grant from AFOSR following the conclusion of the present research grant.

2.7. Conference Papers and Publications

This grant supported APL contributions to many AIAA conference papers, reporting research findings from the BOLT-1 postflight analysis as well as describing pre- and postflight analysis of BOLT-2: The Holden Mission. The papers are summarized below:

- [3] Wheaton, B. M., Butler, C. S., McKiernan, G. R., & Berridge, D. C. (2022). Initial Results from the BOLT Flight Experiment. AIAA Paper 2022-0345. `https://doi.org/10.2514/6.2022-0345`
- [4] Butler, C. S., Araya, D. B., McKiernan, G. R., & Wheaton, B. M. (2022). Supersonic Transition Measurements During the BOLT Flight Experiment Descent Phase. AIAA Paper 2022-4099. `https://doi.org/10.2514/6.2022-4099`
- [5] Kutty, P. M., Butler, C. S., Wheaton, B. M., & Fortier, J. B. (2022). 6DOF Simulation Analysis for the Post-Flight Investigation of the Boundary Layer Transition (BOLT) Experiment. AIAA Paper 2022-3884. `https://doi.org/10.2514/6.2022-3884`
- [6] Melcher, J. T., Radcliffe, E. J., Butler, C. S., & Wheaton, B. M. (2022). Effects of Aeroelasticity on Flight Stability of the Boundary Layer Transition (BOLT) Experiment. AIAA Paper 2022-3748. `https://doi.org/10.2514/6.2022-3748`
- [7] Butler, C. S., McKiernan, G. R., & Wheaton, B. M. (2023). Initial BiGlobal Stability Analysis of the BOLT II Flight Experiment. AIAA Paper 2023-0291. `https://doi.org/10.2514/6.2023-0291`
- [8] Wheaton, B. M., & Dufrene, A. T. (2023). Thermal and Structural Analysis of BOLT-2: The Holden Mission. AIAA Paper 2023-0685. `https://doi.org/10.2514/6.2023-0685`
- [9] Berry, S. A., & Wheaton, B. M. (2023). BOLT II Roughness-Side Flight Results. AIAA Paper 2023-0684. `https://doi.org/10.2514/6.2023-0684`
- [10] Wirth, J., Morreale, B., Bowersox, R. D., & Wheaton, B. M. (2023). Boundary Layer Turbulence Flight Experiment in Memory of Mike Holden: Side A Flight Data 2. Abstract Submitted to AIAA AVIATION 2023.

3. Impacts

This section documents the distinctive contributions, major accomplishments, innovations, successes, or any change in practice or behavior that has come about as a result of this project:

- Although the BOLT flight did not reach its intended hypersonic experiment conditions, the postflight scientific analysis of the supersonic descent phase of the flight supported by this grant resulted in a new flight validation dataset for supersonic transition that complements previous datasets (such as HIFiRE-5A [14]);
- This project supported APL and its partners to identify the cause of the BOLT unexpected flight behavior, and to reconstruct the flight behavior in a postflight simulation;

- The BOLT postflight investigation efforts resulted in new knowledge of sounding rocket flight dynamics that will influence the practices of planning for new low-cost flight experiments with complex asymmetric forebodies;
- This research project supported the first ever implementation of aeroelastic effects into 6-DOF modeling at APL, whereby the aerodynamic force and moment coefficients were a function of dynamic pressure in addition to typical parameters (Mach number and angle of attack). This implementation of aeroelastic effects not typically modeled in sounding rocket flight planning was documented and available for future flight experiment plans;
- The lessons learned from the BOLT flight investigation were directly applied by APL in assessing the risk of similar flight behavior in the successful BOLT-2 flight that would follow;
- This project supported the original BOLT-1 team as team members of BOLT-2: The Holden Mission to assist with knowledge transfer and advisory activities. The involvement of APL in this manner significantly reduced the development cost, timeline, and risks for the BOLT-2 flight;
- APL subject matter experts in aerodynamics, flight dynamics, thermal analysis, and structural analysis were able to mentor the BOLT-2 team including graduate students in their own analysis for planning the BOLT-2 experiment. This mentorship helped improve the resulting BOLT-2 planning and also helped foster improved workforce development for the students;
- APL's independent aerodynamic analysis for the BOLT-2 flight provided a much needed independent check on the results being generated by graduate students for the flight. The independent analysis by APL was cited by NASA Wallops as critical to reducing risk of the first flight at Wallops with user-supplied aerodynamic databases;
- APL performed independent trajectory modeling that influenced the roll-rate scheme employed for the BOLT-2 flight to mitigate unwanted pitch/roll resonance instabilities;
- Trade studies performed by APL with transient thermal modeling and correlation-based heating were instrumental in helping the BOLT-2 team select suitable materials for the design of the flight experiment;
- APL conducted the primary thermal analysis from a database of viscous CFD simulations for the BOLT-2 flight ahead of the program PDR;
- APL assisted in independent thermal analysis of the BOLT-2 transition module and second stage fin thermal protection systems ahead of the program CDR;
- APL assisted the BOLT-2 team in receiving, post-processing, and understanding portions of the flight data;
- APL conducted an independent post-processing analysis of the BOLT-2 Medtherm coaxial thermocouples and identified a reduced-form of reduction of the measured temperatures to heat flux via the Cook-Felderman analytical solution. This method only requires a surface measurement rather than a surface and inner measurement;

- A complete postflight RANS database of laminar and turbulent CFD solutions of the BOLT-2 as-flown flight trajectory were generated by APL, providing computational heat transfer rates and shear stress predictions that assisted the BOLT-2 team in understanding the experimentally-measured flight data;
- A postflight thermal analysis performed by APL of the BOLT-2 flight provided best estimated temperature distributions suitable for use as boundary conditions to future computations performed by others seeking to understand the impacts of temperature distribution on transition and turbulence;
- The postflight BOLT-2 thermal analysis provided validation of the preflight process used to predict temperatures for the flight, and documented the conservatism inherent to preflight assumptions of turbulent heating throughout the flight;
- The postflight thermal analysis of BOLT-2 allowed CUBRC to estimate the expected differential thermal expansion at the nosetip joint in the actual flight;
- This grant supported new CFD and Spatial BiGlobal stability analysis of the BOLT-2 flight experiment at the flown conditions;
- This grant supported APL to participate in the NATO AVT-346 working group, which seeks to understand the behavior of transition in the presence of multiple mechanisms using the BOLT geometry. APL provided new analysis of wind tunnel data on the BOLT geometry gathered by NATO partners.
- APL subject matter experts were able to directly mentor graduate students working on the BOLT-2 flight, providing unique perspective and workforce development.

4. Changes/Problems

In coordination with the AFOSR PO, Dr. Sarah Popkin, the APL team successfully navigated several challenges encountered during this research project:

- The availability of the BOLT flight data was critical to many of the planned research efforts related to postflight analysis of this data in the present project. Due to the COVID-19 global pandemic, the BOLT flight experiment was delayed from May 2020 to June 2021. This meant that the BOLT flight did not occur until approximately mid-way through the 3-year research effort, rather than at the beginning of the project as planned originally. The APL team was able to redirect early project effort to support of the BOLT-2 preflight planning instead. To mitigate the delay in obtaining the BOLT flight data, the spending on the grant in Year 1 was lower than planned and was followed by higher than planned spending in Years 2 and 3 of the grant when the BOLT data was available (see Figure 2).
- The project objectives were to analyze hypersonic flight experiment data from the BOLT flight, however the flight did not achieve this conditions. Instead, a smaller research effort centered on analyzing that data that was received from the flight at supersonic conditions, which still provides value to the field;

- Following the BOLT flight unexpected behavior, research effort was re-prioritized within the scope of the grant to support a postflight investigation of the flight dynamics. This investigation meant a greater emphasis on aerodynamics and flight dynamics research compared to the proportion originally planned in the proposal;
- Since the original proposal, APL developed new capabilities to perform higher-fidelity BiGlobal stability analysis along with planar marching PSE by using the Sandia LST-PACK code. These new capabilities required additional computing resources that were not anticipated in the original project proposal, and were not generally available within APL's existing internal computational resources. APL was able to apply for and be granted a supplemental allocation of computing hours from the Department of Defense (DoD) High Performance Computing Modernization Program (subproject AFOSR49332933). This allocation of resources greatly enhanced the ability of the APL team to meet the research objectives of this project.

Acknowledgments

This work was supported by the Air Force Office of Scientific Research under award number FA9550-20-1-0043 (PO: Dr. Sarah Popkin). Any opinions, finding, and conclusions or recommendations expressed in this material are those of the author(s) and do not necessarily reflect the views of the United States Air Force. This work was supported in part by high-performance computer time and resources from the Department of Defense (DoD) High Performance Computing Modernization Program.

References

[1] Wheaton, B. M., "FA9550-20-1-0043 Year 1 Annual Report," *Grant deliverable to the Air Force Office of Scientific Research*, 2021.

[2] Wheaton, B. M., "FA9550-20-1-0043 Year 2 Annual Report," *Grant deliverable to the Air Force Office of Scientific Research*, 2022.

[3] Wheaton, B. M., Butler, C. S., McKiernan, G. R., and Berridge, D. C., "Initial Results from the BOLT Flight Experiment," *AIAA Paper 2022-0345*, 2022. doi:10.2514/6.2022-0345, URL `https://arc.aiaa.org/doi/10.2514/6.2022-0345`.

[4] Butler, C. S., Araya, D. B., McKiernan, G. R., and Wheaton, B. M., "Supersonic Transition Measurements During the BOLT Flight Experiment Descent Phase," *AIAA Paper 2022-4099*, 2022. doi:10.2514/6.2022-4099, URL `https://arc.aiaa.org/doi/10.2514/6.2022-4099`.

[5] Kutty, P. M., Butler, C. S., Wheaton, B. M., and Fortier, J. B., "6DOF Simulation Analysis for the Post-Flight Investigation of the Boundary Layer Transition (BOLT) Experiment," *AIAA Paper 2022-3884*, 2022. doi:10.2514/6.2022-3884, URL `https://arc.aiaa.org/doi/abs/10.2514/6.2022-3884`.

[6] Melcher, J. T., Radcliffe, E. J., Butler, C. S., and Wheaton, B. M., "Effects of Aeroelasticity on Flight Stability of the Boundary Layer Transition (BOLT) Experiment," *AIAA*

Paper 2022-3748, 2022. doi:10.2514/6.2022-3748, URL `https://arc.aiaa.org/doi/10.2514/6.2022-3748`.

[7] Butler, C. S., McKiernan, G. R., and Wheaton, B. M., "Initial BiGlobal Stability Analysis of the BOLT II Flight Experiment," *AIAA Paper 2023-0291*, 2023. doi:10.2514/6.2023-0291, URL `https://arc.aiaa.org/doi/10.2514/6.2023-0291`.

[8] Wheaton, B. M., and Dufrene, A. T., "Thermal and Structural Analysis of BOLT-2: The Holden Mission," *AIAA Paper 2023-0685*, 2023. doi:10.2514/6.2023-0685, URL `https://arc.aiaa.org/doi/10.2514/6.2023-0685`.

[9] Berry, S. A., and Wheaton, B. M., "BOLT II Roughness-Side Flight Results," *AIAA Paper 2023-0684*, 2023. doi:10.2514/6.2023-0684, URL `https://arc.aiaa.org/doi/10.2514/6.2023-0684`.

[10] Wirth, J., Morreale, B., Bowersox, R. D., and Wheaton, B. M., "Boundary Layer Turbulence Flight Experiment in Memory of Mike Holden: Side A Flight Data 2," *Abstract submitted to AIAA AVIATION 2023*, 2023.

[11] Hodapp, A. E., "Effects of Unsymmetrical Stability Derivative Characteristics on Re-Entry Vehicle Trim Angle Behavior," *Journal of Spacecraft and Rockets*, Vol. 11, No. 5, 1974, pp. 300–307. doi:10.2514/3.62067, URL `https://arc.aiaa.org/doi/10.2514/3.62067`.

[12] Hodapp, A. E., "Effects of unsymmetrical stability derivative characteristics on re-entry vehicle transient angular motion," *Journal of Spacecraft and Rockets*, Vol. 13, No. 2, 1976, pp. 82–90. doi:10.2514/3.27887, URL `https://arc.aiaa.org/doi/10.2514/3.27887`.

[13] Cook, W. J., and Felderman, E. J., "Reduction of Data from Thin-Film Heat-Transfer Gages: A Concise Numerical Technique," *AIAA Journal*, Vol. 4, No. 3, 1966, pp. 561–562. doi:10.2514/3.3486.

[14] Kimmel, R. L., Adamczak, D. W., Borg, M. P., Jewell, J. S., Juliano, T. J., Stanfield, S. A., and Berger, K. T., "First and fifth hypersonic international flight research experimentation's flight and ground tests," *Journal of Spacecraft and Rockets*, Vol. 56, No. 2, 2019, pp. 421–431. doi:10.2514/1.A34287.